Experimental low frequency mooring analysis of a floating offshore wind turbine

Y. J. Metsch

TU Delft

Royal HaskoningDHV

Experimental low frequency mooring analysis of a floating offshore wind turbine

Master Thesis

By

Y. J. Metsch

to obtain the degree of Master of Science
at the Delft University of Technology

Student number: 4668529
Project duration: May 2022 – May 2023
Supervisors: Dr. O. Colomés Gené (chair)
Dr. S. Schreier
Dr. A. van Deyzen (RHDHV)
Dr. X. Jiang

TU Delft

Royal HaskoningDHV

Preface

This document contains the report for my master thesis. With this master thesis I hope to complete the degree of Master of Science at the University of Technology in Delft at the faculty of Civil Engineering and Geosciences. The subject of this thesis is in accordance with my specialisation in Hydraulic Structures and will fulfil the requirements for that master track.

This thesis goes into the physical behaviour of floating offshore wind turbines through the use of experimental research. It follows up on the OC5 project which laid out some of the issues and questions this thesis tries to solve and answer. This thesis also attempts to generate more data which can then be used to improve numerical models of the floating offshore wind turbines. Hopefully, it will help make the world a better place.

I would like to thank Sebastian Schreier, who came with the original push for this thesis and helped me throughout the process. His insight, questions and attention to detail really helped me in making this thesis the best it could be. I would further like to thank Alex van Deyzen for his insight and help in presenting this thesis. I also thank Thijs de Boer and RHDHV for presenting me with the research and opportunity to do it. Furthermore, I would like to thank Oriol Colomés Gené and Xiaoli Jiang for making time for me with their help in the graduation committee. I would also like to thank those that helped me build the model, Jasper den Ouden, Pascal Taudin Chabot and Peter Poot.

I would also like to thank my friends Elise, Regino and Peter for the great times we had together during our time at the university. It was truly the best group to go through university together with and I would not have wanted it any other way. I would further like to thank Jelmar and Arend for their friendship. The many evenings spend playing games, watching movies and making (often off-colour) jokes kept me going. Thank you all for your support.

Finally, I want to thank my family. My parents, Peter and Martine, whose love, support and upbringing made me who I am today. You always pushed me to be better and to improve and I cannot overstate how grateful I am to you for it. And my younger brother, Tycho, and younger sisters, Esther and Nina, who always motivated me to keep going and who made the weekends the best part of the week. Thank you all from the bottom of my heart.

Youri Metsch

Vlissingen, May 2023

Abstract

Previous research into floating offshore wind turbines consistently shows some manner of discrepancy between numerical and experimental simulations when it comes to low frequency forces and motions. A part of solving this issue is the generation of accurate data for the calibration and validation of the numerical models, needed because of the coupled analysis introduced due to the relatively large wind force. The goal of this research thus became to generate accurate experimental data focussed on the low natural frequency of the mooring system in surge direction. This data had to be accompanied by an uncertainty assessment and should encompass multiple mooring systems for a good comparison. It was furthermore deemed preferable to maintain semblance to the OC5 project in order to be able to make a comparison of the data between research projects.

In order to achieve these goals experimental model tests were set up using bichromatic wave sets in a long towing tank. The bichromatic wave sets allowed for the creation of beating patterns, targeting the specific low frequencies on and around the surge natural frequency via the difference frequencies. The long towing tank reduced the amount of reflections and clutter in the tank. Together these factors ensured accurate excitation of model at the desired frequencies.

The model used was a 1:96 semi-submersible model with three buoyancy columns supporting a central tower column, akin to the model from the OC5 project. The depth in the tank being 1.25 m at model scale ensured a relatively deep testing environment. Two different mooring systems were tested, each with a different surge natural frequency but with the same semi-taut fibre rope-chain lay-out. A comprehensive measurement system consisting of force transducers in the mooring lines and wind force device and a camera tracking system enabled accurate measurement of both the force and motion of the model. Experiments revolved around examining the influence of the difference frequency in the wave excitation on the low frequency behaviour of the mooring system and floater.

From the lead mooring line force time series, it could be observed that during the surge natural frequency test the mooring line had triple the force compared to the wave tests with the monochromatic components, showing a clear effect of the bichromatic beating pattern. From the tests it also became clear that mooring system 1 had rear lines which were slack during wind and wave excitation. These slack lines had a number of effects on the behaviour of the model during the tests, such as increasing the mooring line force and surge response. The surge response further showed an asymmetric response, also the effect of the beating pattern and the slack mooring lines.

The tests thus show that the low frequency response comes from the difference frequency in the bichromatic wave sets, as was the goal. The heightening of the response around the natural frequency also shows that getting close to this frequency amplifies the effect. The comparison between the test results and the results from the OC5 project show that this is likely also the case there. At the same time the surge response does not show this heightened response. Which is likely due to the non-linear stiffness of the mooring system.

Furthermore, it was seen that the slack lines have a very large impact on the force in the mooring lines, especially on the lower frequencies and should thus be avoided at all times. The damping ratio as a parameter for the low frequency response is both physically and experimentally (excluding the slacked lined system) consistent and shows potential for development.

Contents

1 Introduction

This introduction gives the reader the necessary tools to understand the other chapters and the aim of this thesis. Concretely this will give a brief overview of the terms used around floating wind turbines, it will pose the research question and its sub questions, states the scope of the thesis and how the thesis answers the questions posed.

1.1 Floating wind turbines nomenclature

Bottom founded offshore wind turbines are a key element is making our power generation renewable and sustainable. However, these wind turbines are economically limited to a depth of 70 m, as the structural requirements grow exponentially with depth (GWEC, 2022). As more and more wind parks are built in the shallower parts of the world's seas, a new solution is needed to be able to harness wind power in deeper areas. This is where floating offshore wind turbines (FOWTs) come in.

As the name implies, the floating offshore wind turbine is a wind turbine that is built on top of a floating platform, thus reducing the need for large foundations to reach the seabed. The floating platform is kept in place by mooring lines anchored to the seabed and stays upright with the help of ballast in most types of FOWTs. A power cable comes off the platform to then deliver the power shoreside. FOWTs are anchored in clusters forming a wind park akin to their bottom founded counterparts, mainly to share energy transport infrastructure and to make maintenance easier. Figure 1 shows an example of a semi-submersible FOWT, with the power line on a buoy to reduce stress.

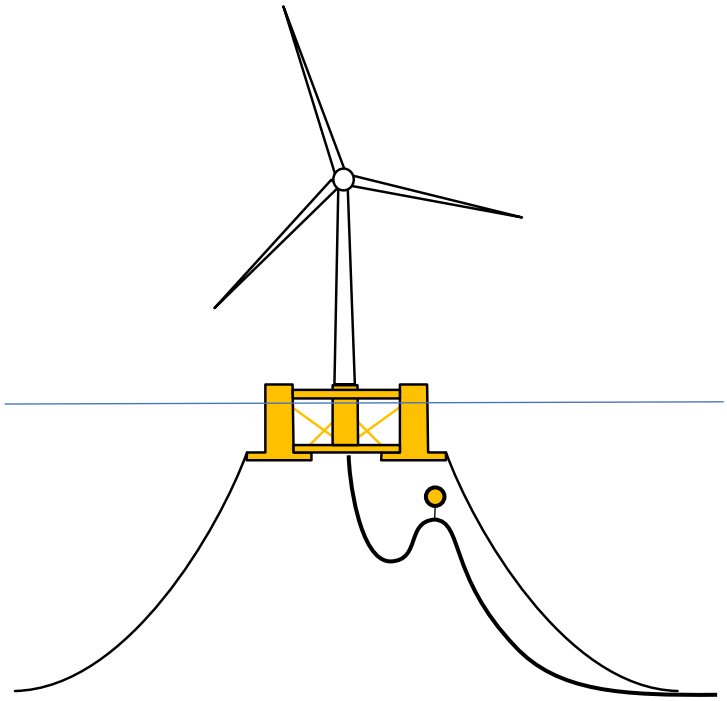

Figure 1: A FOWT using a semi-sub design.

Figure 2 shows the nomenclature of the motions used in this thesis. Due to the IR tracking software used, the coordinate system used is unconventional. Surge is forward, into the waves, but pitch is up away from the waves. Besides the surge no coordinates definitions are used in this thesis.

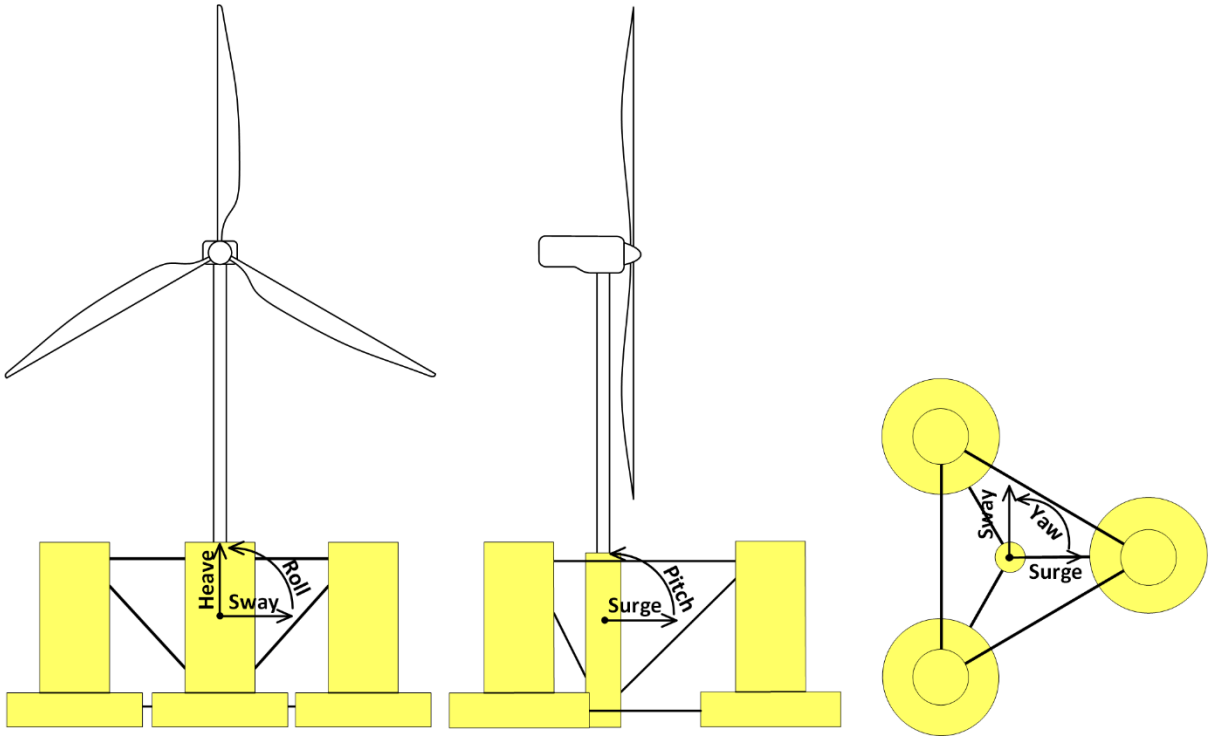

Figure 2: Motion directions of the FOWT

As FOWTs find their niche mainly in deeper parts of the sea, interesting countries for FOWTs are mainly those with a steep seabed and little shallow water surrounding the coast. Islands such as Ireland or Taiwan come to mind as there is little space to build bottom founded offshore wind turbines. Coastal profiles at the edge of the continental plates, such as California, Norway or Chile also look like good options, because of the deep coastal waters.

As space for bottom founded offshore wind becomes sparser, building offshore wind requires going out to deeper parts of the sea, which necessitate floating foundations. To reduce the costs of the energy produced, FOWTs need to be built at a larger depth compared to bottom founded wind turbines for as low of a cost as possible. Which requires simpler and less materially intensive structures, which in turns requires more engineering knowledge.

1.2 Research question

The research question will be posed. Sub questions, needed to answer the main question will also be stated. As the research question requires some knowledge of previous research, this will also make a short appearance before the literature review covers it in more depth.

A lot of engineering knowledge from the offshore oil and gas industry can be used in the design of the FOWTs. However, the FOWTs have some crucial differences with the platforms used in the oil and gas industry. The main differences are the size of the platforms and the disproportionally large wind force exerted on the wind turbine (Jonkman, 2007). These differences, combined with the need to build the FOWTs at mass compared to the one-off oil and gas platforms, means a very different mooring system is needed, which is both tailored to the different force balance but also less complex and easier to maintain.

Traditionally, a decoupled analysis of the mooring system and the floater was possible due to the lower external forces compared to the weight, in the decoupled analysis the mooring system and the floater motion are analysed separately. This is done by inserting a force on the floater in its analysis

to represent the mooring system and introducing a displacement in the mooring system to represent the floater motion. However, due to the increased force in the mooring lines (due to the high wind load) compared to the weight of the floater, a coupled analysis, in which both items are joined in one system, is preferable. To do this, numerical models need to be made to represent the FOWT as a whole, and these have to be calibrated and tested. This has thus been the focus of much previous research into FOWTs.

Past research has focused on calibration and validation of the numerical models and in some a peculiarity has emerged. One prominent piece of research which showed this has been the OC5 project (Robertson, 2017), which aimed to compare numerous numerical models to an experimental data set of the same model. It shows a discrepancy in force between the numerical model and the experiments used to validate them in the lower frequencies. This will be expanded upon in the literature review, but in the OC5 project all the numerical models participating showed an underprediction of the mooring line force compared to the experimental model, which poses obvious problems to be solved. The mooring line force spectra in figure 3 shows this with the black experimental line being more than twofold above even the highest coloured numerical line in the lower frequency peak at 0.01 Hz. Furthermore, the OC5 project showed a need for a good reliability analysis in the experimental data.

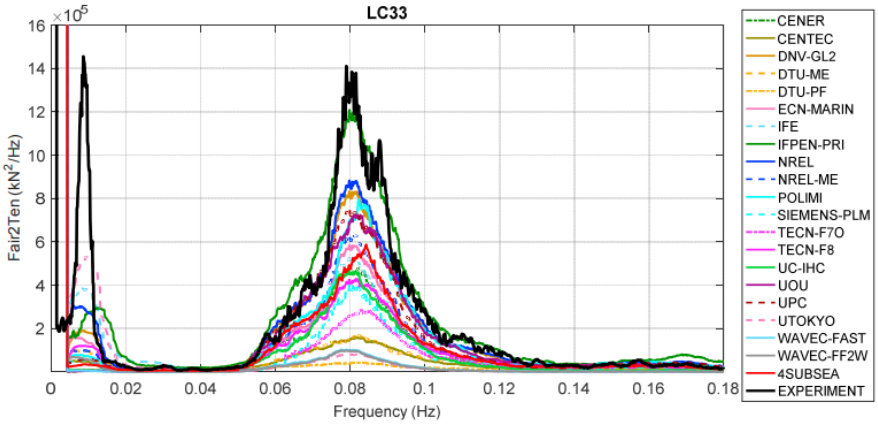

Figure 3: OC5 spectra of mooring line force for the black experiment line obtained by MARIN and the other coloured lines, representing numerical results. (Robertson, 2017)

From this project (more on it in the literature review) an incentive for new research, which builds upon the OC5 project, can be gathered with a few demands:

- Physical tests aimed at a low frequency excitation to validate the large response in the mooring line force, as there seems to be a lack of validation data available compared to the numerical models.
- Accuracy in the measurement in order to get a good representation of what the actual response is.
- Good estimates on the uncertainty in the data.
- A qualitative understanding of what is happening to cause this low frequency response but also the generation of a good quantitative dataset for future numerical research.
- Different test cases with different systems and loads, to better establish the effect of the mooring system.
- Usage of the same FOWT model as the OC5 project, to get a measure of compatibility.

Complying with these demands would allow for a good body of experimental research which can both be used to get a better understanding of the physics of FOWTs but also serve as the basis to help calibrate and validate numerical models, potentially resolving the issues found in the OC5 project.

The demands lead to the research question:

> *What is the low frequency response in the mooring system and the floater motions during the physical test with a scale model floating offshore wind turbine under wind and wave loading?*

This question can be split in a few sub questions to make the subject more approachable. As this research was the first research done with a physical model of a FOWT at the towing tank of the TU Delft, part of the thesis focuses on setting up the experiments.

> *What relevant loading processes can be expected on the FOWT, in what amplitude and which frequency?*
>
> *What physical aspects of the FOWT need to be taken into account?*
>
> *How can these forces, specifically the low frequency ones, and aspects of the FOWT be properly modelled in scale tests?*
>
> *What forces are found in the mooring system and what magnitude are these forces?*
>
> *What movement is to be observed in the floater?*
>
> *What is the influence of the eigenfrequency and load frequency on the response, specifically in the lower ranges?*

The build-up of these sub questions will be reflected in the chapters of the thesis. All questions will be answered in the conclusion specifically. Answering all sub questions will then allow the answering of the main research question of this thesis.

Again, briefly stated: The goal of this thesis is to gain more knowledge into the physics of low frequency wave excitation on FOWTs, specifically looking at the wave difference frequencies. A secondary goal is to generate more data for the calibration and validation of numerical models.

1.3 Approach and scope

The methods used to answer the research question within the limits of the scope is stated.

To start off, an in-depth review of the literature is needed to see what other papers found and if these results match the OC5 project. To do this past experimental research will be examined to look for the same low frequency discrepancy. The OC5 project will be reviewed more in depth as to look for more relevant factors in the research. A good look at the mooring lines is also needed to get a better understanding of their features and design.

With this knowledge the design of the tests can commence. The most important aspect are the forcing conditions as these determine the eventual frequency response of the system, a crucial aspect of the research question. A method to focus on the low frequencies will be examined as it is more efficient than doing irregular tests focused on a broad spectrum. An experimental set up which avoids the need for a cable bundle, which was an issue during the OC5 project, needs to be designed, affecting the measuring devices and the wind forcing. To enable the uncertainty analysis, multiple mooring systems and repeat tests need to be done to ensure adequate data. Repeatability and good knowledge of the model parameters are key factors in this.

The test data will be verified to ensure the proper forcing was applied during all different tests and all model parameters are correctly applied to the actual model. All peculiarities noticed during the tests are examined.

After the tests are done the test data can then be filtered and analysed. As with the OC5 project spectral analysis will play a key part here. A causal path needs to be established to examine the origin of the model response. Only when the origin is sufficiently determined can the low frequency response be properly examined. As mentioned before an uncertainty assessment will be done with the data. The results will then be discussed and placed in the context of the literature review.

After all that a conclusion to this research will be presented in which the general flow of the research is repeated, and the more important points highlighted. This conclusion also gives recommendations for future research.

2 Literature review

This chapter aims to give a brief overview of the previous research into FOWTs as it applies to the research question, so consisting mostly of experimental research in addition to mooring lines. Two literature reviews, namely from Dong et al. (2022) and Lei et al. (2022) provide additional insight, also in numerical models.

Through time a few different concepts for FOWTs floater concepts have appeared each with their own advantages and disadvantages. Many of these designs have their origin in the offshore oil and gas industry. The designs are shown in the figure 4 below:

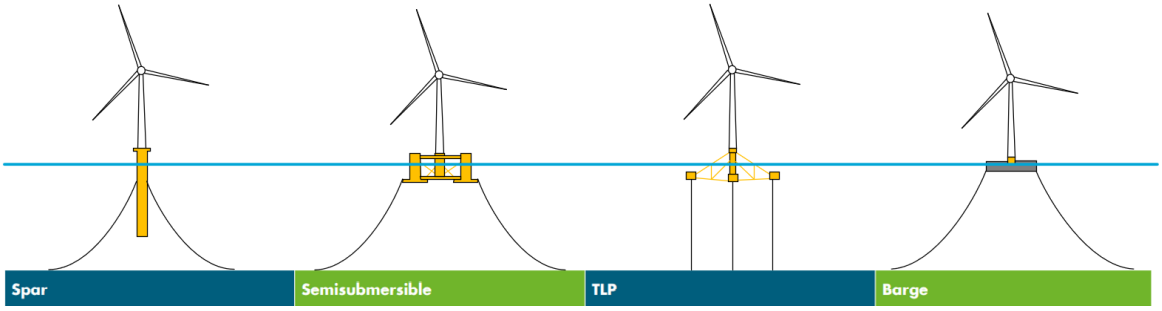

Figure 4: Different FOWT floater concept types

As the drawings above show there are four main concepts. These are discussed below per type, partially based on (GWEC, 2022):

- The spar type consists of a single column with ballast at the bottom to keep it upright. It is quite stable in rougher sea states and is relatively simple to build. Its main issues are the complex installation and the requirement of a large depth at the installed site. It also has the drawback of not being able to be taken back in port. This design was the most popular in the earlier days of FOWT design and the commercial Hywind FOWT uses spar type floaters.
- The semi-submersible, a platform consisting of a few interconnected ballasted columns, seems to be gaining in popularity at the moment to be the leading type in FOWT design. This is because it alleviates some of the negatives of the spar type. It is easier to install and doesn't have a large depth requirement due to the shallow design. Furthermore, the semi-sub design often has heave plates to reduce heave motion. The drawback in this design is the complex construction requiring a large drydock and more skilled labour.
- The TLP design uses a relatively buoyant floater which is tied down to the anchors in the seabed creating a tensioned leg system. This has the distinct advantage of having a very small mooring footprint compared to other designs, whilst retaining high stability. It also requires relatively few materials to build the platform as it does not need ballast. The downside of this system is the complex anchoring system, which has a very high load and thus requires a very good anchor. It also poses several operational risks and is all in all quite expensive.
- The barge design is a bit more obscure, but it finds its theoretical application mainly in calmer waters such as lakes. This is because of its high susceptibility to waves, making for a more unstable design. The advantage of this design is the ease of its construction and installation. Its low draft making it further suitable for lakes.

2.1 FOWT concept and early numerical models

Only a year after the first bottom founded offshore wind park was built in 1992 in Denmark (EESI, 2010), Tong and Cannell (1993) proposed the concept of floating offshore wind. Their floater took the shape of a SPAR design.

In 1994 Bertacchi et al. (1994) proposed a TLP design and did experimental model tests with this design. The tests were done using a JONSWAP wave spectrum and found that the platform mostly responded to the wave frequencies. Additional responses were also found at the higher natural frequencies.

And although FOWTs are relatively new, the floater designs are not, the oil and gas industry has had many years of experience designing and operating these floaters. Although a large difference being the balance between the forces (Jonkman, 2007). As FOWTs are considerable lighter than oil and gas platforms but quite literally build to catch wind, the wind force is relatively much larger than the weight. This has obvious impacts on the mooring system which is thus the main focus of research into floating offshore wind turbines (Bashetty, 2021).

Numerical models for FOWTs were also developed for this research purpose. Early models focused on creating a hydrodynamic simulation capability and coupling these with existing structural and aerodynamic models from bottom founded wind turbines (Jonkman, 2007). These models are then called aero-hydro-servo-elastic models. An overview of the different aspects of a FOWT numerical model is shown below. As can be seen there are a number of different dynamic elements working together, as this is a coupled analysis, seen by the interaction in platform and mooring dynamics. The main structural model (here called the FAST & ADAMS model) takes care of the structural element by taking everything from the mooring dynamics to the control system. Then different smaller forcing models like HydroDyn used here are added for the loading processes.

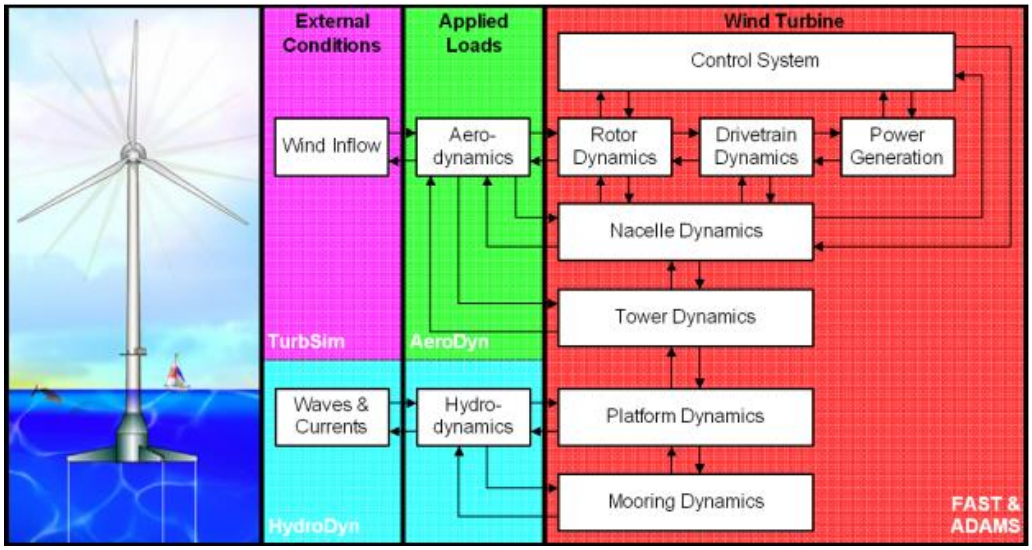

Figure 5: The schematic of the FAST & ADAMS numerical model of a FOWT, taken from (Jonkman, 2007)

Nowadays many different numerical models for FOWTs exist, one only has to look at the OC5 project (Robertson, 2017) to get a good overview of some of the main ones. Most modern models are dynamic but there are a few quasi-static models which also participated in the OC5 project. As this thesis does not do a comparison with a numerical model, the individual models will not be examined. For more research into the models, it is advised to look into the OC5 project and its participants.

2.2 OC3-6

The OC3-6 research is a large project that aimed to compare different numerical models. OC5 included experimental modelling in this and the questions stemming from that research form the basis of the research in this thesis.

The OC3 (Offshore Code Comparison Collaboration) (NREL, 2010) project was started by the national renewable energy laboratory of the United States government in order to discuss and develop modelling strategies for both bottom founded and floating offshore wind turbines. The difference between this project and earlier projects with this objective was in the scale and number of participants. Because of the worldwide participation with this project most of the aero-hydro-servo-elastic models for wind turbines were tested and compared in this project.

The OC4 project (NREL, 2014) continued (the 4th C) the OC3 project, again looking at the models for floating wind turbines. Three different designs were used, a SPAR buoy, a TLP and a semi-submersible type floater. Participants again made numerical simulations that were compared to each other. Although provisions were made to model the semi-submersible design in wave tanks the main focus of OC4 was again a comparison between different tools. The results of OC4 will be discussed together with the OC5 project as that way they can then be compared directly to the experimental results.

The objective of the OC5 project (Robertson, 2017) was to see if the numerical results were comparable with experimental research. This is where the fifth C comes in, correlation. The goal thus being a validation of the numerical tools available, and improvement where needed. The numerical tools to be examined were the ones from OC4 and the model used was the semi sub design from OC4 as well.

As a response to the findings of the OC5 project the OC6 project (Wang & Robertson, 2021) was started and is as of writing still ongoing. This project focusses on the unCertainty aspect (the 6th C). To do this the project zooms in on the hydrodynamic properties of the semi-submersible by using CFD modelling and simpler bi-chromatic waves.

The OC3 project used the Hywind project, a SPAR type as the base to model with the different numerical tools. Seven different tools were used to model the motions of the wind turbine using aero, hydro, servo and structural models. These models generally gave similar results with some exception. For the purposes of this research one of the more noteworthy results were the very spread predictions for the tensions in the upwind mooring line. Figure 6 shows a RAO (response amplitude operator) of the upwind mooring line, each line representing a numerical model. As can be seen the results vary by orders of magnitudes between the different models around wave excitation frequencies. What is also notable is the difference in prediction in the lower frequency band. Here the models “only” vary by a factor two. As can be seen the models not only have different maximums but these are also located at different locations, although all models show a peak at the lowest frequency.

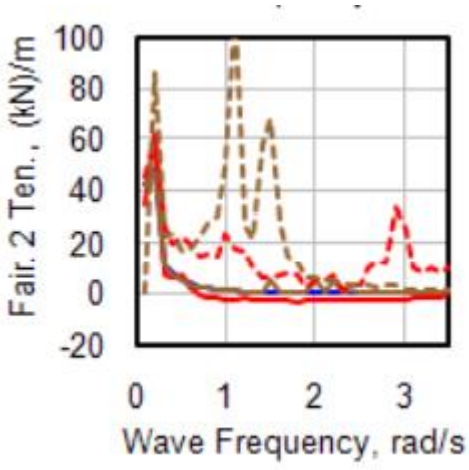

Figure 6: Graph of the mooring line force, taken from (NREL, 2010)

The model tests for the OC5 project (in order to validate the OC4 numerical results) were done at MARIN. The tests were full systems with both a wave tank deep enough for full mooring lines and a wind generator to simulate wind load. Two iterations of the model were made as the wind turbine performance of the first model did not match that of the real system. Both models were Froude scaled 1:50 for the hydraulic part, but they differed in their scaling of the wind turbine with the second wind turbine being scaled to take the low Reynolds number environment into account. The towers were scaled to match the real sized eigenfrequencies in both cases. Research continued with the second iteration.

Figure 7: An image of the tested FOWT in the MARIN basin, note the large data cable bundle, taken from (Robertson, 2017)

Comparison between the experimental results and the numerical ones led to a number of findings, the main one being that there is a discrepancy between the numerical prediction of the mooring line forces and the experimental findings, especially at the lower frequencies. The difference is clearly shown in figure 7 below. The black line indicates the experimental results while the other lines indicate the numerical simulations. Around 0.01 Hz the difference has more than a factor of two at best. The predictive value at the wave frequency around 0.08 Hz is better than that of the lower frequency but still shows an underprediction. The load case 33 is an irregular JONSWAP pattern with a T_p of 12.1 seconds.

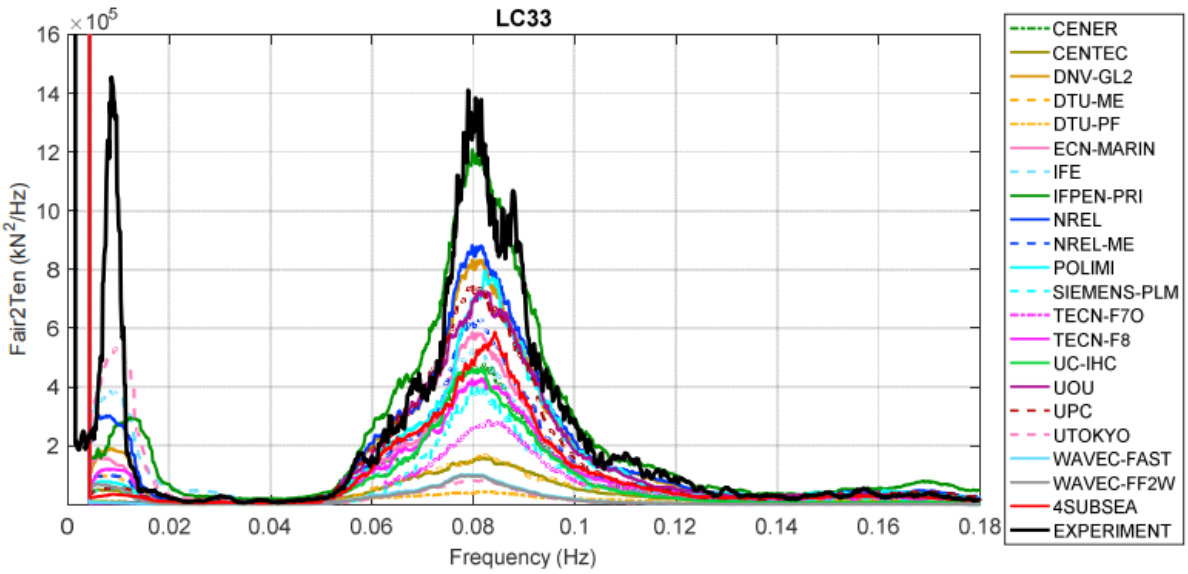

Figure 8: PSD of the mooring line force, taken from (Robertson, 2017)

Figure 9 shows the ultimate and fatigue load (page 48 of the OC5 project for the precise calculation (Robertson, 2017)) per participant relative to the experimental result. The blue colour indicates the dynamic models, and the pink colour indicates quasi-static models. As mentioned earlier, these latter ones tend to give lesser results. The obvious issue is that a consistent underprediction of the mooring

line force in (almost) all numerical models means that in design mooring lines will be made too weak which would lead to failure.

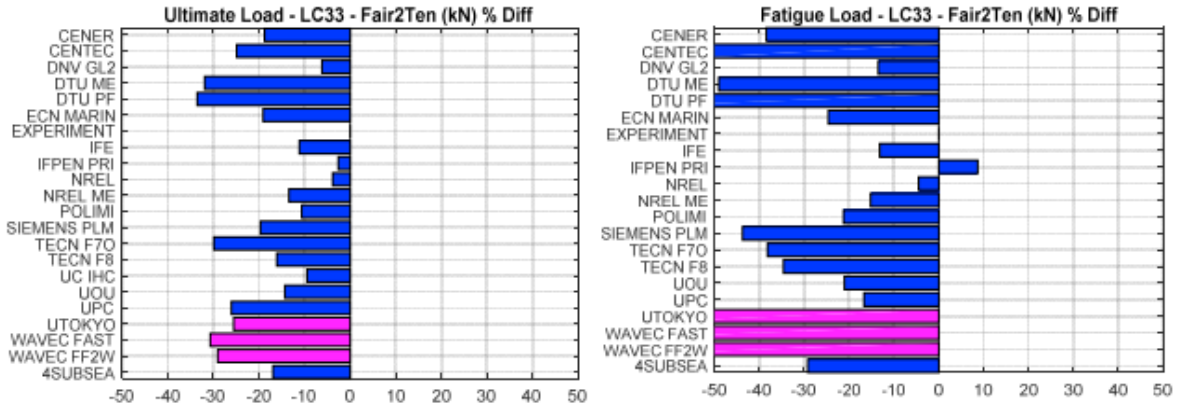

Figure 9: A bar graph of the percentage difference of individual numerical models relative to the experiment, taken from (Robertson, 2017)

It was also noted that during some more extreme testing scenarios the mooring lines would go slack and then re-tension themselves. This also leads to large forces in the mooring lines and should of course be avoided.

Robertson (2017) notes, however, that to determine the reasons for this difference with certainty more research is needed as an uncertainty assessment is not possible due to the limited data. This limited data is due to the limited test campaign and needs to be addressed in future research. It was also noted that the cable bundle from the sensor leading off the model could impact the stiffness of the model. A further note is that differences between aerodynamic models were masked by the difference in the hydrodynamic models and that tower and nacelle drag were not important.

To solve the uncertainty issue the OC6 project started the use of CFD modelling. As the bichromatic waves are simpler and the CFD modelling can be done with more insight into what actually goes on an uncertainty assessment can be made. These CFD models were then validated with new experimental research, where the model was simplified. The model was tested without wind and mooring lines, opting instead to hold the model at a fixed location with a force meter attached. In general, a good correspondence between the CFD modelling and the physical experiments was found, which showed that the CFD models can be used to fine-tune the numerical tools.

With the new knowledge around CFD modelling, the numerical models are being improved in for example (Wang & Robertson, 2022a) and (Wang & Robertson, 2022b). These were then generally in very good correspondence with the experimental results, as can be seen in figure 10, the black line being the experiment, with the red the older model and the blue the new model. The bar graph also shows that the new model is much closer than the older model. It was also found that the general underprediction in the OC5 project was partly caused by a discrepency in the incident waves between experimental and numerical tests. And especially during extreme wave events large discrepencies remain.

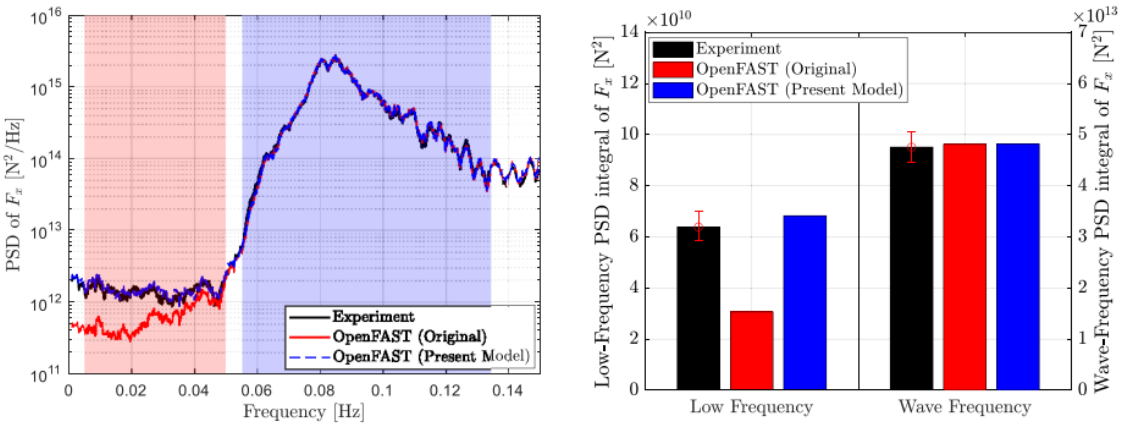

Figure 10: Graph and bar plot showing a comparison of the mooring line forces for both the older and the improved numerical model FAST, taken from (Wang & Robertson, 2022)

2.2 Experimental research

As mentioned before many numerical models for FOWTs are made, these have to be validated using experimental tests. This section highlights a few findings from these experiments, also focussing on relevant research to the research question posed in this thesis.

The introduction discussed the four main types of floater concepts. Of these, the barge type is not often tested as research mainly focusses on sea conditions for which the barge is not very suitable. The most popular of the three remaining types is the SPAR which also has the first commercial application.

Hong et al. (2015) tested a SPAR type design which was simplified in order to aid in numerical modelling. The scale used was 1:100 and the model featured regular waves, but no wind force. The mooring lines were taut but used an extra spring to simulate elasticity. It was found that nacelle displacement, pitch motion and mooring line force increased as the wave frequency came closer to the respective natural frequencies. The numerical model followed the experimental data very well.

Duan et al. (2016) tested a 1:50 Froude scaled SPAR type design with a wind generator set up for wind simulation in order to aid with the validation of numerical models. It tested an irregular JONSWAP spectrum and found again a strong influence of the surge natural frequency on the mooring line force, due to resonance.

Utsunomiya (2017) aims to compare experimental data with a numerical model of a SPAR type design. For this he used an existing SPAR 2 MW design in Nagasaki, Japan and compared its natural period with that of the numerical model of the same design. It was found that in general the numerical model had good correspondence with the existing model, with the exception of the surge natural frequency which was significantly underestimated by 10%. The suspected reason for the surge discrepancy is a mismatch between the numerical and experimental model when it comes to the mooring installation.

Fowler et al. (2017) describes the development of a 1:52 semi-submersible design and a comparison to some other data sources, including a numerical model. The semi-submersible design is based on the VolturnUS design and uses full wind simulation with a wind generator. Different types of waves were tested including a JONSWAP spectrum. It was generally found that the model produced the same results as the target data. Low frequency data however is not compared.

Krishnan et al. (2017) looks at a vertical axis FOWT semi-sub design and aims to compare experimental free decay results with CFD modelling. The FOWT is scaled at 1:75 and is not moored as this is a free decay test. A regular wave test is also done. The CFD model finds good correspondence with the experimental free decay tests and the wave tests find the pitch, heave and roll responses the strongest around the respective natural frequencies.

Caillé (2017) tests a TLP design and compares this design with a numerical model. The experimental tests were done at MARIN with a full wind simulation and were compared to a few numerical models. It was found that the numerical models after some tuning represented the experimental results well, including in the lower frequencies. It should, however, be noted that the lower frequency response in TLP designs is dominated by the pitch frequency and not the surge frequency.

Naqvi (2012) tested both a TLP and a SPAR type experimentally to look at the gyroscopic effects of the wind turbine. The experiments used irregular waves and a sheet to catch wind with a (non)rotating mass with a wind generator for wind and rotor simulation. It was found that the gyroscopic effects of the rotor changed little in the results. It further showed a dominance of the surge response.

In (Tomasicchio, 2017) a SPAR type is tested and as with the OC5 project the paper found a large discrepancy in the mooring line tension as seen in figure 11. In this figure a power density spectrum for the mooring line force is given. The blue line represents a numerical model using a static mooring simulation and overpredicts the low frequency force, whilst the red line represents a numerical model which uses a dynamic mooring simulation and underpredicts the force compared to the black experimental line. It should be noted that in this particular case the under and overprediction of the force do not really impact the maximum force on the mooring line as this is located at the wave frequency. From this it follows that the ratio of the surge frequency response at around 0.01 Hz and wave frequency response at around 0.1 Hz is an important aspect in this issue.

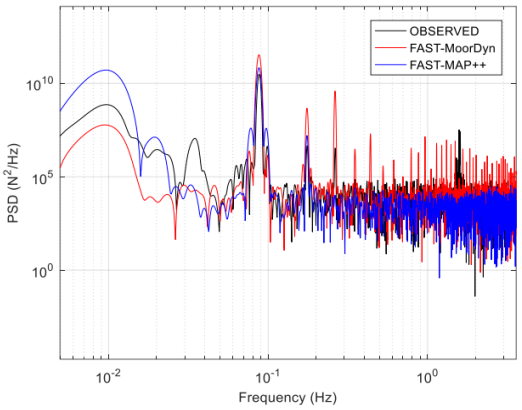

Figure 11: PSD of the leading mooring line force, taken from (Tomasicchio, 2017)

One paper that did find a good correspondence at the lower frequency between the experimental and numerical model was Karimirad et al. (2017). It tests a semi-submersible design against a few different variations of a numerical model. The wind in this research was simulated with the use of a hybrid method. With this method the FOWT model has a few rotors at the location of the nacelle powered by electric motors. The rate at which these spin and thus the force they deliver is determined by the pitch and surge, thus simulation drag on the rotor blades. This is in contrast to the earlier mentioned research which either uses a wind generator and passive rotor blades or do not simulate wind at all. Figure 12, which again shows a power density spectrum of the mooring line force, shows that the lines representing the different data sets overlap with a small exception around the peak were the red experimental line is

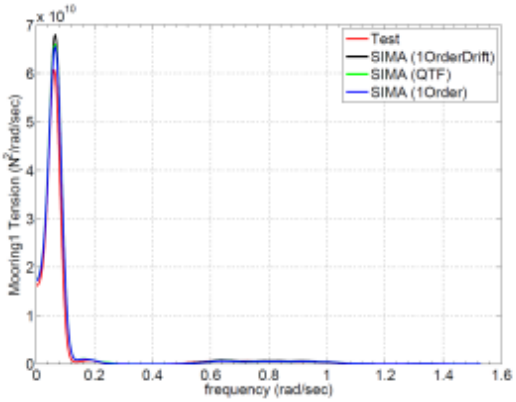

Figure 12: PSD of the leading mooring line force taken from (Karimirad, et al., 2017)

slightly lower. What also stands out is the very large peak at the determined surge natural frequency at around 0.04 rad/s compared to the wave frequency at 0.6 to 1 rad/s. The ratio of this peak over the wave frequency peak is enormous compared to the OC5 project in figure 3.

Yan et al. (2021) propose a new method for the estimation of damping in mooring lines. This is done by splitting the line in segments and estimating the fluid drag on each part. This is then integrated to get the damping in the entire line. An experimental comparison shows that this method is feasible to estimate mooring line damping.

2.4 Mooring lines

Below a few papers on the design and calculation of mooring lines are covered. These will provide some knowledge on the mooring lines of FOWTs but might also be applicable to other floating offshore structures.

As previously mentioned, there are both dynamic and quasi-static models for the mooring analysis. Research by Guo (2017) goes into the dynamic mooring system and compares it with the quasi-static results. He finds a large increase in the top tension when using a dynamic model. This again corresponds with the findings in the OC5 project where quasi-static models were found to underpredict the mooring line tensions more than dynamic models, although with a lesser degree than Guo found.

Although not specifically focused on FOWTs, Ma et al. (2018) provides a good basis for offshore mooring design. Specifically, chapters 4 and 5 go into the important aspects that make up the design and calculation of a mooring system.

In (Trubat, 2020) an approach to the discrepancy issue from OC5 is examined by looking at the wave forces on the mooring lines themselves. This results in a slight improvement of the prediction of the numerical models but the gap between the numerical and experimental research remains. Meaning this is probably not the fundamental issue.

Carlos (2020) does a sensitivity analysis on mooring line modelling. This is done by comparing the results of different numerical models to each other. He finds that a relatively low inaccuracy in parameters can lead to large changes in the mooring forces. This emphasizes the importance of accurate parameters that was also found as a result of the OC5 project. This paper also shows the same large difference between quasi-static and dynamic models as Guo did earlier.

2.5 linear wave theory

As waves will be the main way to excite the model, a quick dive into linear wave theory is in order. Linear wave theory is based on the mass and momentum balance equations. Combined with the assumption of irrotationality this leads to the Bernoulli equation. Non-linear terms can then be removed by assuming a small wave height compared to both the depth and the wavelength. Combining the equations then leads to the orbital velocity equations:

$$\phi = \hat{\phi}(z)\cos(\omega t - kx) \text{ where } \hat{\phi}(z) = \frac{\omega a}{k}\frac{\cosh(k(d+z)}{\sinh(kd)} \quad (1)$$

Particularly relevant for this research is the fact that this allows a standard to be set for deep water, namely when k*d >> 1, or in more practical terms, when d>0.5*L. This then replaces the hyperbolic functions with e^{kz}. From this the speed of the wave(group) can be calculated using the dynamic boundary, thus, in deep water: $c = g * \frac{T}{2\pi}$ and $c_g = \frac{1}{2} * c$.

Wave loads are another aspect that can be glanced from linear wave theory and also important in this context. The Morrison equation is often applied to slender cylinders and consists of an inertia and a drag term to express the force on the cylinder. These terms require knowledge of the acceleration and the velocity, both difficult to measure directly in this context. However qualitatively it can be said that this first order wave load, because of the velocities involved be focussed around the wave frequency as here the velocity is present. A second order force occurs due to the difference between the affected area of the structure during waves. The wave impacts the structure the forward moving particles will have a larger are to affect (as the wave is higher) than the other way around, thus inducing a net (constant) force.

Besides the wave frequency, loads occur when the frequencies of two or more waves interact at the sum and (the focus of this research) difference frequencies. When two waves have an unequal frequency the difference between the two becomes an additional excitation. The difference frequencies can excite the low frequency surge motion of a floating structure slowly varying the previously mentioned second order force due to constructive and destructive interference. This effect is exactly what this thesis is after and will be used all throughout. These forces are called wave drift forces due to the fact that they do not have a zero mean and thus tend to move the floating structure in the propagation direction.

2.6 Spectral analyses

This section will explain the process of turning the time series into a spectral series. This will be used later in the data analysis part.

The main purpose of a spectral analysis is to convert a dataset from the time domain to the frequency domain. This is done via the application of a Fourier transformation and allows the observation of individual periodic components, which allows the separation of low frequency and wave frequency effects. The Fourier transform circles the time series in on itself at different frequencies. The frequency domain can then be found by looking at the distance of the centre of mass of this circled time series from the origin. A great visual representation of this can be found at (Sanderson, 2018).

The actual calculation of the Fourier transform is done by taking the infinite integral of the multiplication of the time series with the complex exponent, shown below.

$$\hat{x}(f) = \int_{-\infty}^{\infty} x(t) * e^{-i2\pi ft}\, dt \tag{2}$$

This Fourier transform then gives the frequency components of the time series which are then transformed into a power spectral density via the formula below. Note that T here is the period and not time.

$$S(f) = \lim_{T\to\infty} \frac{1}{T} |\hat{x}(f)|^2 \tag{3}$$

In general, the power spectrum density (PSD) is well suited for long continuous signals. It also removes negative and non-real elements, making it easier to understand. For this reason, it is used for the data analysis in this document.

3 Model and test design

This chapter, the first of the three main parts, explains the design of the experiment. The general design is meant to approach the OC5 experimental design within the scope and approach of this thesis. It is divided into a few subchapters each covering a part of the design.

3.1 The OC5 model and scaling

The floater design is based on the OC5 floater and called the DeepC model. The important parameters of this model are shown in the table below.

Table 1: parameters of the full scale OC5 model

parameter	value	unit	parameter	value	unit
mass	1.40*10^7	kg	yaw inertia	1.37*10^10	kgm2
draft	20	m	hub height	90	m
Centre of Mass above base	12	m	water depth	200	m
			pretension	1.11E6	N
pitch inertia	1.56*10^10	kgm2	stiffness	46200	N/m
roll inertia	1.39*10^10	kgm2	mean wind thrust	719000	N

The DeepC model is a semi-submersible design with three outer columns and one inner column, which supports the wind turbine. The three outer columns have heave plates, and these heave plates provide the connection points for the mooring lines. The three outer columns are connected to each other and the inner column with rods at the top and bottom and three inclined rods towards the inner columns provide shear resistance. A photograph of the model is shown in figure 13. Apart from the scale, the above-mentioned parameters remain very similar, specifications for the floater are given in this subchapter nonetheless. The mooring system is very different however and will be explained in the next subchapter. A larger scale technical drawing can be found in the appendix A.

The OC5 project had a Froude scale of 1:50, with the very deep MARIN basin this enabled the project to have a mooring system of a depth of 200 m at full scale. These tests will be performed at the 3mE towing tank number 2, which has a maximum depth of 1.25 m (see next section). With the lower tank depth during this project, the increased amount of blockage and the relative shallowness of the mooring system a 1:50 scale was not deemed suited to this tank, furthermore, a 1:50 would not allow for the rear mooring lines to be fully placed as the tank width would have become limiting. The scale was thus increased to 1:96 to take account of the tank dimension but also the construction method of the floater. Besides the model the wind force applied, taken from the mean thrust of the OC5 project, is also scaled to 1:96 and comes to 0.81 N.

The model is constructed using PVC piping which eases the creation of the round pieces for the columns and heave plates. The PVC piping was available in the 125 mm and 250 mm sizes, which allowed for a 1:96 scale in the high columns and the heave plates respectively. The middle column is then build using a 63 mm pipe, which is 0.5 mm more than needed for a 1:96 scale of the DeepC model, so no significant effect is to be expected. The tower and nacelle simulated via a 2 m vertical rod installed in the central columns, made from carbon fibre, with added weight.

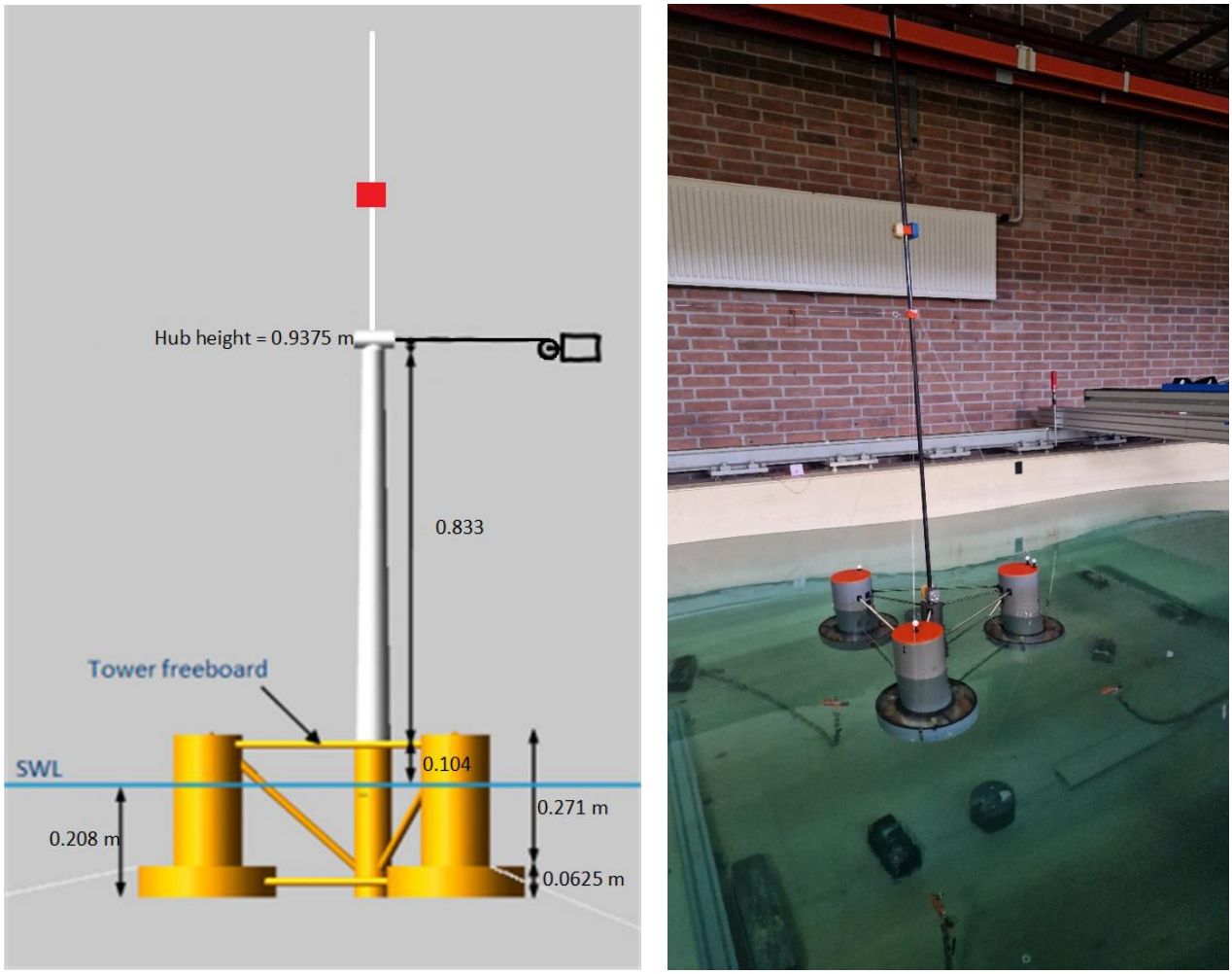

Figure 13: Schematic and photograph of the DeepC model, schematic adjusted from (Robertson, 2017)

The properties of the model are displayed in table 2. These concern the properties of the model as measured after testing was completed.

Table 2: properties of the DeepC model at 1:96 scale as measured after testing.

property	tested	goal	unit	relative difference [%]
mass	15.81	15.77	kg	0.25
yy – mass moment of inertia (pitch)	1.80	1.907	kgm^2	-5.94
xx – mass moment of inertia (roll)	1.78	1.710	kgm^2	3.93
zz – mass moment of inertia (yaw)	1.22	1.679	kgm^2	-37.6
centre of gravity height w.r.t. the bottom	125	124	mm	0.80
draft without mooring lines	208	208	mm	0

3.2 Testing layout

The experiments were performed in the small towing tank of the 3mE faculty in the TU Delft (TU Delft, 2022). This tank and its features supplied key input parameters in the design of the tests. For example, the lower depth and width compared to the OC5 project meant an adjustment of the scale from 1:50 to 1:96. These features and their effect on the design will be explained in this section.

The 3mE Ship Hydromechanics lab has two tanks, the experiments were to be performed in tank number 2. This tank is the smaller of the two which brings a few practical advantages to this research. These include easier switching of mooring systems, as multiple systems need to be tested and the presence of an advanced camera tracking system. The general dimensions of the tank are shown in figure 14. As can be seen, the tank has a length of 85 m, a width of 2.75 m and for these experiments has a depth of 1.25 m. The model is located 28.8 m away from the wave maker, as can be seen in figure 14.

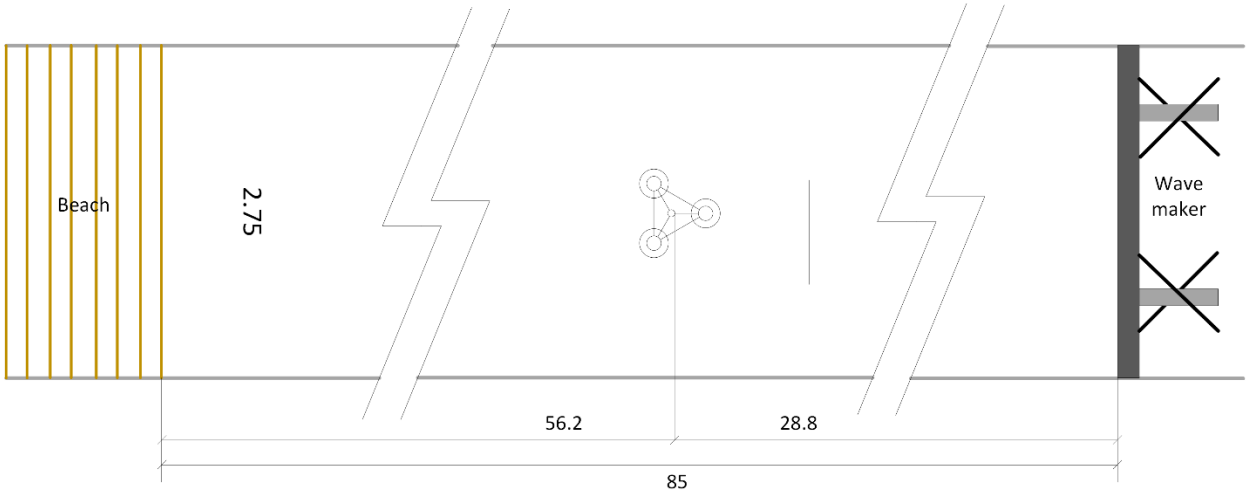

Figure 14: Map of the towing tank number 2 with the distances between key locations, dimensions in meters

For wave generation a wave maker operating in piston mode was present at one end and for wave damping a beach on the other. The wave maker was hydraulically operated and steered via an electronic signal in from a steering file on a computer. Data on the position of the wave maker was recorded. The beach consisted of ribs made with wooden beams attached at an angle. Pictures of the wave maker and the beach are displayed in figures 15 and 16 respectively.

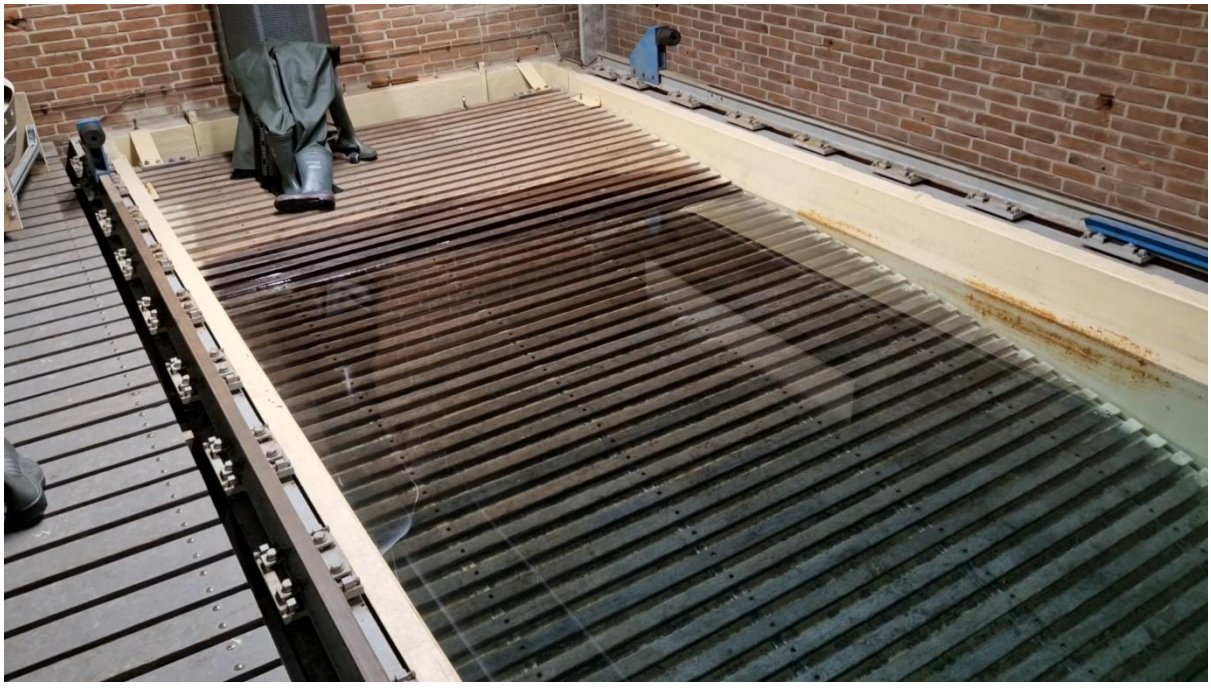

Figure 15: Wave damping beach of towing tank number 2.

Figure 16: Wave maker of towing tank number 2 in piston configuration

Another added benefit of this tank is the presence of windows in the wall at the location of model shown on the tank map in figure 14. These windows allowed for easy observation of the model and mooring lines. As one of the goals of this research was a better understanding of the behaviour of mooring lines, optical access was deemed very beneficial. The model was thus at a distance of 28.8 m from the wave maker. Besides the model, four wave gauges were also present (indicated by the upside-down extended triangles) as was a device for simulating the wind force. Figure 17 shows the distances of the different elements from each other. Note that during wave tests without the model present, the fourth wave gauge was present at the location of the model, this was then moved to the lead anchor point during model tests. Also note that the lead mooring line is mooring line number 2.

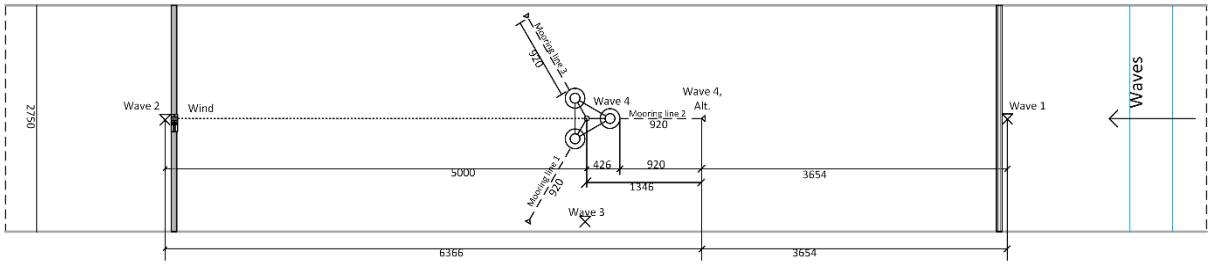

Figure 17: top view of the total tank and the area around the model, dimensions in millimetres

3.3 Mooring lines

The focus of this research is on the mooring lines and their interaction with the FOWT. Thus, the design of the mooring lines will be described in this section. Limitations in the depth required a different design compared to the OC5 experiment. The setup in the tank is also touched upon as it follows from the mooring line design.

The depth of the tank means that it is not possible to emulate the chain of the OC5 project as the full-scale depth is 118 m versus 200 m. To keep the results comparable to the best degree possible and dynamically similar, the mooring system was still designed with the intention of having the same surge natural period of 107 s (Robertson, 2017), which at this scale translated to 10.9 s. To reduce weight

on the model and prevent the chains from pulling the floater down too much a fibre rope (Dyneema) upper part was introduced, which lead to considerable weight savings.

This hybrid system made it difficult to calculate the mooring line analytically, leading to an iterative design. The calculations were done by combining the analytical design of a catenary system (Schreier, 2022), the formulas for this are shown below, with a reduction in height and offset based on the taut part of the mooring system. The angle was calculated by taking the angle of the horizontal force (this was an applied parameter, based on the OC5 pretension with deviation) and the vertical force.

$$F_z = sinh\left(\text{acos}\, h\left(\frac{hw}{F_x} + 1\right)\right) \tag{4}$$

$$\alpha = \text{atan}\left(\frac{F_x}{F_z}\right) \tag{5}$$

In these equations *Fz* is the vertical force, *Fx* the horizontal, *h* the height of the catenary mooring line. *w* the submerged weight and *α* the angle of the taut part of the vertical.

The distance of the model was then determined by:

$$x_{\text{tot}} = S_{chain} - \frac{F_x}{w} * sinh\left(\text{acos}\, h\left(\frac{hw}{F_x} + 1\right)\right) + \text{acos}\, h\left(\frac{hw}{F_x} + 1\right) + S_{taut} * \cos\left(\alpha\right) \tag{6}$$

In which the S_{chain} and S_{taut} are input parameters for the length of the chain and fibre rope parts.

The reduction in height and offset are calculated for the fibre rope part of the mooring system and found by the use of the top angle of the chain part. By increasing the angle of the top of the catenary part compared to the vertical the reduction of the offset is increased whilst the reduction of the height is decreased. This leads to an amplification effect of the extension of the mooring line, as the floater is moved further additionally due to the change in angle whilst there is more force due to the increase in height. As it is not possible to get an analytical function for this reduction in height and offset it is necessary to introduce it in an iterative way. After three iterations the solution converged on the mooring line in figure 18, shown in a neutral stance with the pretension as determined in section 3.1.

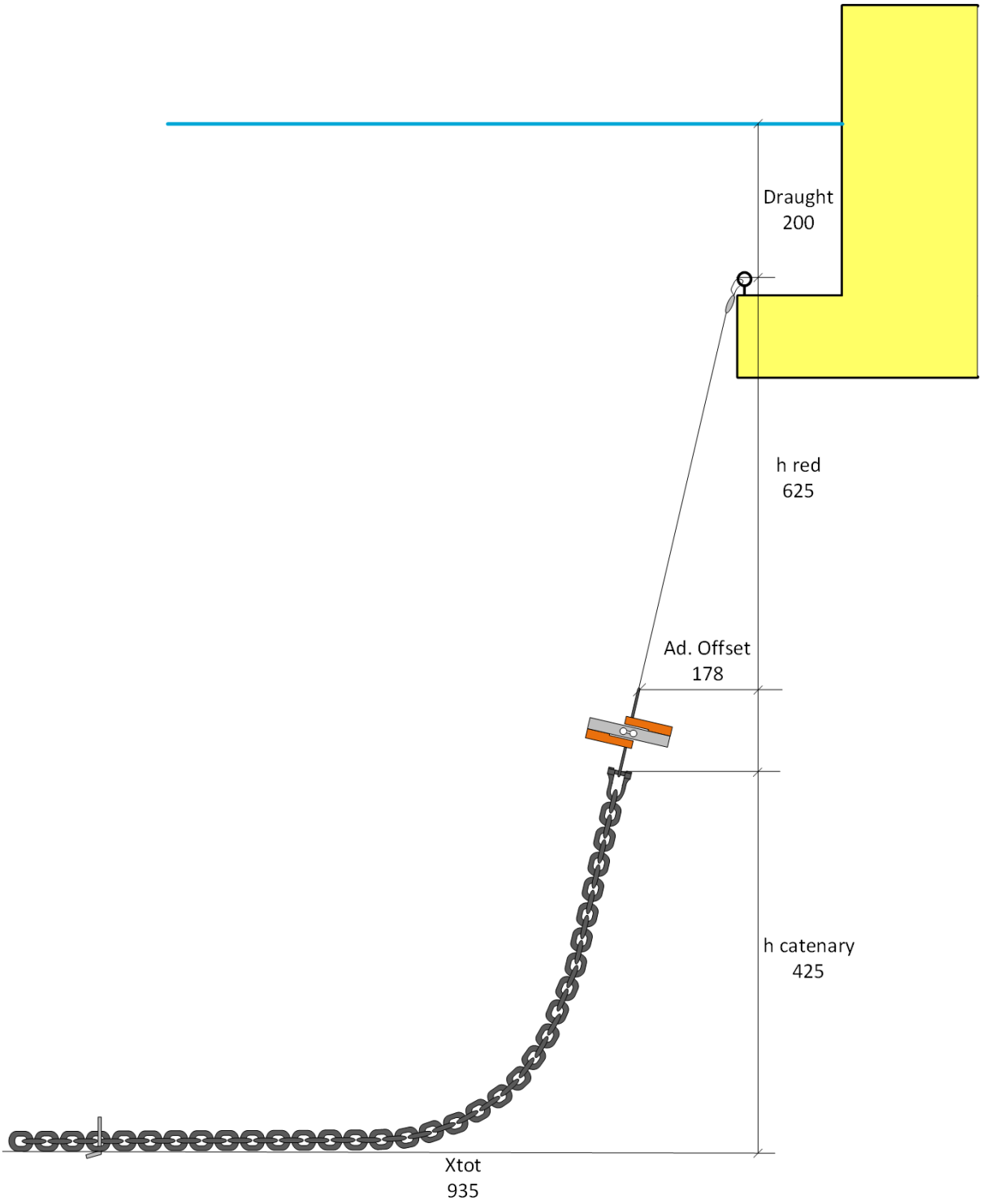

Figure 18: sketch of the mooring line in the model

As can be seen the fibre rope part of the mooring line reduces the height and the offset of the catenary part, amplifying the effects of the mooring line. The line was optimized in the length of chain and fibre rope to yield the desired stiffness of 5.01 N/m, as was found in the OC5 project. A calculation example of the third iteration is given. By taking a pretension of 1.01 N, as the OC5 project used, the top angle of the catenary part can be calculated at 1.32 rad by formula 5 using an estimated catenary height of 0.425 m, adjusted by earlier iterations. Using a fibre rope length of 0.65 m this angle gives additional offset of 0.178 m. This is then added to the offset of the catenary part to get a total offset of 0.953 m.

The earlier estimated height of the catenary part is checked by the now more accurately calculated height using the angle of the fibre rope part, the difference is negligible. The stiffness was found by imposing different forces on the mooring line and calculating its displacement using the iterative method found above. So, an additional force of 0.05 N was introduced in the system, which led to an offset of an additional 11 mm. The difference was then used to calculate the stiffness. This was repeated for -0.05 N additional force. Appendix G shows the iterative calculations to achieve the desired mooring line stiffness. The mooring line further featured a force transducer in between the chain and the fibre rope part, its data cable being weaved through the chain. This measuring device and its data cable were not considered in the design calculations.

The mooring line thus featured a 629 mm long fibre rope part at the top, connected to the heave plate via a screw eye and a hook. Then in between the fibre rope and the chain a force transducer was located weighing 64 grams and with a length of 146 mm from end to end. A coupler then connected the block with the chain, which was a DIN 766 size 5 chain. This chain weighed 0.5 kg/m above water and 0.438 kg/m underwater. This gives the 1142 mm chain used in the mooring line a weight of 532 gram above water and 500 grams under water. The mooring line has a 920 mm horizontal footprint between the anchor point and the attachment point on the model at a neutral stance. The anchor was attached at seven links down the end of the system, giving the chain between the anchor point and the force transducer a length of 1022 mm reducing the effective underwater weight to 447 grams. This mooring system will be referred to simply as mooring system 1. A second mooring system, mooring system 2, was made as well to test a second configuration with more stiffness. Mooring system 2 changes the length of the fibre rope part by inserting a plastic spool that reduces the fibre rope part length to 422 mm, thus increasing the stiffness of the mooring system. Figure 20 shows figures of both systems making clear the difference.

As the tank did not have any attachment points on the floor, it was necessary to sink a plate with attachment points to the bottom to serve as an anchor. The advantage of this approach is that it allows for the freedom to place the anchors wherever, but it does introduce some blockage on the tank as the plates were joined by beams. Figure 19 displays the bottom plates at a lower water level. A technical drawing of this lay-out is given in the tank set up section with figure 17.

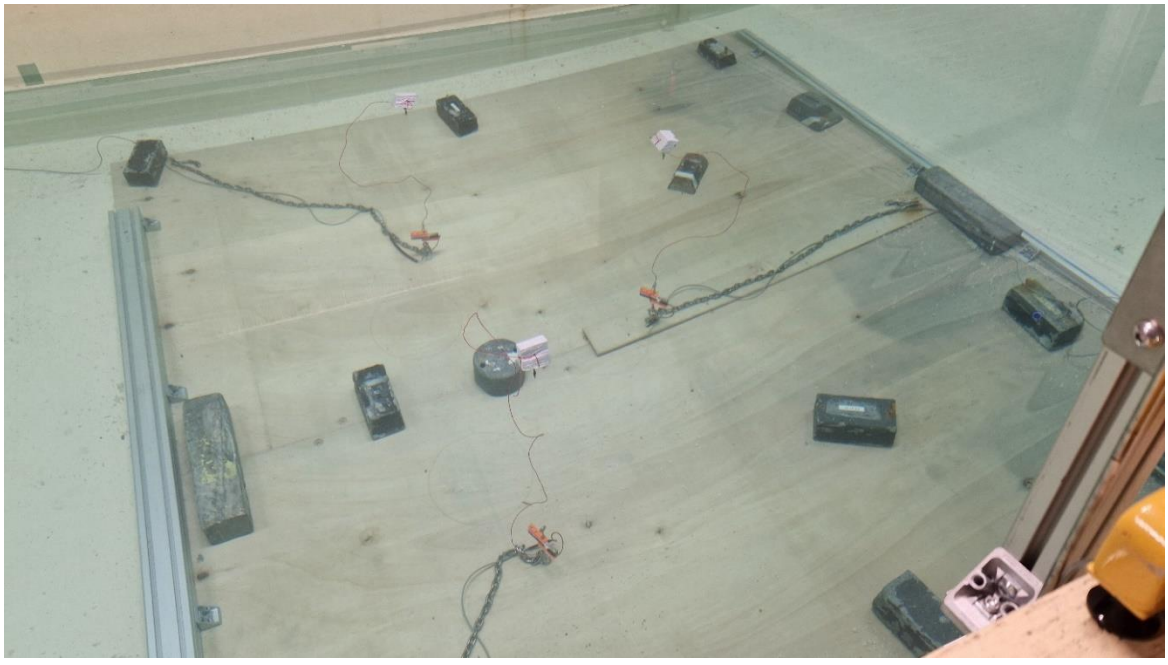

Figure 19: Picture of the bottom plate

In figure 20 a photo of mooring system 2 and a sketch of the mooring system 1 and 2 is shown. The threaded data cable mentioned earlier is visible in this photo as well.

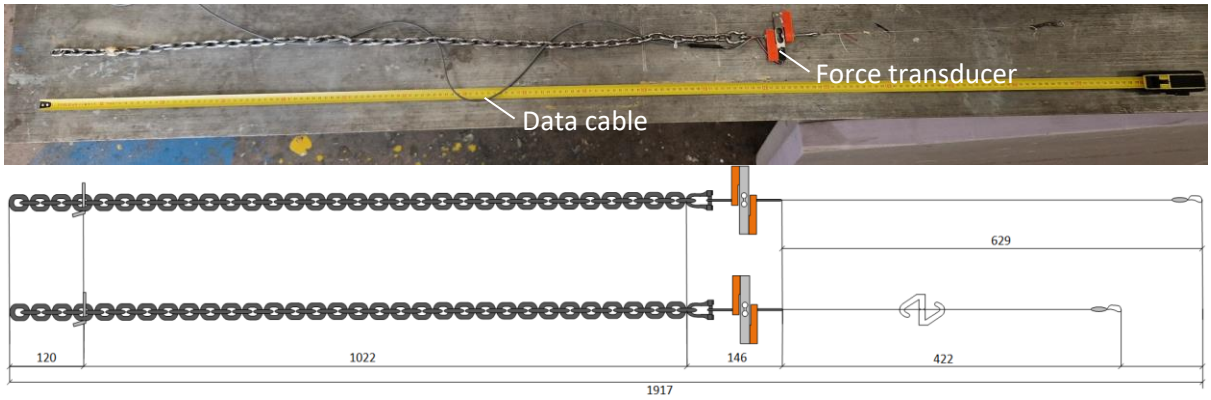

Figure 20: Photo and sketch of the mooring lines, mooring system 1 being the top sketch and mooring system 2 the lower

It should be noted that the most important mooring line is mooring line 2, this is the lead mooring line and will thus be taking most of the load of the wind and waves. However, the other two mooring lines participate as well, for example the wind load will be counterbalanced by an increase in the force in mooring line 2, but also a reduction in force in mooring lines 1 and 3.

3.4 Wind

Contrary to the OC5 experiment, wind was not simulated using a wind generator. To keep this part of the experiment simple, as the main interest laid in the wave excitation, a constant force was deemed adequate, meaning that the quite complex system of aerodynamic drag influenced by the movement of the rotor blades was excluded. The force was applied by using an electric motor connected to a winch via a magnetic clutch. This winch was then connected to the model via a fibre rope (again Dyneema) at the nacelle height. The winch allowed for a tension on the rope at all nacelle distances and the magnetic clutch enabled a constant torque to the winch. The magnetic clutch consisted of two disks, a steel disk laced with neodymium magnets and one aluminium disk. By spinning the magnetic disk magnetic fields would be created putting torque on the aluminium disk in the backward direction (looking at the model from the wind device). If the model moves forward because of a wave the torque on the disk would be overpowered forcing the winch to let some rope go, if the model moved backward the torque would force the winch to take rope in. A schematic with the different parts is shown in figure 21.

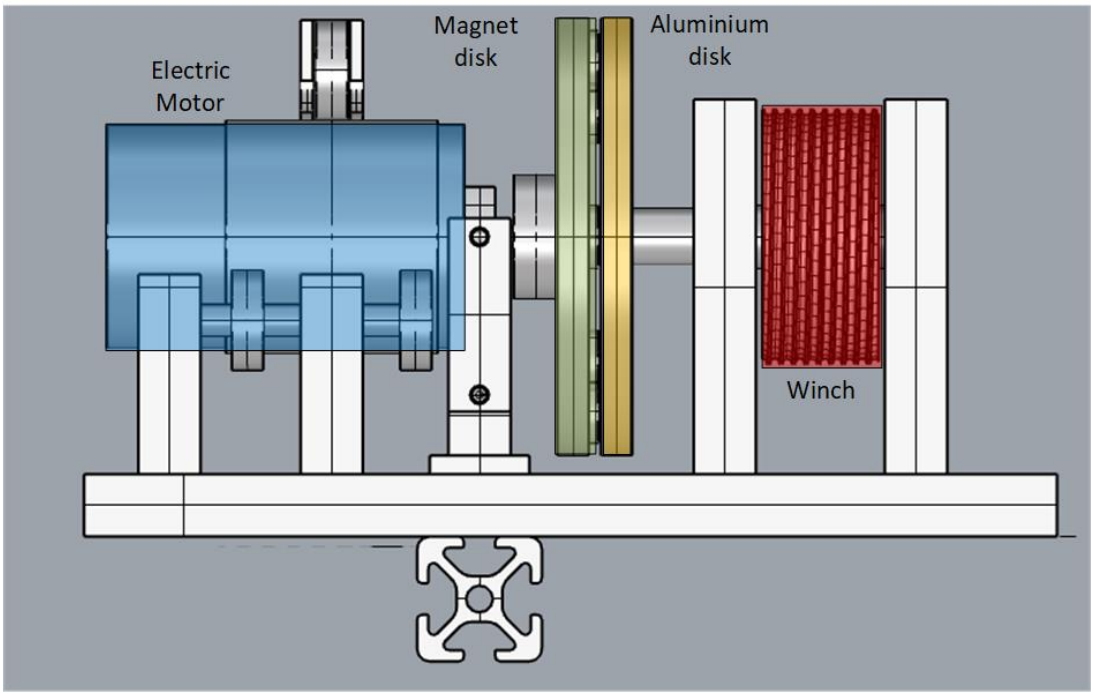

Figure 22: Sketch of the wind force device, created by (Taudin Chabot, 2022)

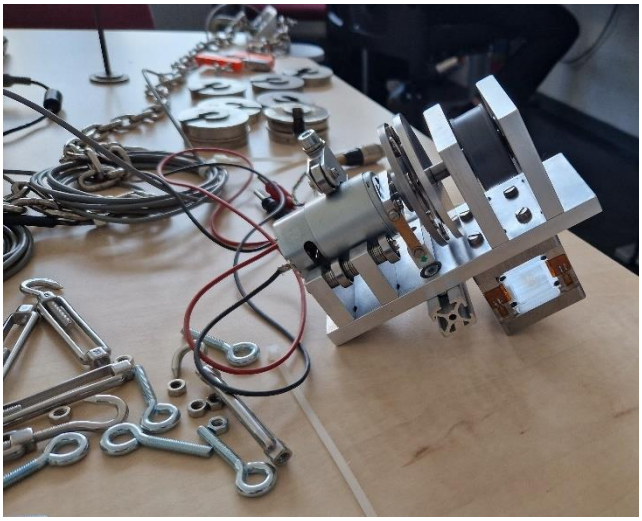

Figure 21: Photo of the wind device, clearly showing the two disks, these were later covered up for safety. The winch is visible on the right. The background shows some of the weights used for calibration.

Together with the mooring system this wind simulation thus created an equilibrium position for the model influenced by the waves. As mentioned, the targeted force applied to the nacelle was 0.81 N. As is expected the force would fluctuate somewhat during a test but was recorded with a measuring device, to both facilitate later analysis and to enable application of the force at the right magnitude.

3.5 Waves

To effectively aim for the low frequency surge natural frequency the difference frequency of bichromatic waves is used. These waves consist of two waves which have a close but not equal frequency, the small difference between the waves then forms a new wave via constructive interference. As the waves line up the amplitude gets summed, which cause the total wave height to increase. If the waves then move apart again the amplitude is reduced or even destroyed. This

changing of the amplitude then forms a wave envelope with the difference frequency, effectively creating drift forces on the model. That way wavemakers can make relatively low frequency waves whilst not moving too slow to not push water around. This is then generally called a beating pattern. A graph the electronic wave maker input file of bichromatic wave named b1, with voltage to the wave maker on the y axis and time on the x axis is shown in figure 23. As can be seen there are seven large low frequency waves made up of many high frequency waves in this beating pattern. The envelope curve thus has a much lower frequency than the wave frequency itself has, but this much lower frequency is closer to the surge natural frequency than the wave frequency and thus makes it likely that the mooring system will respond to it.

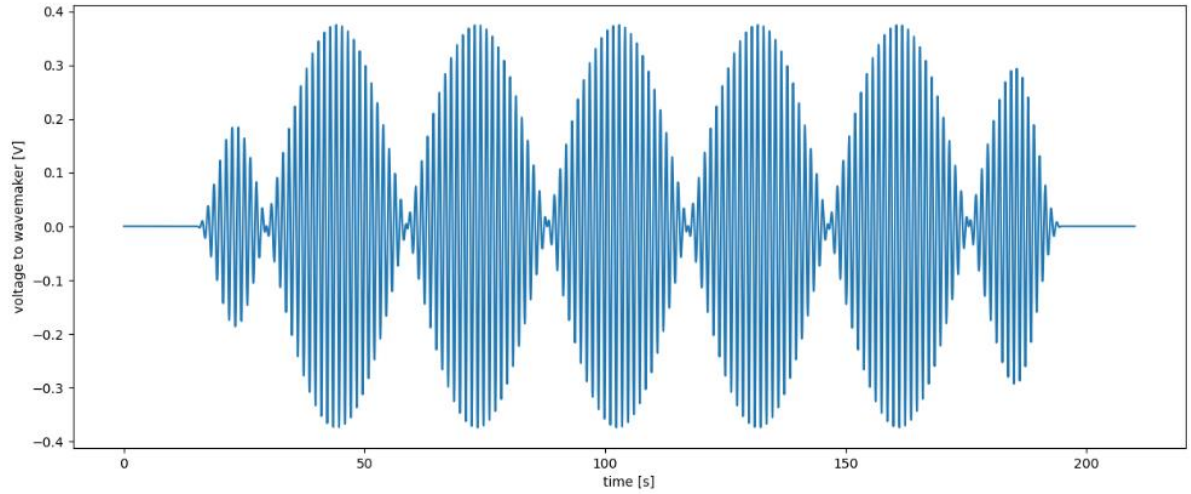

Figure 23: Wavemaker file for b1

3.6 Measuring devices

Multiple measuring devices were used to collect information from the experiments. This subchapter goes into the measuring system used during the experiments and discusses decisions made surrounding their use. In total there are five different sets of measuring devices, these include the force transducers in the mooring lines, the wave gauges, the wind force transducer, the wave maker recorders and the camera system for measuring motion. Appendix H provides additional information on the measurement set-up.

The most important measuring devices are the force transducers in the mooring lines. These three transducers are attached between the fibre rope part and the chain part of the mooring line. This means they will measure the tension pulling down on the fairlead as the fibre mooring line is taut. They consist of a tension meter with two 3D printed attachment blocks bolted on to keep the force in line.

The force transducer make is a Zemic Type 1R1-K Load Cell (Zemic, 2023) with a 2 kg range. Their connection to the central data collection point was done via data cables weaved through the chain down to the anchor. Figure 24 shows a force transducer outside of the mooring line.

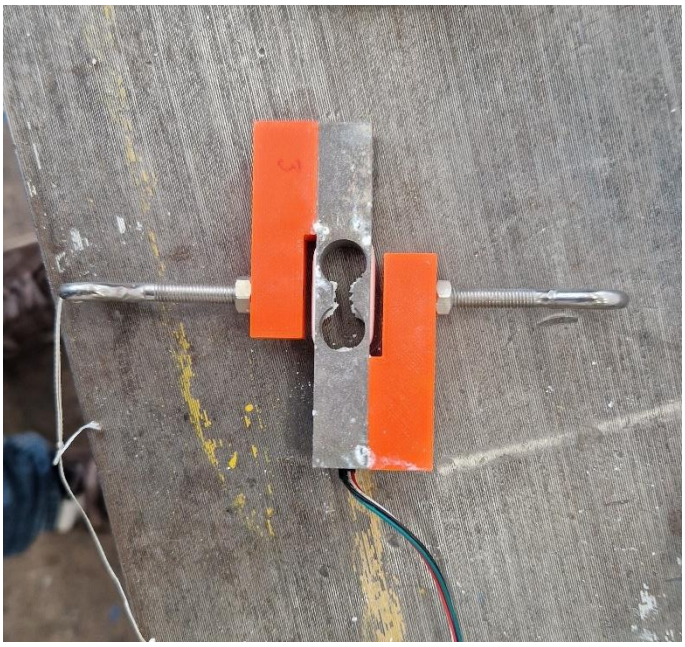

Figure 24: Force transducer of mooring line 3

Waves were measured via four water gauges called Ultrasound Sensor USS 13-HF by General Acoustics. These devices measured the distance between the sensor and the water sonically. This distance was then translated to a water elevation graph, which allows for waves to be observed. As can be seen in figure 17 two wave gauges were put on either side of the model at a distance of 5 m. A third was placed alongside the wall at the neutral position of the model. The fourth wave gauge was placed in the middle of the tank at the neutral position during empty tank tests and above the anchor point of mooring line 2 during tests with the model.

The device to simulate wind was also fitted with force transducers. Both the direct tension in the line was measured as well as the torque the motor applied. This was done to enable the application of the correct force during the test and to evaluate the feasibility of simulating wind in this manner. The force in the line was measured using a shear block between the device and its mount, thus any force on the line would have to go through the block into the mount. The torque was measured by giving the motor a free rotation and then blocking that rotation using a small beam on a force meter, thus turning a torque into a force. The wind device can be seen in figure 21.

The wavemaker was equipped with a threefold of measuring devices to measure input and output. Firstly, a digital system measured the input signal of the wave maker, to ensure the correct signal was sent. Then the wave maker moves and an internal system measures the movement of the plate. In case of an impossible movement, a discrepancy would be found between these two measurements. A third measuring device, a spring-loaded potentiometer was attached to the wave maker plate to measure the movement of the plate again, but this time externally.

The movement of the model is measured through the use of cameras. These cameras track in the infrared spectrum four IR markers attached to the model. These can be seen in figure 17 on top of the outer columns. There are six cameras aimed at the model which all feed into software (Optitrack) (Optitrack, 2023) that makes a digital 3D space. In this space then allows the user to select dots to consider as a vessel, the software then automatically calculates motion in the six degrees of freedom of the model.

The mooring line force transducers and the wind force transducers were calibrated by the use of the ITTC guideline (ITTC, 2021). The calibration was done by coupling the devices (and all the necessary cables to connect them when placed in the tank) to the central measuring computer and then putting known weights in the measuring direction. By increasing the number of weights in increments a relation can be found for the voltage output of these devices versus the amount of weight added. For

additional precision the precise weight was examined thoroughly by taking both the buoyancy due to air pressure and the local gravitational field into account. The spreadsheets created during this calibration are to be found in appendix D.

The camera system was calibrated before the tests using an infrared stick to enable the cameras to give the cameras a sense of their position by comparing it to other cameras. This way the 3D space was made and calibrated.

Uncertainty for the measuring devices is very low in general. The mooring line force transducers show a RMSE of 0.02%, the wind force transducer a RMSE of 0.5%, the torque 1.5%. The wave gauges have a 95% uncertainty range of 0.6 mm (Bouvy, n.d.), and the camera system a RMSE of 0.1 mm, measured by looking at the distance between the individual markers during a test, which should stay constant as the model is very rigid.

The data rates (due to the filter settings) of the mooring lines and wind force and torque transducers are limited to a 100 Hz. The wave gauges measure at rate of 100 Hz as well and the camera system measures at rate of 40 Hz. Although possible, making these rates any faster would not have helped the research as the main focus was on the low frequency excitations and thus a high recording rate would not have added much except the need for additional storage space. The camera system specifically also had a resolution downgrade at capture rates higher than 40 Hz.

Apart from the movement tracking all devices are recorded by an electronic recording device (National Instruments, 2023) after being amplified and filtered (BMCM, 2023). The complete set-up is shown in appendix H. The recording device sends the data to a laptop where it is all collected in a single environment called Labview. This means that all the data is automatically synchronized for these devices. The Labview data records at a 1000 Hz however, meaning that ten consecutive data points are (more or less) equal as the input is only 100 Hz.

The cameras are on a different system and thus need to be synchronized to the data. This is done via the use of a light signal imbedded in the wavemaker signal. This light signal triggers a LED light which is then recorded by two additional cameras in the camera system. This then gives a time synchronization which can be used to synchronize all data.

The Labview data is stored on a laptop and the moving tracking data on a separate desktop. This stored data was then processed and filtered (more on that in the data processing section). The processed data (with exception of the wavemaker data, as that was deemed unnecessary) was stored in csv files to be used in the data analysis. These csv files are available via the appendix B.

3.7 Test matrix

A test matrix is made to show what tests were performed during the experiments and on which model. Different wind and wave conditions and different mooring systems make for a quite complex test regime which will be explained. Appendix C shows a complete overview in tables.

First up are the moored decay tests, as the surge natural frequency is needed for the construction of the waves. These were performed both with and without wind force applied. They tested all 6 different degrees of freedom, so surge, heave, sway, pitch, roll and yaw. Both configurations of the mooring system were tested for all six freedoms. The surge decay test got an additional repeat test as this provides more data for the uncertainty analysis. Free decay tests were also performed on the roll, pitch, and heave movement.

For the experiments six sets of bichromatic waves are then created, consisting of combinations of six monochromatic waves. Five sets were tested on mooring system 1 called b1 through b5, b1 being the

one with the lowest frequency. For the creation of these bichromatic wave sets six individual wave components were set up called m1 to m6. For the creation of a bichromatic wave set, the number of the set would be combined with m6. So, to create set b3 components m3 and m6 are combined. Mooring system 2 was tested with b4, b5 and b6. b6 was an additional set made up from two of the earlier components, m2 and m5 to get a specific period. Below a table of the waves and wave sets is given.

Table 3 overview of the wave components and their periods

wave	period [s]	frequency [rad/s]
m1	1.251	5.02
m2	1.270	4.95
m3	1.307	4.81
m4	1.369	4.59
m5	1.436	4.38
m6	1.2	5.24

Table 4: overview of the wave sets, their periods, constituents and their constituents' frequencies

wave set	set period [s]	set frequency [rad/s]	component 1	1 – frequency [rad/s]	component 2	2 – frequency [rad/s]
b1	29.2	0.215	m1	5.02	m6	5.24
b2	21.9	0.287	m2	4.95	m6	5.24
b3	14.6	0.430	m3	4.81	m6	5.24
b4	9.73	0.646	m4	4.59	m6	5.24
b5	7.3	0.860	m5	4.38	m6	5.24
b6	10.95	0.574	m2	4.95	m5	4.38

These waves were made with the results of the decay tests. The middle wave set for both mooring configurations was aimed at the surge natural frequency. So mooring system 1 has a natural period of 14.6 second, which was replicated with b3. The other sets were then made to be half the frequency with b1, two thirds the frequency with b2, one and a half times the frequency with b4 and twice the frequency with b5. For mooring system 2 the middle wave set, b4 was focused on the natural period of 9.8 s, b5 and b6 were then added to provide two additional sets to test with one on either side. All wave components were around 40 mm high, meaning a bichromatic has an amplitude of 80 mm at the maximum. The waves are run in full for 150 seconds, with a ramp up and ramp down time of 15 seconds added to enable the wave maker to start up. Hence why the first and last low frequency wave in figure 23 are smaller. These 150 seconds allowed for the completion of 5 b1 waves. This does mean that a single reflection can return from the beach as discussed during the tank overview. As it would cut down on too much measuring time to stop before this reflection it is accepted.

Taking from the linear wave theory discussed previously the reflection time of the waves can be calculated. The formula for the group wave speed in deep water (most wave cases are in deep water, but there are a few edge cases which deviate from this calculation by a few percent) is as follows:

$$c_g = \frac{1}{2} * g * \frac{T}{2\pi} \tag{7}$$

To examine the reflection, the highest period of the waves used is 1.436 s. This period leads to a group speed of 1.12 m/s. This means that after 2*56.2 m / 1.12 m/s the waves will return, which is after 100

s. To then return from the wave maker again an additional 51 seconds would be needed. As the tests only take 150 seconds (again more in the wind and wave section) this means that the model will experience only a single reflection during the experiment.

The complete test schedule can be seen in appendix C with the different codes for each test.

3.8 Testing process

This section aims to give the reader a good overview of the different steps taken during one of the test runs. To improve the repeatability of the test and to act as guidebook for other research.

1. A zero measurement is done with the wave and wind force transducers for 30 seconds. this allows for zeroing the measurement data later collected. No wave excitation takes place during this measurement.
2. A zero measurement with the camera system is done for 30 seconds as well.
3. This data is then saved and logged.
4. Wind force is applied to the model by turning on the wind device.
5. Wavemaker is (checked to be) disconnected from the computer and a wave is selected. The disconnect is done to prevent shocks in the system which would disturb the still water as a new file is loaded.
6. Measurement devices are all checked, the Labview recording time is set to 300 s.
7. Model is selected in the 3D environment of the camera software.
8. Measuring devices and cameras are all checked to see if they provide output.
9. Wavemaker is connected to the computer.
10. Measurement is started and wave is turned on.
11. Experiment takes place, peculiarities are noted, and data streams continually checked.
12. After 240 seconds the cameras are stopped and saved.
13. Wave maker is disconnected from the computer to prevent shocks.
14. Wind device is turned off.
15. Approximately 20 minutes of wait time before the next test, to make sure the water calms down again. The water is deemed calm enough once the wave gauges no longer show a clear wave pattern in combination with a visual inspection of the water surface. The data is checked, named and logged in the meantime.

4. Verification

The goal of this chapter is to verify the tests in order to see if they were given the correct input and yielded usable results. The actual interpretation of the results is done in the data analysis chapter after this.

4.1 Decay tests

A good look at the model is on order to check if the desired dynamic similarity is achieved. This is done via decay tests. The decay tests were done to determine the eigenfrequencies of the system. Although, they were performed for all six degrees of freedom, the most important one is surge, which will get some extra attention in the form of an uncertainty and damping analysis as well.

Decay tests are performed by placing the model in still water and giving it a slight excitation in the intended degree of freedom. The excitation will be counteracted by either the buoyancy or the mooring lines and will cause it to move in the opposite direction like a spring attached to a weight. Besides the oscillating force, a damping force causes the model to slowly lose speed. From these two elements the natural frequency and the damping of the model can be determined. The response was measured using the camera system.

The natural period is determined using the zero-crossing method. This means that a period was measured by taking the time difference between two points crossing the y = 0 line. Figure 25 shows a surge versus time plot with the aforementioned method in the blue dots, the red dots indicate the alternative, a method based on looking at the peaks. The data used is the completely unfiltered data from the camera system, which leads to some issues with the peak method. The exact point in time where the zero crossing happens is done by letting an algorithm search for the value of the motion data set that is closest to the zero line in a bounded box in between the peak and through. An optimization could be done by interpolating the exact value where the motion crosses the zero line, but as will be seen later, the standard deviation from the decay tests is an order of magnitude larger than what could be gained by this optimization.

As can be seen in figure 25 the zero-crossing method has twice as many dots as the peak method and the dots are more accurately placed allowing for a more accurate assessment of the period. A 95% certainty range (2 standard deviations either way) of the calculated half period is also indicated around the blue dots, calculated by taking the standard deviation from the formula below over all the intervals between the dots.

$$std = \sqrt{\frac{1}{N}\sum_{i=1}^{N}(x_i - \bar{x})^2} \tag{8}$$

It can be seen that this uncertainty is beyond what is reasonably caused by the zero crossing placement, meaning that the uncertainty comes from the changing of the period during the damping of the oscillations. The reason the red dots tend to go astray later in the test is due to small bumps in the data, most likely caused by small reflections generated during the decay test. The zero-crossing method has less issues with these small reflections because at a zero crossing the model is already moving and is thus less impacted.

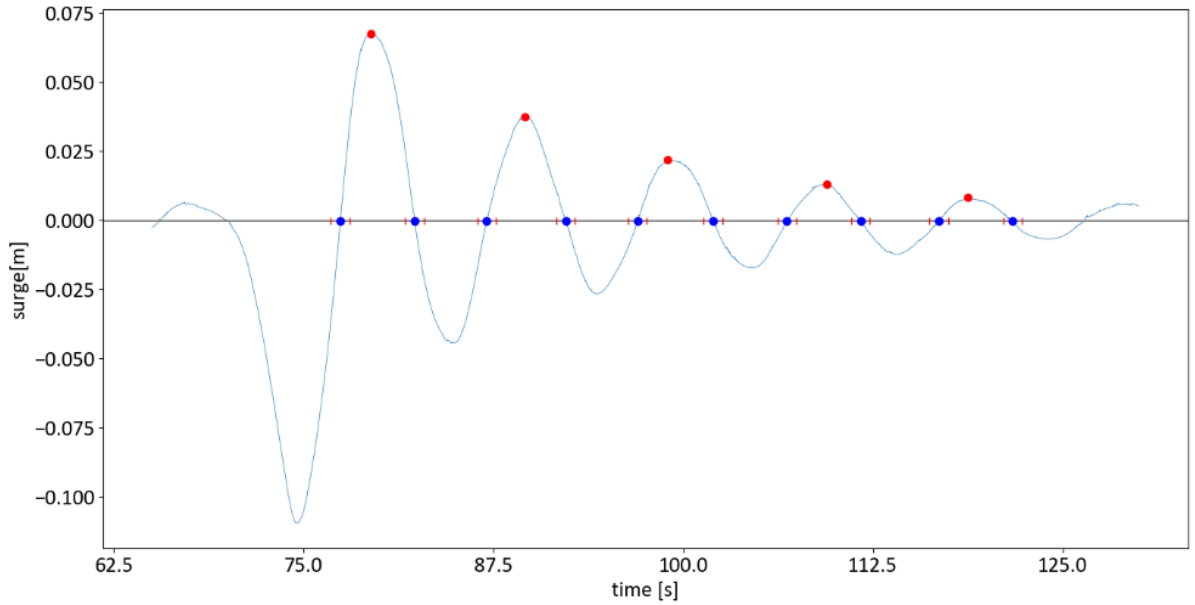

Figure 25: Graph showing the surge in m versus the time, for the surge decay test of mooring system 2 with wind.

As stated previously the two mooring line configurations (see figure 20, with mooring system 2 being the stiffer of the two) are tested in their six degrees of freedom, both with and without wind load. As the wind pulls back on the front mooring line this has an influence on the stiffness of the mooring lines. The natural periods and frequencies are shown in the tables below.

Table 5: Overview of the eigen periods of mooring system 1 with wind

mooring system 1 with wind			mooring system 1 without wind	
motion	period [s]	frequency [rad/s]	period [s]	frequency [rad/s]
surge	12.7	0.49	14.6	0.43
sway	15.4	0.41	14.5	0.43
heave	1.77	3.54	1.77	3.54
pitch	2.78	2.61	2.90	2.16
roll	8.85	0.71	10.4	0.60
yaw	8.80	0.71	8.80	0.71

Table 6: Overview of the eigen periods of mooring system 2 with wind

mooring system 2 with wind			mooring system 2 without wind	
motion	period [s]	frequency [rad/s]	period [s]	frequency [rad/s]
surge	9.24	0.67	9.80	0.64
sway	10.1	0.63	9.75	0.64
heave	1.78	3.54	1.79	3.52
pitch	2.73	2.30	2.85	2.20
roll	6.06	1.04	6.13	1.03
yaw	5.08	1.24	5.08	1.24

Because of the relatively slack mooring lines in mooring system 1, the decay test of this configuration does not have a clean single neutral line which can be used for zero crossings. To take this into account a 1000 different ‘zero’ lines were tried at different y values. The one which yielded the periods with the lowest standard deviation between them was chosen. This is shown in figure 26, which shows a

surge decay test, against the time. The grey horizontal line indicates the eventual zero line. It deviates from the actual y axis zero value as can be seen. Figure 27 shows a graph of the standard deviation for the 1000 different tested heights, ranging from -0.01 to 0.01 m. The red dot indicates the lowest value, which becomes the height for the grey line in the graph. This was done for the surge decay tests of all models for consistency.

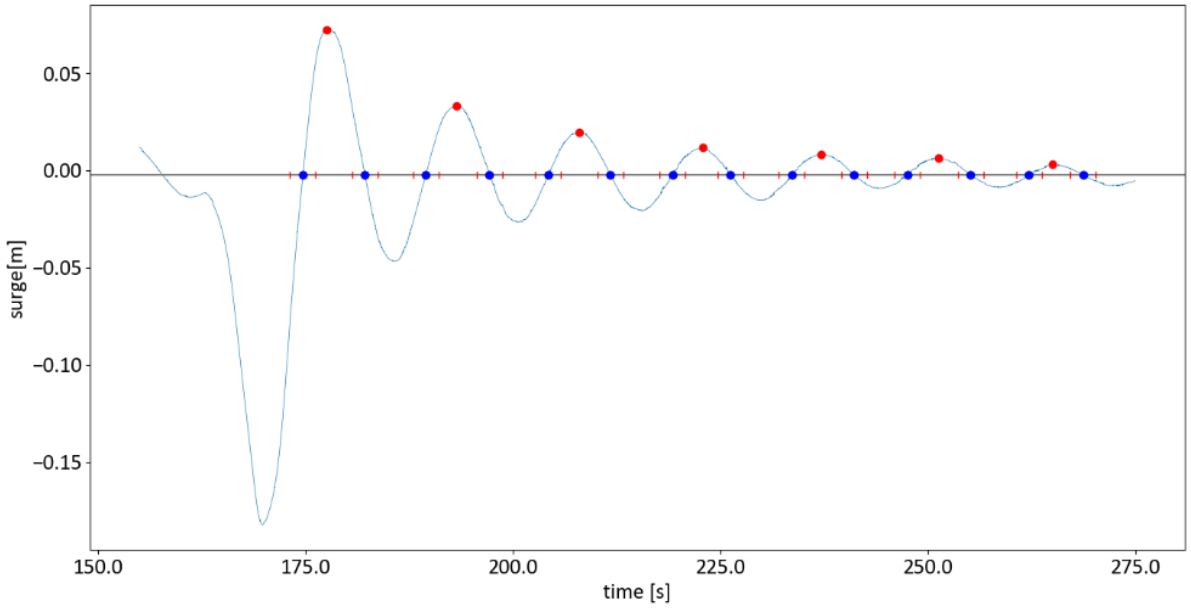

Figure 26: Graph showing the surge in m versus the time, for mooring system 1 without wind.

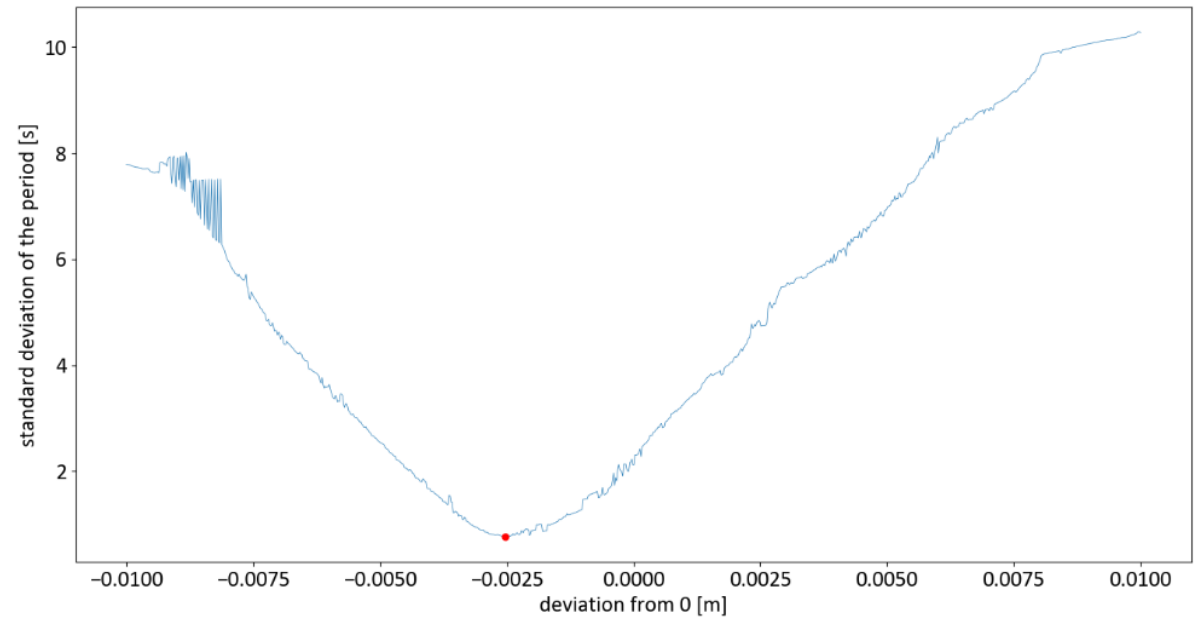

Figure 27: Graph showing the standard deviation in the period versus the deviation from the y= 0 axis for the zero line

The uncertainty per system can now be calculated for the surge movement with the formula shown above. Table 7 indicated both the absolute and relative uncertainty in the eigenfrequencies. As can be seen mooring system 2 without wind has a lower relative standard deviation, why this is, is not known.

Table 7: overview of the mean natural surge period per system and its standard deviation

system	mean natural surge frequency [rad/s]	absolute standard deviation [rad/s]	relative standard deviation [-]
mooring system 1 with wind	0.492	0.0104	0.021
mooring system 1 without wind	0.429	0.0092	0.022
mooring system 2 with wind	0.672	0.0147	0.022
mooring system 2 without wind	0.638	0.0085	0.013

The damping is determined for the surge motion as well. This is done by the use of the logarithmic decrement. The logarithmic decrement is based on the theory of a linear damped mass spring model, which the mooring system is not, but can and will be approximated as. The logarithmic decrement aims to quantify the damping by looking at the reduction of the height of the peaks per oscillation. These values can then be used to find the damping ratio. The formulas are as follows:

$$\delta = \frac{1}{n} \cdot \ln\left(\frac{x(t)}{x(t+nT)}\right) \quad \text{and} \quad \zeta = \frac{1}{\sqrt{1+\left(\frac{2\pi}{\delta}\right)^2}} \qquad (9 \ \& \ 10)$$

with ζ being the damping ratio, x indicating the x-position of the peaks, T the period and n the number of periods.

When converted to a simple line value starting at the first peak, it can be seen that this damping ratio fits the decay well. Figure 28 shows a plot for the surge decay test with the peak damping line in orange.

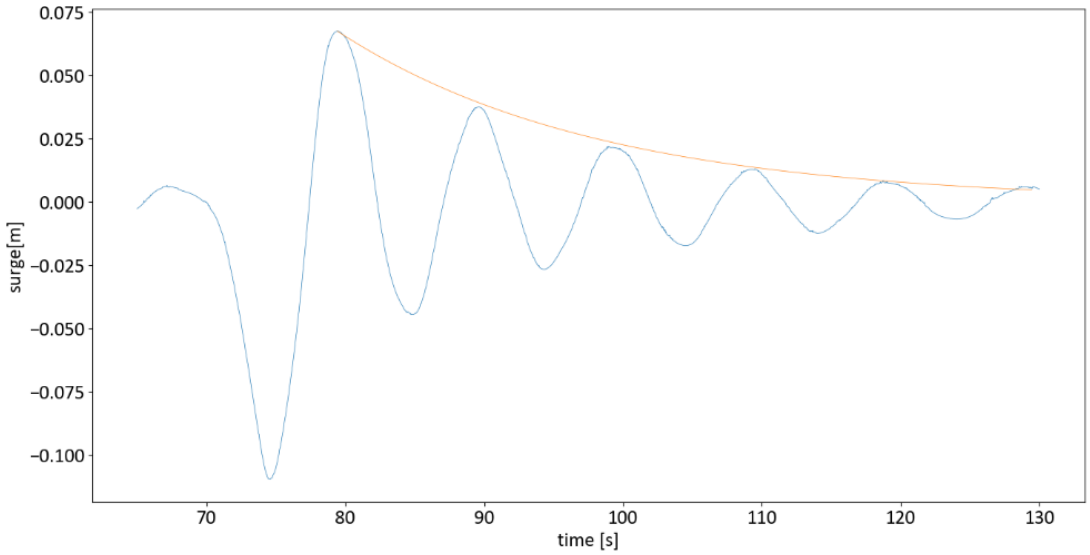

Figure 28: Graph of the surge excitation versus the time, with an orange line indicating the found damping, for mooring system 2 without wind load.

The damping ratios of the different mooring systems are shown below.

Table 8: overview of the damping ratios of the different systems

system	damping ratio
mooring system 1 with wind	0.120
mooring system 1 without wind	0.050
mooring system 2 with wind	0.085
mooring system 2 without wind	0.074

4.2 Wave verification

Wave data of both the tank without the model and the tank with the model are shown and analysed. This will be used to determine whether the waves are actually at the correct input values. This will concern two parameters, wave frequencies, and wave height, the first taking precedence.

Before experiments with the model are carried out, tests with the same waves but in an empty tank are performed. This allows the testing of the response of the tank to the waves and enables later comparison of the wave data with and without model. That way it can be determined whether possible phenomena come from the model or the tank. The tank was not entirely empty during the empty tank test, however, as the foundation plate and a few buoys for the mooring lines were present. These can be seen in figure 19, although it should be noted that the water level was lowered when that picture was taken. The remaining items in the tank should however not significantly impact measured data as the have a very small surface area compared to the wet area of the tank or in case of the foundation plate are located at a the bottom and thus away from wave action.

Figure 29 shows a water elevation graph measured by wave probe 4 for the tested m3 wave. The graph shows that the wave is very consistent during the first part of the test in amplitude, staying around 18 mm. When the reflection from the beach comes back, approximately 100 seconds after the first contact an increase in the height can be seen, which ends at approximately 20 mm. This implies that some wave energy is being send back from the beach, as it increases the wave height by roughly 10%, and energy thus by 20%.

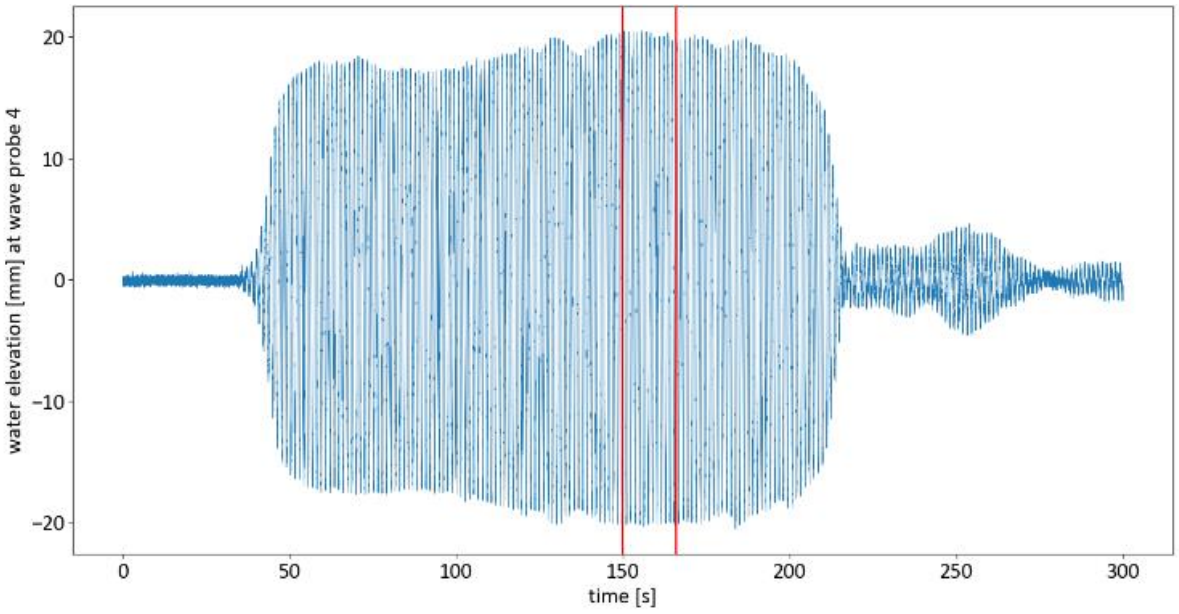

Figure 29: Water elevation versus measuring instance for the empty tank test of m3

Figure 30 then shows a zoom of the same graph, centres the y-axis to the mean and adds the wave maker input signal, scaled to the same height as the water elevation for visibility's sake. Apart from the phase shift due to the distance between the wave maker and wave probe the two graphs line up nicely and show that the frequency of the input signal is matched. From the y axis the actual wave height can now be estimated to be about 40 mm. This was the intended height and was achieved by linear interpolation of two earlier wave tests with a known height and wave maker input voltage. The first phase of the wave test had a lower height as mentioned, which should be taken into account during the analysis.

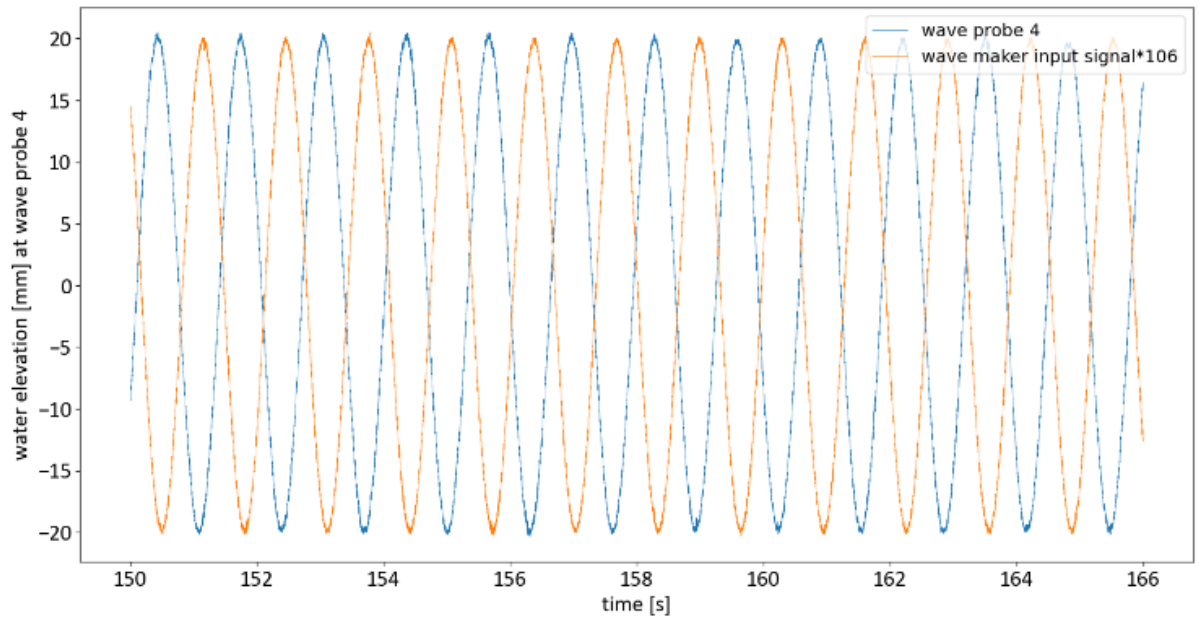

Figure 30: Graph showing the water elevation and the wave maker input signal for the empty tank test of m3, zoom indicated by red lines in figure 29.

This is then repeated for the bichromatic wave b3. Figure 31 shows the wave elevation at wave probe 4 versus time for the entire wave test showing the consistency in the wave data. The maximum wave height can now be estimated to be about twice that of m3 at 80 mm. But again, the wave height increases slight during the experiment due to the reflections returning from the beach.

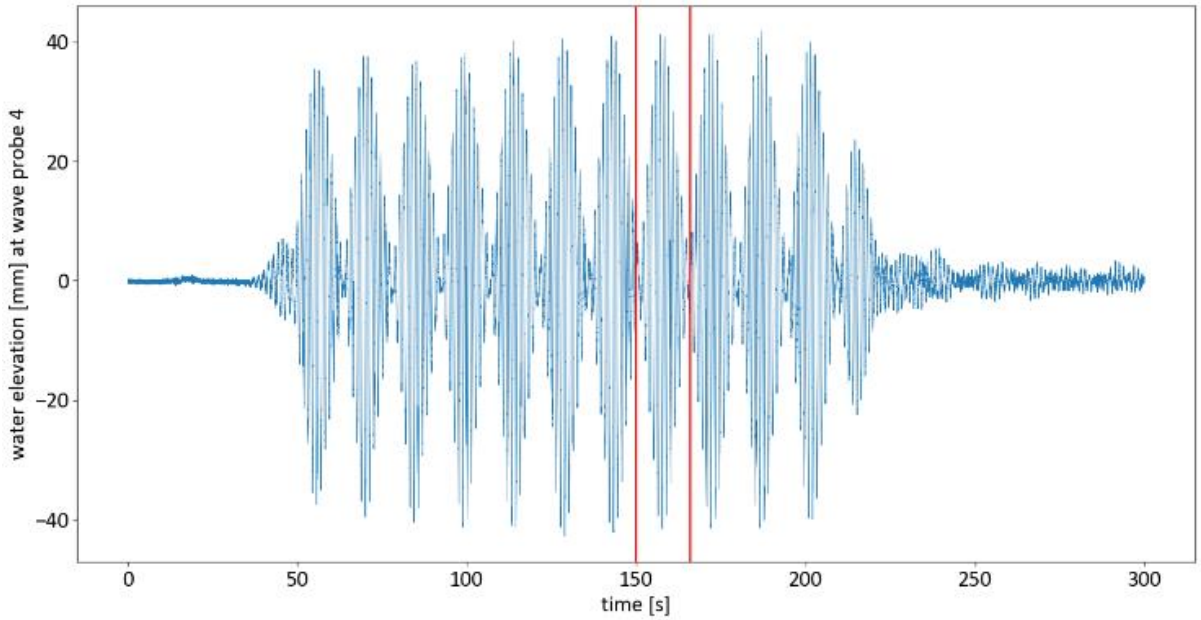

Figure 31: Water elevation versus measuring instance for the empty tank test of b3

Figure 32 shows the same zoom for the b3 wave and again adds the wavemaker input data, centring and scaling the two to match in height. Now the bichromatic wave becomes clearer in the data. It is clearly visible that the wave is made up ever increasing and decreasing small waves due to constructive interference. It can also be seen that the data lines up well with the input signal.

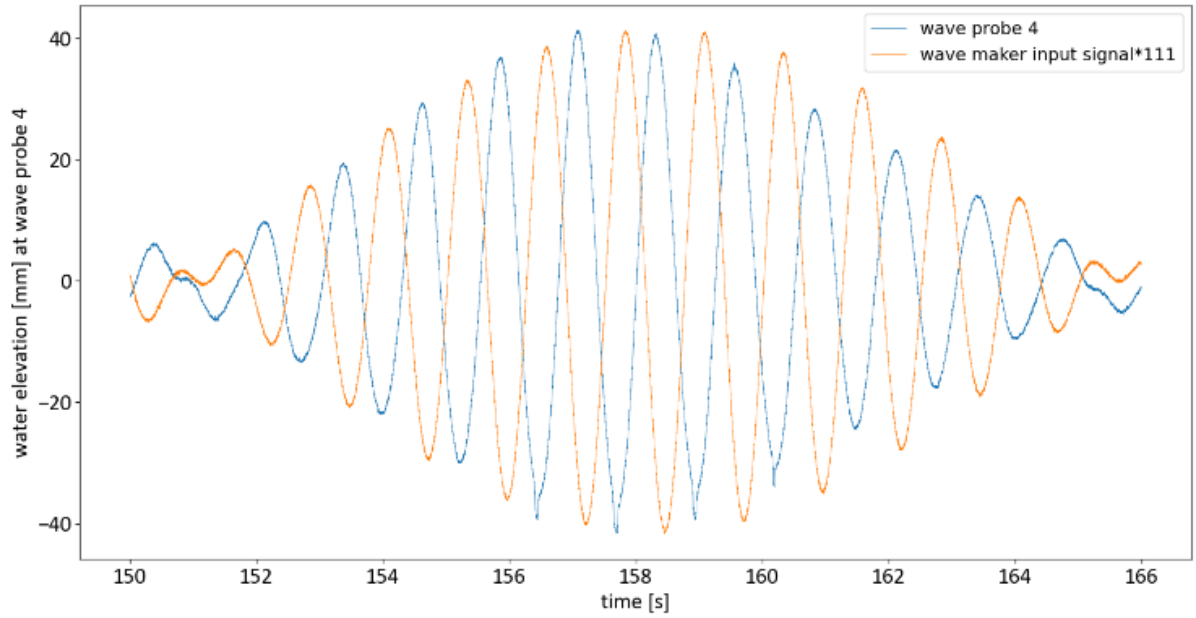

Figure 32: Graph showing the water elevation and the wave maker input signal for the empty tank test of b3, zoom indicated by red lines in figure 31.

Figure 33 shows the repeat test for the bichromatic wave b3 empty tank test. As can be seen when comparing it to figure 31, there are very little observable differences between the two tests, showing that the waves have a high degree of repeatability.

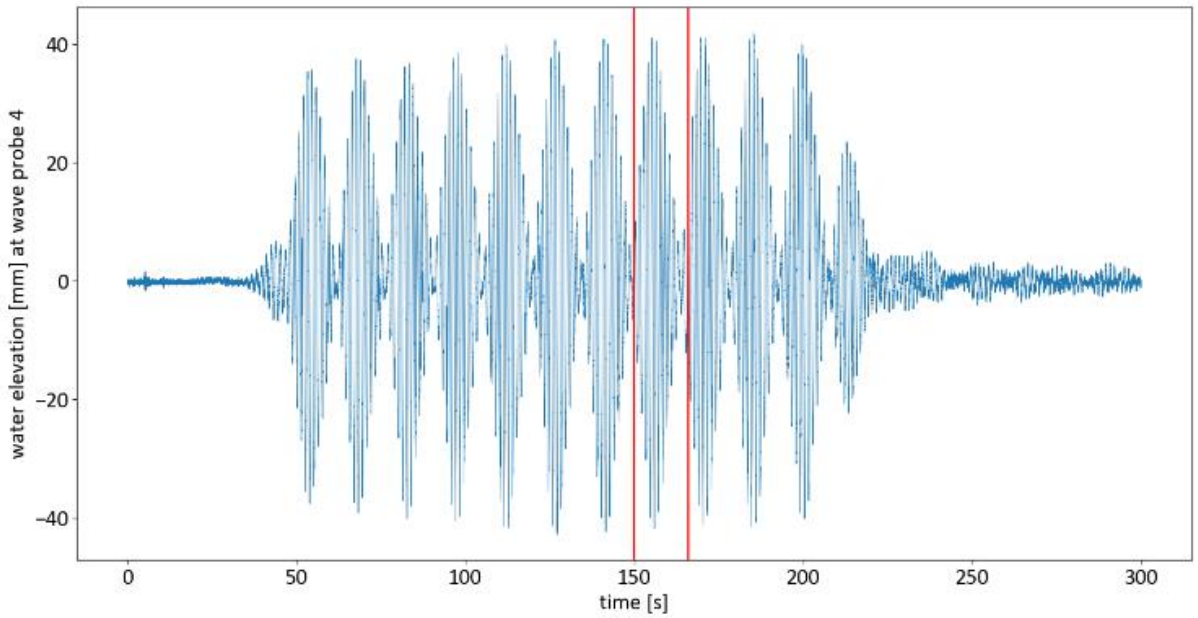

Figure 33: Repeat test for wave test b3

This check was repeated for other waves and can be done using the data from appendix B. In all cases it was observed that the waves follow the wave maker input frequency very well and are consistent throughout the test. A short spectral analysis of this data is also performed see if the data matches the desired frequency. Figure 34 presents a spectral analysis of figure 31, showing the very sharp peaks on the frequencies of 4.81 and 5.24 rad/s, which as recalled by table 4 are exactly the frequencies of bichromatic wave b3.

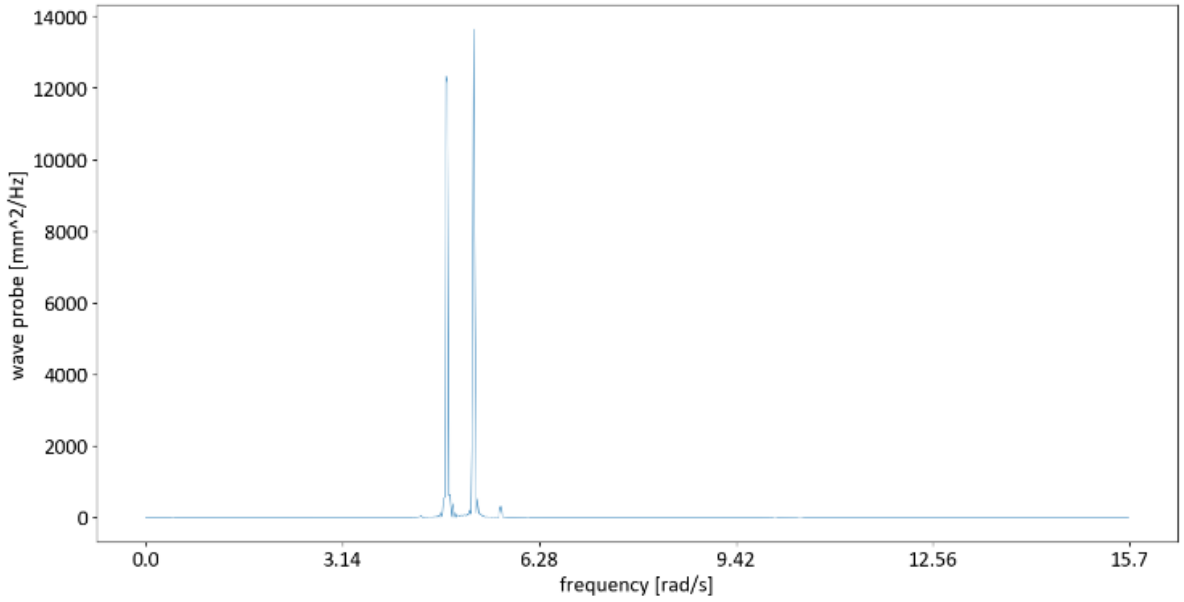

Figure 34: Spectral analysis of the wave test for wave b3

A more elaborate analysis establishing the causal chain of excitation is provided later in the data analysis chapter.

Using the wave data, a further check can be performed on the group speed, thus validating some of the assumptions made around the linear wave theory. This is done by checking the two outer wave

probes, number 1 and number 2. These are spaced 10 m apart and thus by taking the time between when wave trains appear the wave speed can be calculated. This is shown in figure 35, where the wave data from wave probes 1 and 2 are shown. Here in blue is wave probe 1, and in orange wave probe 2, separated by roughly 10 seconds going forward. It should be noted that this is from experiment b3 which includes both the m3 and m6 waves. The m6 wave has a group speed of roughly 0.93 m/s, whereas the m3 wave has a group speed of roughly 1.03 m/s. The average of these, 0.98 m/s would correspond nicely with the 10 sec gaps observed, thus validating the linear wave theory group speed used.

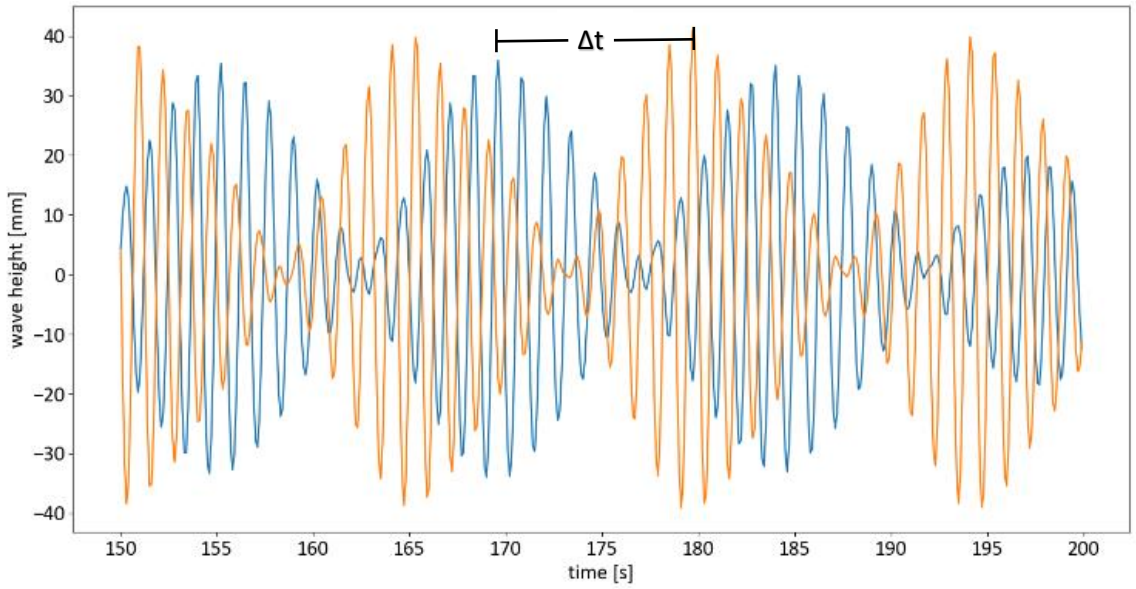

Figure 35: Wave speed comparison wave test b34. The reason for the difference in maximum wave elevation is not known, but most likely due to improper calibration.

4.3 Wind verification

As with the wave data, the wind data is shown and analysed to determine if the correct load was applied to the model. Additionally, the torque in the wind motor is displayed to get a better sense for the mechanical needs of the wind simulator for future research.

The main goal of the simulated wind force was to provide a constant force. The mechanical and measuring devices set up to do that are described in the previous chapter. Figure 36 shows the force in the shear block underneath the wind device (and thus the force in the cable) versus the time for a wind application test. As can be seen there is a lot of noise in the graph, but the force centred close to the desired 0.81 N when the wind is applied. The standard deviation in the wind force when the force is applied is 0.164 N, which is a rather large standard deviation and would pose a problem for this research. Thus, an investigation of the source of this noise is in order.

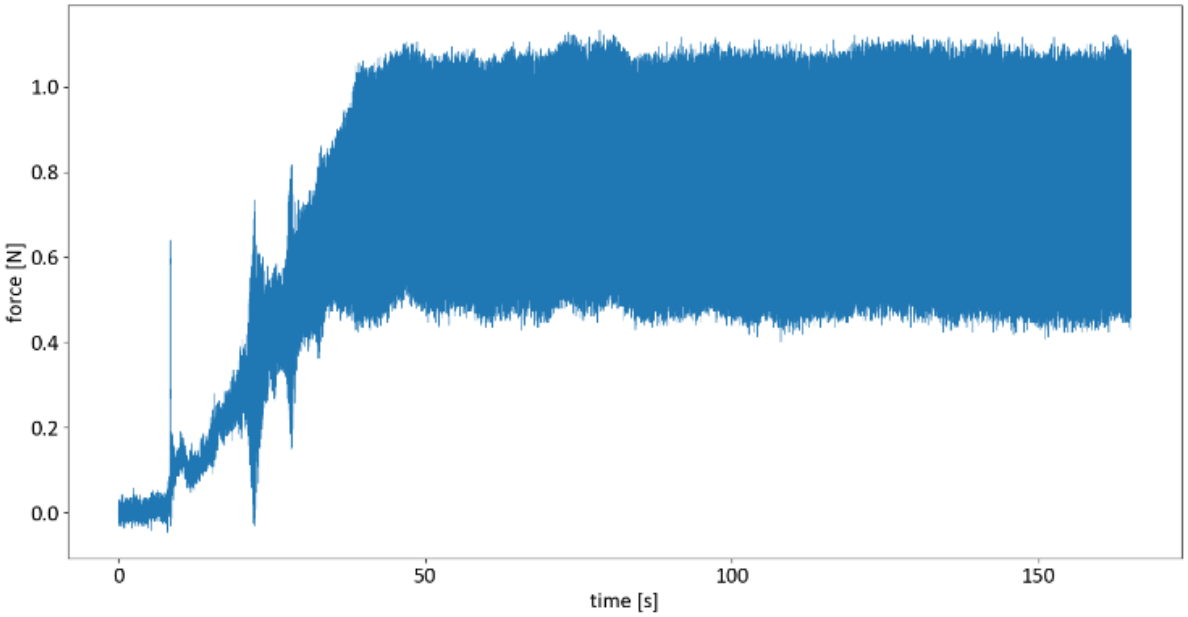

Figure 36: Graph showing the wind force during a wind application test.

Figure 37 shows a zoom of this graph on to the middle 2000 points, at a 1000 Hz, this is 2 seconds. It can be concluded that the source of the large variation most likely mechanical in nature, as the data shows 30 oscillations, so 15 Hz, which will thus probably have its source in the rotation of the motor.

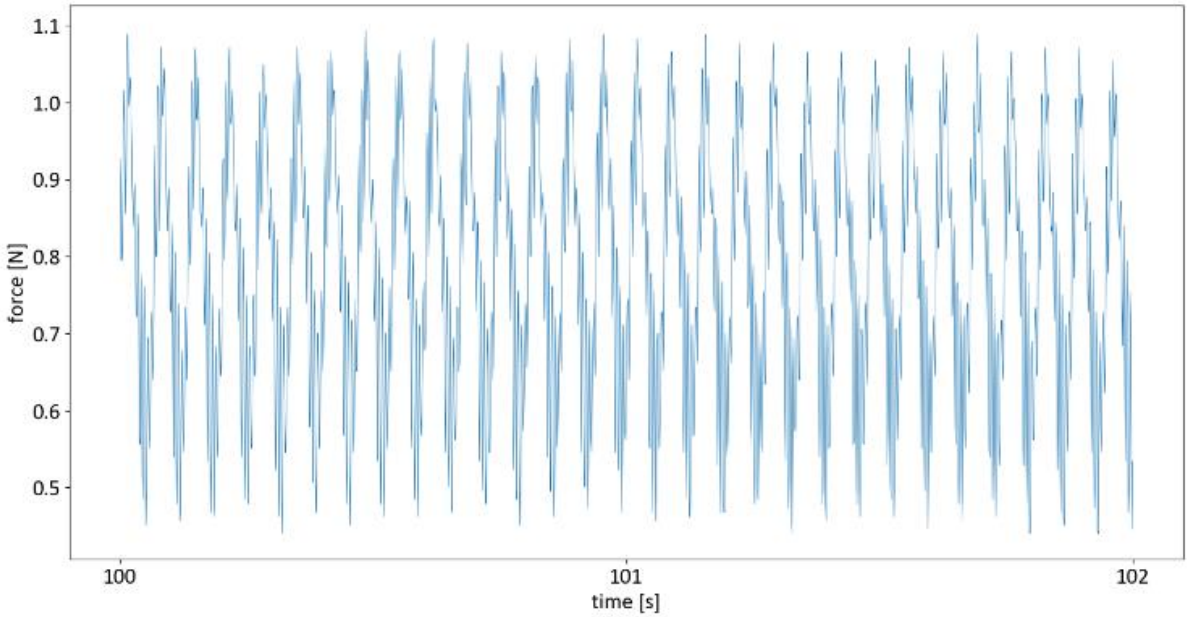

Figure 37: Zoom in on figure 36 around the 100 s mark.

From this graph it can be concluded that there is a high frequency variation in the wind force. The most likely source will be the electric motor as this motor turns and a small imbalance in this motor would cause the observed oscillation. This high frequency oscillation however does not pose much of a risk to research as the frequency is way too high to be seen in the results later on.

To further show that this oscillation is mechanical in nature the zero measurement of this test, where the engine is turned off, is shown below in figure 38. Here it can be seen that the large amount of noise is absent, pointing to the fact that it is in fact mechanically caused.

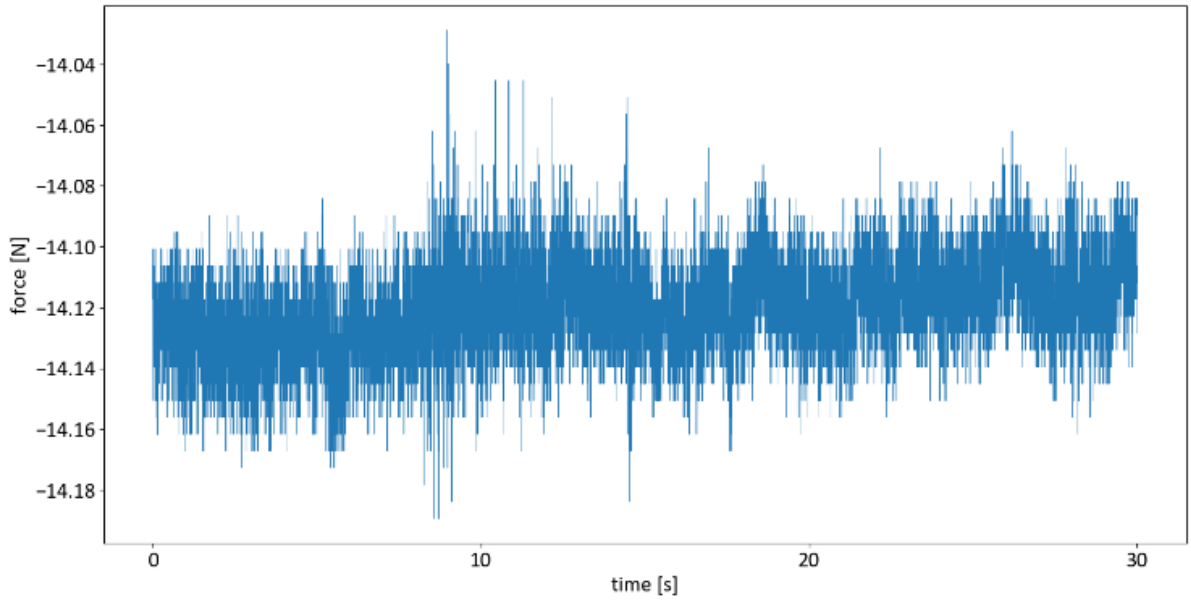

Figure 38: Zero measurement for the wind application test

Figure 39 then shows the wind force during model test b3. Here again a large variation is visible in the data. Note that the application of the wind force is not recorded.

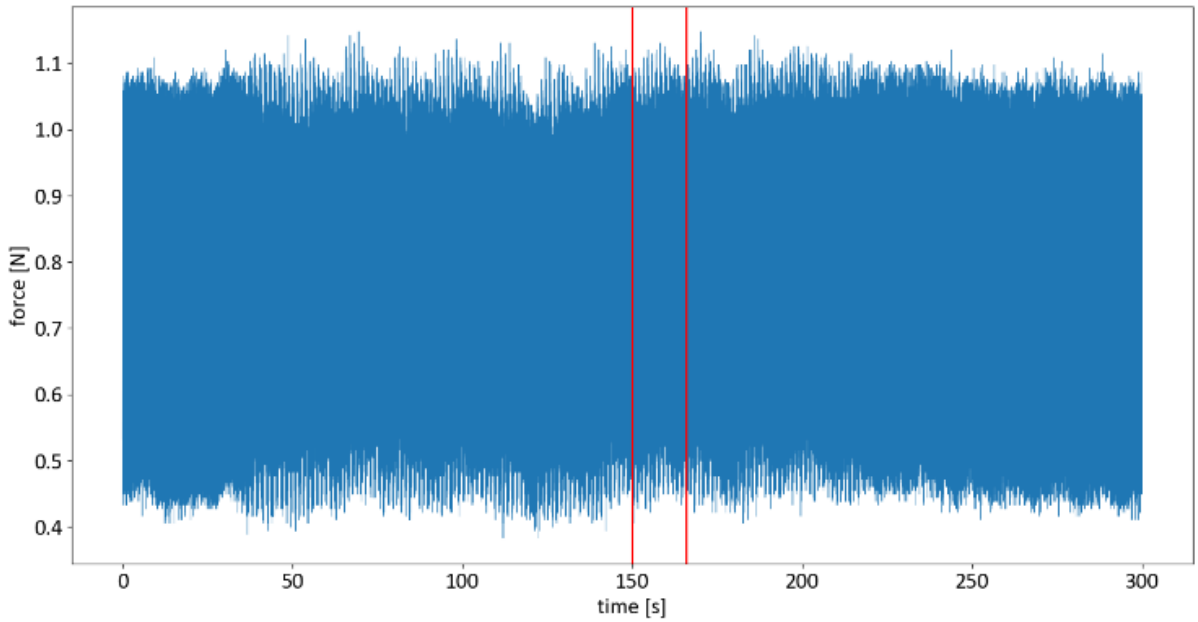

Figure 39: Wind force data for model test b3

Again, a zoom in on the graph is shown in figure 40. Here again the high frequency oscillation can be seen.

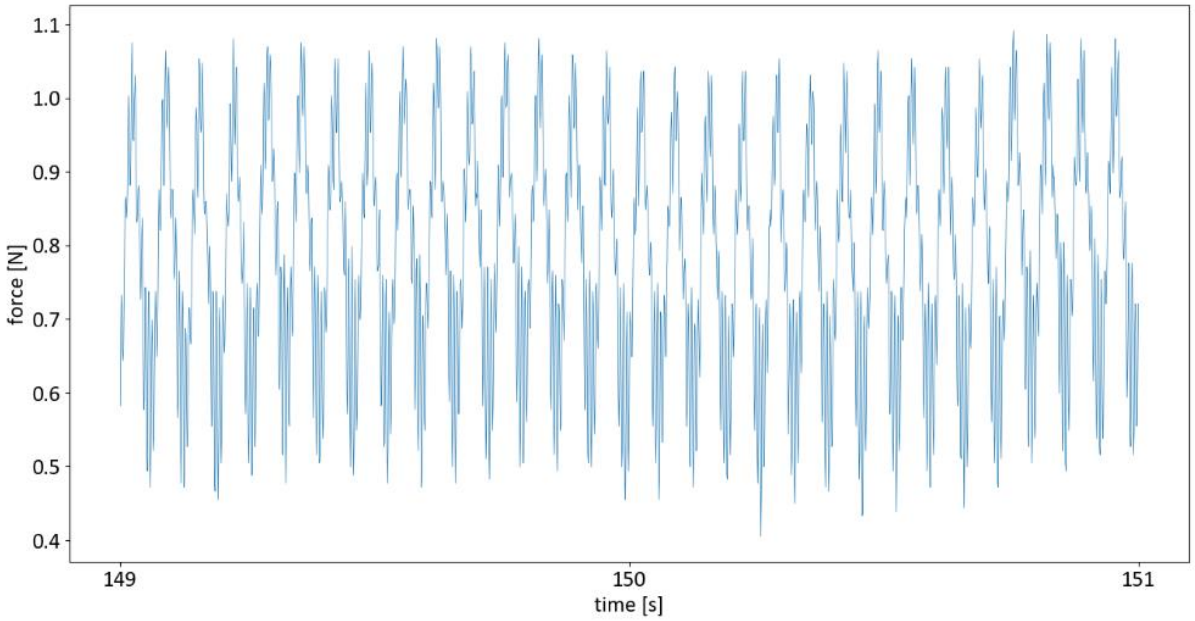

Figure 40: A high frequency zoom in for the wind force data for model test b3, taken one second on either side of the 150 sec mark.

Besides the high frequency oscillations, the wave excitation can also clearly be seen in the wind data. Figure 41 shows the wind force data for a larger measuring instance indicated by the red bands in figure 39 and one can clearly see the bichromatic wave in the force. This makes sense as the waves cause pitch which would then allow the winch to reel in line, which reduces the relative speed between the discs and thus the torque on the motor.

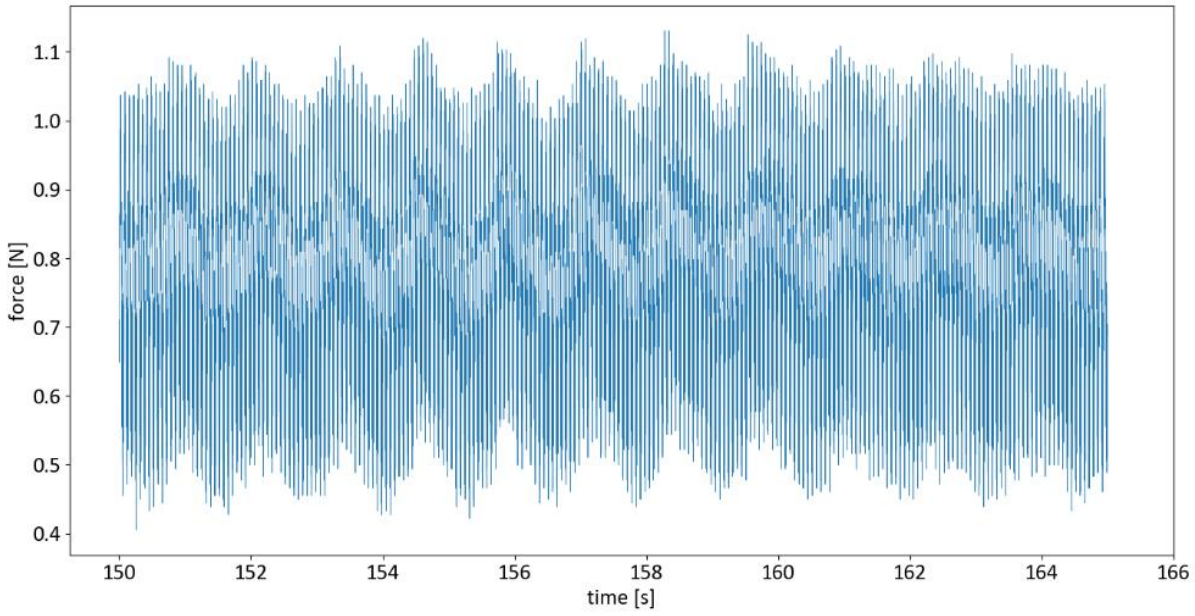

Figure 41: Wave frequency zoom in of the wind force data or model test b3, indicated by the red lines in figure 39.

Figure 42 shows the presence of the waves even better. In this figure the high frequency oscillations have been filtered out and the wave probe data has been added. It can clearly be seen that the blue wind force data is linked to the orange wave probe data.

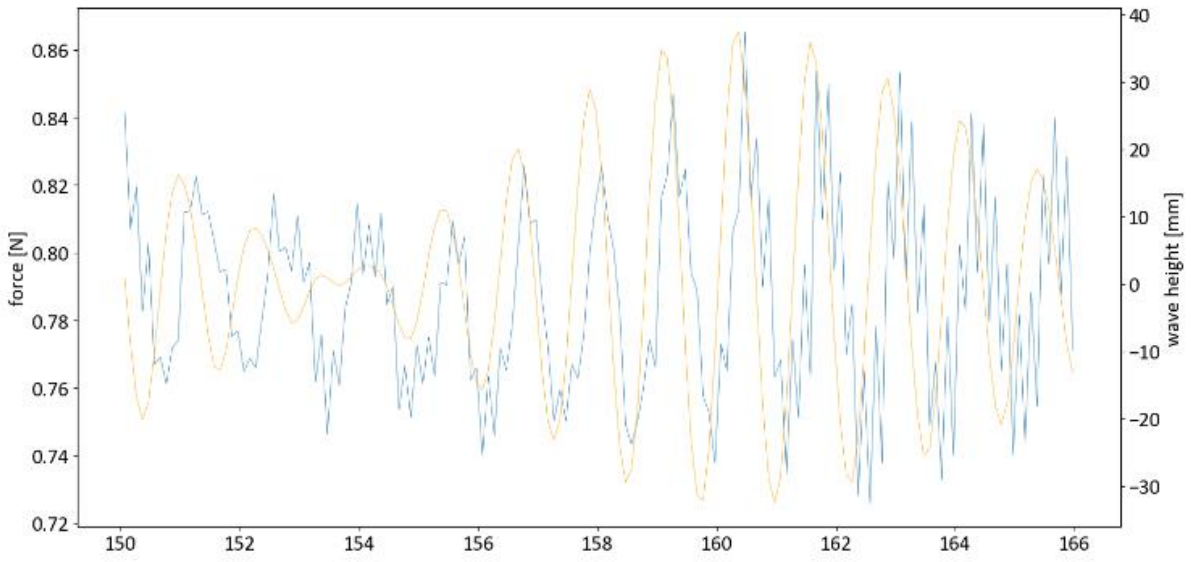

Figure 42: zoom in on the same period, high frequency filtered out (similar to data analysis method later) and with an added wave data.

The same phenomena can all be seen in the wind torque starting with figure 43, which is for model test b3, where now the torque of the motor is displayed versus the time. Again, a very thick band can be observed with a mean of 22.2 Nmm.

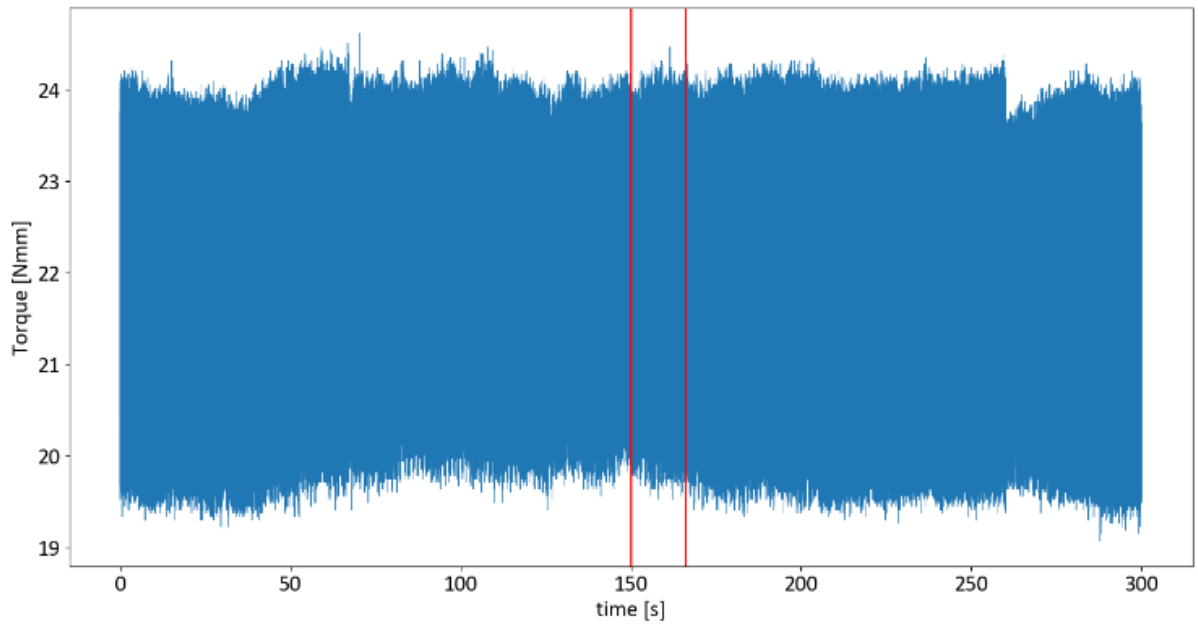

Figure 43: Wind torque data for model test b3

When taking a closer look in figure 44, focusing on the same range, the oscillations again become apparent. As with the force there appear to be 30 large oscillations, but there are now also a lot of smaller oscillations. These will be due to variations in the mechanical output of the electric motor as a result of the poles that the motor switch between during each cycle.

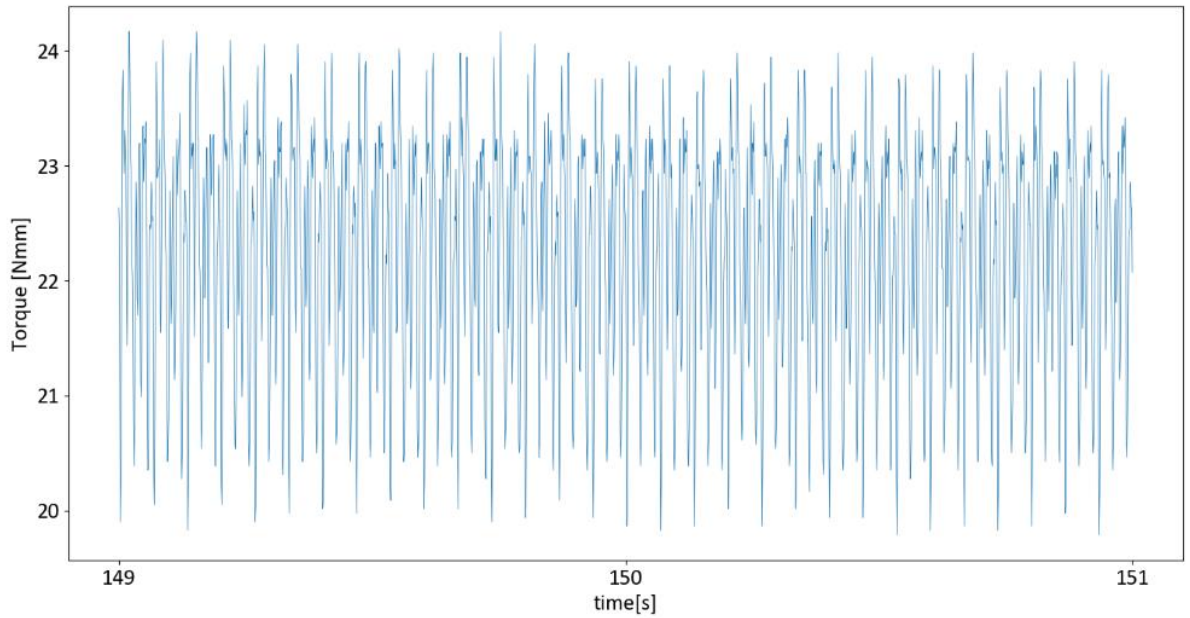

Figure 44: A high frequency zoom in for the wind torque data for model test b3, taken one second on either side of the 150 sec mark.

And again, in figure 45 another zoom in of the wave data can also be observed in the torque data although to a lesser extent than with the force data.

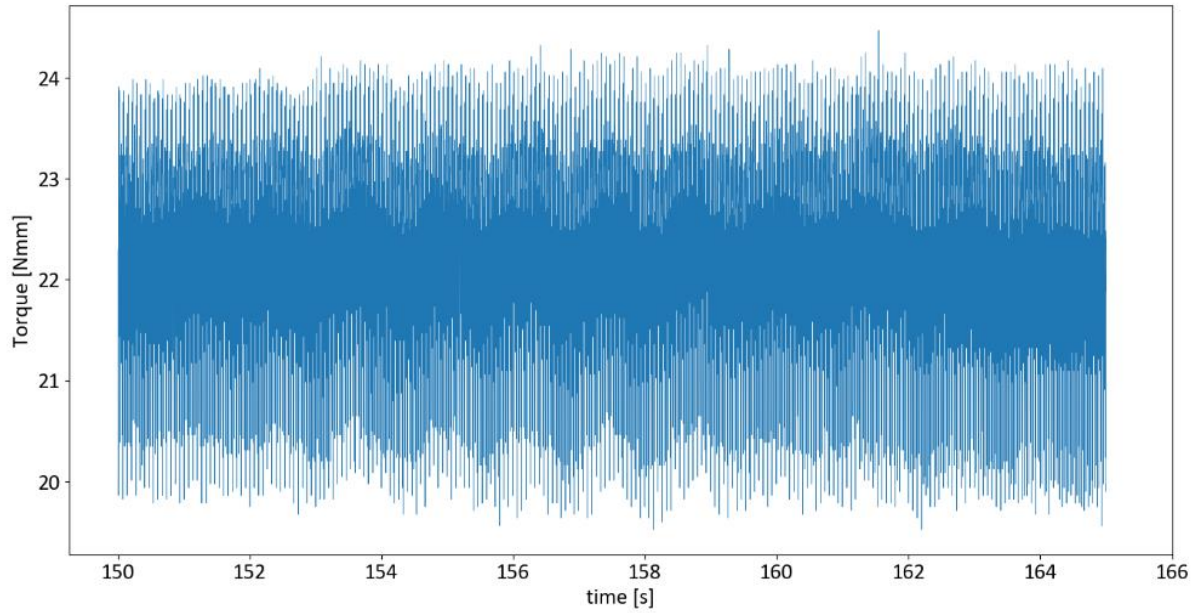

Figure 45: Wave frequency zoom in of the wind torque data or model test b3, indicated by red lines in figure 43.

As can be observed in the previous figures there is a large high frequency oscillation of about 15 Hz in the force and torque provided by the engine. However, as this research focuses mostly on the low frequency response of the mooring system (around 0.1 Hz) this is not much of a concern as neither the model nor the mooring lines could move at such a frequency. Some other research into FOWTs focuses on the tower structural response, which has a much higher frequency. This type of research might want to look into other methods of simulating wind force. The wave force oscillation is relevant for this research, and although it is smaller than the high frequency oscillation at only about 0.1 N

difference, it does have an influence. This effect will, however, be hard to split apart from the effect of the waves on the force in the mooring lines, which will be looked at next. It should further be noted that this wind data was only for one test but is representative for all wind data. Appendix B provides the data set to look up the other model tests and their wind data. During the experiments it was noticed that to keep the wind force at the desired force of 0.81 N the voltage of the electric motor needed to be increased as the experiments continued. The voltage during the last experiment was 50% higher than during the first. This means something in the wind device is losing aptitude, although it is completely unknown what part.

4.4 Mooring line data

The main source of data during the data analysis chapter is the data from the mooring line force blocks, this data is shown for a few selected experiments. Furthermore, issues with mooring line 3 will be discussed. As mentioned before during the model and test design, mooring line 2 is by far the most important of the mooring lines as it is the leading mooring line. Focus is thus put on mooring line 2 over the other two, although they will still be treated.

Figure 46 shows mooring lines 1, 2 and 3 during a zero measurement for the model test m3, so without wind or waves. Here it can be seen that mooring lines 1 and 2 have a roughly static force with some noise of a range of 0.01 N, but that mooring line 3 has significantly more noise at 0.08 N. The garble was determined to be at 50 Hz as can be seen in the spectral analysis in figure 47, indicating an electric issue as the power grid frequency is also at 50 Hz. This already points to issues with mooring line 3 which will be expanded upon further.

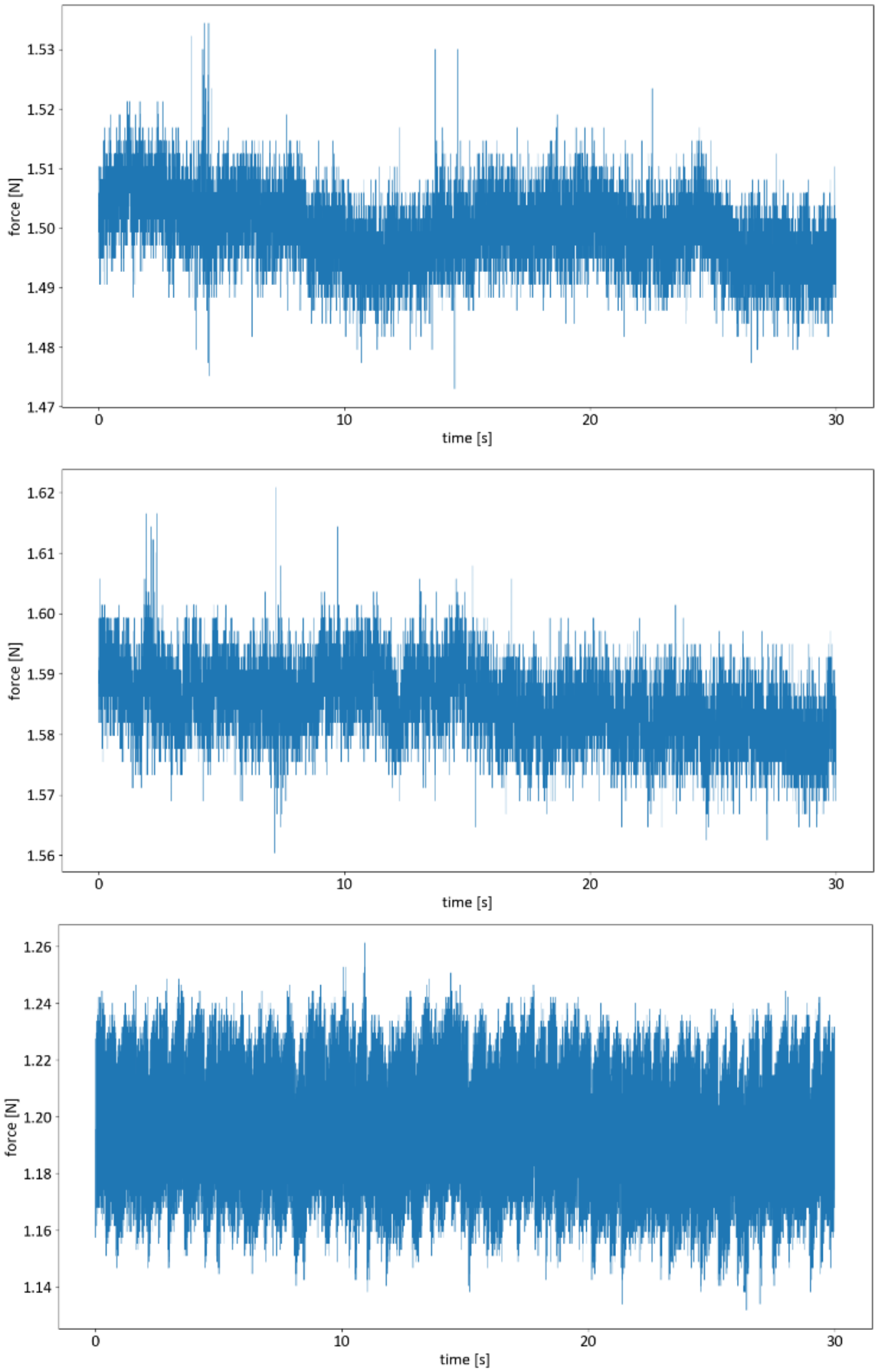

Figure 46: Zero measurement of the mooring line force before model test m3

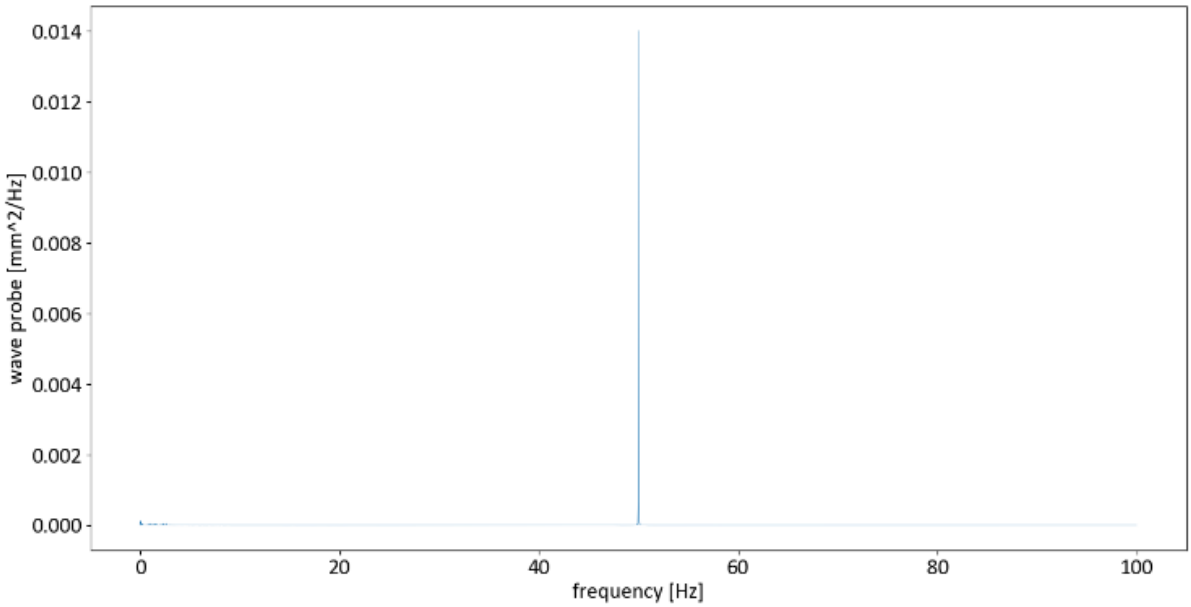

Figure 47: Spectral analysis of the mooring line 3 noise

Figure 48 shows the mooring line force for mooring line 2 during model test m3. The graph shows an average mooring line force of roughly 0.69 N at the start which seemed to have increased further on. Note that the average force found during the previously shown zero measurement has been subtracted to only show the increase in force. After the wave excitation is done (figure 29 of the corresponding wave test serves as indication), a clear low frequency oscillation can be seen at the end of the test where the model slowly comes to rest. It can be seen that the average of the mooring line force seems to have shifted up a bit from roughly 0.69 to 0.71 N. This is most likely due to slack lines which were observed and will be treated later on.

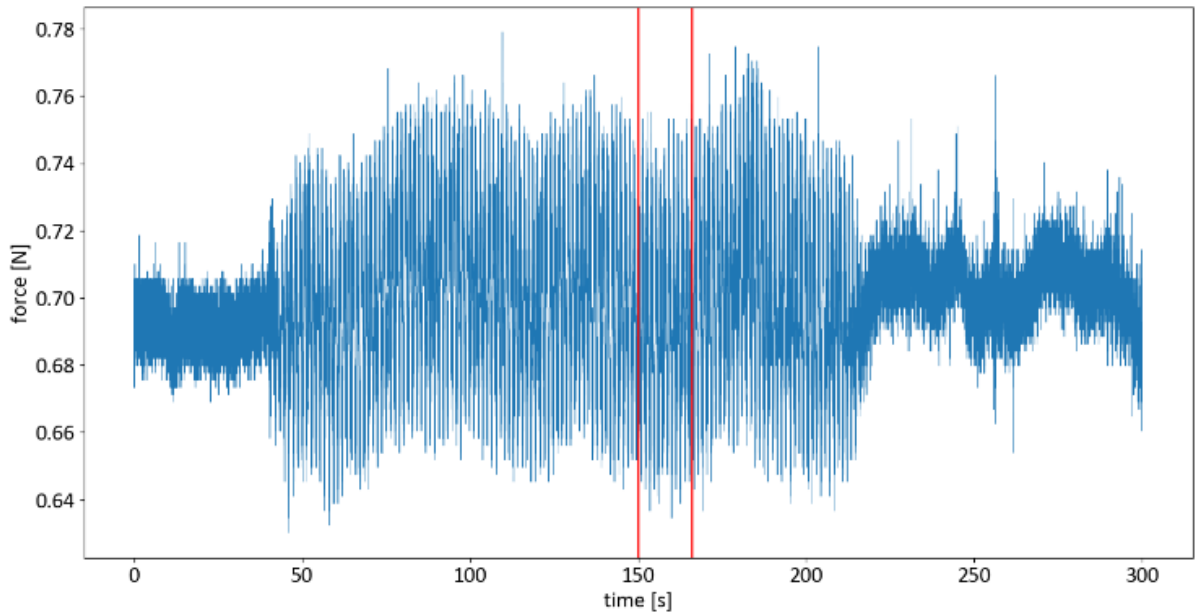

Figure 48: Graph of the force in mooring line 2 for model test m3

Figure 49 shows a zoom in on a part of the above graph. Now the oscillation caused by the waves becomes clearer. As a quick check one can see roughly 11.5 oscillations in this 15 second section,

which corresponds with the 1.3 sec monochromatic wave of m3. Some large spikes can be observed but in general the data also seems to be tightly packed, indicating good confidence.

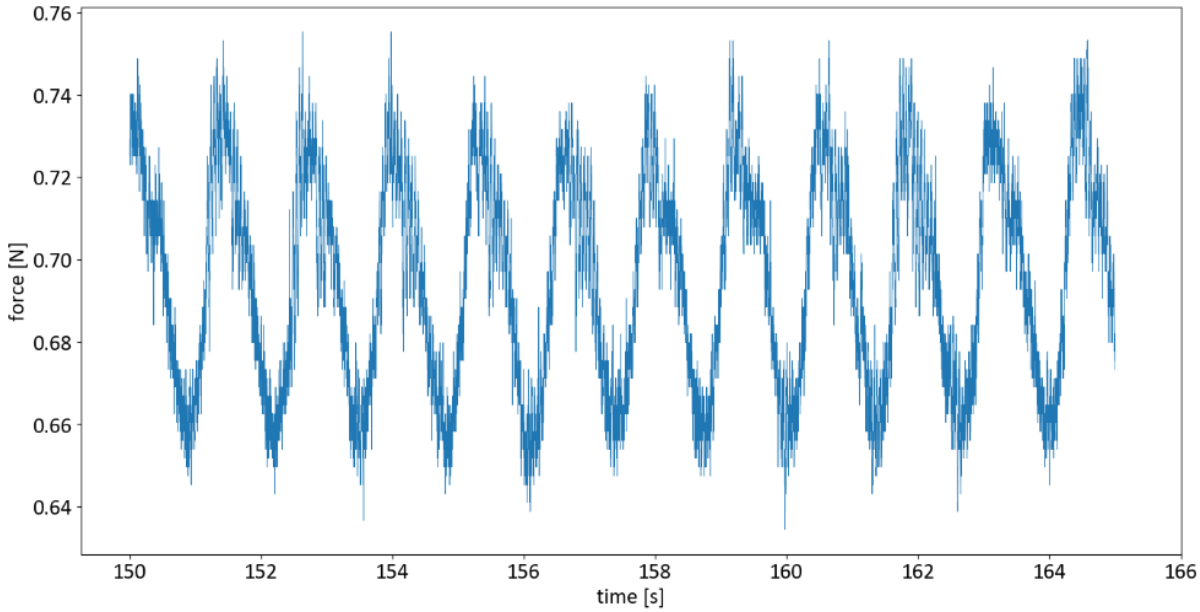

Figure 49: Zoom in of the graph for mooring line 2 force, indicated by red lines in figure 48.

Figures 50 and 51 show two more zoom-ins of the force graphs for mooring line 1 and 3 respectively. Mooring line 1 seems to behave normally and shows a similar response to mooring line 2. Note however that due to the zeroing of the force to the zero measurement the force is negative. This does not indicate that there is a compressive force but that there is reduction in the pretension. Of some concern is again the large amount of noise of mooring line 3 and the introduction of spikes into the data at evenly spaced intervals.

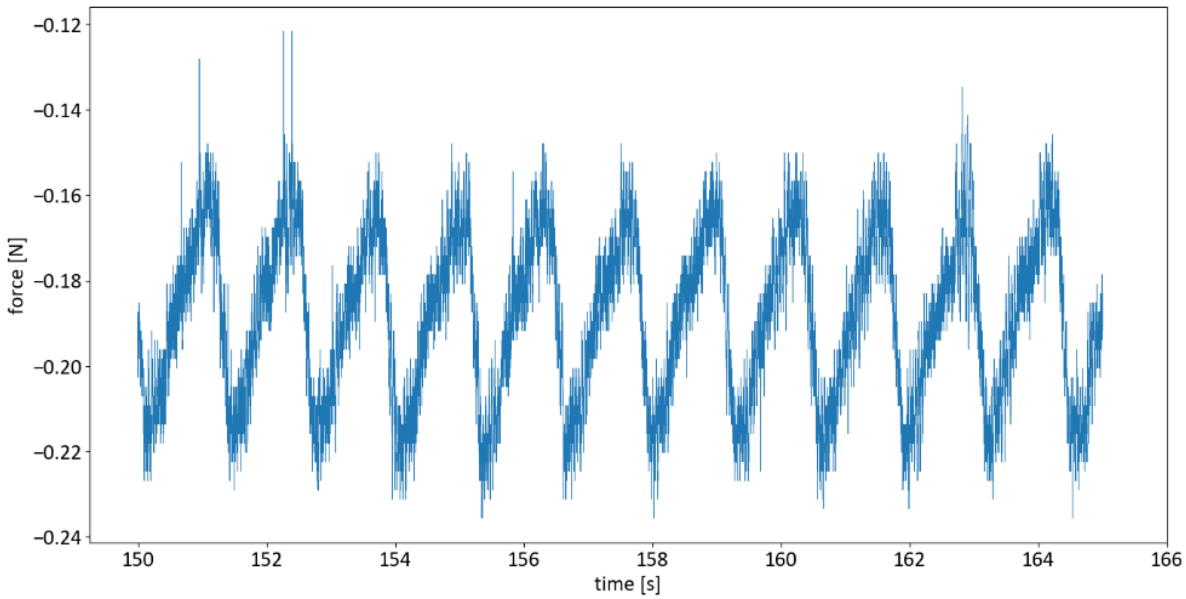

Figure 50: Graph showing the force in mooring line 1 on a short interval.

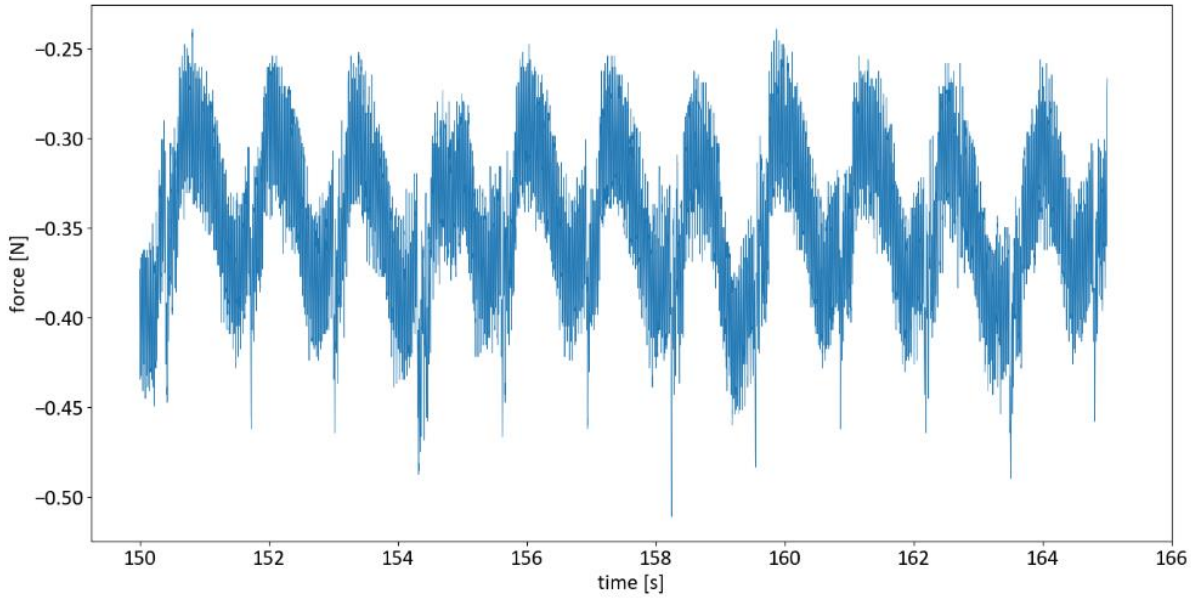

Figure 51: Graph of the force in mooring line 3 shown for a short interval.

Besides the garble mooring line 3 also showed a large drift of about 0.1 N, versus the 0.05 N amplitude of the wave frequency. Figure 52 shows this drift over the entire test run. This drift is especially troublesome as it interferes with the low frequency response research of this thesis. The issues with mooring line 3 could not be resolved in the timeframe of this project. The symmetry of the model also means that mooring line 1 can stand as a good data source on its own, analysis is thus based solely on mooring line 1 and 2.

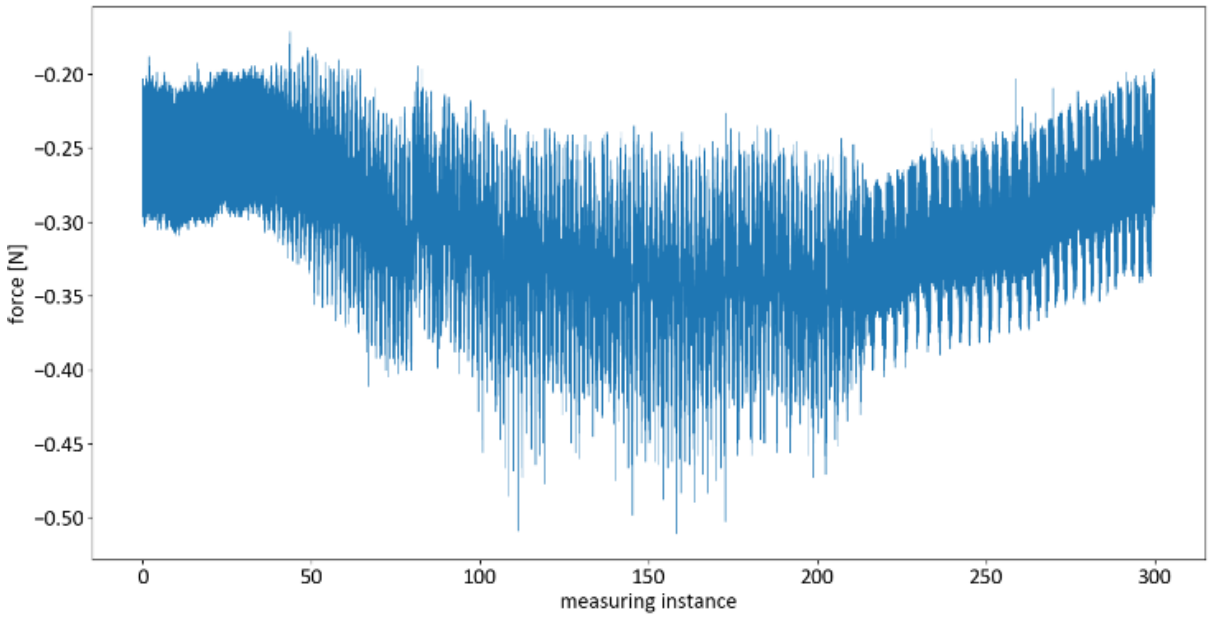

Figure 52: Graph of the force in mooring line 3, showing a large drift in the overall response.

Figure 53 shows the force in mooring line 2 for model test b3 with mooring system 1. When the bichromatic wave is tested it can be seen that the force has a very different response than with the monochromatic wave m3. Now the shift after the test becomes clearer, as the test began at 0.67 N and ended on an average of 0.71 N. This is again the consequences of the slack lines which are discussed later.

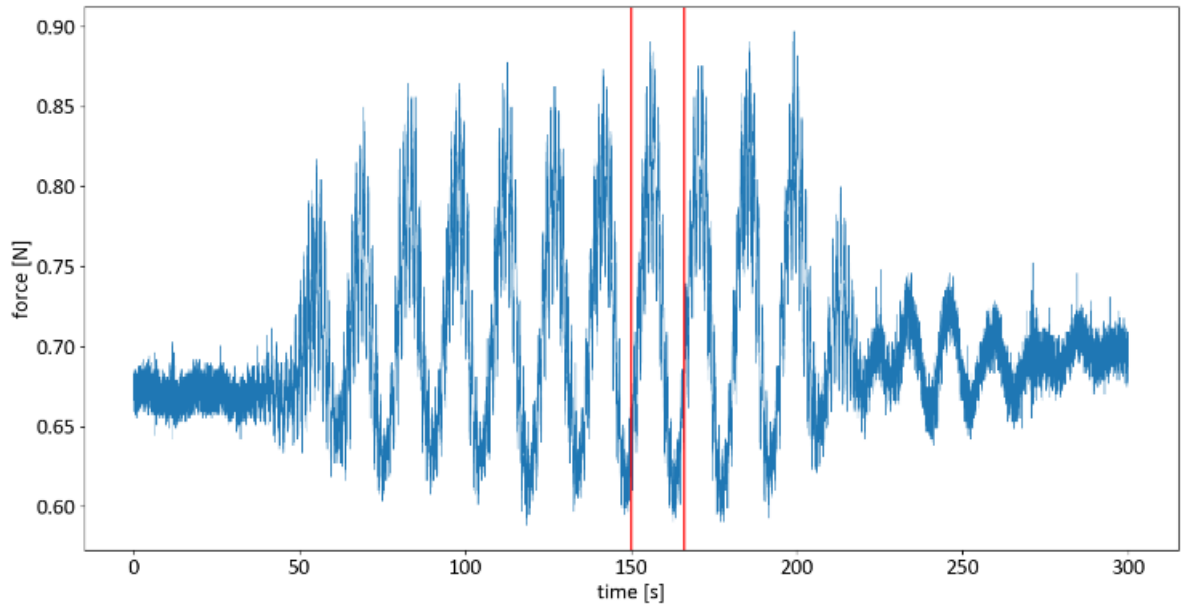

Figure 53: Graph showing the force in mooring line 2 during model test b3.

Figure 54 shows the repeat test for the b3 model test. As can be seen the tests show a large amount of similarity the small spikes found in the repeat tests will be filtered out during the post processing. A similar check has been performed for all other data, which shows that the data is very consistent between repeat tests.

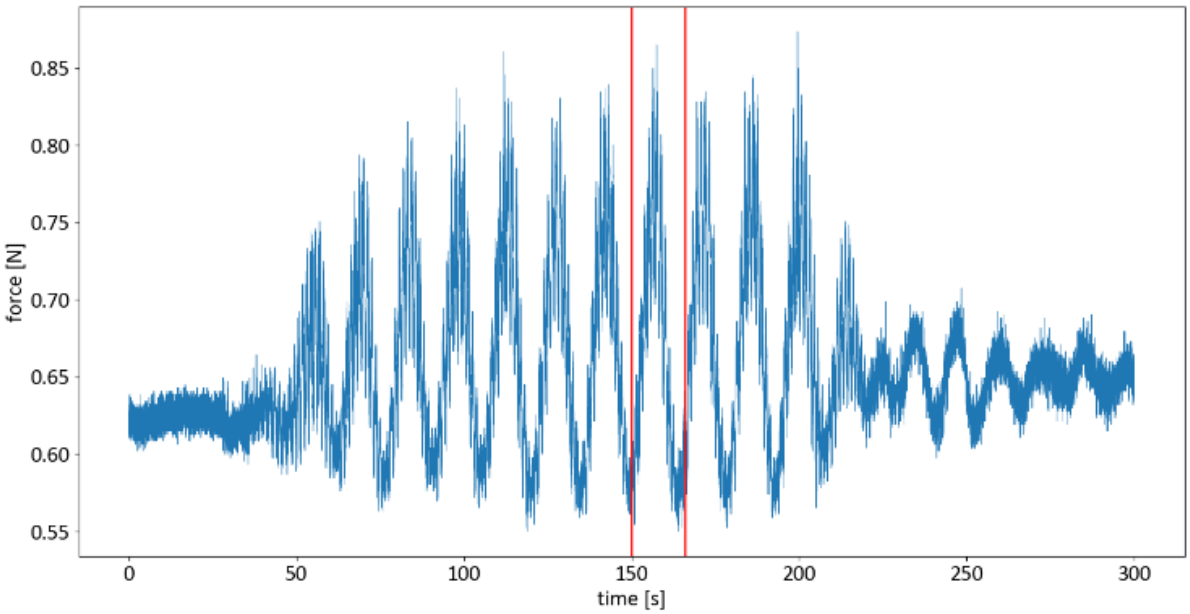

Figure 54: repeat test for model test b3, showing the force in mooring line 2.

Figure 55 shows the force in mooring line 1 of mooring system 1 again for model test b3. It can be seen that this data shows a different pattern from mooring line 2, where the response is more symmetrical. This is a consequence of slack lines present in mooring system 1.

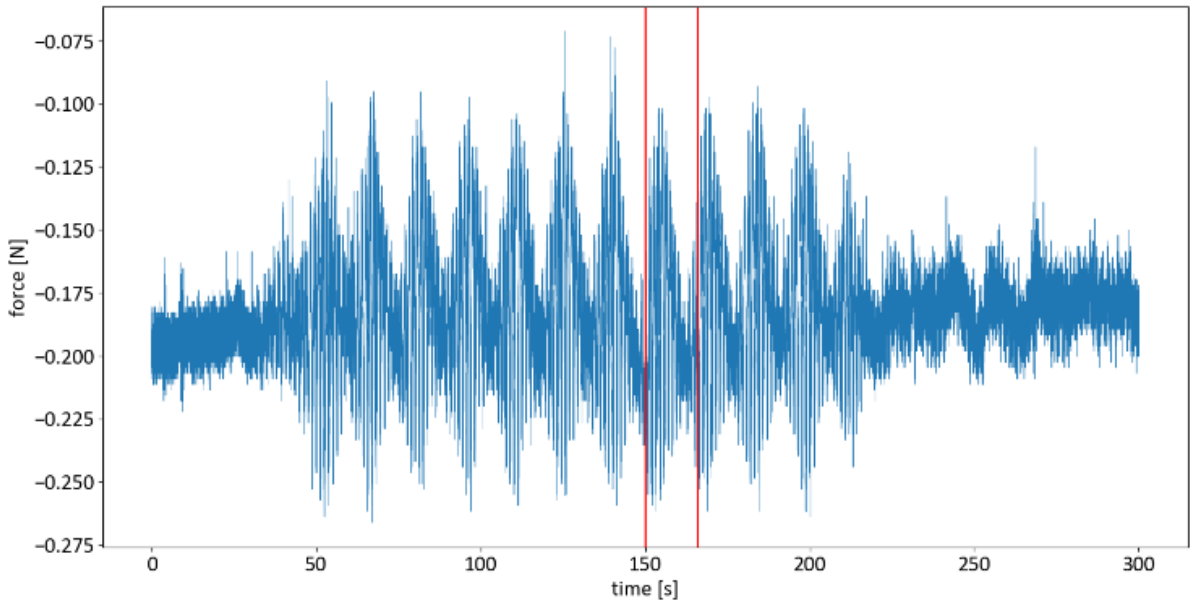

Figure 55: mooring line 1 force for model test b1

During the experiments for mooring system 1 with wind it was noticed mooring lines 1 and 3 were slack. Implications of this will be discussed as it might provide the key to later findings.

As one might notice the total length of the mooring line in system 1 of 1.9 m was quite long for a 0.92 m footprint and a 1.25 m depth. This caused the back mooring lines to tend towards hanging slack in this configuration when the wind force was applied. Especially during low frequency wave tests, which were aimed at the eigenfrequencies of the mooring configuration the back mooring lines would be slack during backwards motion. Figure 56 shows a photo of the back mooring lines being slack during a wave test. The lines are completely vertical from this perspective with the only catenary shape remaining in the sideways direction. The mooring line moves to the anchor points by turning on the bottom plate.

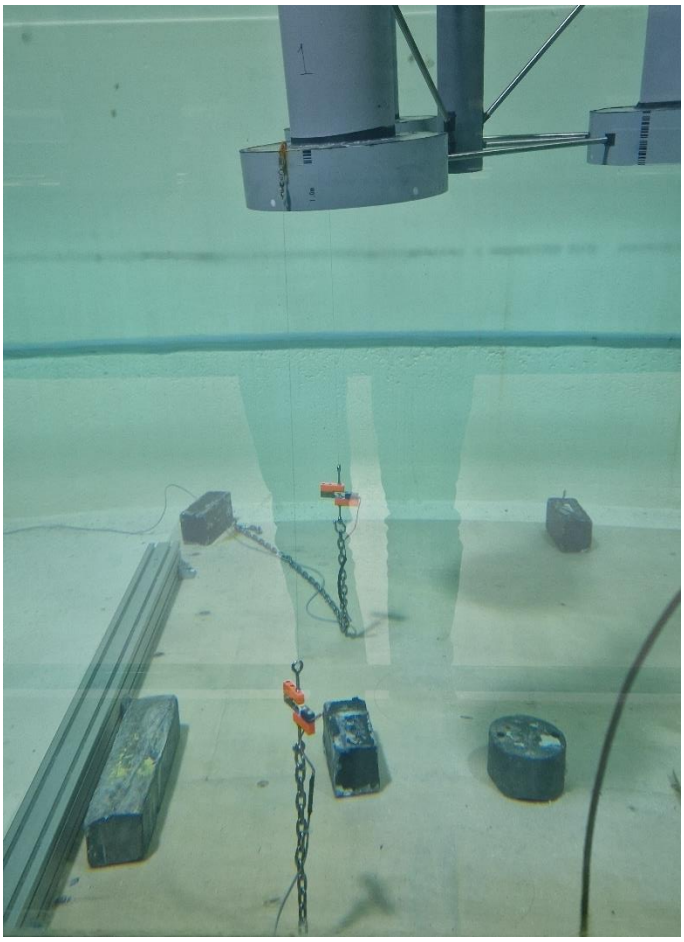

Figure 56: Photo of the two back mooring line hanging slack.

This had a number of consequences. For starters, this meant that there were two neutral positions, which became apparent during the mooring line data. This could be seen by the fact that after a test the model would lay still in a different position than before the test. This is because the slack mooring lines would partially pull back on the model and form a new equilibrium with the front mooring line.

A second consequence is that during the bichromatic tests the front mooring line would regularly become the only mooring line resisting backwards motion, effectively giving the model a single point mooring system. This increased the force on the front mooring line. During strong forward motion however, the back mooring lines would pick up their slack and resist the motion. This caused mooring line 2 at the front to have an asymmetric response to the waves as the stiffness of the mooring system would change suddenly.

It should be noted that due to the position of the force transducer the force on the mooring lines was not 0 as there was still the vertical weight of the chain and the sideways catenary line shape present. The catenary shape in the surge direction, however, was not present anymore.

Mooring system 2 was made to be more stiff than mooring system 2 by taking in some of the fibre rope used in the upper part thus counteracting this issue. This removed the phenomena from the tests. The difference can later be seen in the data analysis chapter.

Mooring system 2 data is also verified below to check for repeatability and inconsistency. Figure 57 shows the force on mooring line 2 with this system during the b4 model test. Please note however that the y-axis is shifted down by 0.05 N compared the examples from figure 53.

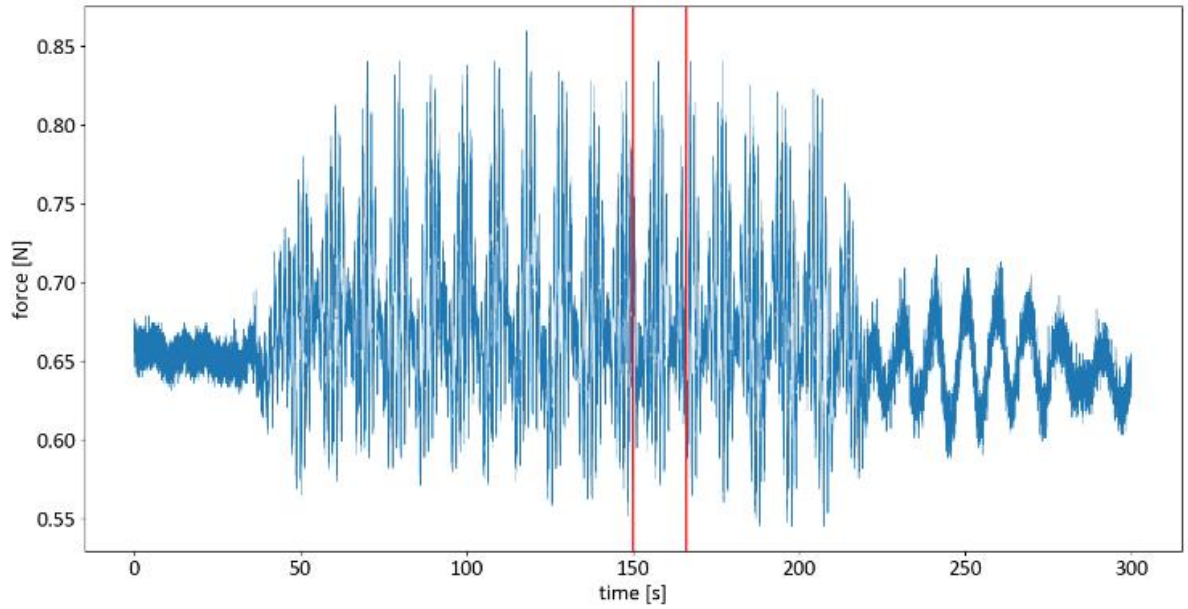

Figure 57: mooring line 2 force during model test b4 with mooring system 2

Figure 58 then shows the repeat tests for this model test. As with mooring system 1 good repeatability is observed. Although the repeat test shows a slightly smaller response in general. With peaks not reaching as far up or down as in the first test.

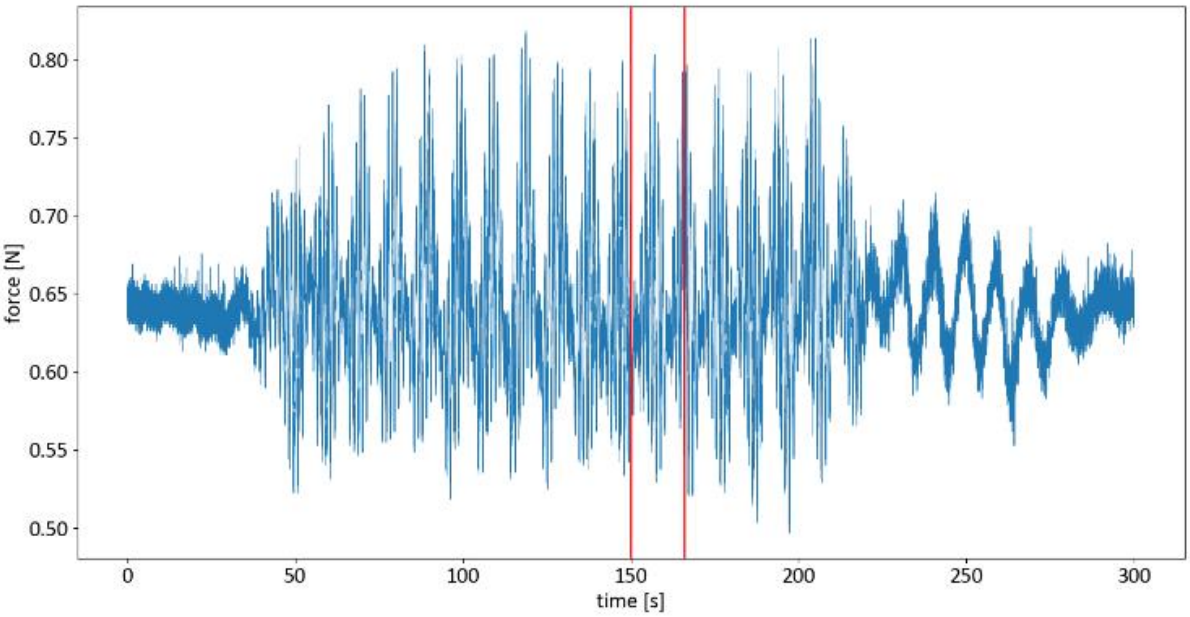

Figure 58: mooring line 2 force for the repeat test of model test b4 with mooring system 2

Figure 59 show the force in mooring line 1 for this same test. As can be seen the mooring line force is now more symmetric compared to the one in mooring system 1, although it is a bit hard to see due to the shift in neutral position.

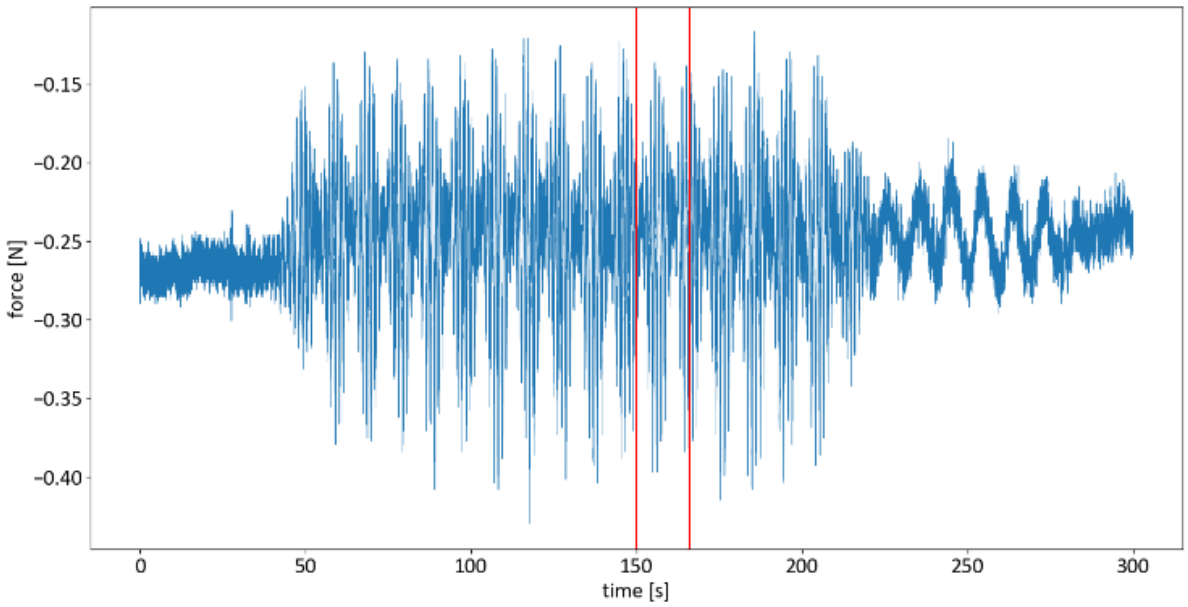

Figure 59: mooring line 1 force for the repeat test of model test b4 with mooring system 2

4.5 Surge data and stiffness

In this section the surge data will be verified to check for repeatability and to check for large inconsistencies. The stiffness of the mooring line will be calculated to see if it matches original intension.

Figure 60 shows the surge data for the monochromatic m3 model test. Plotted is the surge in meters. It got a zero position before wind application, so the wind force gives it an offset slightly over 160 mm. As can be seen the overall reach of the surge is about 20 mm back and forth and here the phenomena of the slack lines becomes more apparent as the model ends about 5 mm further back than it started.

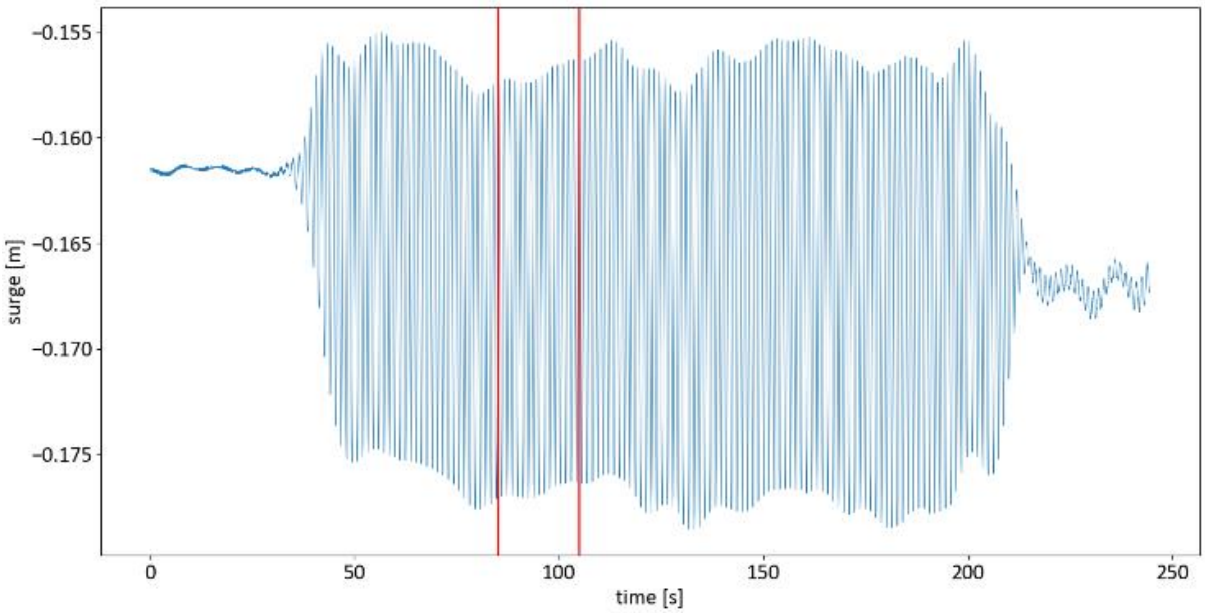

Figure 60: Graph showing the surge data versus the recording frame for model test m3.

As with the mooring line data a zoom of the data shows a better picture of the waves. Figure 61 shows this zoom. This particular section shows a slight increase in the average as can be better seen in figure

60. In general, the amplitude of the data seems to vary during the experiment by a few mm. At that scale it might simply be the case that a link in the chain falls one way or the other.

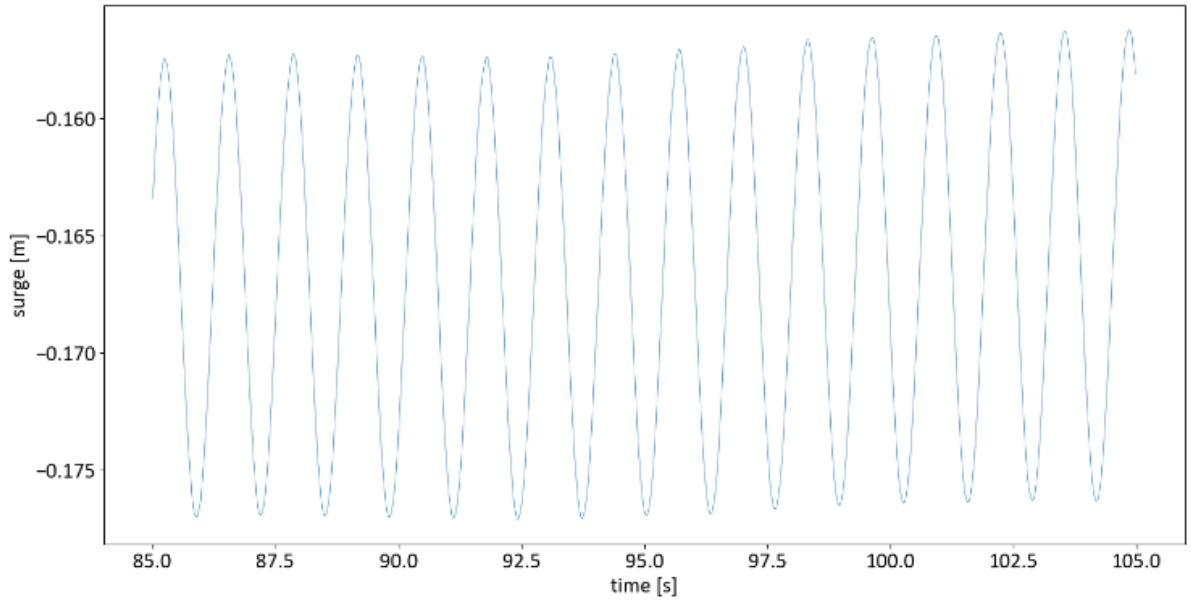

Figure 61: Zoom of the graph of the surge per frame for model test m3, indicated by red lines in figure 48.

Figure 62 shows again a surge plot versus the time, this time of b3. And the zoom in in figure 63

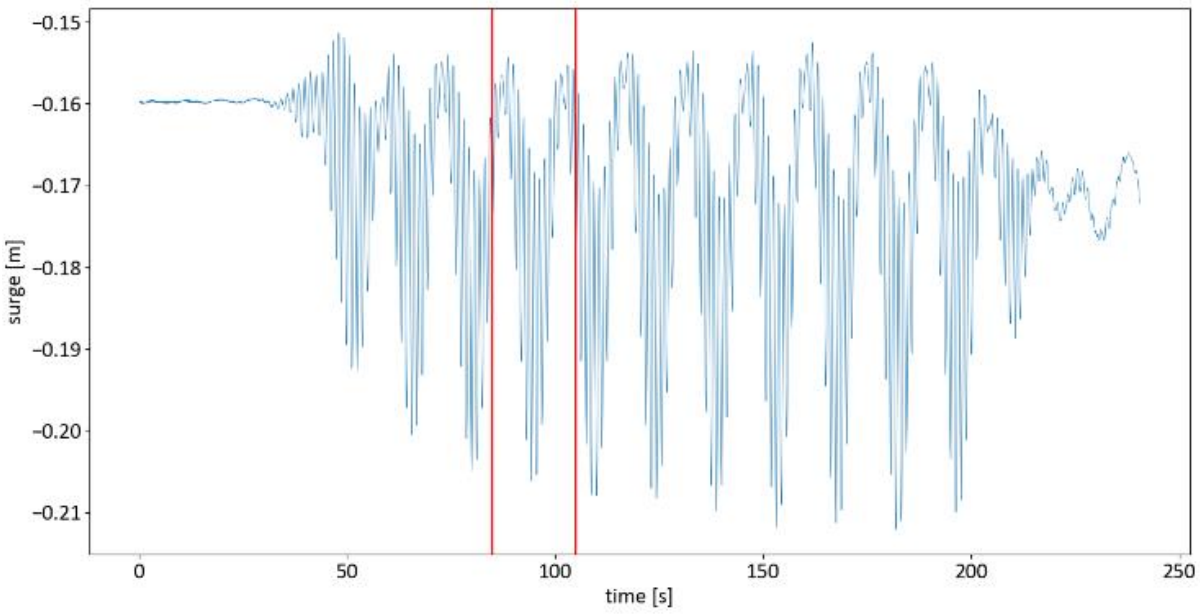

Figure 62: Graph showing the surge data versus the recording frame for model test b3.

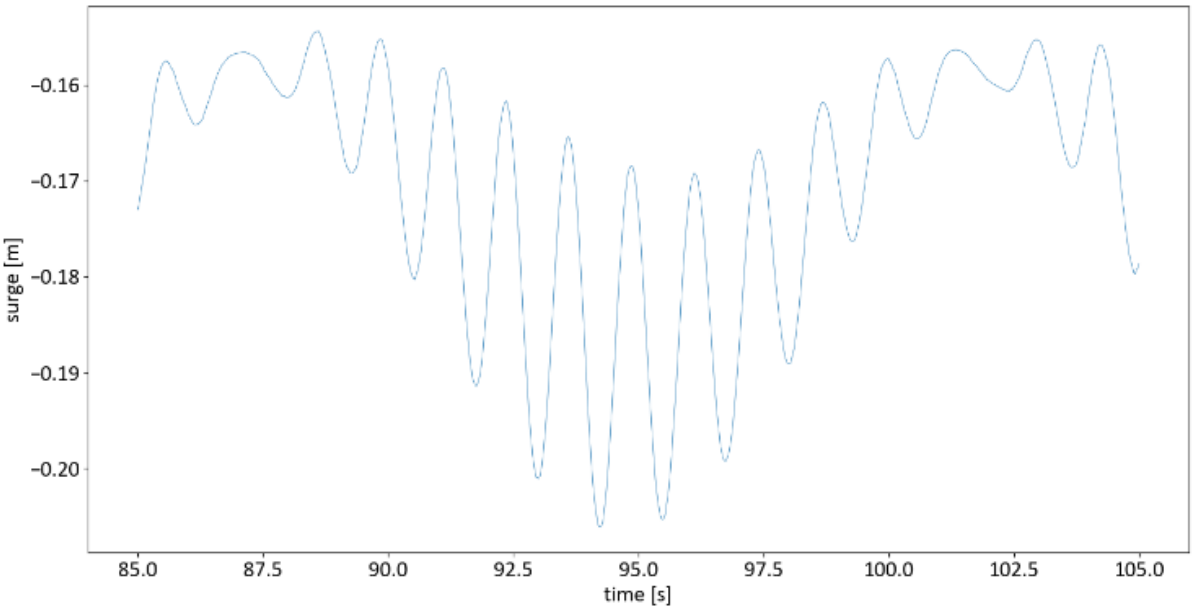

Figure 63: Zoom of the graph of the surge per frame for model test b3, indicated by red lines in figure 50.

Figure 64 shows the repeat test for the b3 model test again showing a very repeatable experiment.

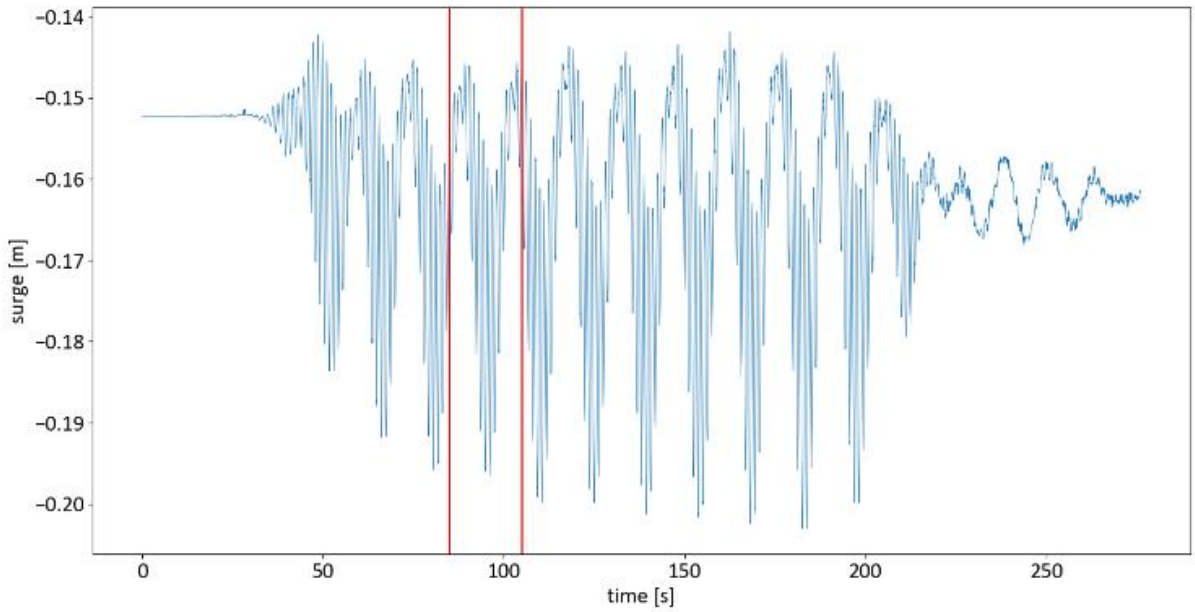

Figure 64: surge in repeat test for model test b3

Now that both the surge and the mooring line force have been examined, the two can be combined to take a look at the stiffness of the mooring lines. The original goal for the stiffness in mooring system 1 was a stiffness from OC5 project scaled down to 5 N/m. The designed mooring line matched this scaled stiffness numerically. Using the wind application tests performed to catalogue the performance of the wind, the stiffness for both mooring systems can be determined. To do this the data first had to be synchronized as there was no synchronization light during these tests. This was achieved relatively simply by taking the maximum of both the surge and the mooring line force as these would both correspond to the short overshoot when the equilibrium position was reached.

After the data is synchronized short intervals of about 500 ms are taken in which the increase in surge and force are recorded. The force difference is then divided over the surge difference to get a stiffness for each interval. Figure 65 shows the mooring line force during the wind application test with mooring system 2 with the intervals indicated with the vertical bars and the maximum indicated with the red dot.

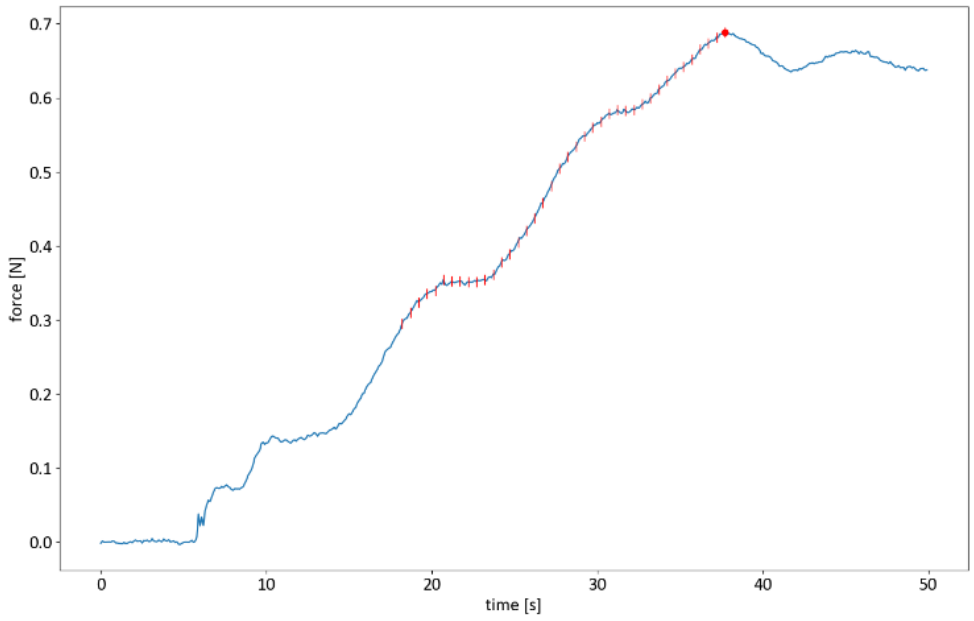

Figure 65: wind application test mooring line force for mooring system 2

Doing the calculations this leads to the following graph for the stiffness per interval for mooring system 1, shown in figure 66. As can be seen there seems to a bit of an oscillation motion, which is due to the wind force being applied incrementally. There is also a slight upward trend in the stiffness, indicated here by a linear trend line for simplicity (although the increase is most likely exponential). This increase is most likely due to the non-linear behaviour of mooring line stiffness, as it becomes harder to extend the line further as extension is applied. The average stiffness found is 4.7 N/m, which is not far of the desired 5 N/m value.

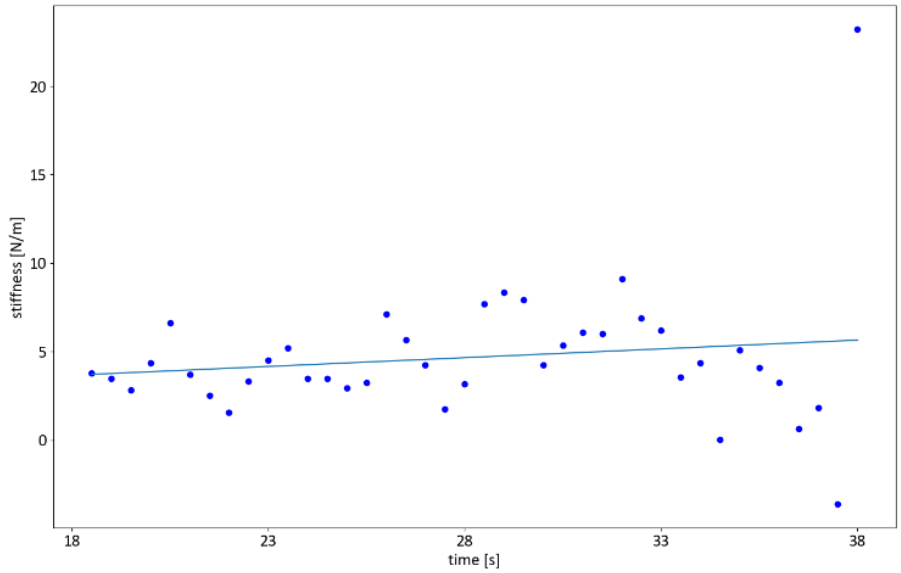

Figure 66: Stiffness per interval for mooring system 1

Figure 67 shows the mooring line stiffness per interval for mooring system 2. Here the oscillations are a lot larger, but the underlying behaviour remains the same. As with mooring system 1 an increasing trend can be found. The average stiffness is 5.5 N/m, which would correspond with the increased tension on the system.

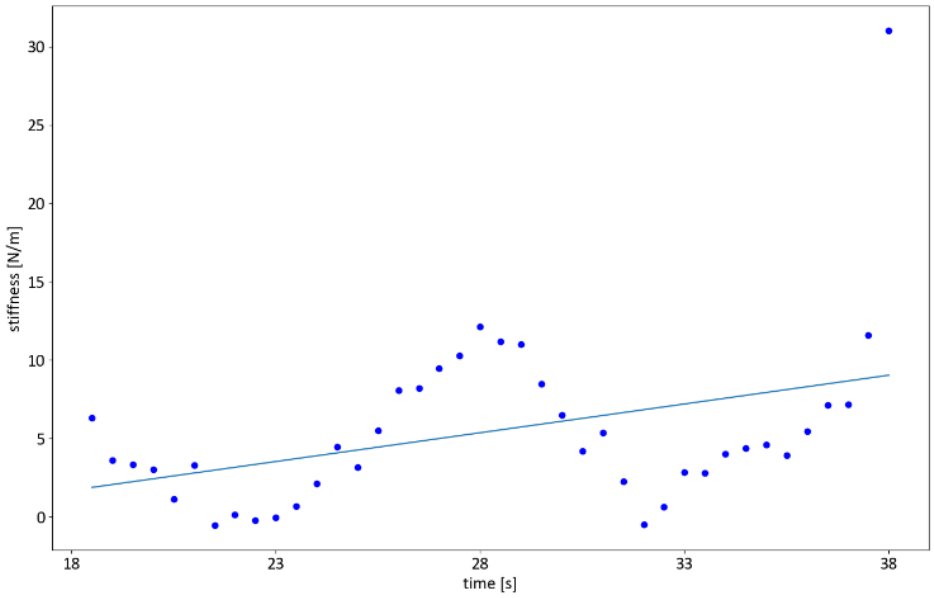

Figure 67:Stiffness per interval for mooring system 2

As mentioned before the stiffness shows large oscillations, this is because of the start stop behaviour seen in figure 65. To get another reading of the stiffness the differences between the plateaus in figure 65 are used. The points taken for this are shown below in figure 68. This analysis yields a stiffness of 3.5 N/m for the first difference, 4.5 N/m for the second difference and 5.6 N/m for the third. This again shows a clear increasing trend line, but also yields and average stiffness the entire range of 4.3 N/m. This is significantly lower than with the short interval method and crucially lower than mooring system 1. A clear number for the stiffness is thus not obvious and for future research dedicated stiffness tests are advised.

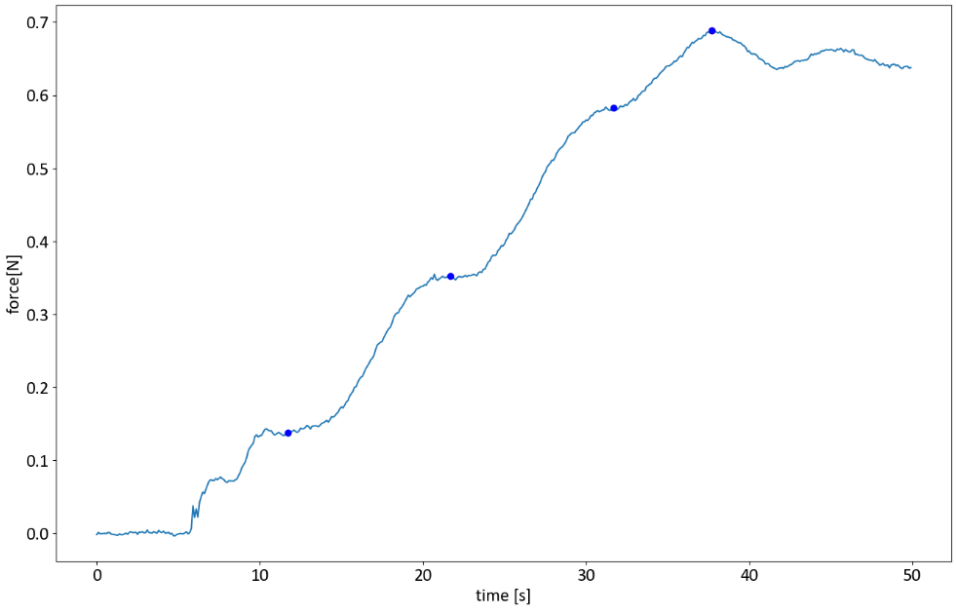

Figure 68: Force in the mooring line during the wind application test, with points indicating the used plateaus.

As the tests were performed with and without wind and as the stiffness analysis does show a changing stiffness based on surge, it has been decided to separate the mooring systems further from this point into systems with and without wind. This thus effectively creates four different mooring systems: mooring system 1 with wind, mooring system 1 without wind, mooring system 2 with wind and mooring system 2 without wind. In the coming chapter these four systems will be treated as such where applicable.

5 Data analysis

The goal of the data analysis is to find out what causes the forces in the mooring lines, what the influence of the surge natural frequency is and what other effects are at play, but to achieve this goal more than just the time series data is needed. To achieve this a spectral analysis was performed. This chapter discusses this analysis and the results than can be drawn from them.

5.1 Data preparation

This section provides an explanation of all the steps taken to make the data more accessible and usable. Choices in down-sampling, filtering and the synchronization are expanded upon. With this processed data the rest of the analysis can then be done. A flowchart is provided in figure 69 to visualize the process.

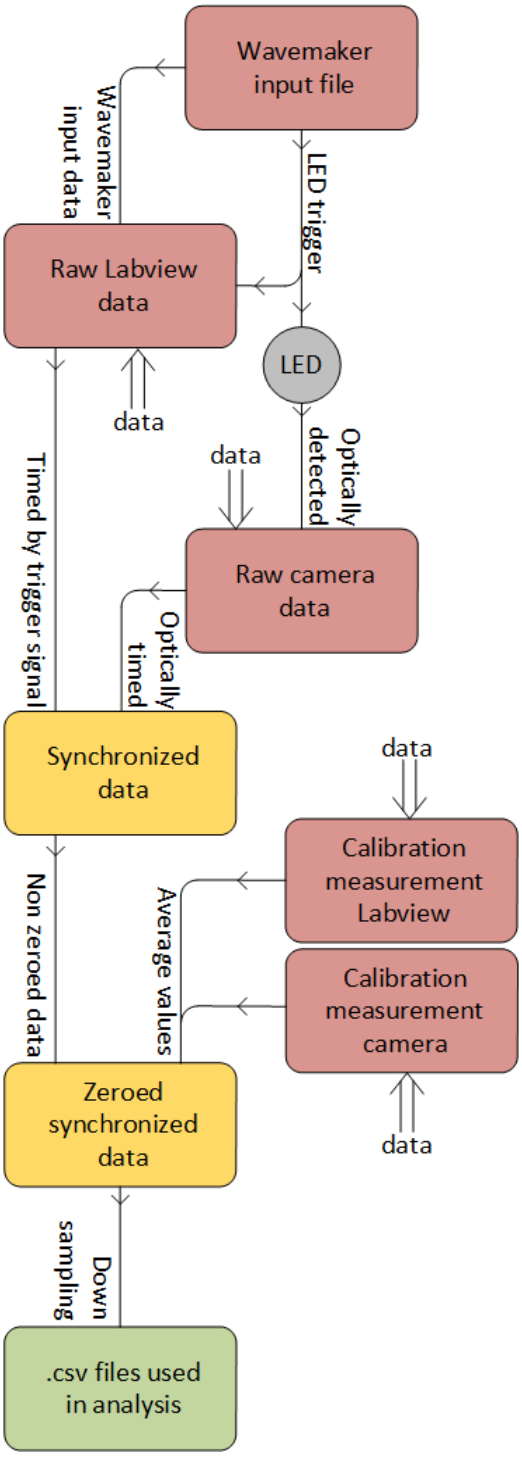

Figure 69: Flowchart of the data preparation

If you count the measuring devices in the device section, there are eighteen different data sources which need to be put together. The bulk of the data (everything apart from the movement) is already put together in the Labview environment. These sources are thus already synchronized. The second data source is the movement recorded by the cameras which needs to be matched in time with the Labview data. This was done by a timed LED visible in the camera system. The trigger signal for this LED was recorded in the Labview data. The actual synchronization then happens in python (code provided in appendix B) by simply analysing the footage frame by frame until a large increase in the brightness at the LED's location is recorded. The moment this trigger signal happens and the first frame it is seen then provide the synchronization point of the data collected, which is also the start of the data as everything before that is not relevant.

It should be cautioned that the end of the data is not limited, as the camera system had to be turned off manually. This leads to differing end times in the movement measurement, the target was to do 240 seconds, but some do way more. Thus, when handling the data, one should watch out that the data is only in sync looking from the starting values and not from the final values.

Data is then zeroed to the static position, this is done by the use of the zero-measurement taken at the start of each test, mentioned in the section on the testing process. The average of the measuring parameters during this zero-measurement become the baseline, meaning that if nothing happened at the tests all data

sources would output 0, so 0 N of force on the mooring lines and 0 m of surge. However apart from the tests where no wind is applied and where the wind application is tested all tests have the application of wind unrecorded. This means that most tests do start with a force in the mooring line and some surge. For future research it is advised to record the application of the wind as well.

As was stated in the section on the measuring devices the Labview systems measure with 1000 Hz, while the camera system measures at 40 Hz. During the data preparation these data streams were both down sampled to 10 Hz. The 10 Hz was chosen to still provide a high resolution in time for all measured data whilst removing high frequency phenomena such as the spinning of the motor in the wind device and the 50 Hz power grid frequency in mooring line 3. This down sampling was done by simply taking the average of the 100 data points in lab view or the 4 data points in the camera system. This average would then be moved to the first location of the two value arrays averaged. This does mean that the higher resolution data may be shifted forward in time, but the effect should be negligible at 10 Hz, especially when looking at low frequency effects. And although the camera system is averaged way less than the Labview system, the accuracy of the camera system readily makes up for that, having less noise during positioning and thus giving a very accurate picture of the data.

This down sampled data is saved in a comma separated values file, or .csv for short. In these each row is a new time instance and each comma separated values a data source. The link to these files is provided in appendix B.

Due to the down sampling to 10 Hz the PSD cannot have any higher frequency components than a frequency of 5 Hz or 15.7 rad/s. This should however not present a challenge as it is more than triple that of any wave frequency.

Figure 70 shows a power spectral density graph for wave test b2 on mooring system 1 as an indication for how these graphs look in the end. As can be seen two larger spikes around the wave frequencies can be seen at 4.95 rad/s and 5.24 rad/s. These can be traced back to be at the used wave frequencies, but more on that in the next section. Three peaks can be seen in the lower frequency, going from left to right these are the static displacement at 0 rad/s (corresponding to the pretension and wind force), the difference frequency of wave set b2 and the surge natural frequency (these are the low frequency oscillations seen in the earlier time series like figure 53).

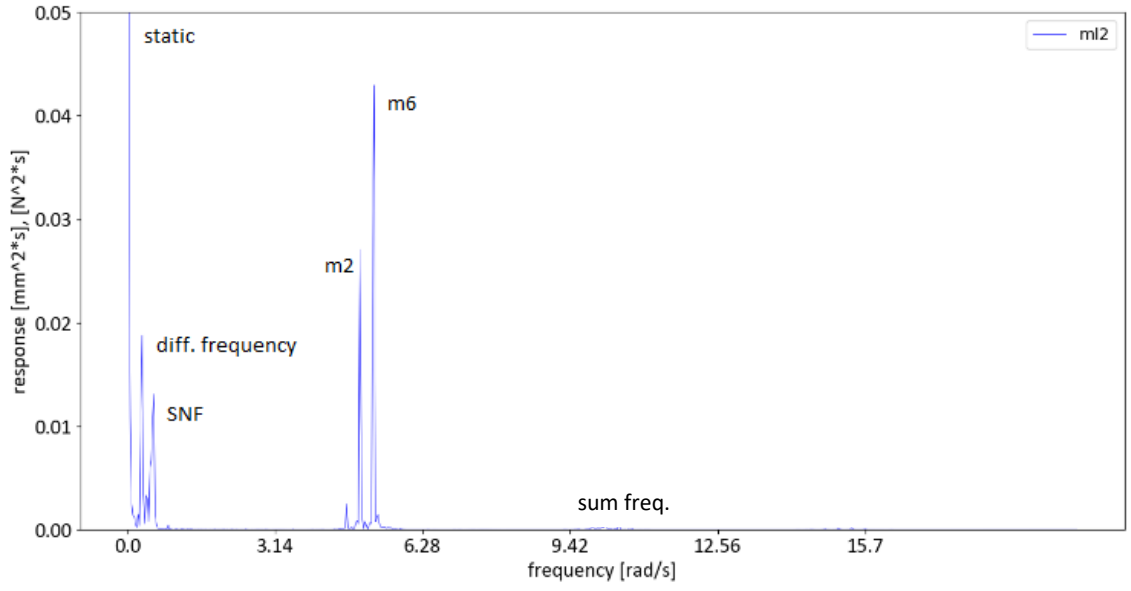

Figure 70: PSD of the mooring line force in line 2 for test b2

In order to achieve a good representation of the data it is furthermore important to look at a steady state situation during a spectral analysis. The range of the data to be analysed was thus chosen based on the consistency within the data. This range was determined per test, with repeat test of the same condition getting the same range for repeatability. The range for every can be seen in appendix F by taking the first and last red vertical line and in general can be summarised as every beating pattern minus the first and last. Some manual exceptions were made when the beating pattern became too inconsistent.

5.2 Wave Data analysis

Figure 71 shows the PSD of the wave elevation measured by wave probe 3 during the b3 model test with mooring system 1 (see figure 20 for the differences between the mooring systems, mooring system 2 being the stiffer of the two). It can be seen that there are two large peaks in the wave frequency corresponding to the wave components that make up bichromatic wave b3. There is also a very small peak, with the height of 35 mm^2*s located at the combined frequency. This peak is not visible on the PSD. This clearly shows that the waves consist of almost exclusively wave frequency excitations and that there are no low frequency excitations found in the wave data.

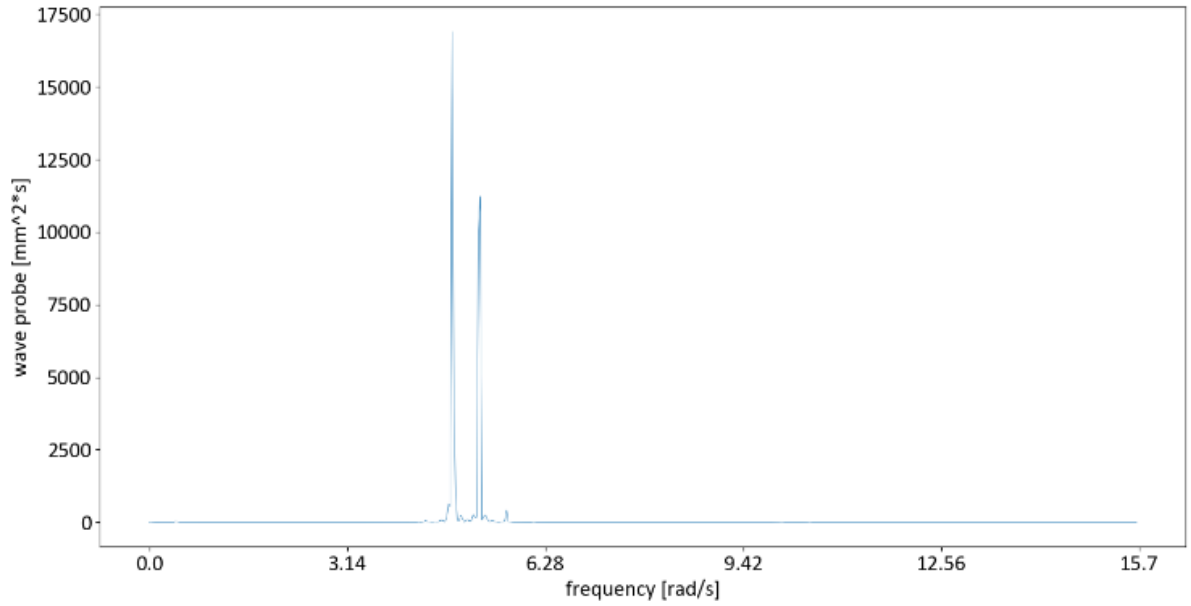

Figure 71: Wave elevation from wave probe 3 during model test b3 with mooring system 1

Figure 72 shows the wave elevation measured from wave probe 3 for model test b4 with mooring system 2. Although it can be seen that the peaks are somewhat lower at 10000 mm^2*s versus 14000 mm^2*s, the general picture remains the same. Two large peaks corresponding to the components and a very small peak at the low frequencies.

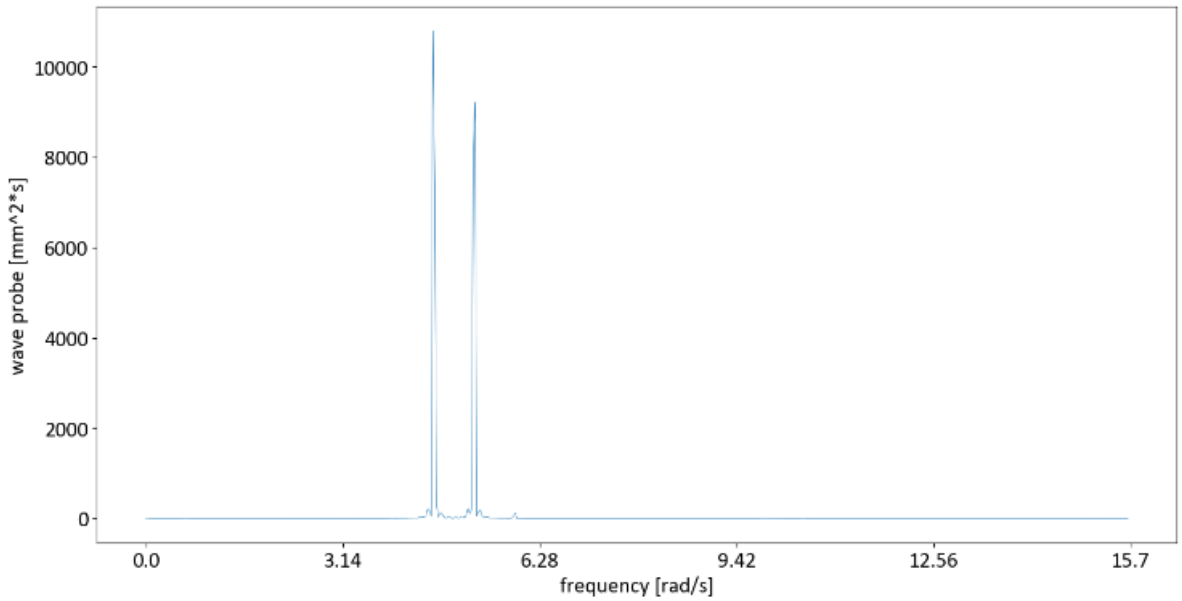

Figure 72: wave elevation from wave probe 3 during model test b4 with mooring system 2

5.3 Surge data analysis

Figure 73 shows again a surge plot versus the time, this time of b3. As can be seen the larger amplitude is clearly visible. An asymmetric response is also very visible, this is caused by the wave drift forces which move the model in the propagation direction of the waves. The overall peak to peak difference is about 50 mm. Which is more than twice the 20 mm amplitude found during the monochromatic tests.

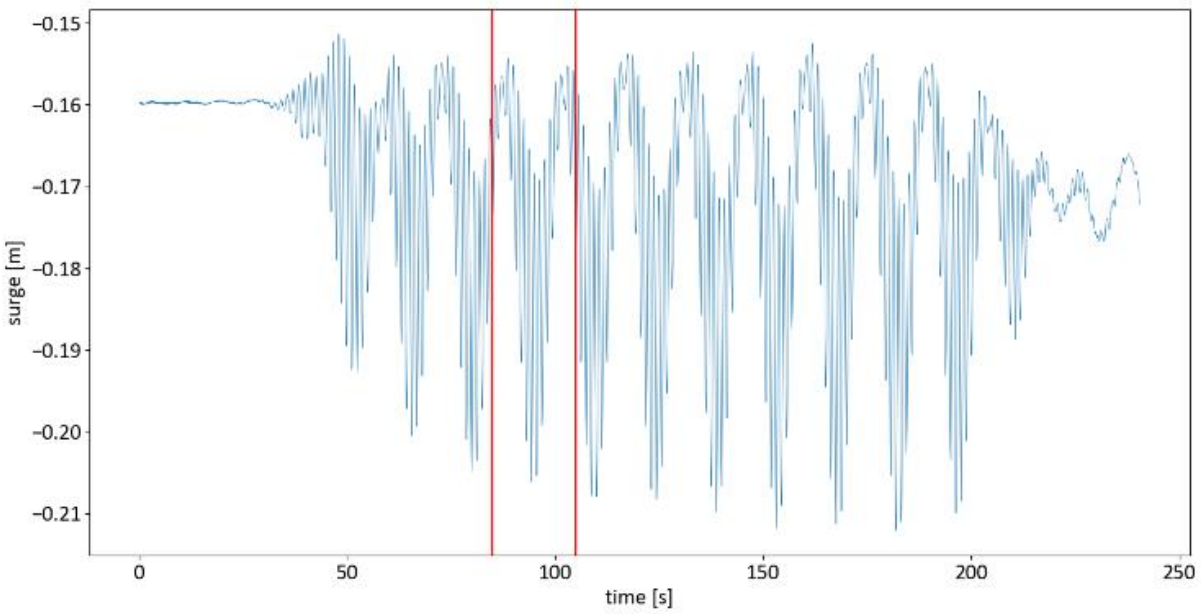

Figure 73: Graph showing the surge data versus the time for model test b3.

Furthermore, figure 74 shows a zoom on one of the low frequency waves in this graph, where the individual wave is more clearly visible. The asymmetry also stands out as the upper part of the graph goes down about 10 mm at the peak with the lower part going down 30 mm.

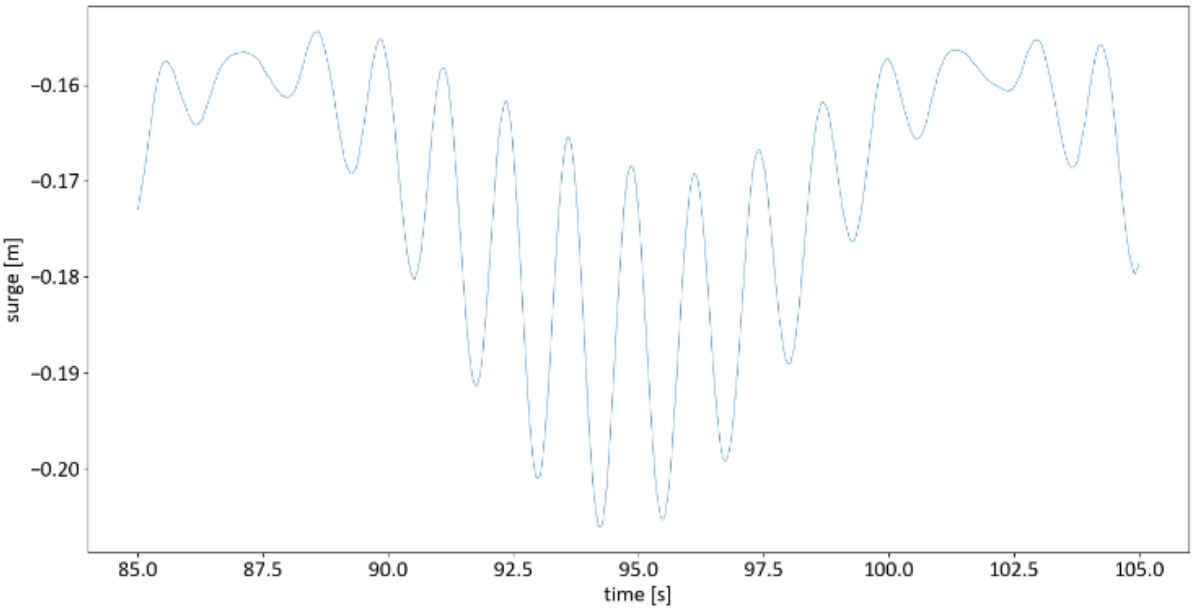

Figure 74: Zoom of the graph of the surge versus time for model test b3, indicated by red lines in figure 50.

Figure 75 shows a PSD of the surge of the b3 model test with mooring system 1. Here the low frequency peaks of the difference/natural surge frequency are very clearly visible compared to the wave probe PSD. Also visible is the static frequency associated with an offset. This is caused by the asymmetry in the response discussed earlier.

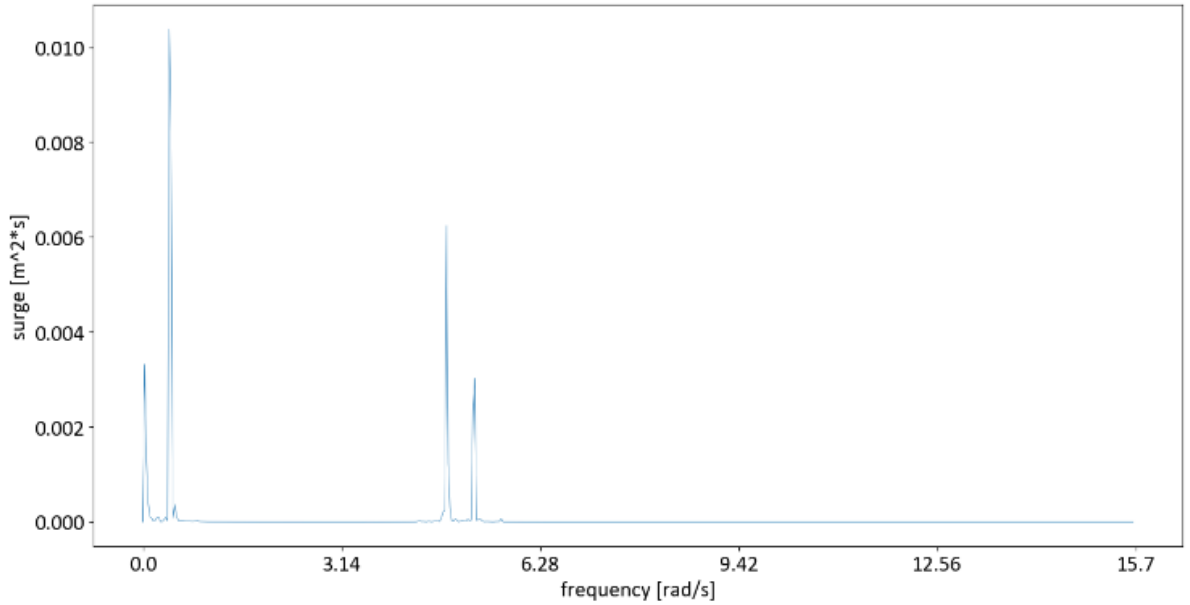

Figure 75: PSD of the surge movement for model test b3 with mooring system 1

Figure 76 shows the surge movement for the b4 model test with mooring system 2. Here the surge is considerably less asymmetric than in figure 73. There is still some asymmetry as the movement back is 5 mm larger than movement forward, but the effect is clearly smaller. The amplitude of the movement is also significantly decreased as it is now roughly 25 mm compared to the 50 mm before.

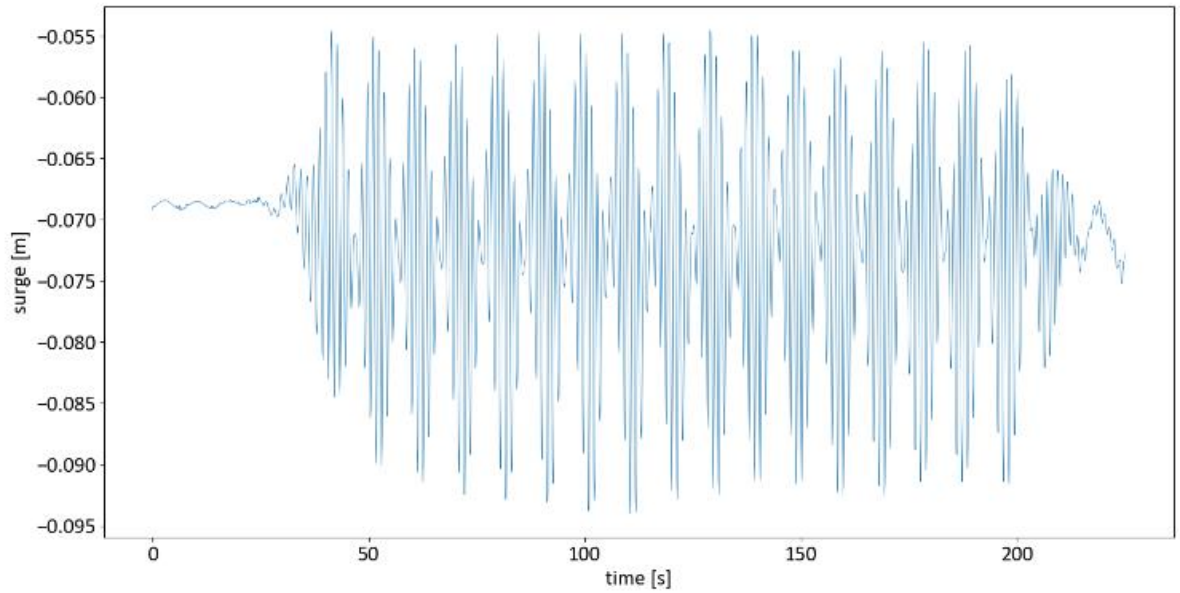

Figure 76: Graph showing the surge data versus the time for model test b4 with mooring system 2.

Figure 77 now shows the PSD for the model test b4 with mooring system 2. This system shows a similar but more muted response compared to figure 75. As can be seen the peaks at the difference frequency is still present but now the peak is only a fraction of the wave peak height. This shows that the difference frequency movement is indeed a lot smaller as was noted from the time series. To be noted as well is the smaller peak of the static offset, associated with the asymmetry. This is also smaller compared to the previous results, again also visible in the time series as well. It still however indicates a low and wave frequency response as opposed to the purely wave frequency response in the wave height PSD.

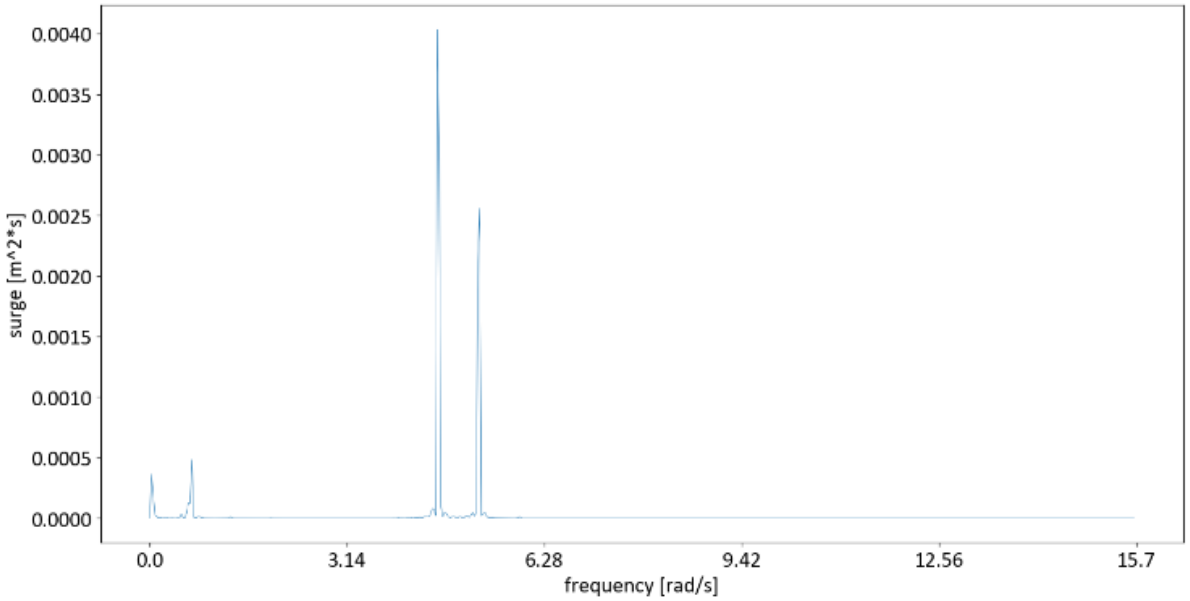

Figure 77: PSD for surge for model test b4 with mooring system 2

5.4 Mooring line analysis

Figure 78 shows the force in mooring line 2 for model test b3. When the bichromatic wave is tested it can be seen that the force has a very different response than with the monochromatic wave m3 shown

during the verification. The low frequency element becomes the dominant feature of this graph and it can be seen that the individual waves become a small part of the overall force. Whereas in figure 48 the amplitude was roughly 0.05 N, now the amplitude goes to 0.15 N. More than the simple doubling one would expect from the doubling of the wave height. This is because that natural frequency is being hit. This effect is even larger than the one found during the surge analysis, most likely due to the non-linear stiffness of the mooring lines which would giving increasing amounts of force for the same amount of movement.

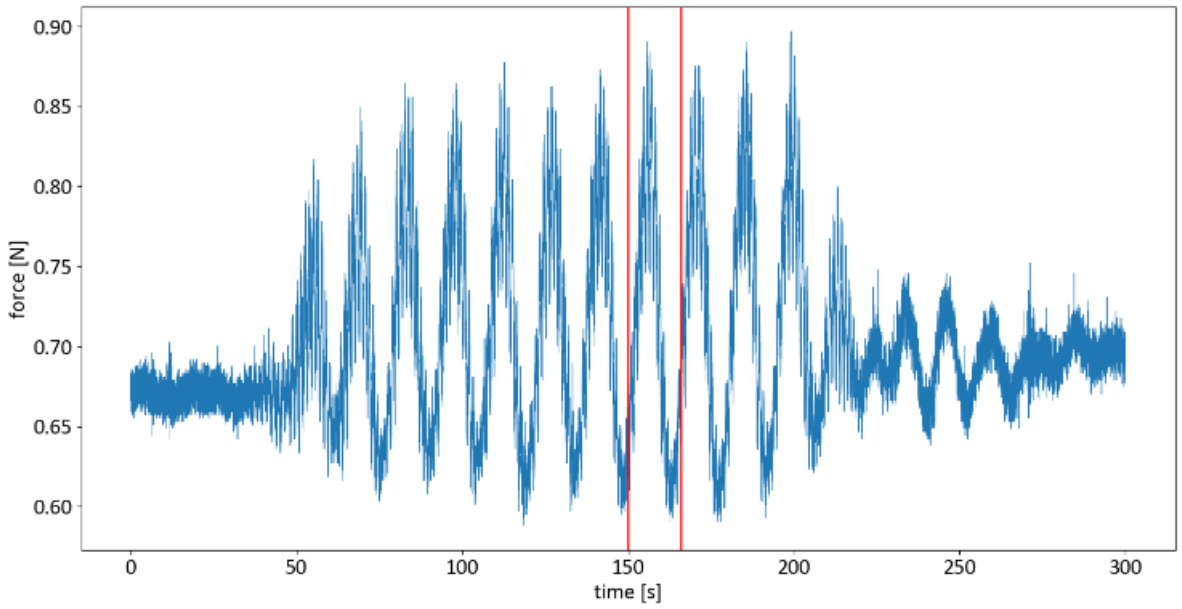

Figure 78: Graph showing the force in mooring line 2 during model test b3 with mooring system 1.

When zooming in in figure 79 the individual waves become a bit more visible. It can also be seen that the low frequency wave shows a one-sidedness in the response as there are no force below the 0.6 N line where the force seems to be at rest during the bichromatic wave. This is because of the wave drift forces which have a non-zero mean, although this might be combined with the slack lines, which creates and asymmetric mooring system. This is because the mooring system moving backwards loses the stiffness of the rear two mooring lines and transfers force to the front mooring line, and when there is movement forwards the mooring lines at the back take up some force again reducing the force on the front mooring line. This does need to be set in motion by the wave drift forces, however.

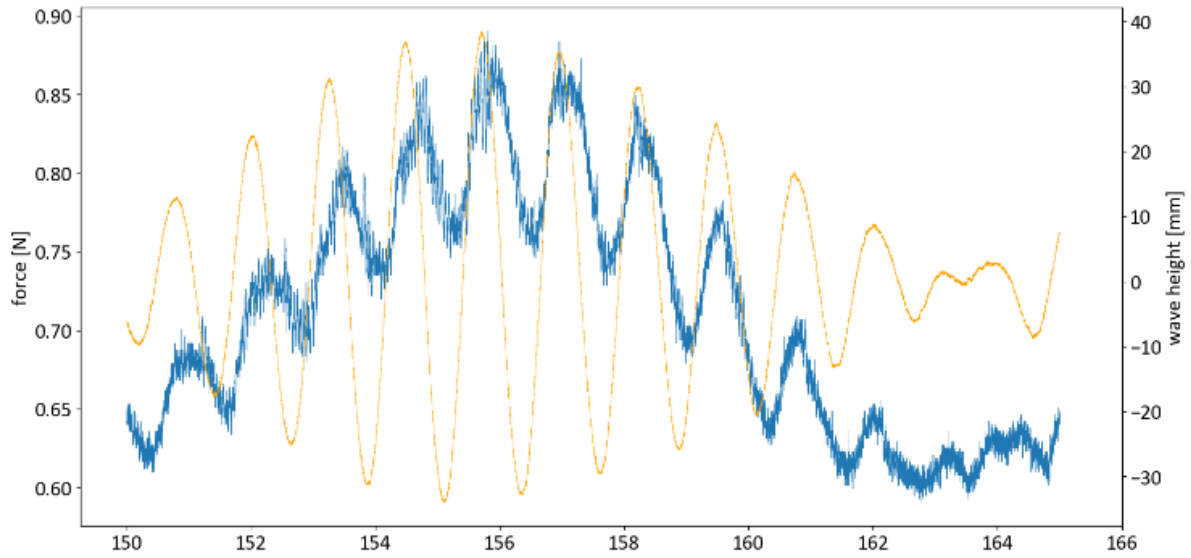

Figure 79: Zoom in on the force in mooring line 2 for model test b3, indicated by red lines in figure 78, the wave elevation from wave probe 3 is indicated in orange.

Figure 80 shows the PSD of the mooring line 2 force for model test b3 with mooring system 1. Here it can be seen that the low frequency aspect becomes very dominant. This concurs with the large low frequency force that can be observed in the time series. The asymmetry is also visibly represented by the static amplitude.

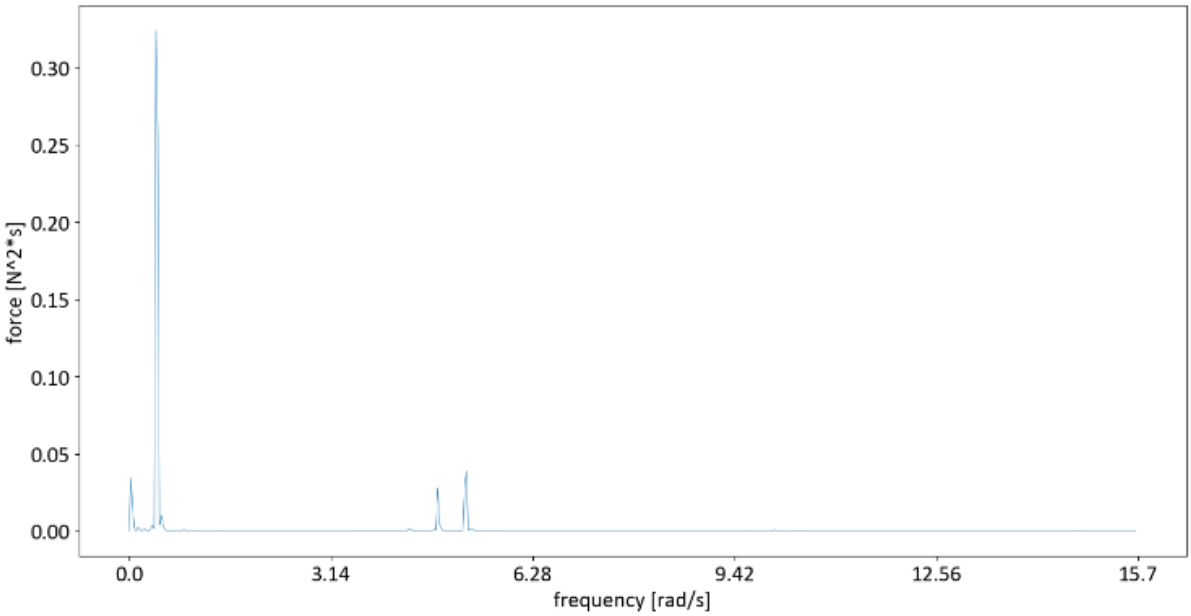

Figure 80: PSD of the mooring line 2 force during model test b3 with mooring system 1

Figure 81 takes a look at the force in mooring line 1. As can be seen the mooring line now has a more symmetrical shape, where there is a much closer response in the positive as in the negative direction. Again, the mooring lines fall slack at a backwards movement causing the force to reduce to the vertical force. The lack of force in the back mooring lines then causes the front mooring line 2 to spike causing an asymmetric shape.

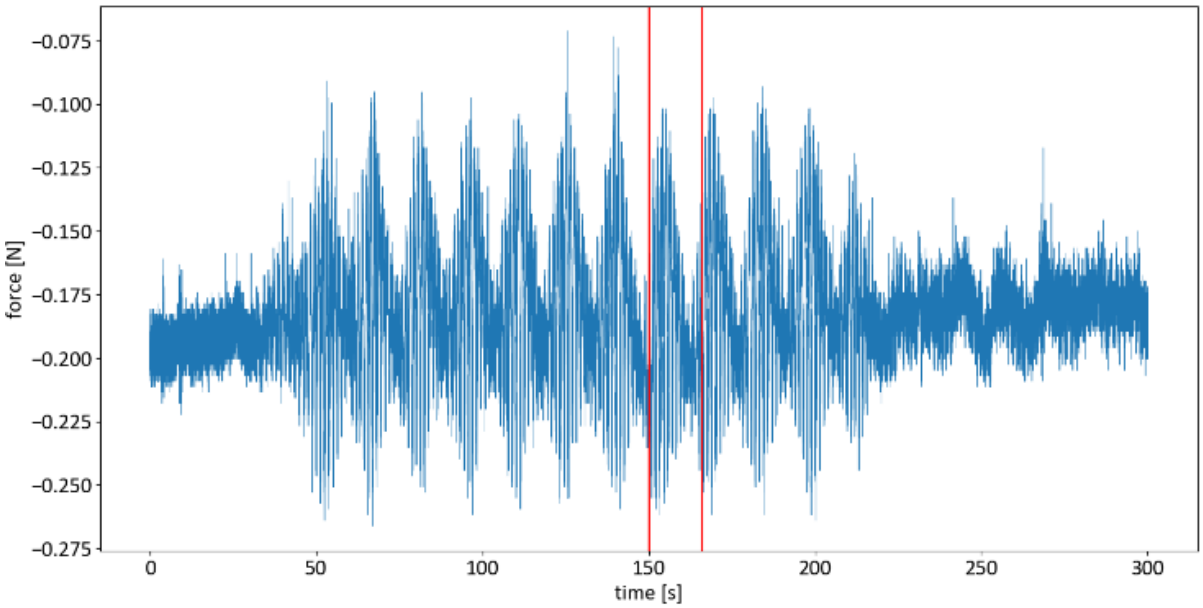

Figure 81: Graph of the force in mooring line 1 for model test b3

Figure 82 shows a zoom of figure 81, where the shape is more symmetric around the average. Now the mooring line force follows the waves better, showing less one sidedness. This is because although the drift forces are still pushing a one-sided solution the enhancing effect of the slack mooring lines seen in mooring line 2 now works against the force in this mooring line, reducing asymmetry.

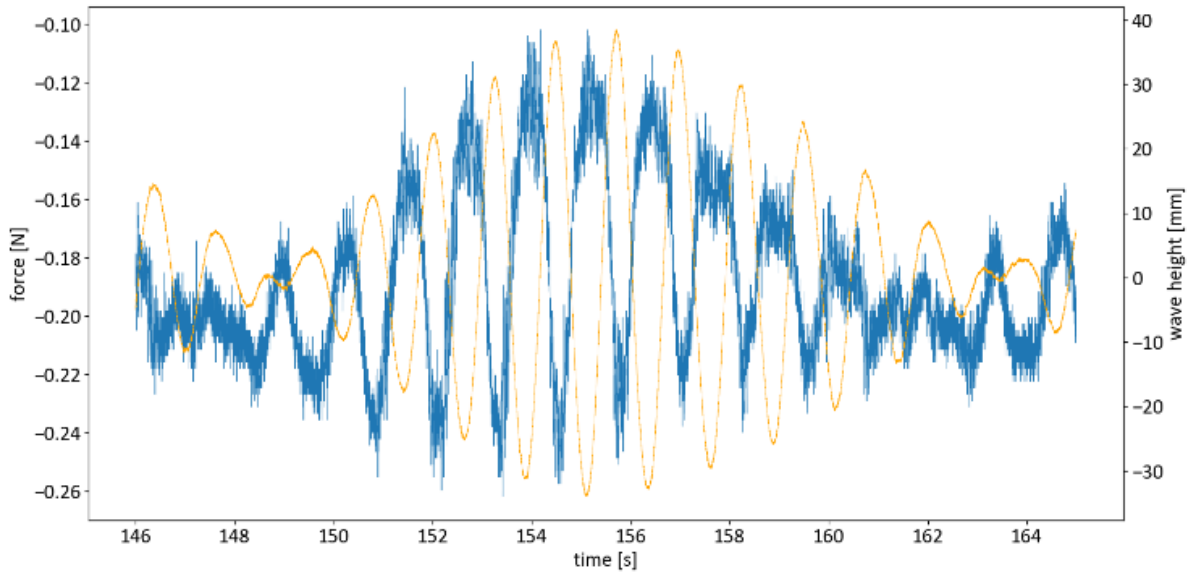

Figure 82: Zoom in on the force on mooring line 1 for model test b3, indicated by red lines in figure 46.

Figure 83 shows the force in mooring line 2 during model test b4 with mooring system 2. Here it becomes clear that, as with the surge, the asymmetric response seen with mooring system 1 is muted. It is still present, but the beating pattern is harder to see, and the asymmetry is now only a factor 2 rather than a factor 3 seen earlier.

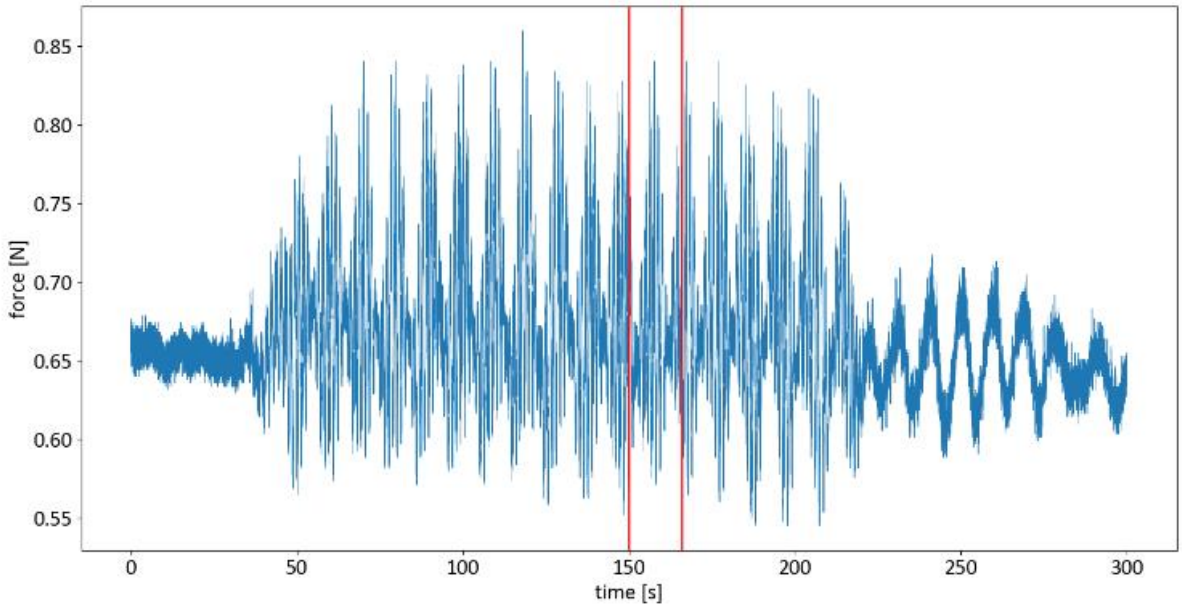

Figure 83: Graph showing the force in mooring line 2 during model test b4 with mooring system 2.

Figure 84 shows the zoom in of the range indicated by the two red lines. Here again the more muted response can be seen as the mooring line force in blue seems to follow the yellow wave height plot very well.

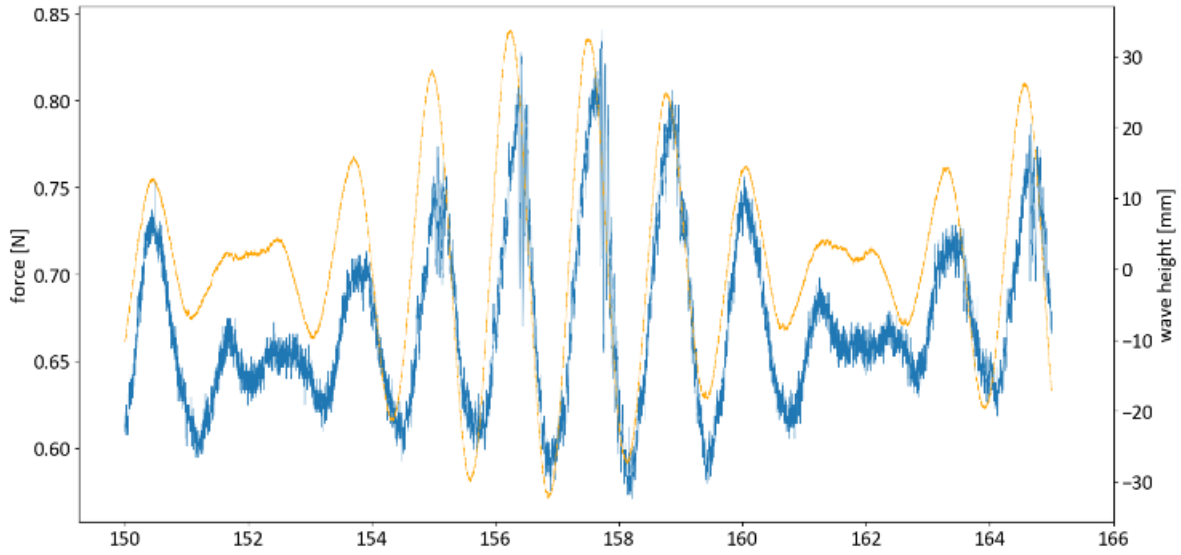

Figure 84: zoom in of the mooring line 2 force for model test b4 with mooring system 2, combined with wave height

Figure 85 shows the PSD of the mooring line 2 force for model test b4 with mooring system 2. Here it can be seen that the low frequency peaks are a lot smaller than with the previous test. This corresponds to what can be seen in the time series and what was observed with the surge.

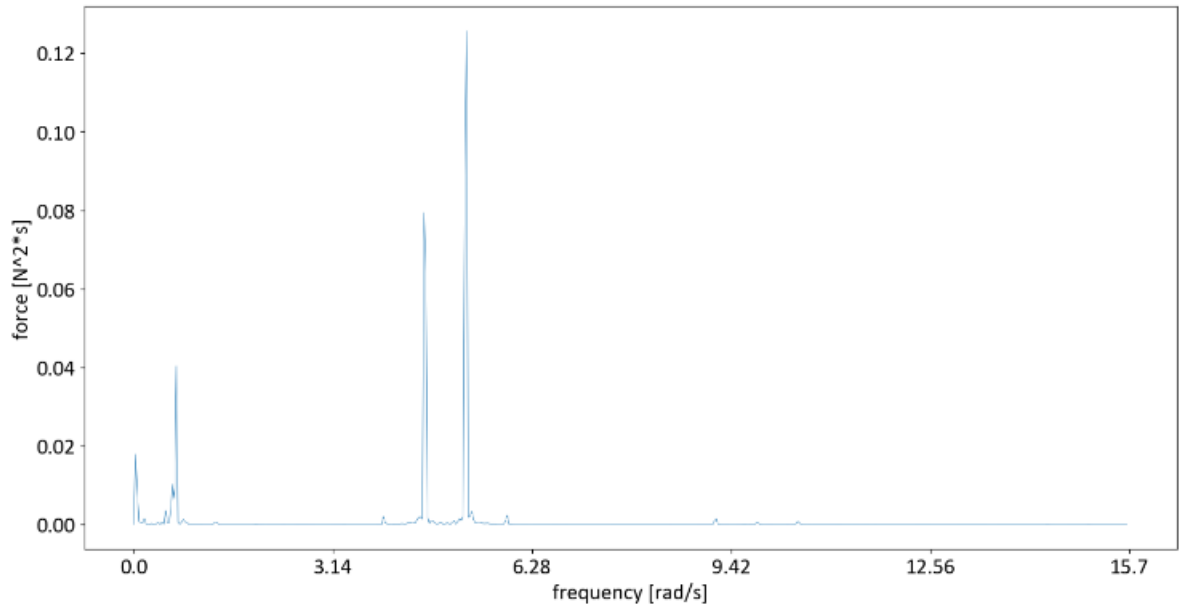

5.5 Causal path

Spectra of different data sources are compared within the same test. This will show the translation between different steps of the experiments. So going from the wave maker to the waves to the eventual mooring line force.

This will be done to show the causality of the low frequency response. By observing changes between the different PSDs, it can be established that a certain response comes from the transformation done in the chain of response during the test. The PSDs plotted in figure 85 are for test b1 with mooring system 1. They are representative of the different steps in the forcing process, the wave probe 3, the surge data and the mooring line 2 force. Additionally wave probe 3 from the empty tank test is also added to indicate the difference in waves caused by the model. Note that the mooring line force has been amplified by 10000 to make it visible on the multi-unit y-axis.

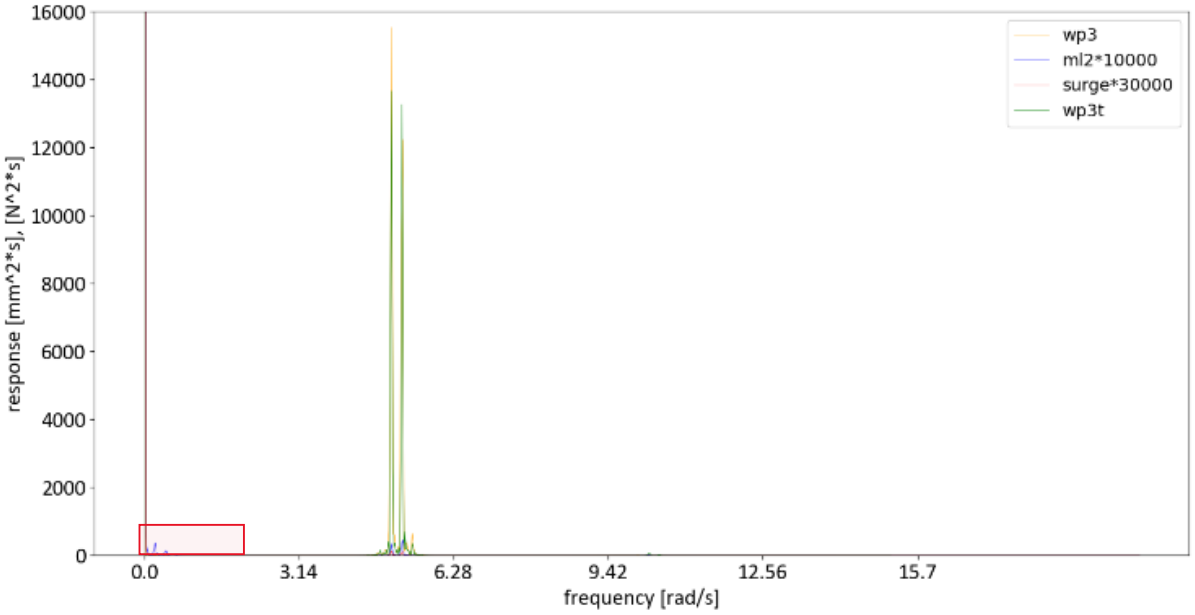

Figure 85: PSDs overlayed to show the chain in response of b1.

In this figure, four PSDs are laid on top of each other for comparison. Starting at the top of the legend the orange line indicates the PSD from wave probe 3. The blue line then indicates the mooring line force in mooring line 2. This force has been multiplied by 10000 to make it barely visible. The red line is for the surge, this time multiplied by 30000, and lastly the green line is for the wave test without model.

The two large peaks are at 5.02 and 5.24 rad/s and values of 14000 mm^2*s for the wave test without model, 16000 mm*s for the wave test with model. Showing only a minor difference.

It can be seen that the response is mainly in the wave frequency aspect where the wave probes have a very certain (narrow) response on the wave frequencies. The blue mooring line force is also slightly present at this frequency with a peak of about 300 N^2*s. The surge however is barely visible. In figure 86 the low frequency area is enhanced to show that here the blue mooring line force dominates here, together with the surge.

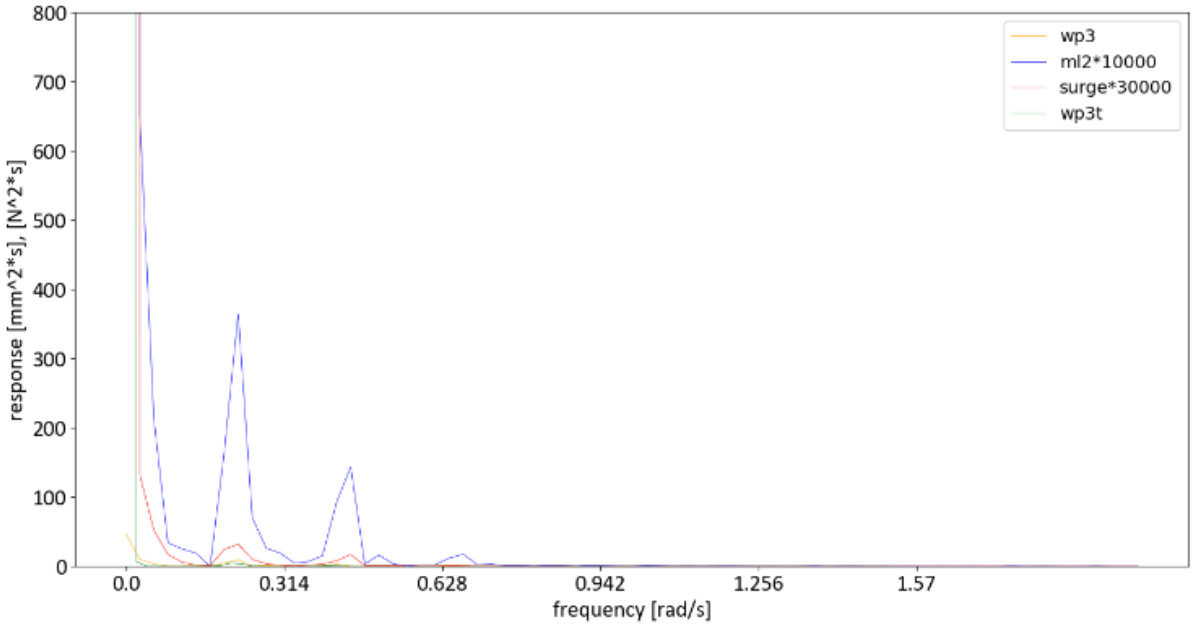

Figure 86: Low frequency zoom in of the PSD comparison.

The wave probe data is almost perfectly flat, as it should be, as this was created to be purely bichromatic around the wave frequencies. The probes do however show a small response around the difference frequency. This bump is very small though so a conclusive reason for its existence cannot be given, although reflections from the model cannot be the case as the bump is equal for both wave test. Most striking in figure 86 however are the two large peaks of the mooring line in blue and surge motion in red at the surge natural frequency and the difference frequency. Whereas at the wave frequency the wave response dominates, now the mooring line and surge motion are much higher, showing that this low frequency response really comes from the low frequency response of the mooring system. As otherwise the blue and red response would have been a lot higher at the wave frequency as well. This visual comparison of course only works when the mooring line and surge data is scaled to a large degree, but the main purpose of the comparison is to establish a causal chain of excitation. The wave gauges all show very strong response around the wave frequencies but lack the reaction at the lower frequencies. Whereas the mooring line and surge show a relatively strong response at the low frequencies. The lack of wave excitation but presence of mooring line excitation means that somewhere along the way the model must translate the second order effects into the low frequency excitations. Together with the fact that there is a peak at the difference frequency, this

shows that the low frequency response is indeed caused by the bichromatic beating pattern, thus enabling the analysis to continue with that finding.

A thing to note is that the resolution of the PSDs starts to show when you zoom in this much. For the mooring line the resolution is approximately 0.0218 rad/s. For the goal of establishing a causal chain this is accurate enough as it is only a qualitative assessment.

To provide another example, but this time with the difference frequency at the surge natural frequency, figures 87 and 88 take a look at model test b3. Here the bichromatic waves were exactly aimed at the surge natural frequency. The blue mooring line plot clearly shows a much stronger response in the lower frequencies and when zooming in, it is clear that this comes from the low frequency response of the mooring system. Note that the y scale is different from figure 86.

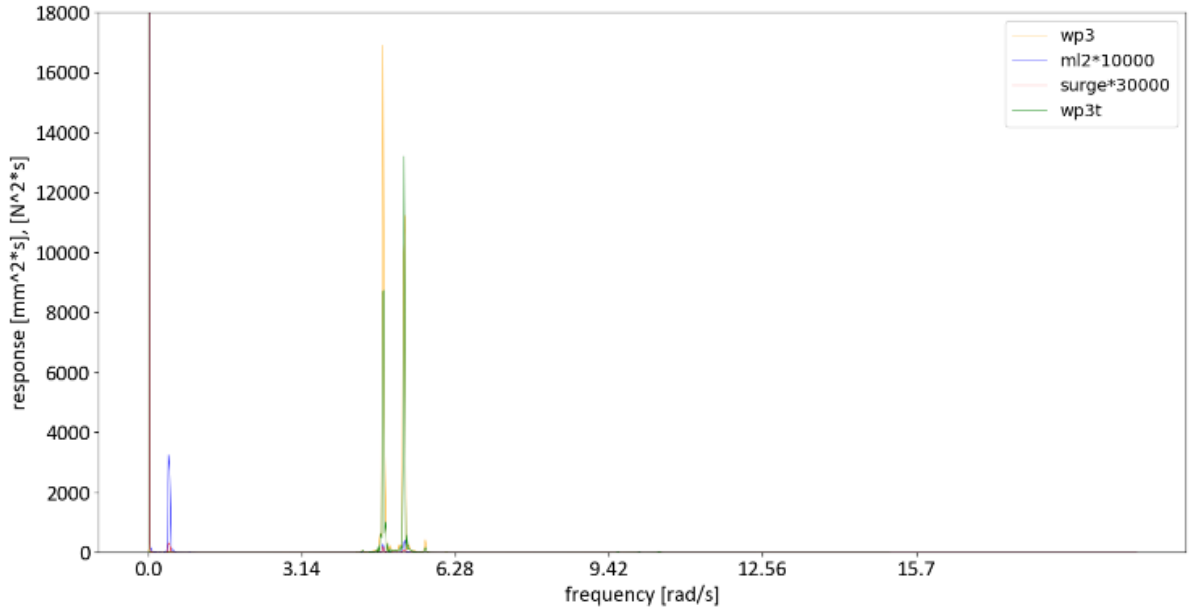

Figure 87: PSDs overlayed to show the chain in response of b3.

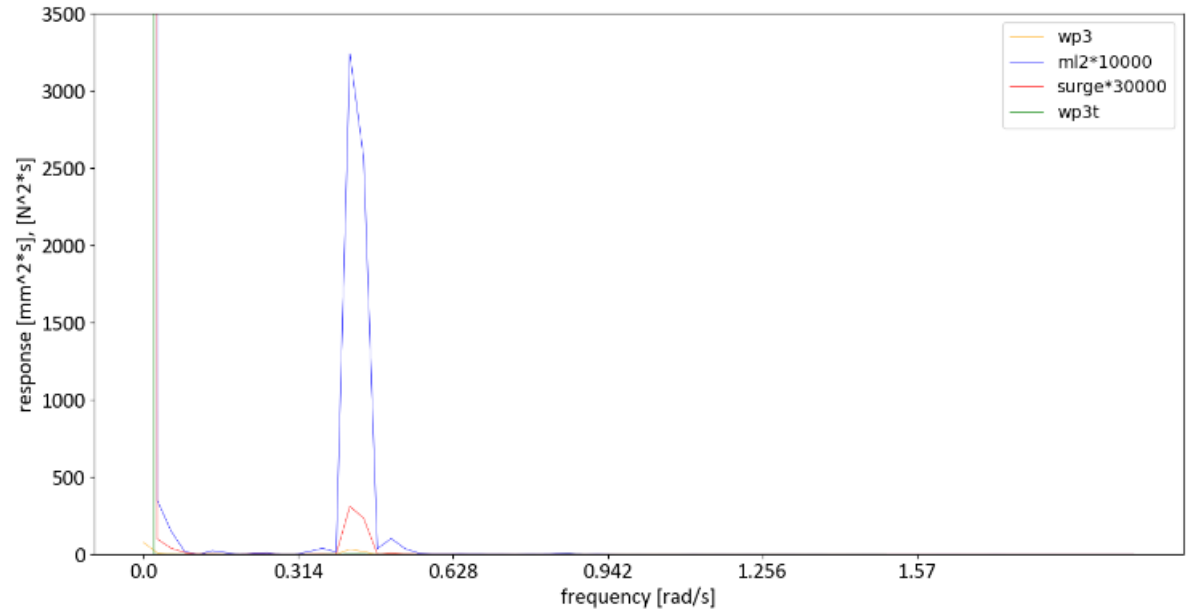

Figure 88: Low frequency zoom in of the PSD comparison.

Lastly the b4 model test with mooring system 2 is examined, where the natural surge frequency and difference frequency match as well. Figure 89 shows that in the wave frequency range the dominant response is in the wave height with the two peaks corresponding to the components of the bichromatic wave. Figure 90 then zooms in and shows that in the low frequency range the mooring line force dominates. Contrary to the b3 & mooring system 1 comparison the surge frequency is not very clearly a factor, only having a small peak at the natural frequency.

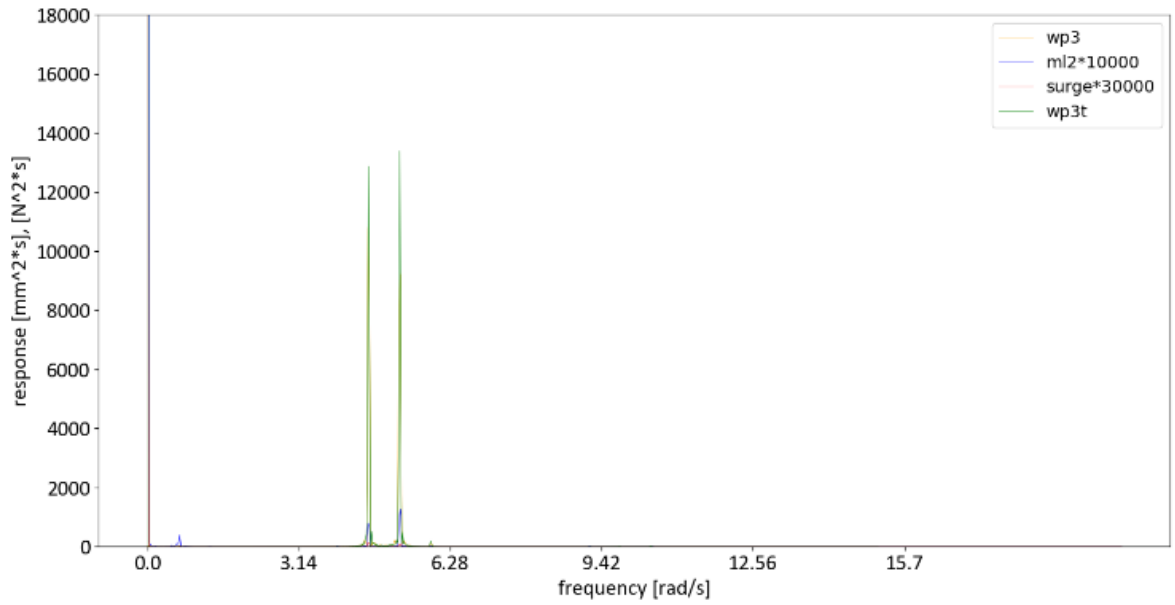

Figure 89: PSDs overlayed to show the chain in response of b4.

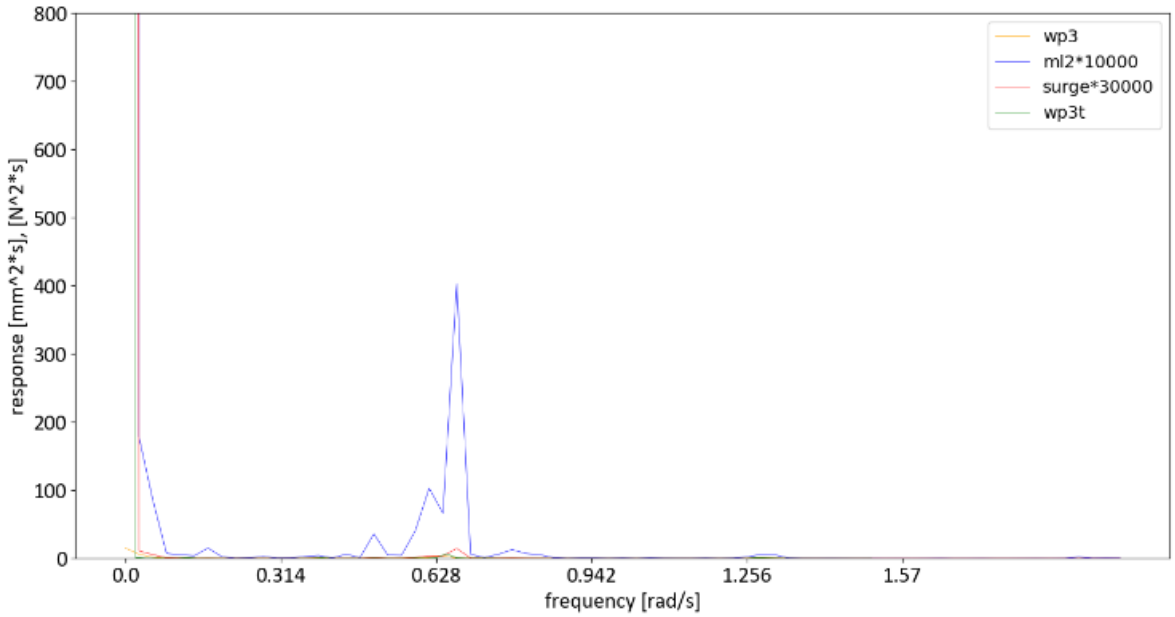

Figure 90: Low frequency zoom in of the PSD comparison.

All in all, it can be concluded that the low frequency response in the mooring line force and the surge movement comes from a translation made by the model. The previous PSDs all show an almost non-existent wave height at the lower frequency whilst there is a clear mooring line force response and in the case of b3, mooring system 1 also a clear surge response.

5.7 Resonance analysis

As was noted in the causal path section the tests which were aimed at the surge natural frequency, b3 and b4 for mooring system 1 and 2 respectively, had very different responses. This begs the question of a comparison between low frequency response of the different tests measured against the ratio of the forcing and mooring system natural frequency. Three different methods are tried to characterize this low frequency response.

In the first method the peak value in the low frequency range of 0.05 to 1.57 rad/s is taken. This peak is then laid out per test with on the x-axis a ratio of the difference frequency of the test divided by the eigenfrequency of the system. Figure 91 shows the results of this method. As can be seen the initial mooring system with wind, the red dots, has very high peaks during test b3 (near the 1.0 ratio). Other tests have smaller responses. Besides the large responses in mooring system 1, likely due to the slack lines observed earlier, no clear pattern is visible in this analysis. Of note is the relatively large response of model test b5 with mooring system 1 at a ratio of 2. It is especially noteworthy as one of the repeat tests shows a large response and one does not, whereas other repeat tests are closer together. What causes this one test to go astray is not clear as the time series of the two tests is very similar as can be seen in appendix F.

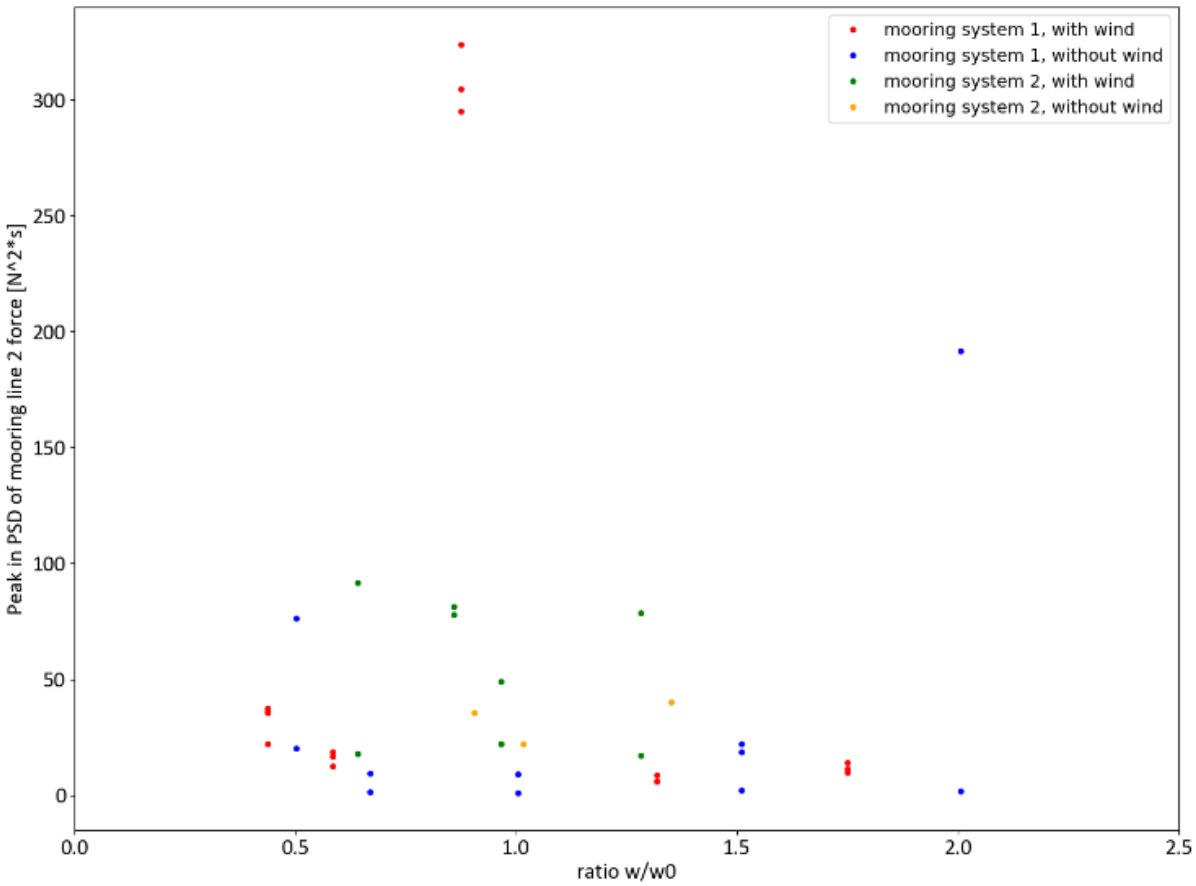

Figure 91: Comparison of peak low frequency mooring line force response of different tests.

A similar analysis is shown for the surge in figure 92. Here it can be seen that the b5 test is even higher than with the mooring line force, although it is still the one test. It can also be seen that the b3 tests of mooring system 1 again show a larger response. The rest of the tests again does not really show a pattern.

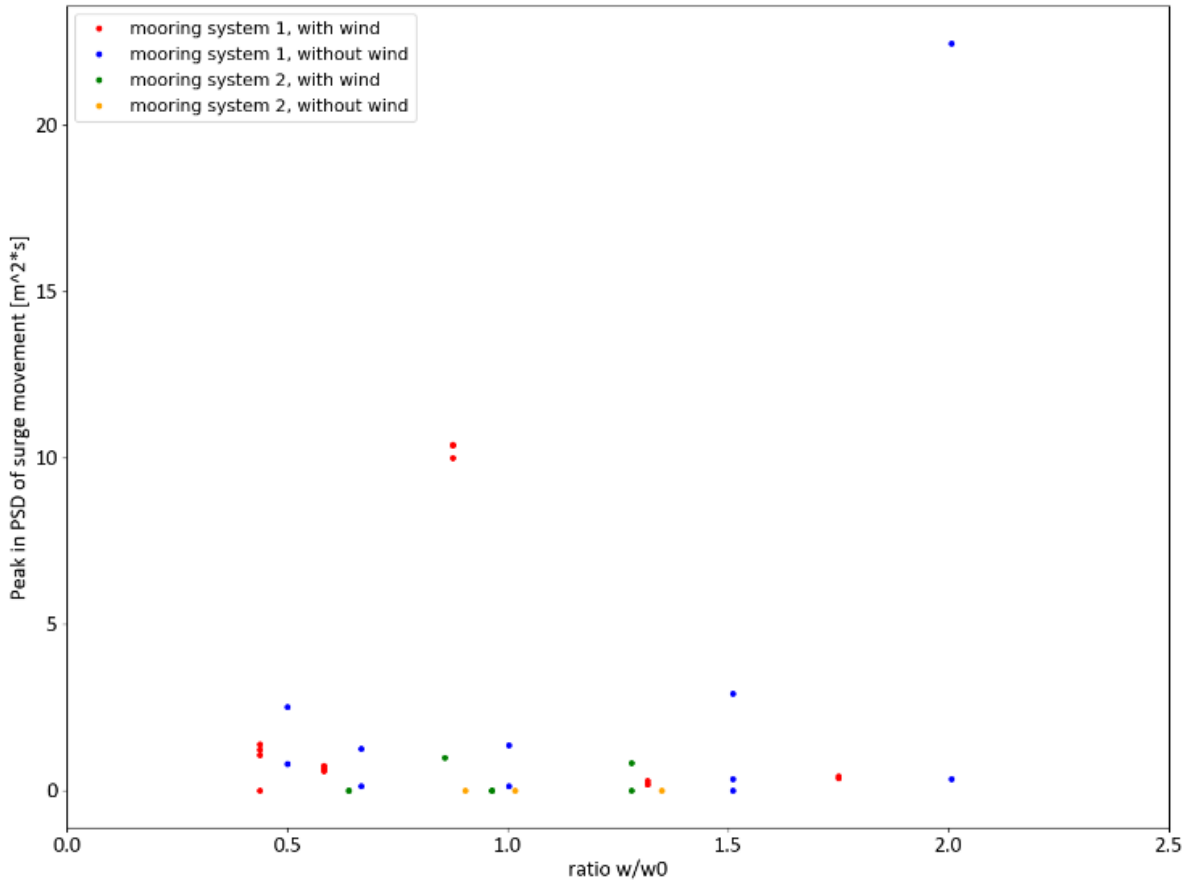

Figure 92: Comparison of peak low frequency surge response of different tests.

As can be seen from some of the earlier PSDs however some graphs have multiple peaks. To accurately take the response into account the different low frequency spikes should all be taken into account. However, the static force located at 0 rad/s should not be measured. To accurately represent the low frequency response, it was decided to take the area below the graph from everything above 0.05 until 1.57 rad/s. The reason to take an area rather than, for example a peak value, is to be able to take all the low frequency responses into the analysis. All test with the exception of the b3 on mooring system 1 and b4 on mooring system 2 have two peaks in the low frequency response, one corresponding with the surge natural frequency and one with the difference frequency. Both of these should be taken into account. Furthermore, any build up to the peak should also be taken into account as this would also contribute to the low frequency response. To meet all these demands, taking the area becomes a good choice.

This leads to the following response graph for the mooring line 2 force, shown in figure 93. As can be seen qualitatively not much changes but most of the repeat tests do get closer together, thus coming closer to the result found in the verification that the tests have a high degree of reliability.

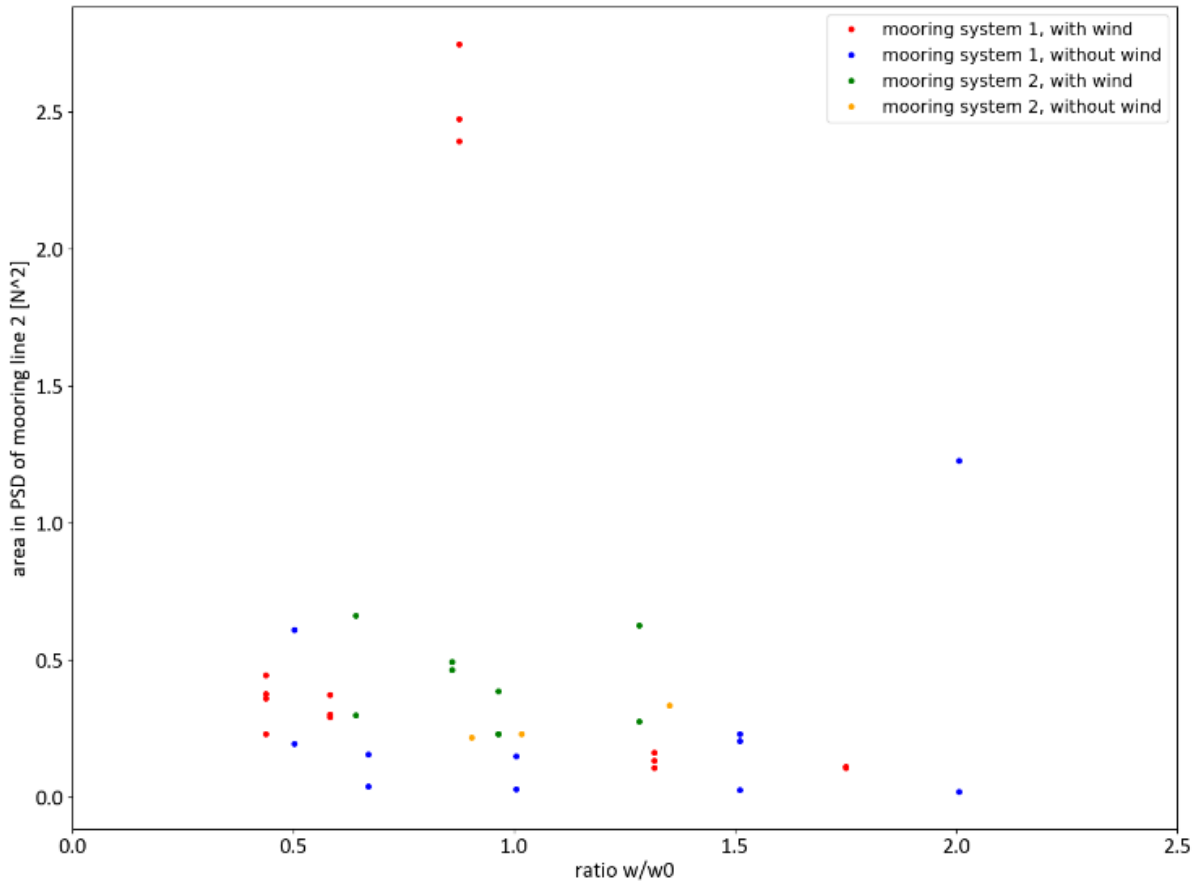

Figure 93: Comparison of area low frequency mooring line force response of different tests.

Another method of comparison is by taking the net force in the mooring system. This net force was calculated by taking the mooring line 2 force minus the force in the two rear lines. In this the force in mooring line 1 stands in for the force in mooring line 3. The angle of the lines taken into account to remove the sway component of the force. This is done 'live' by using the surge data and trigonometry. The net force is then transformed to a PSD and the low frequency area is taken as with the previous method. As can be seen in figure 94 this calculation tends to suppress the low frequency response of most tests, whilst increasing the response in the b3 model test. The results however are still qualitatively similar.

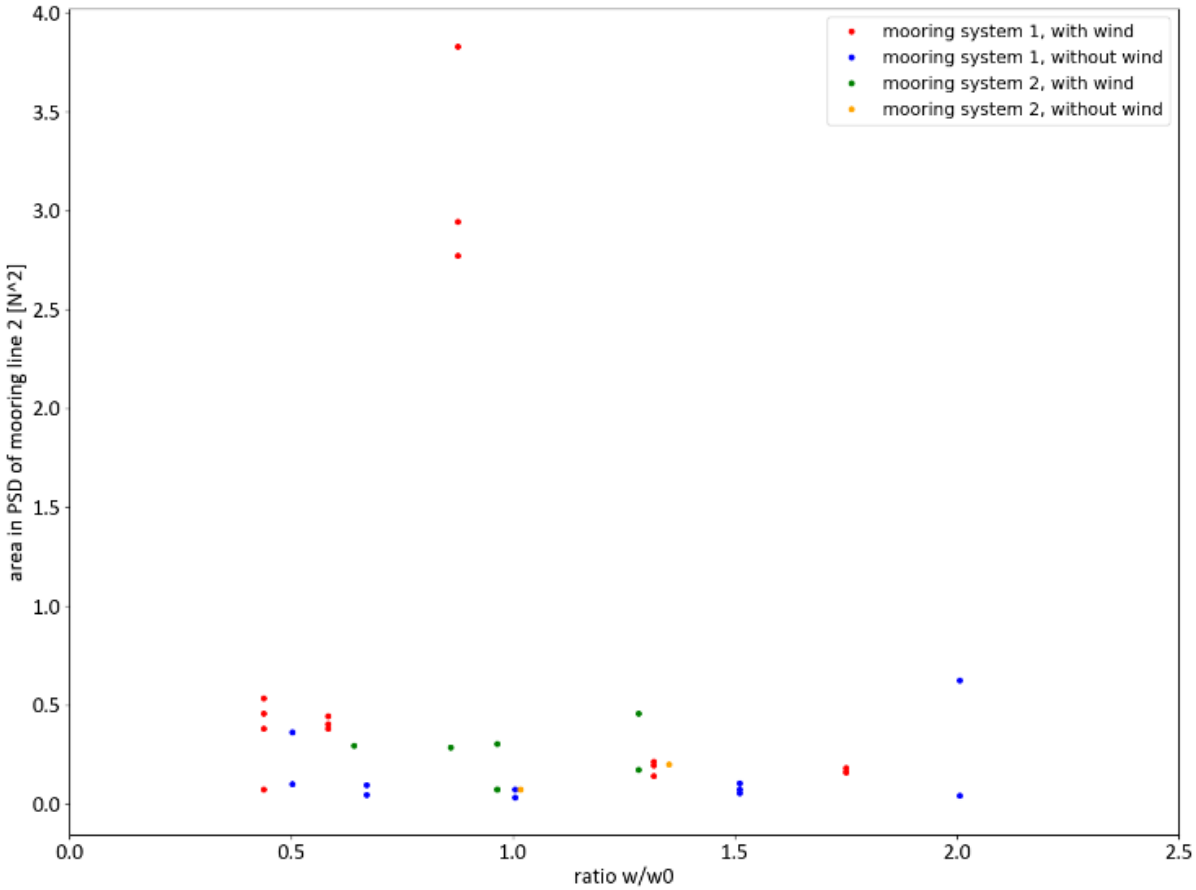

Figure 94: Comparison of area low frequency net mooring force response of different tests.

Of the three different calculation methods the area method is preferred for further analysis as it is more representative of the low frequency response than the single peak method, whilst also being easier to execute than the net force method. It also remains more comparable to both the surge, which cannot utilize the net method and the OC5 project which looks at the lead line force.

5.8 Uncertainty

In order to get a measure for the uncertainty around the experimental data, a key recommendation of the OC5 project, an unusual method of splitting the data is used. This method is explained and used to determine the uncertainty around the amplitude of the response in the force and surge.

The difficulty in an uncertainty assessment of these types of tests is the fact that it is hard to do a large number of them. As can be seen in the testing schedule, tests are repeated thrice at most. An N of 3 would be too few to do a meaningful uncertainty measurement. Thus, the uncertainty assessment was done by splitting the data akin to the method described by Werkman (2019), which could easily be done due to the steady state beating pattern of the test design. The time series data is split into different blocks of a number of low frequency movements. Figure 95 shows a time series of model test b1 being split into three blocks. This is done by splitting the main low frequency events into four sections. These sections then form three blocks by taking two consecutive sections at a time. Appendix C shows the splitting for each time series.

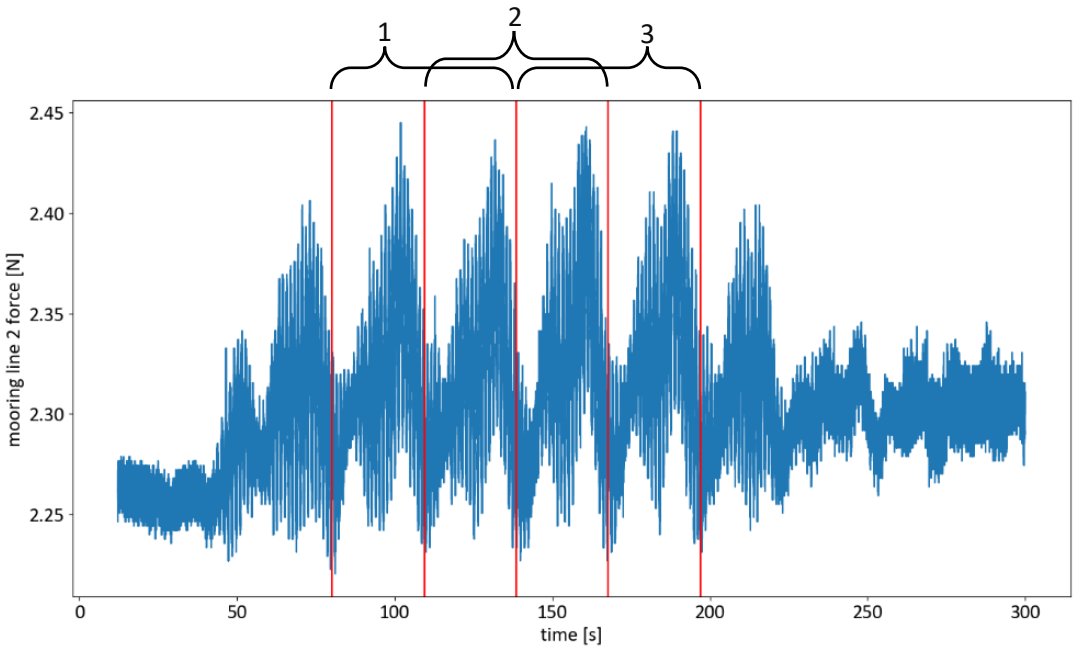

Figure 95: Time series of the mooring line 2 force being split into sections, with the block numbers indicated.

These three blocks then have individual PSDs made shown below in figure 96. The three different blocks have a very similar trajectory, showing that they are comparable to each other and can be used in the same uncertainty assessment.

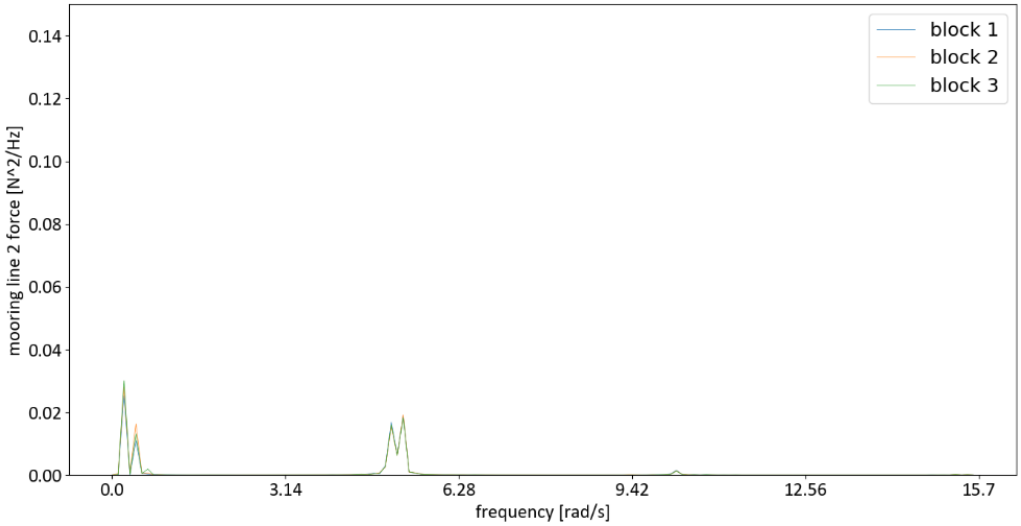

Figure 96: PSDs of the three different blocks from b1.

This method elevates the number of data points to compare to nine in the case of model test b1, a significant improvement. Other tests have an even better outlook as they have more usable low frequency oscillations, as can be seen in for example figure 58.

Some optimizing is required as it comes to how many sections form a block. Having more sections makes the block more accurate but reduces overall data points. Experience showed that two already shows good results, where the blocks get a very good representation of the data, which can be glanced from figure 96. Only one section showed significant deviation from the data, especially around the low frequency, as the PSD only had one wave to work with. Two was thus chosen to be the optimum number.

The uncertainty in the data can now be collected for all tests. As mentioned before the area under the graph from just over 0, changing per test, based on the length of each block, to 1.57 rad/s is taken to

be representative of the low frequency response. This is done for every block of every model test, giving a larger data set of which, the standard deviation can be calculated than with individual tests.

The standard deviation (in this case for the data set x is calculated via an inbuilt python function using the following formula:

$$std = \sqrt{\frac{1}{N}\sum_{i=1}^{N}(x_i - \bar{x})^2} \tag{11}$$

From table 9 it can be seen that there is a larger standard deviation in the b3 model tests with mooring system 1 (b3) and b4 model tests with mooring system 2 (b4_NM). This is however because these tests have a very large general response. When normalized to the mean area under the graph b3 actually shows a smaller relative standard deviation than other tests whilst b4 becomes comparable. Besides b3, b1 with mooring system 1 also shows less relative uncertainty than other tests. Table 9 shows the different values concerning the mooring line 2 force for all the tests done. A similar analysis was done for the surge, a visual representation of the two parameters will follow later.

Table 9: overview of the LF response per test, with uncertainty included.

test name	wave difference frequency [rad/s]	surge natural frequency [rad/s]	mean LF area [N^2]	STD LF area [N^2]	STD/mean [-]
b1	0.215	0.492	0.0207	0.0071	0.344
b2	0.287	0.492	0.0149	0.0203	1.366
b4	0.648	0.492	0.0033	0.0089	2.724
b5	0.861	0.492	0.0037	0.0037	1.017
b3	0.43	0.492	0.1196	0.0542	0.453
b1_2	0.215	0.492	0.0182	0.005	0.275
b2_2	0.287	0.492	0.0111	0.0211	1.899
b4_2	0.648	0.492	0.0022	0.0065	2.942
b5_2	0.861	0.492	0.0033	0.004	1.223
b3_2	0.43	0.492	0.1078	0.0363	0.336
b1_3	0.215	0.492	0.0186	0.0047	0.255
b2_3	0.287	0.492	0.0114	0.0179	1.566
b4_3	0.648	0.492	0.0027	0.0057	2.080
b5_3	0.861	0.492	0.0034	0.0044	1.279
b3_3	0.43	0.492	0.1103	0.0476	0.431
b3XL	0.43	0.492	0.1382	0.0401	0.290
b3XL_2	0.43	0.492	0.1388	0.0227	0.163
b1wl	0.215	0.429	0.0087	0.0036	0.415
b2wl	0.287	0.429	0.0045	0.008	1.786
b3wl	0.43	0.429	0.0429	0.0137	0.319
b4wl	0.648	0.429	0.0006	0.0011	1.782
b5wl	0.861	0.429	0.0008	0.001	1.156
b3wl_2	0.43	0.429	0.0458	0.0148	0.324
b2wl_2	0.287	0.429	0.0042	0.0063	1.507
b4wl_2	0.648	0.429	0.0009	0.0025	2.596

b1wl_2	0.215	0.429	0.0089	0.0028	0.310
b5wl_2	0.861	0.429	0.0008	0.001	1.285
b6_NM	0.576	0.672	0.0335	0.023	0.687
b5_NM	0.861	0.672	0.0199	0.0235	1.184
b6_NM_2	0.576	0.672	0.031	0.0225	0.726
b5_NM_2	0.861	0.672	0.0195	0.0218	1.118
b1_NM	0.43	0.672	0.0139	0.0106	0.759
b1_NM_2	0.43	0.672	0.013	0.0041	0.315
b6wl_NM	0.576	0.637	0.0419	0.0315	0.752
b5wl_NM	0.861	0.637	0.0088	0.0111	1.264
b4_NM	0.648	0.672	0.0132	0.0232	1.764
b4_NM_2	0.648	0.672	0.0159	0.0322	2.032
b4wl_NM	0.648	0.637	0.0092	0.0202	2.203

Spectra of different tests are now compared. Firstly, data of repeat tests are compared to get a measure of repeatability, then the data between different test configurations are compared in order to draw conclusions about the effect of the changed parameters.

Figure 97 shows the time series of the mooring line 2 force for test b3. The red lines indicate the borders between the different sections that form the blocks.

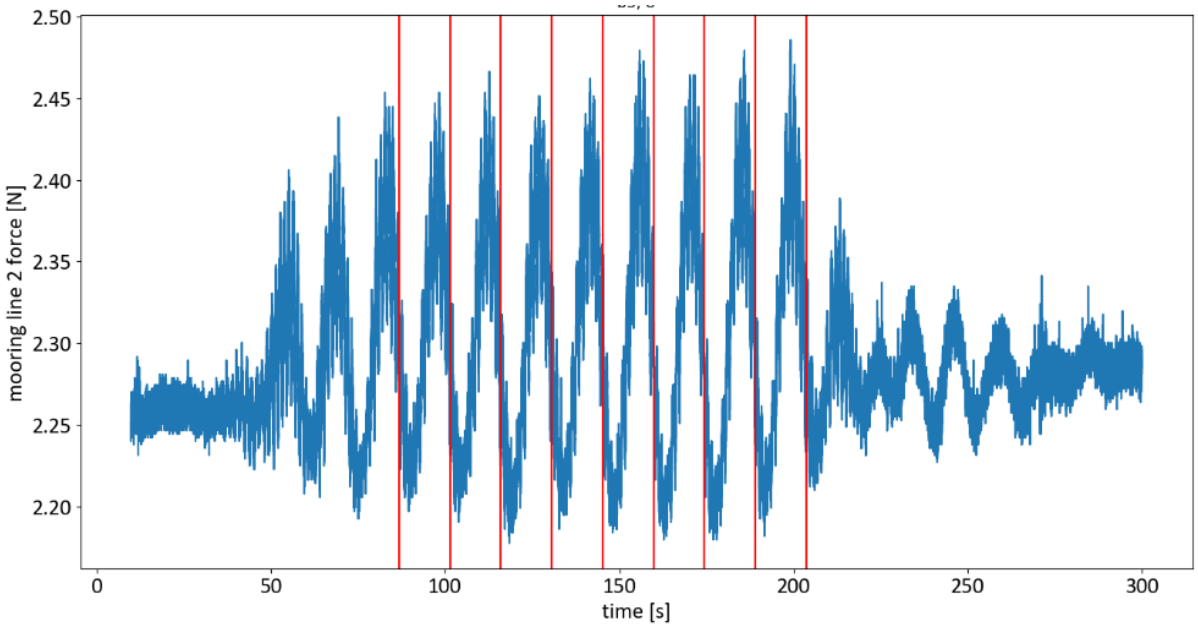

Figure 97: Time series of the mooring line 2 force for test b3.

Figure 98 then shows the PSDs for the first four blocks of this time series, block 4 has a higher peak than the others but in general good agreement is again shown between the different blocks.

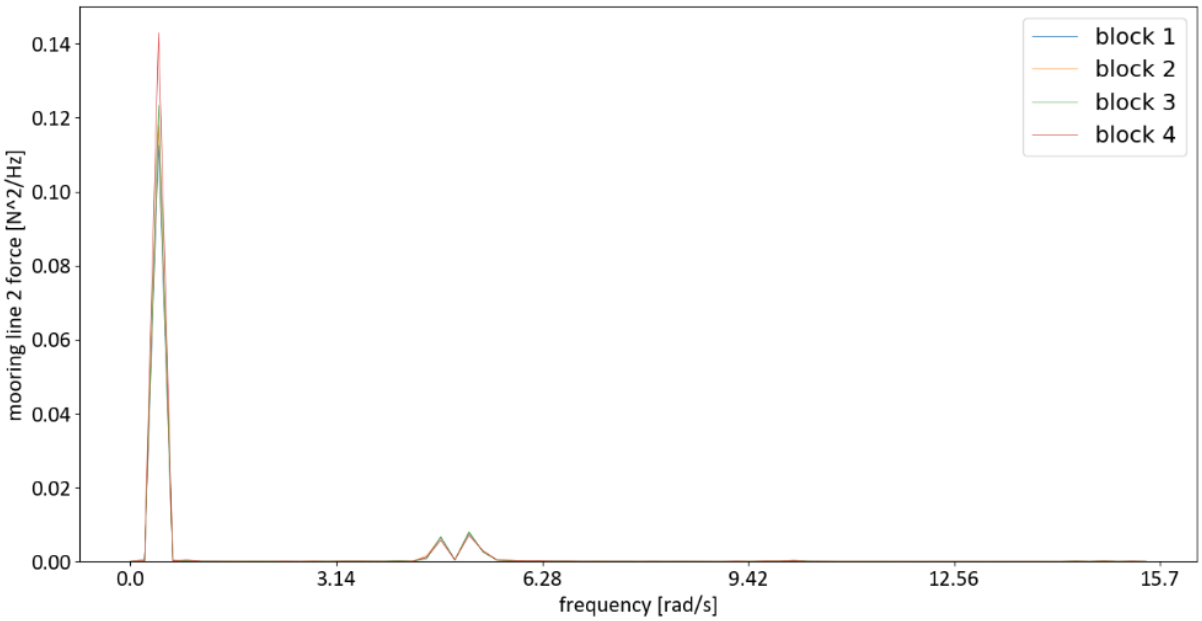

Figure 98: PSDs of the first four blocks of the mooring line force during test b3.

Figure 99 now shows the same time series of the mooring line 2 force, but now for the repeat test of b3, called b3_2. Again, red lined indicate the borders between sections which form the blocks.

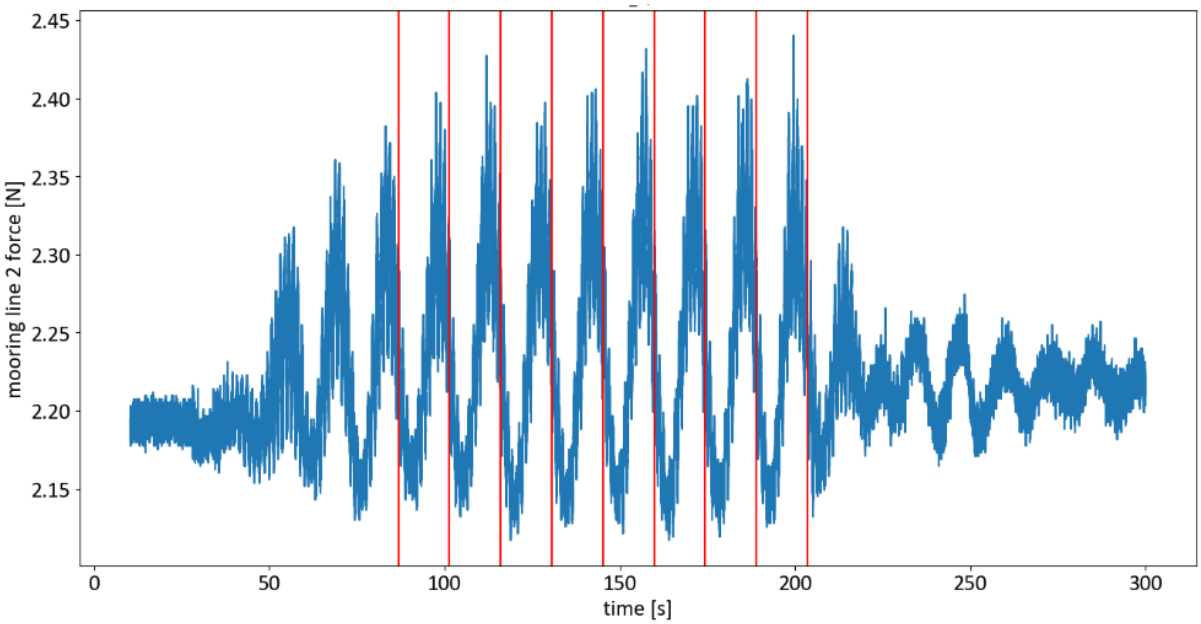

Figure 99: Time series of the mooring line 2 force for test b3_2.

Now again the PSDs for the first four blocks are shown in figure 100.

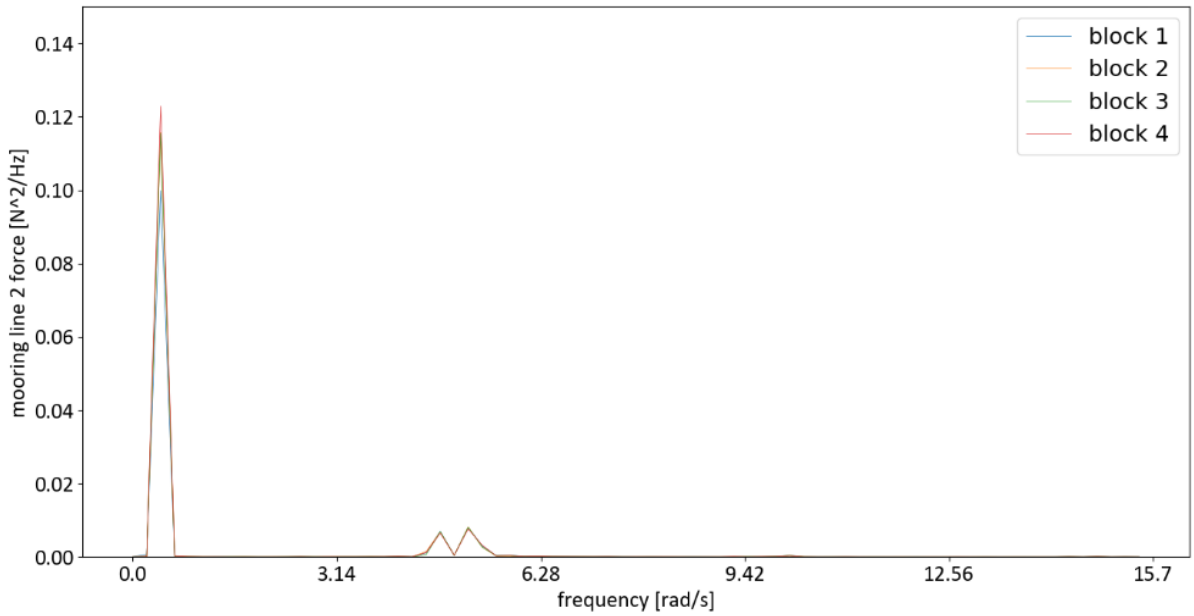

Figure 100: PSDs of the first four blocks of the mooring line force during test b3_2.

From the similarity of figures 98 and 100 it can be concluded that the repeat tests follow very similar responses compared to each other. Figure 101 further illustrates this by showing the average height of each peak and a 95% certainty range per experiment, showing that they are not significantly different. That allows the repeat tests to be bundled together to generate more data for the uncertainty assessment as discussed before, but it also allows the data to be plotted together to get a less cluttered picture later.

To show the comparability between the repeat test further, the other focussed test, wave b4 on mooring system 2 is also shown. Figures 102 and 103 show the PSDs of the first four blocks again to illustrate the repeatability of the tests.

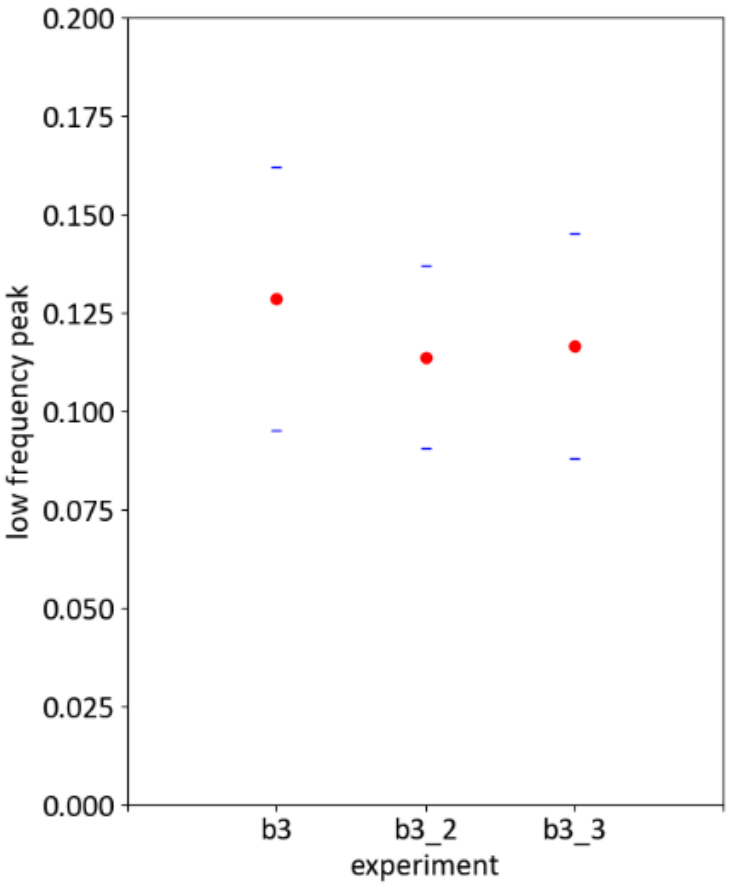

Figure 101: Comparison of peak height per b3 experiment, with b3_2 being the first and b3_3 the second repetition.

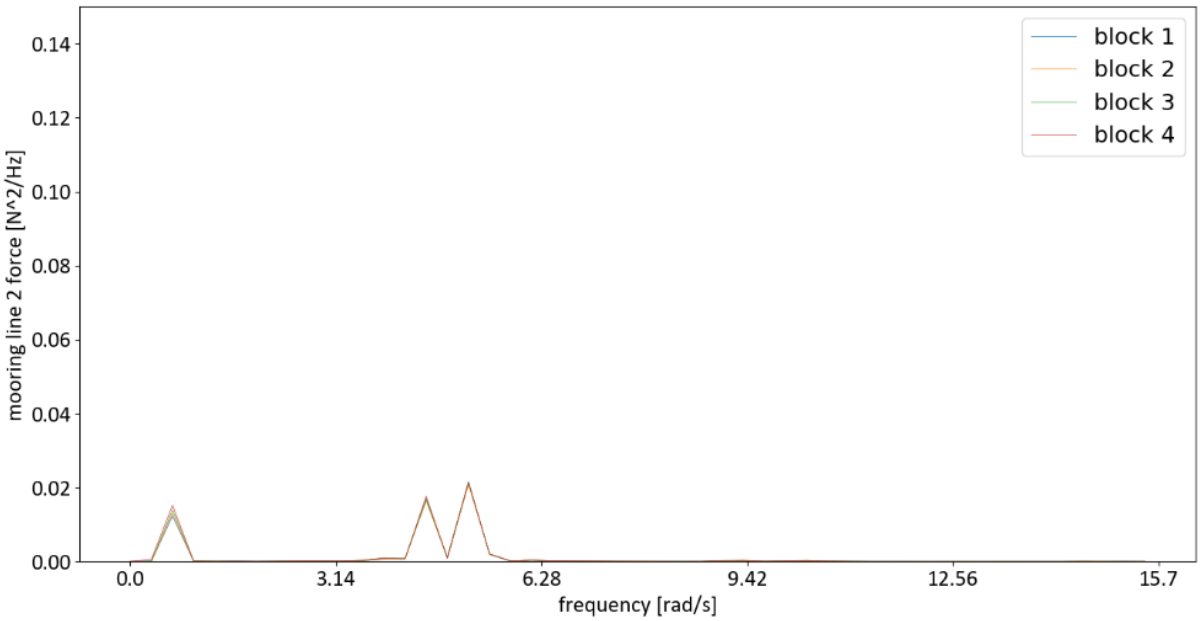

Figure 102: PSDs of the first four blocks of the mooring line force during test b4_NM.

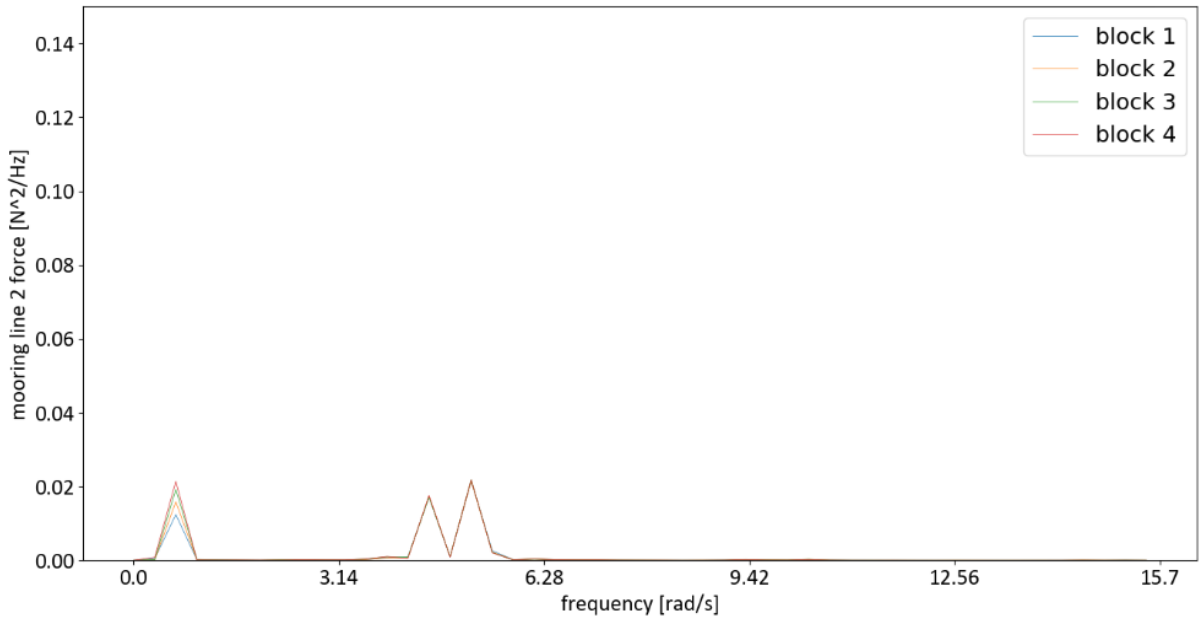

Figure 103: PSDs of the first four blocks of the mooring line force during test b4_NM_2.

Figure 104 shows the comparison of the different b4_NM tests, which also show that the different blocks are not significantly different.

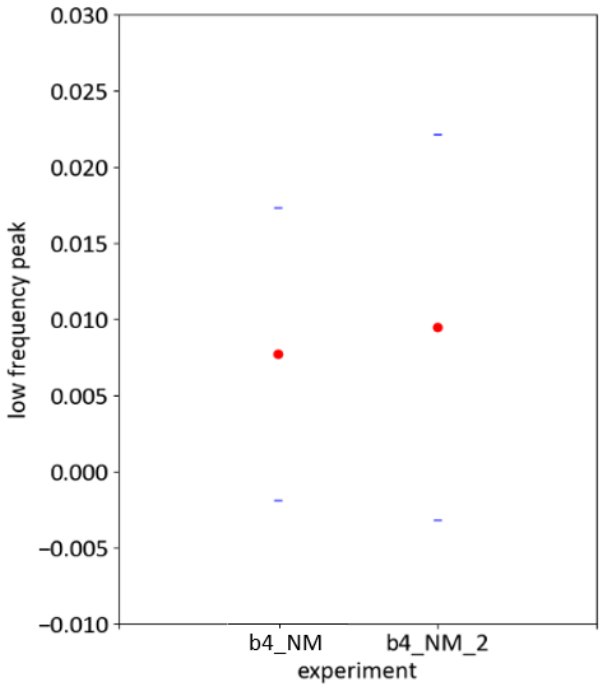

Figure 104: Comparison of the height of the peaks between the different b4_NM experiments.

Figures 105 and 106 show the comparison for surge again in test b3 and b3_2. So, PSDs of the first four blocks of the surge movement in the first test are compared with PSDs of the first four blocks of the repeat test.

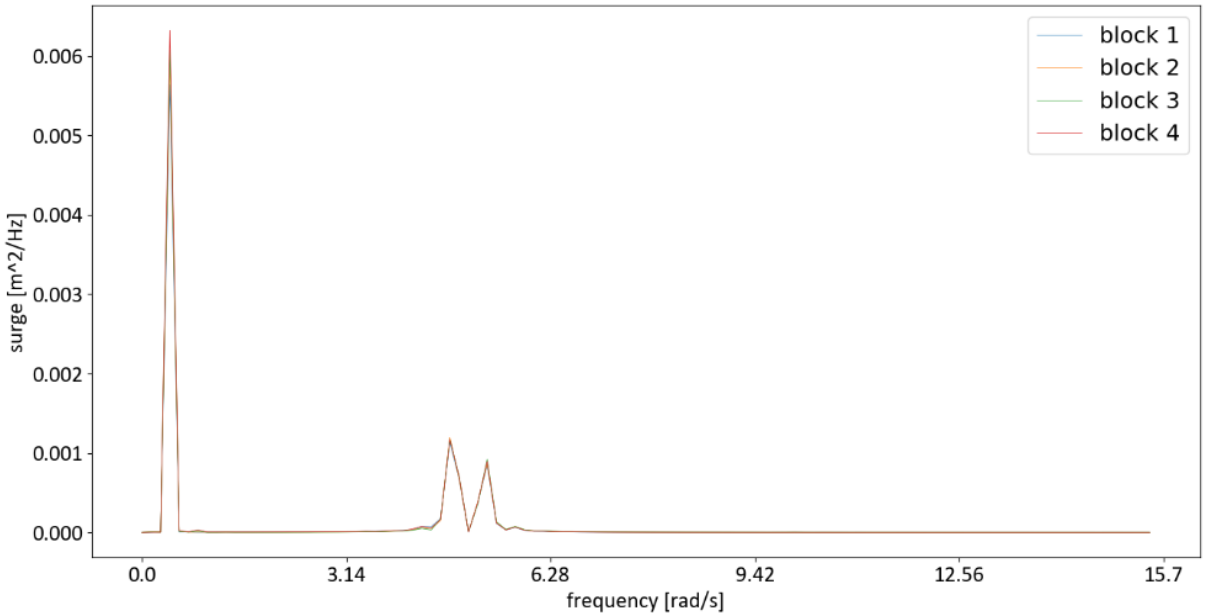

Figure 105: PSDs of the first four blocks of the surge during test b3.

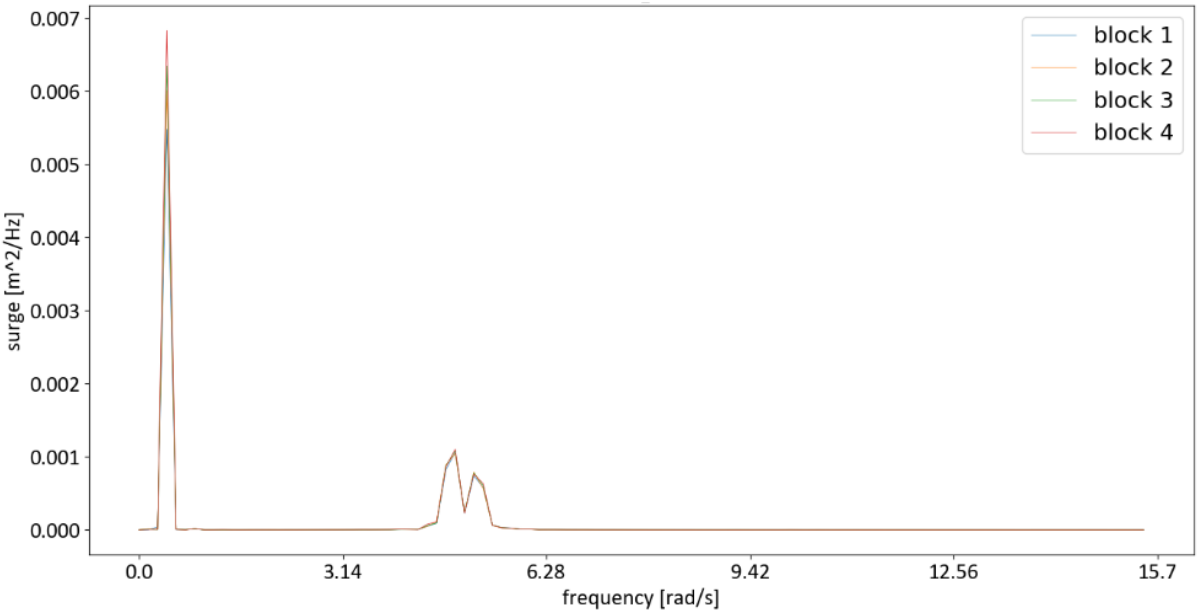

Figure 106: PSDs of the first four blocks of the surge during test b3_2.

Although the wave frequency shows some difference, around the interesting low frequency peak a very similar response can be found. This then also clears the way to cluster this data in a single point.

What follows now is a general overview of all this data bundled together per system, visualizing table 9, with the uncertainty around the period and the bundling of repeat tests included. Figure 107 through 110 show graphs of the areas under the low frequency range of the bundled blocks per system/bichromatic wave combination against the ratio of wave frequency to natural frequency. So, all the b3 wave tests for mooring system 1 with wind have been bundled together and the average area under the low frequency range is calculated (from table 9 it can be seen this comes down to roughly 0.12 N^2 taking the b3XL tests into account). Then the difference frequency of b3, 0.43 rad/s is divided by the surge natural frequency of 0.49 rad/s, giving a ratio of 0.87. The marker for this combination can then be found at {0.87, 0.12} in figure 107. The 95% uncertainty range in period and amplitude are also indicated. This is done per mooring system wind condition combination to prevent clutter.

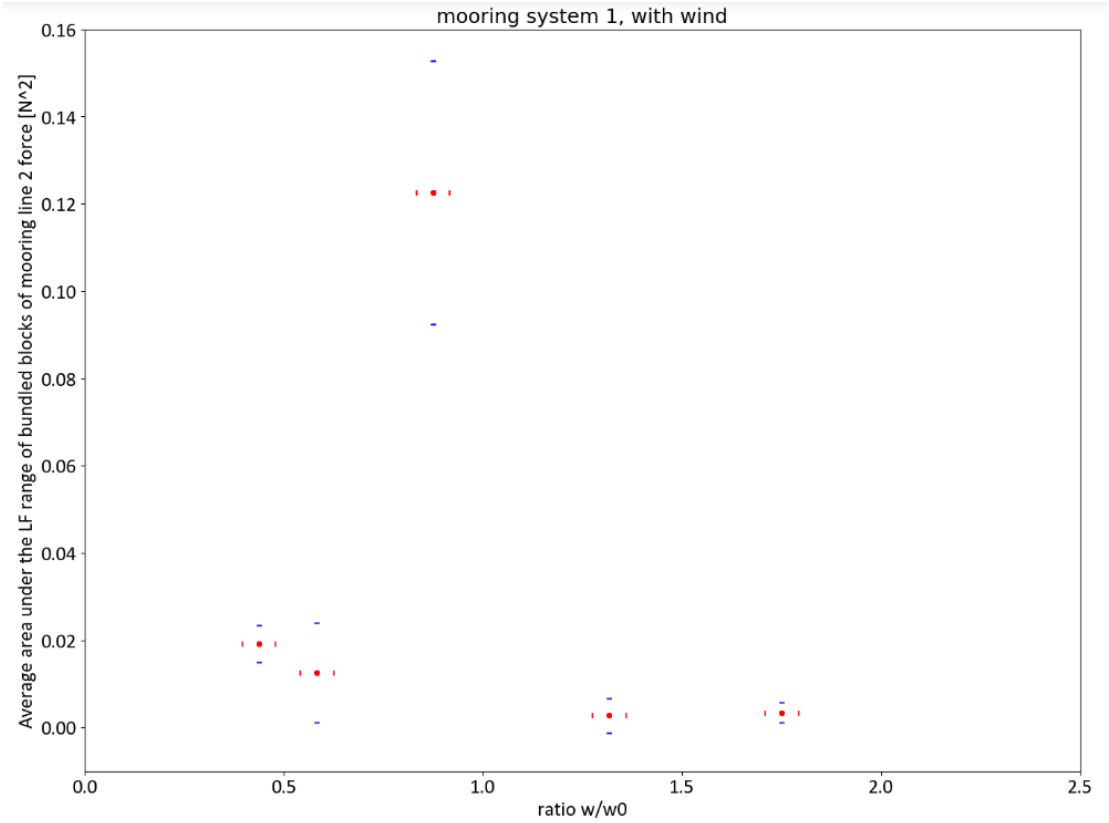

Figure 107: Graph showing the average system/wave combination response in mooring line force over the ratio of frequencies.

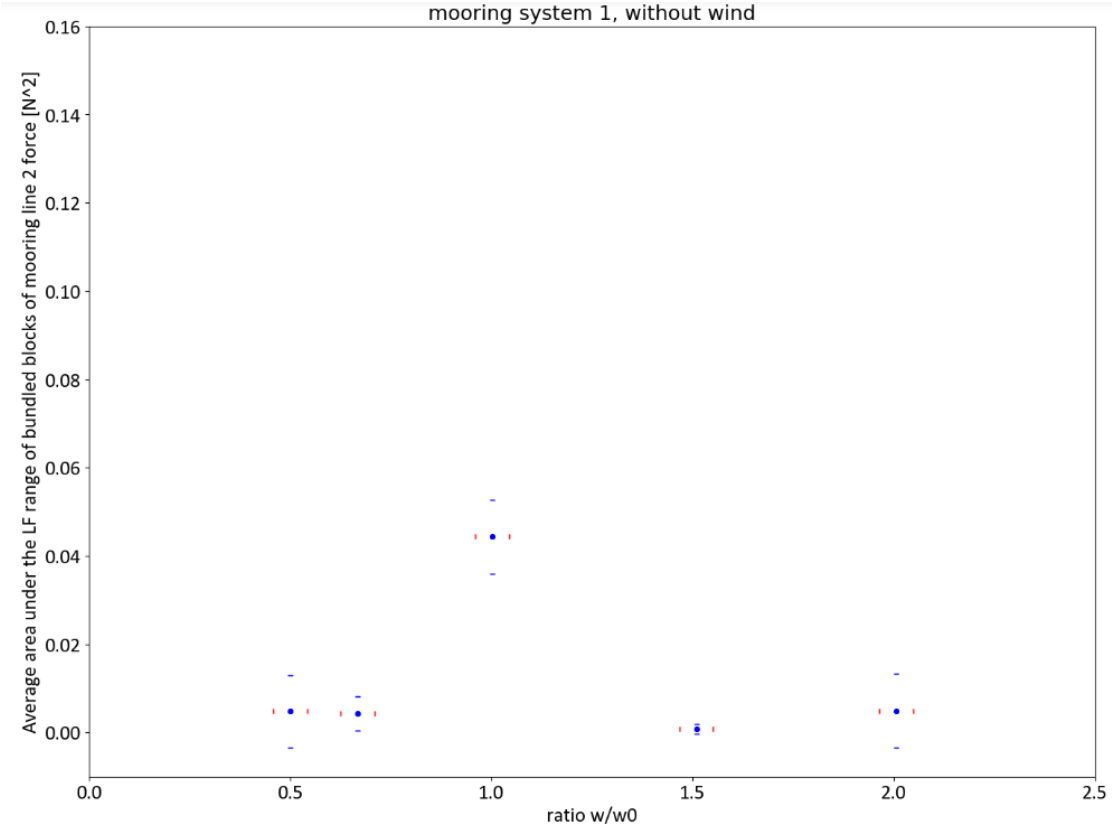

Figure 108: Graph showing the average system/wave combination response in mooring line force over the ratio of frequencies.

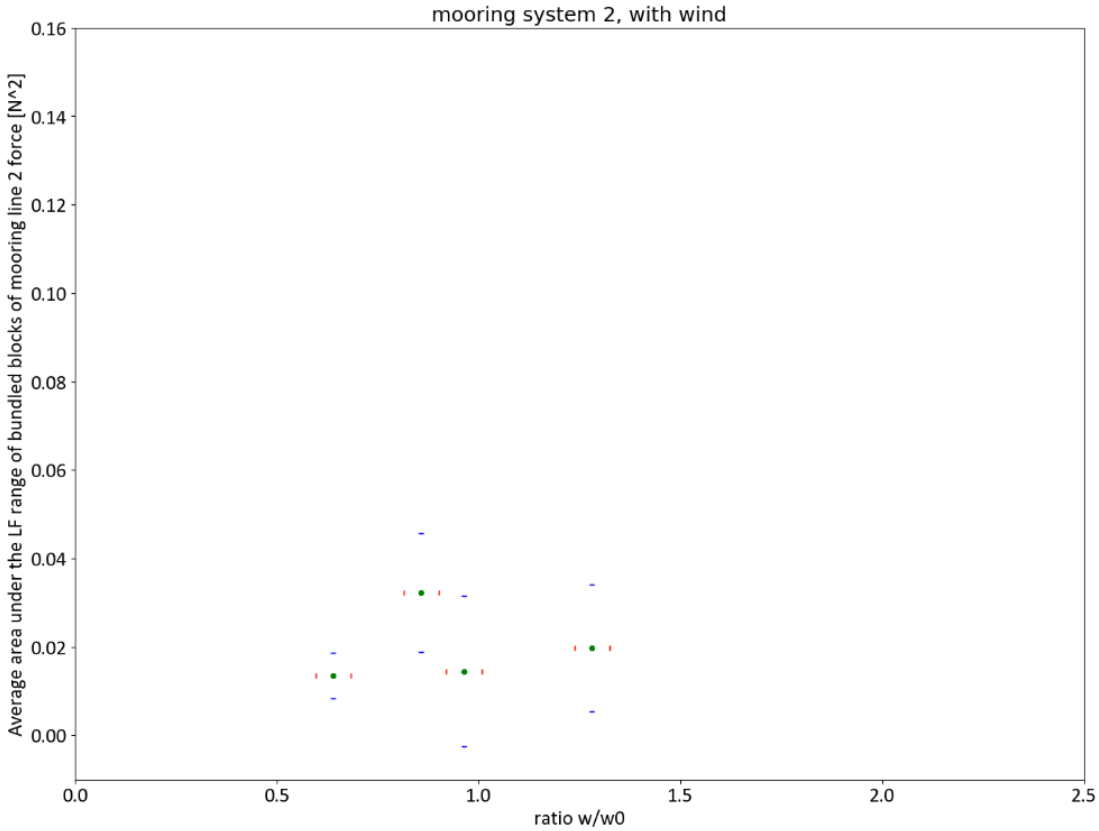

Figure 109: Graph showing the average system/wave combination response in mooring line force over the ratio of frequencies.

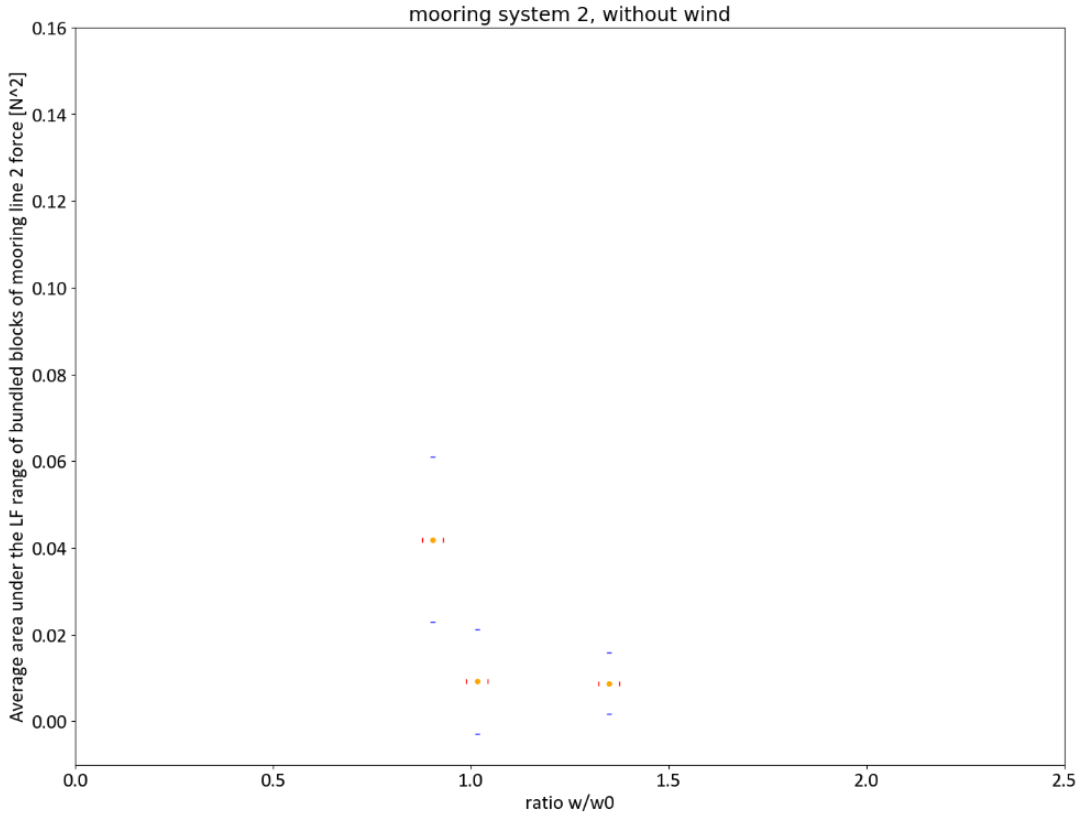

Figure 110: Graph showing the average system/wave combination response in mooring line force over the ratio of frequencies.

It can be seen that most tests have a relatively low response, but that an uptick can be seen slightly before a frequency ratio of 1 in most systems. The highest response is from mooring system 1 with wind and wave set b3 at 0.12 N^2. As was described during the verification chapter this system (mooring system 1 with wind) had the slack lines which are probably the reason for the large response as the mooring system becomes a single point mooring system and drastically increases the amount of force in this mooring line. A conclusive statement on this cannot be made and further research to isolate this effect would be necessary. A good way to tackle this would be to remove the two rear mooring lines and see if the response is similar. From the (lack of) difference between the responses one could establish whether the slack mooring lines during this experiment were indeed the cause. It is however perhaps not very relevant as any actual FOWT design should not have slack lines.

Besides the very large response in figure 107 it can generally be observed that the different figures show a test with an increase in the response. This would be expected as the system comes closer to moving in resonance with the bichromatic waves. Another remark would be the higher valued red marker at a ratio of 0.45 in figure 107, corresponding with wave b1 on mooring system 1 with wind. This could again be a consequence of the slack mooring line, but a definitive reason is hard to give. Some evidence pointing in that direction is the fact that the force in mooring line 1 during this test is not asymmetric as one would expect due to the drift force and the consequently asymmetric surge motion. The disconnect between the surge motion and mooring line 1 would suggest that the mooring line is not a functioning part of the mooring anymore.

Figure 108, showing mooring system 1 without wind, has the best representation of the desired effect in the test data. As can be seen the test located right at the natural surge frequency has the highest response with the located away from that location showing very little low frequency response. This figure thus best shows the low frequency effects of the resonance.

Noticeable is that in figures 109 and 110, corresponding with mooring system 2, the tests closest to the ratio of 1 are not the tests that have the heightened response but instead earlier tests around a ratio of about 0.8. The reason for this shift is not quite clear, the possibility that it is due to the ''damping shift'' of the resonance peak is explored in the discussion but does not seem to be the case. A shift due to measurement errors is also explored by the introduction of uncertainty bars in the x direction, but again does not seem to explain the phenomena. It should however be noted that the mooring system 2 tests have less data available than the mooring system 1 tests, which makes it more difficult to draw hard conclusions. In general, it can also be said that more data also in between the points might be a good recommendation for future research.

Figure 111 shows the same kind of graph but now for the surge and all systems combined as the clutter does not impede the observations. Again, the b3 test stands out but it should also be noted that the general increase in response around the frequency ratio of 1 is no longer present. Two blue markers corresponding to mooring system 1 without wind show a large uncertainty band, this is because here the repeat tests do not match, making the bundled uncertainty very large, even as the deviation of the results inside a single test (via the blocks) is quite good. This even makes the lower range estimate run negative which is unrealistic. In both cases, one of the two tests has a low frequency response of basically 0, where the other has a relatively high response, which is most likely somehow related. What the precise cause is, is unknown. It should be noted that most 95% uncertainty ranges overlap, meaning there is not real significant difference between the experiments, as the ranges are even smaller than in the force graph.

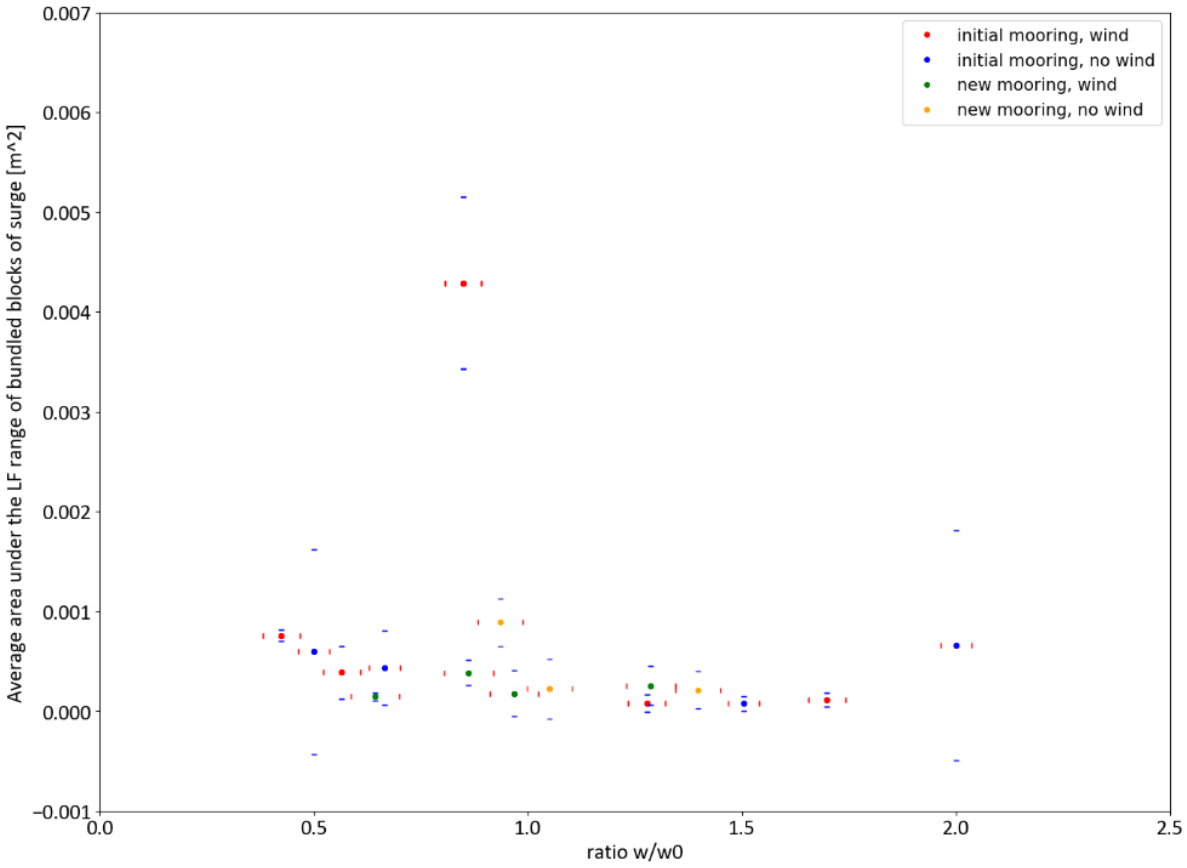

Figure 111: Graph showing the average system/wave combination response in surge over the ratio of frequencies.

6. Discussion

The discussion goes into the analysed results previously found. This is done via a comparison with a damped mass spring system and a general discussion. This general discussion will place some of the findings back into the previously discussed research such as the OC5 project.

6.1 Comparison with damped mass spring model

A comparison with a damped mass spring system is made using the damping from the decay tests. This comparison shows unexpected results further supporting the theories around slack lines.

The x-axes from figures 107 through 111 were chosen with a reason and that is to allow for a comparison with a damped mass spring model. This will be large simplification of the system using a mass excited by a force attached to a solid surface by a spring and a damper. This resembles the FOWT on a fundamental level, with the mass resembling the mass of the floater, the spring simulating the return force exerted by the mooring system and the damper resembling the damping of the movement as a result of drag. The goal of this model will be to compare the different systems in behaviour as a result of damping. There are some fundamental inaccuracies in this method however, the first being that this model uses linear springs whilst the mooring system changes its stiffness based on excitation. The second inaccuracy is that the model uses linear damping, based on velocity whilst drag on the mooring line will be dependent on the amplitude for low pretensions (Webster, 1994). Nonetheless, this can be a good way to look at the fundamental influence of the damping. Figure 112 shows a diagram of the damped mass spring model.

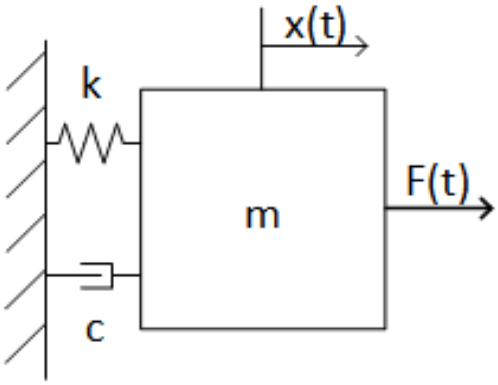

Figure 112: Diagram of a damped mass spring model.

In this model the damping ratio ζ can be calculated with the damping c, the spring constant k and the mass m via the following formula:

$$\zeta = \frac{c}{\sqrt{2km}} \tag{12}$$

This is the same damping ratio as found during the decay test, displayed in table 8 per system. The equation of motion of the model is as follows, based on a force (F) balance, centred on the displacement x:

$$m\ddot{x} + c\dot{x} + kx = F(t) \tag{13}$$

After a while the differential equation damps out any initial movement and only reacts to the force in what is called a steady state solution, which follows:

$$x_{steady} = \lim_{t \to \infty} x(t) = |X| \cos(\omega t - \varphi) \tag{14}$$

Wherein an amplification factor |X| can be described using the static displacement X_{static} and the frequency ratio ω/ω_0:

$$\frac{|X|}{X_{static}} = \left(\left(1 - \frac{\omega^2}{\omega_0^2}\right)^2 + 4\,\zeta^2 \frac{\omega^2}{\omega_0^2}\right)^{-\frac{1}{2}} \tag{15}$$

Plotting this function for the amplification factor with different values for the damping ratio ζ leads to the graph in figure 113.

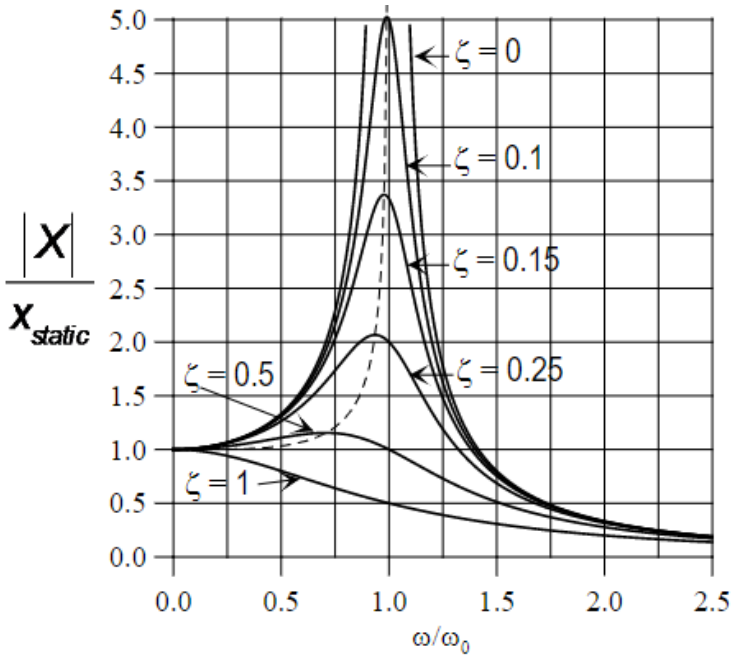

Figure 113: Graph showing the multiplication factor as a function of the frequency ratio, taken from (Tsouvalas & Metrikine, 2022).

From figure 113 the same effect of an increase in response around a frequency ratio of 1 as can be seen in figure 107 through 110. The figures differ in that figure 113 shows movement rather than force, as figure 111 does. However, because of the linear spring the force amplification is the same as the movement amplification shown in figure 111, so the comparison still holds.

When looking at figure 107 through 110 and including the damping ratio from table 8 however the comparison has some problems. As figure 113 shows the lower the damping ratio the higher the amplification factor, but the highest valued system, mooring system 1, has the highest damping (see 4.1 for the damping and figure 20 for the mooring systems). As with the peculiarities this is probably due to the slack mooring lines, which besides increasing forces on the remaining mooring line also increase drag as they are lose weight dragging over the bottom, decreasing the speed at which the floater moves. This increases the c parameter in the damping ratio, linked to drag. It also has an effect on the k parameter, or the stiffness of the system, as the single mooring line will be less stiff, a lower k, than the three mooring lines together again increasing the damping ratio. Note that due to the non-linear stiffness of mooring lines this individual line might have a higher stiffness compared to being with three but that the mooring system in general will be less stiff, at least until the non-linear stiffness becomes dominant way further in the motion.

To show that the system responses do follow the general trend set in figure 113 the individual systems with their damping ratios will be repeated in figure 114 through 117. This shows that apart from mooring system 1 with wind the systems tend to show that a lower damping ratio leads to a higher response of the singular frequency aimed at the natural frequency. Although mooring system 2 with and without wind does not show this heightened response on the test at a ratio of 1, but a bit earlier. These both correspond with wave b6. Why this wave has the heightened response and not the b4 wave aimed at the natural frequency is not known. Do please note that the amplification ratio axis has been scaled to roughly match the highest point and differs per figure.

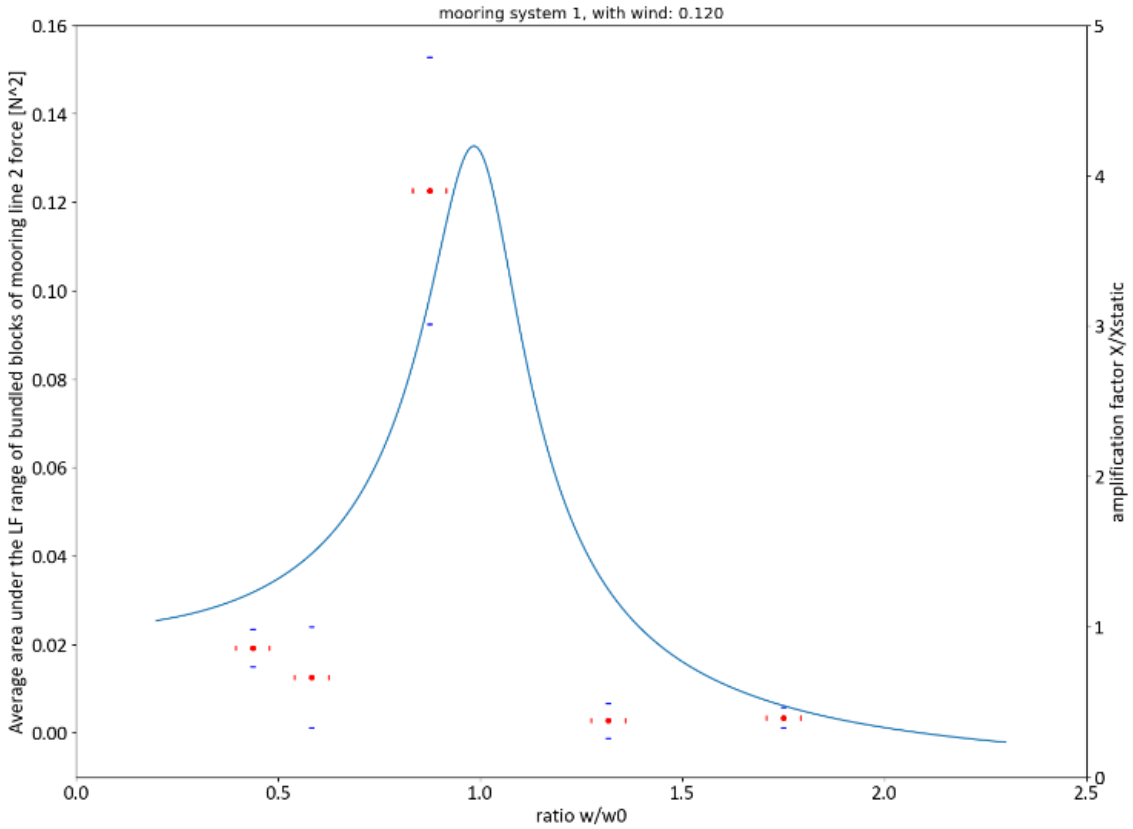

Figure 114: The response in the low frequency range as a result of the frequency ratio for mooring system 1 with wind

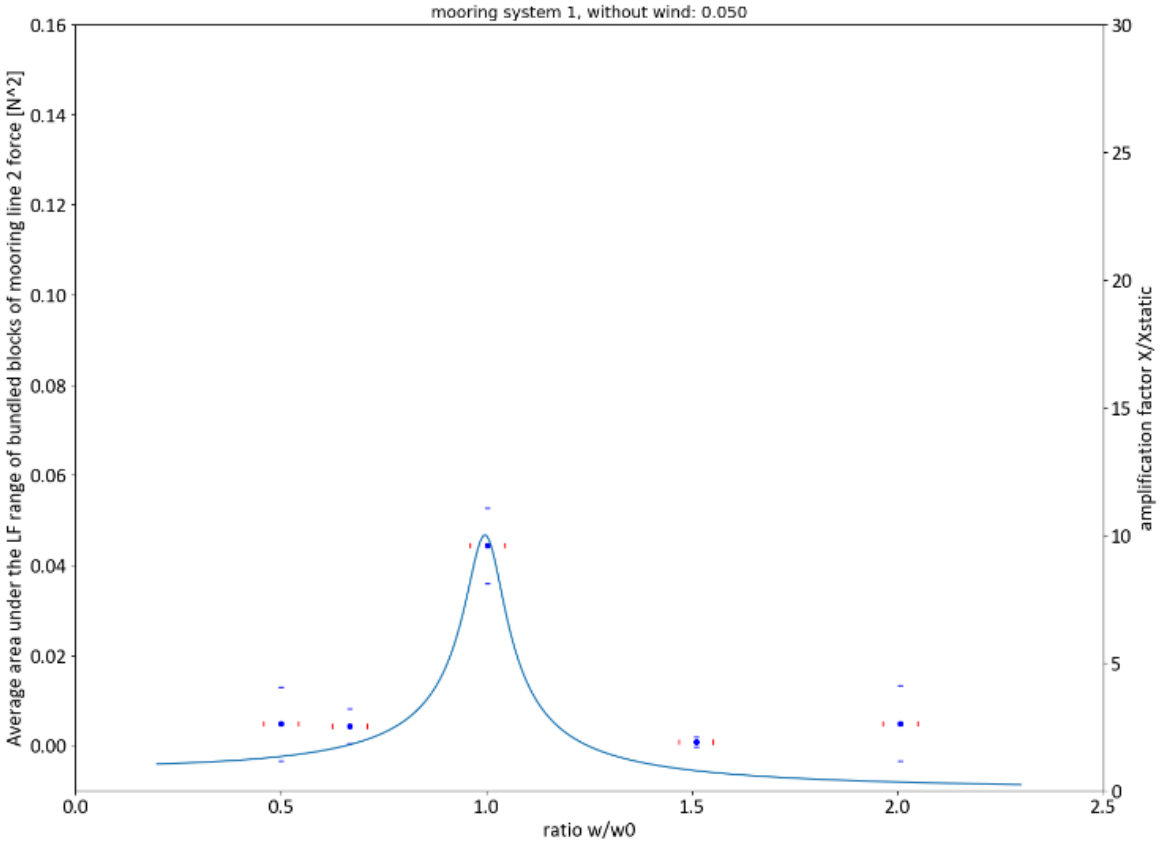

Figure 115: The response in the low frequency range as a result of the frequency ratio for mooring system 1 without wind

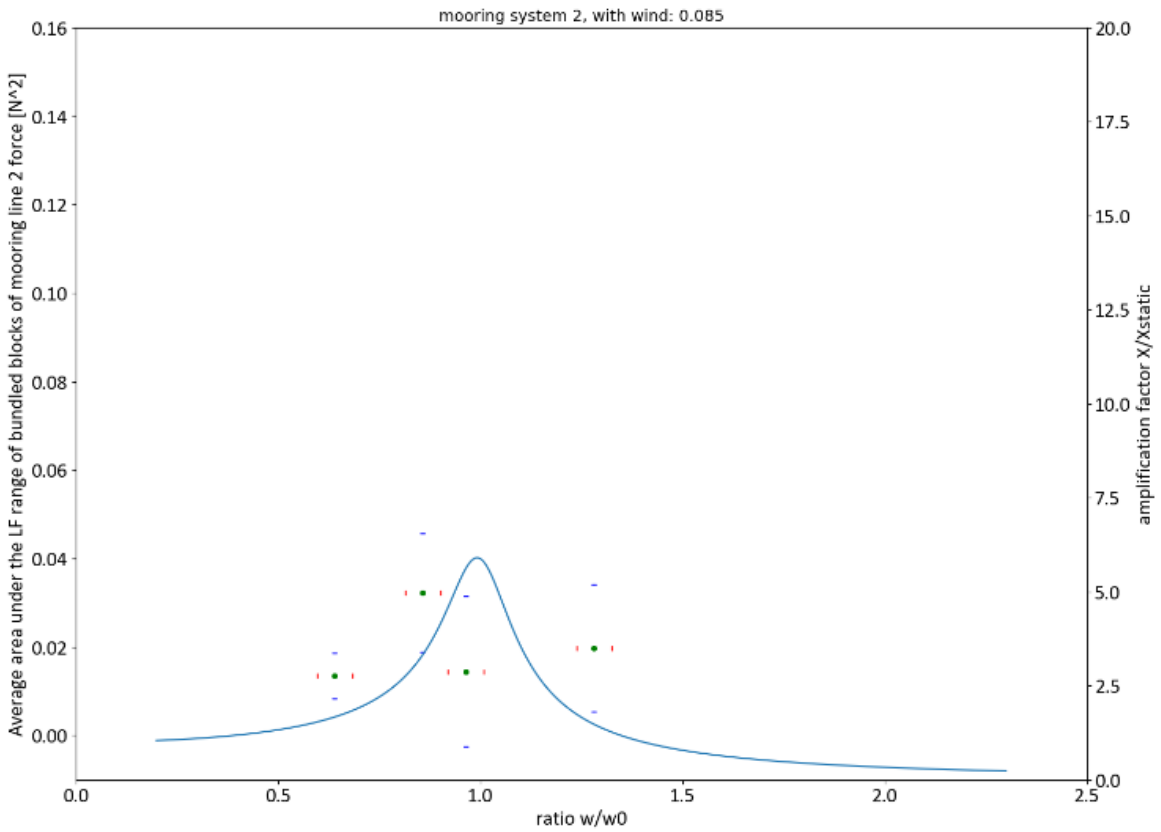

Figure 116: The response in the low frequency range as a result of the frequency ratio for mooring system 2 with wind

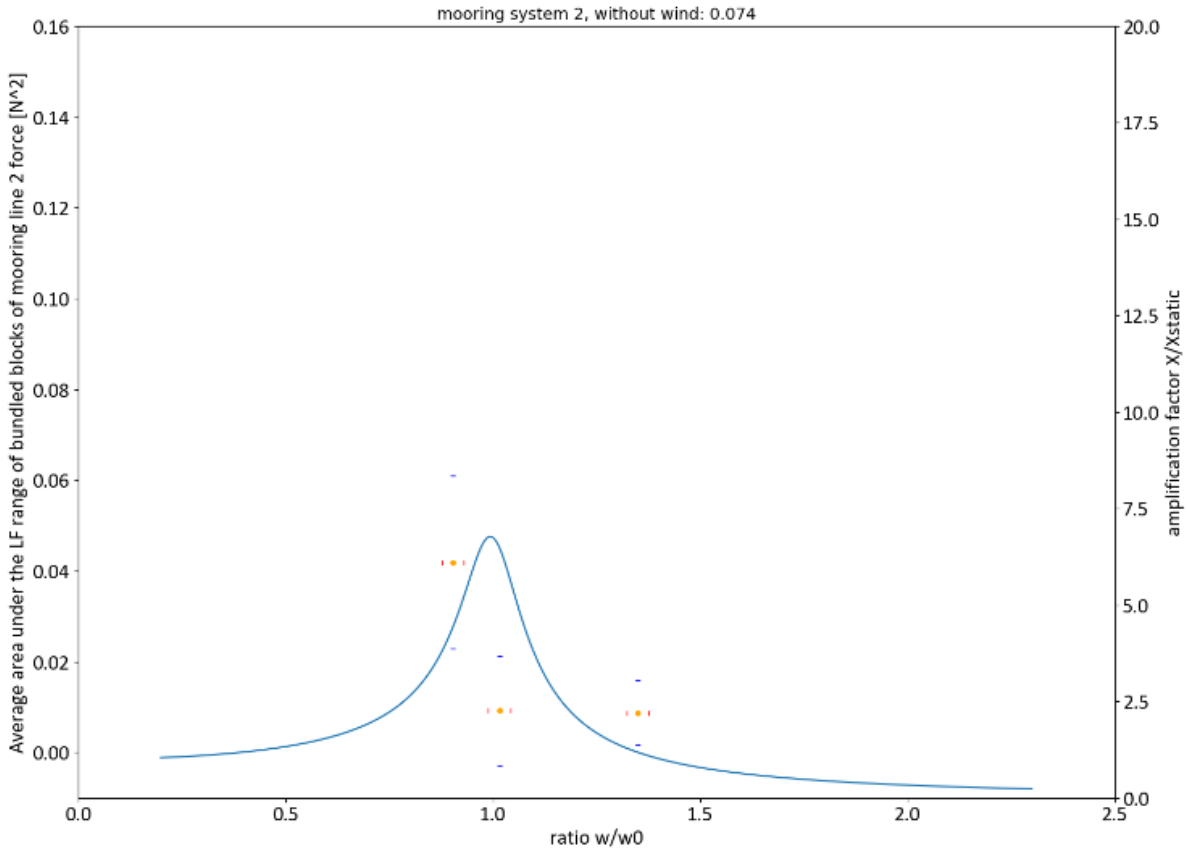

Figure 117: The response in the low frequency range as a result of the frequency ratio for mooring system 2 without wind

6.2 Reflection

A bird's eye view is given of how this thesis fits into the bigger research picture. It will take the findings and compare them to the findings from earlier papers and see if the conclusions drawn fit within the general research context.

The main goal of this research was to examine the behaviour of FOWTs at low frequency near the surge natural frequency. This was coupled with a few other goals as well, such as documenting the setup of the model, providing the data set in an easy-to-use way, making a good uncertainty assessment and testing different mooring systems. All whilst staying close to the OC5 project.

Numerous modelling decisions had to be made along the way starting with the way the low frequency was reached. This was done using bichromatic wave set to create a beating pattern which would excite the low frequency. This approach had the upside of being at all possible to implement at this project scale and being a lot clearer in exactly what frequency was being excited. However, this single frequency excitation is also its largest downside, as in the end only a few frequencies were excited. This can be seen in figures 107 through 110, were there are also some large gaps in the datasets on either side of the frequency ratio of 1. Ideally the response in these gaps would also have been known but that is not the case. Looking at the future the bichromatic wave do make it easier to repeat the test in any following research either experimental or numerical.

A second large decision was the scale. Rather than the 1:50 of the OC5 project this research was done at 1:96. Naturally a smaller scale gives truer to life results but is also harder to implement. The main advantage of the 1:96 scale was that it became possible to switch the mooring systems relatively easily. A smaller scale, and thus a larger depth would have made it very difficult to quickly switch systems. It also would have removed the optical access enjoyed because of the towing tank number 2 windows. A consequence of the scaling choice when it comes to a comparison between this project and the OC5 project is that the natural frequency was harder to get right. The scaling changes the added mass off the model relative to the mass of the model due to scale effects of viscosity. Because of this additional added mass, the natural period of mooring system 1 was too high compared to the OC5 project at 14.6 s versus 10.9 s. This was remedied with mooring system 2, which showed results more in line with the OC5 project (more on that later).

A further point was the wind simulation. The OC5 project and numerous other projects examined the wind using a wind generator and Reynolds scaled blades. Besides the difficulty of this approach, it would have added relatively little value to this project as the main focus was on the low frequency behaviour. The main difference between the two methods being the damping and the ability to produce an oscillating wind force. Damping experienced during a wind simulation via wind generator and blades would mostly impact the pitch frequency movement as velocity in the lower surge frequencies is too slow. The device used however does simulate some damping because of the way it operates. As the pitch movement comes forward for example the aluminium disk needs to start spinning forward, increasing the relative velocity, increasing the force on the winch and thus the nacelle. The other way around the disk moves backwards as the tower pitches backwards, decreasing the relative velocity, decreasing force. This is somewhat akin to drag due to tower pitch, although the exact magnitude and accuracy of this effect is unknown. The behaviour of the model using the method from this thesis is only significantly affected by the wind via the change in mooring line stiffness due to the forcing. The approach used in this research of a theoretically constant force would thus suffice to simulate the influence of the wind in the purposes of this research. The advantage of this approach, its simplicity, allowed for a very distinct upside in the lack of a data bundle coming from the model. This data bundle would have influenced the low frequency movement and the elimination of it is thus

very welcome. One practical downside of the device however seems to that the device degrades over time, as it became necessary to increase the voltage into the electric motor as the tests went on in order to keep the force equal. What part of the device was responsible for the degradation is not known. An improvement of the device would be to introduce a low frequency oscillation to simulate wind gusts found in real life situations (Wichers, 2013). This could easily be done by varying the motor output via the voltage.

A last major modelling decision to be discussed are the mooring lines, contrary to the full chain mooring lines of the OC5 project, the mooring lines of this research were chains with a fibre rope top part. This was to reduce the weight pulling down on the model as the chains had to be relative heavy to get enough stiffness out of the limited depth. The fibre ropes on mooring system 1 however were too long such that the rear lines would be slack. This unintentionally led to the collection of data on how the front mooring line behaves if the rear mooring lines are slack. The OC5 project had this issue as well during extreme wave events so having it repeated in a more consistent environment might prove to be a useful addition.

The main result found is that the force response tends to increase as the frequency ratio goes closer to 1, figure 107 illustrating this best. This tends to correspond with the findings in the OC5 project and other research such as (Tomasicchio, 2017). This earlier research also found a very large response around the surge natural frequency of their models.

One remarkable finding is that the surge response does not show this increase. Figure 111 shows the response remaining largely flat with the exception of mooring system 1, which had the enlarged response due to the slack mooring lines. Why the surge response is different to the force response is not strictly known but the nonlinear behaviour of mooring lines is the most likely cause. As the mooring lines might have had sharply increasing stiffnesses keeping the surge limited whilst drastically increasing the force around the natural frequency. To test this a study into the stiffness of the mooring lines should be conducted.

To facilitate a comparison between this project and the OC5 project, figure 118 shows the PSD of the mooring force of the b6_NM model test. This is the highest responding wave with mooring system 2 with wind and is thus the best to extract from this research as it has both wind and non-slack mooring lines. Figure 119 then shows the graph from the OC5 project shown in the introduction presenting PSDs of the experimental (black) and numerical (colour) results of the force in their mooring line. One can see that the proportion of the wave frequency response and the low frequency response looks very similar between the two experimental results, although the scale is completely different.

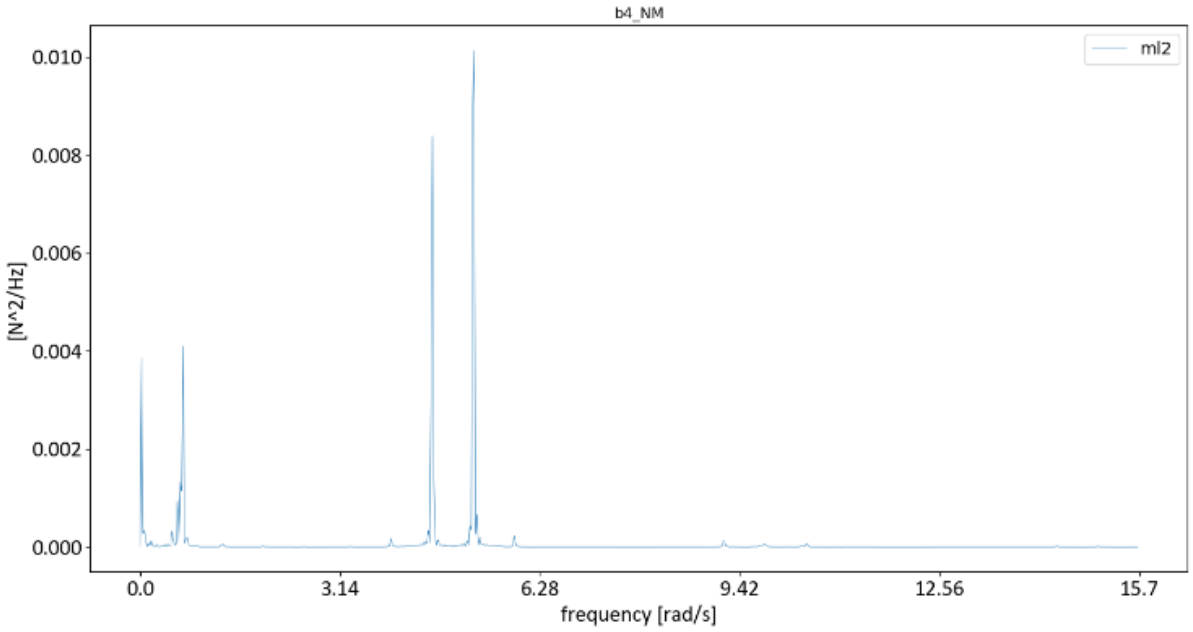

Figure 118: PSD of the mooring line 2 force for the b4_NM test on mooring system 2 with wind

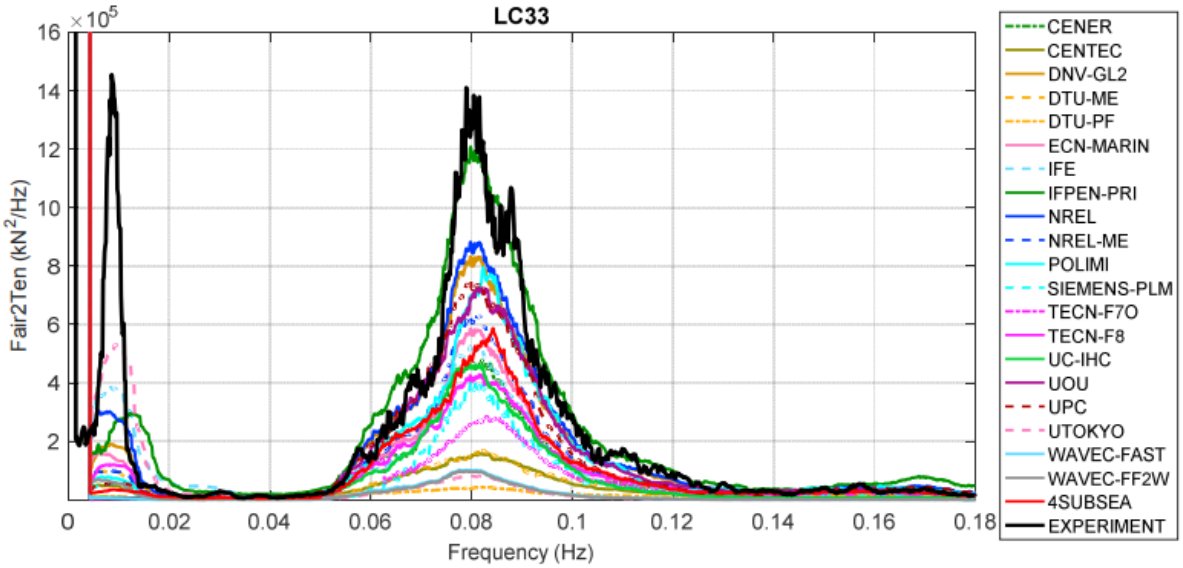

Figure 119: PSD of the lead mooring line force for the OC5 project with the experimental results in black, taken from (Robertson, 2017)

There are of course some changes such as the more spread out forcing in the OC5 project at the peaks due to the irregular waves but both cases show a similarity in that the response in low frequency is a quite significant fraction of the response in the wave frequency even though the results from this thesis are not as high as the one from OC5. The fraction of low frequency response during the current experiments are also significantly higher than the numerical simulations done. It also means that for the OC5 project a bit more certainty can be established in the fact that this low frequency response comes from the difference frequencies between their irregular waves as this effect is now isolated.

During the OC6 project (Wang & Robertson, 2022) already mentioned in the literature review, tank tests were done as well. These tank tests tested bichromatic waves at the surge and pitch natural frequency. Although rather than mooring line force, a force in the surge direction on the model was

measured. The results still showed that the force on the model increased on the surge natural frequency more so than on the pitch natural frequency. This is comparable to the finding in this thesis that the force increases near the surge natural frequency.

This thesis also introduces some new aspects not seen in the literature review performed earlier, such as the damping ratio and the slack mooring lines. Although only limited data is available in this thesis the damping ratio does seem to provide a reasonable indication of the heightened response around the frequency ratio of 1. The slack mooring lines also provide an insight and comparison of what happens when the mooring lines are not tensioned properly, leading to a larger force. These two elements provide nice first steps into more research opportunities.

As mentioned in the literature review (Yan, et al., 2021) established a new method for estimating damping in a mooring line. This research could help better estimate mooring line damping to enable numerical models get closer to the damping experienced by experimental models, thus closing the numerical experimental gap.

The slack mooring rear lines are a hard subject to find research on. The OC5 project also had slack lines during some more extreme wave events but not much information is available on what happened during those events. The closest research available is on platforms with failed lines, but understandably this tends to focus on the front mooring line failing and is not really comparable.

7 Conclusions and recommendations

A conclusion to the thesis is given by a way of presenting the findings and answering the research question in short form in the section below. Besides an answer to the research question, recommendations for future experiments are given based on the experience of performing this research.

7.1 Research question

The research question will be answered by answering each of the sub questions again in short form.

As mentioned in the introduction the main goal of this research was to do physical tests which looked at the low frequency response in the mooring lines and the surge motion. Additionally, uncertainty assessments and different test cases (see figure 20 for the differences between the mooring systems) were included in the requirements as well as a good set up of the model. The main research question was split in multiple sub questions which are answered in short order below.

What relevant loading processes can be expected on the FOWT, in what magnitude and which frequency?

As mentioned in the introduction this research is based on the OC5 project, which also gives rise to the answers to these sub-questions. The two main external loading processes are the wind and the waves. Concerning the wind, a conscious decision was made to do a theoretically constant force via a magnetic clutch rather than a wind generator and Reynolds scaled blades. This constant wind force was successful, providing relatively constant wind force on the model.

The waves were changed compared to the OC5 project to better focus on the low frequency. Rather than irregular sea states a bichromatic wave set was used to be able to specifically focus on certain low frequencies via the difference frequency, causing a beating pattern. These focussed frequencies corresponded with the natural frequency of the model in surge direction.

What physical aspects of the FOWT need to be taken into account?

The main aspect to be modelled was the mooring system, as this system had the largest influence on the eventual results. This system had two configurations; one was designed with the intention to be dynamically similar to the OC5 project. These mooring systems consisted of a chain with a fibre rope top part to reduce weight, which was different from the OC5 project.

In general, it can be concluded that the mooring system was suitable to determine the influence of the forcing frequencies. Although it must be noted that mooring system 1 could have been better designed to exclude the slack mooring lines. The comparison between the results of the OC5 project and this thesis done in figure 118 show that the results are qualitatively similar showing that the attempt to replicate aspects of the OC5 project was successful.

How can these forces, specifically the low frequency ones, and aspects of the FOWT be properly modelled in scale tests?

The 1:96 scale allowed for a smaller more manageable model which eased the switching of the different mooring systems. It also allowed the usage of a tank equipped with glass windows allowing for good optical access. The smaller scale model and the thus relatively higher added mass did obfuscate the dynamic similarity with the OC5 project.

Measuring devices were installed in key locations around the model, namely force transducers in the mooring lines and the wind simulation device, wave gauges and a camera system for movement tracking.

A mix of different tests were performed to be able to isolate certain effects. These include tests with the single components of the bichromatic wave sets and tests without the wind force applied. All this test data was collected, synchronized and filtered to get an extensive database. Publicly providing this database hopefully adds an interesting option for others wanting to do future research into this topic.

What forces are found in the mooring system and what magnitude are these forces?

The focus of this research is mostly on the mooring line force caused by the beating pattern. From the output of mooring force during test b3 a time series can be generated, which is shown in Figure 53. Here it is determined that the amplitude of the total force oscillation is 0.15 N, a tripling of its monochromatic counterpart. A spectral analysis of the results is performed and shown in Figure 98, where it can be seen that there is a significant low frequency peak, especially compared to the wave frequency response.

An aspect to mentioned is the fact that one of the mooring system configurations tended to have slack rear mooring lines. This of course has some effect on the front mooring line, which took over the load. These slack mooring lines thus increase the mooring force in the system not necessarily due to the influence of the frequency. The b3 model test shown earlier suffers from this response but the b6 test shown in Figure 118 does not. From this figure it can be seen that the low frequency response is half the wave response, a finding not too far of the OC5 project, especially taking into account the different conditions.

What motion can be observed in the floater?

The other side of the coin of the force in the mooring lines is the surge movement of the model as the two are linked via the stiffness. The surge recorded during test b3 can be seen in Figure 62, showing a large asymmetry in the response. The general peak to peak differnce is about 50 mm in the low frequency response but Figure 74 shows that this amplitude is not centred around the middle line. This is again because of the slack lines experienced during this test.

What is the influence of the eigenfrequency and load frequency on the response, specifically in the lower ranges?

The eigenfrequencies were also determined via decay tests. These decay tests also enabled the determination of the damping. The low frequency response found in the Fourier transform can then be plotted against the ratio between the load frequency and the natural frequencies of the systems. This leads to Figure 107 through 110 for the mooring force. In this figure it can be seen that the low frequency response grows when closer to a frequency ratio of 1.

Notable in this is the large response from mooring system 1 with wind, which had slack lines. The response with this system is much larger than the other system even though the system had more damping than the other systems. This can be seen from Figures 114-117 where the damping seems to be a reasonable indicator of the response with the exception of mooring system 1 with wind.

Figure 111 shows the same frequency ratio-low frequency response graph but now for the surge. Here the exception of mooring system 1 becomes even more clear. It can also be noted that apart from mooring system 1 the responses seem remarkably flat. This would indicate that the surge is less

affected by the natural frequency than the force is, which might be caused by the nonlinear nature of the mooring line stiffness.

With these sub questions the main question can be then be answered.

What is the low frequency response in the mooring system and the floater motions during a physical test with a floating offshore wind turbine under wind and wave loading?

From the results of the tests the theory that the low frequency response comes from the difference frequency in the bichromatic wave sets is reasonably confirmed. The asymmetry visible in the time series further indicates that the wave drift forces are responsible for the low frequency behaviour. The heightening of the response around the natural frequency as shown in figure 107 also shows that getting close to this frequency amplifies the effect, as was also found in the OC6 project. The comparison between the test results and the results from the OC5 project done in the discussion also show that these findings can be applied to the OC5 project.

Furthermore, it was seen that slack lines have a very large impact on the force in the mooring lines, especially on the lower frequencies and should thus be avoided at all times. It should be noted as well that these slack lines were caused by the wind force, meaning that this is an important aspect to take into account during the design. Some indication in the test results for a factor determining the response can be found in the damping ratio as this parameter is both theoretically and experimentally (excluding the slacked lined system) consistent with the strength of the response around the natural frequency.

In practice increasing the damping ratio could be used to get less low frequency response in a FOWT. This could be of importance as it might reduce peak design load of the mooring system and thus reduce cost. Increasing the damping on a mooring system, however, might prove costly in itself as it would, for example, consist of additional grids attached to the chain near the bottom or loosening the mooring line, letting it drag more. A cost benefit analysis would need to be made to study the feasibility during design.

7.2 Recommendations for future experiments

Recommendations on future research is given based on experience of these experiments.

For future research, a few recommendations and interesting aspects can be proposed. A good continuation of this research would be to do additional tests but now focused on the narrower band around the frequency ratio of 1, for example between the inner two experiments done during this experiment, at 0.67 and 1.5. During this research a wider band of ratios was assessed which showed that not much response is to be expected far away from the ratio of 1. Furthermore, large gaps in the examined band made it harder to draw conclusions about the exact shape of the response curve. It would not be needed to cover every single frequency ratio, but a denser field could help in this aspect.

To expand on some of the findings of this research, a comprehensive study on the influence of the damping on the low frequency response could be performed. Theoretically, from the damped mass spring system, the damping is the limiting factor when operating at the resonance frequency. As the surge natural frequency is low for moored systems, the damping ratio could be important in understanding the low frequency response of the FOWT. Research around damping when it comes to FOWTs seems to be scarce and both experimental and numerical modelling could prove valuable in the design of more cost-effective mooring systems.

Additionally, the data generated in these experiments is provided in the appendix enabling a numerical comparison of this model to be made. This numerical model could be amply tested,

calibrated and validated to the large amount of data available from these tests. Making a numerical model where one can use the known damping ratio, for example, rather than have to estimate it, allows for the examination of the influence of the estimation of such a factor in numerical modelling.

Of specific interest could be CFD modelling as well as the bichromatic tests enable shorter runs. These CFD models could then, like OC6 help the calibration of numerical models. And as the wind force is recorded separately, the wind simulation aspect could even be isolated to get just the hydrodynamic effects in. These CFD models could then aid in better estimation of the parameters of numerical models, making those more accurate.

The wind simulation technique used seems to be suitable to low frequency research. An interesting addition might be to introduce a low frequency oscillation in the wind force as well. Introducing this oscillating wind would extend the wind force to the low frequencies, where it might play a crucial role due to the nonlinear stiffness of the mooring lines. Adding this low frequency oscillation will also improve real life similarity and can be done relatively easily by adjusting the voltage of the electric motor.

Hopefully this thesis adds something to general knowledge base around FOWTs, whether it is in the physics aspect and bringing to light an important and maybe overlooked parameter with the damping ratio. Maybe it serves as a conformation of the suspicion, during the OC5 project, for the causes of the low frequency excitation. That being the difference frequencies and showing their influence more clearly. It could help as a guide for future experimental research, trying some new things with wind simulation. The dataset might be useful to help develop or validate numerical models, or in the use of CFD modelling. And maybe, just maybe, it might remind someone to design their lines, so they don't go slack. One way or another, the overall intention of this thesis was to add something to the pool of engineering knowledge surrounding FOWTs, making them cheaper, safer and easier to build, thus furthering the energy transition.

References

Bashetty, S., 2021. *Review on Dynamics of Offshore Floating Wind Turbine Platforms,* Kingsville: MDPI.

Bertacchi, P., Di Monaco, A., de Gerloni, M. & Ferranti, G., 1994. *Elomar — A Moored Platform for Wind Turbines,* Milano: Sage Publications.

BMCM, 2023. *MA-UNI,* s.l.: BMCM.

Bouvy, A., n.d. *ACOUSTIC WAVE HEIGHT MEASUREMENTS IN A TOWING FACILITY,* s.l.: MARIN.

Caillé, F., 2017. *MODEL TEST AND SIMULATION COMPARISON FOR AN INCLINED-LEG TLP.* Trondheim, ASME.

Carlos, B., 2020. On the importance of mooring system parametrisation for accurate floating structures design. *Marine Structures.*

Dong, Y. et al., 2022. Review of study on the coupled dynamics of performance of floating offshore wind turbines. *Energies.*

Duan, F., Hu, Z. & Niedzwecki, J., 2016. Model test investigation of a spar floating wind turbine. *Marine Structures.*

EESI, 2010. *Offshore wind energy,* s.l.: EESI.

Fowler, M. et al., 2017. *1:52 Scale Testing of the First US Commercial Scale Floating Wind Turbine, VolturnUS:.* Trondheim, ASME.

General Acoustics, 2023. *Sensor USS 13-HF for UltraLab "Advanced and HF" controller,* s.l.: General Acoustics.

General Acoustics, 2023. *UltraLab ULS Advanced,* s.l.: General Acoustics.

Guo, S., 2017. *dynamic response of floating wind turbine under consideration of dynamic behaviour of catenary mooring lines.* Trondheim, ASME.

GWEC, 2022. *Floating Offshore - A Global Opportunity,* s.l.: GWEC.

Hong, S., Lee, I., Park, S.-H. & Chun, H. H., 2015. An experimental Study of the effect of Mooring Systems on the dynamics of a SPAR Buoy-Type Floating Offshore Wind Turbine. *International Journal of Naval Architecture and Ocean Engineering.*

ITTC, 2021. *ITTC quality system manual, calibration of load cells,* s.l.: ITTC.

Jonkman, J., 2007. *Dynamics Modeling and Loads Analysis of an Offshore Floating Wind Turbine,* s.l.: NREL.

Karimirad, M., Bachynski, E. E., Berthelsen, P. A. & Ormberg, H., 2017. *COMPARISON OF REAL-TIME HYBRID MODEL TESTING OF A BRACELESS SEMI-SUBMERSIBLE WIND TURBINE AND NUMERICAL SIMULATIONS.* Trondheim, ASME.

Krishnan, R. & Seeninaidu, N., 2017. *HYDRODYNAMIC RESPONSE OF THREE COLUMN SEMI-SUBMERSIBLE.* Trondheim, ASME.

Lei, Z. et al., 2022. A review of research status and scientific problems of floating offshore wind turbines. *Energy Engineering.*

Ma, K.-T., Luo, Y., Kwan, T. & Wu, Y., 2018. *Mooring System engineering for offshore structures.* Houston: Gulf Professional Publisher.

Naqvi, S. K., 2012. *Scale model experiments on floating offshore wind turbines,* Worcester: WORCESTER POLYTECHNIC INSTITUTE.

National Instruments, 2023. *USB-6211 Specifications,* s.l.: National Instruments.

NREL, 2010. *OC3,* s.l.: NREL.

NREL, 2014. *Offshore Code Comparison Collaboration Continuation,* s.l.: NREL.

Optitrack, 2023. *Optitrack documentation.* [Online] Available at: https://docs.optitrack.com/

Robertson, A. N., 2017. OC5 Project phase 2. *Energy Procedia.*

Sanderson, G., 2018. *But what is the Fourier Transform? A visual introduction..* [Online] Available at: https://www.youtube.com/watch?v=spUNpyF58BY

Schreier, S., 2022. *Catenary Mooring.* [Online].

Taudin Chabot, P., 2022. *Wind Device.* [Art] (TU Delft).

Tomasicchio, G. R., 2017. *DYNAMIC MODELLING OF A SPAR BUOY WIND TURBINE.* Trondheim, ASME.

Tong, K. & Cannell, C., 1993. Technical and Economical Aspects of a Floating Offshore Windfarm. *Wind Engineering.*

Trubat, P., 2020. Wave hydrodynamic forces over mooring lines on floating offshore wind turbines. *Ocean Engineering.*

Tsouvalas, A. & Metrikine, A., 2022. *Lecture 3 slides.* [Online] Available at: https://brightspace.tudelft.nl/d2l/le/content/288963/viewContent/1833944/View

TU Delft, 2022. *Towing Tank No. 2.* [Online] Available at: https://www.tudelft.nl/3me/over/afdelingen/maritime-and-transport-technology/research/ship-hydromechanics/facilities/towing-tank-no-2

Utsunomiya, T., 2017. *NUMERICAL MODELLING AND ANALYSIS OF A HYBRID-SPAR FLOATING WIND TURBINE.* Trondheim, ASME.

Wang, L. & Robertson, A., 2022. Validation of CFD simulations of the moored DeepCwind offshore wind semisubmersible in irregular waves. *Ocean Engineering.*

Webster, W., 1994. *MOORING-INDUCED DAMPING ,* s.l.: Pergamon.

Werkman, J., 2019. *Determining and predicting the seakeeping performance of ships based on jerk in the ship motions,* Delft: Delft University of Technology.

Wichers, J., 2013. *Guide to single point moorings.* s.l.:s.n.

Yan, J. et al., 2021. An improved method of mooring damping estimation considering mooring line segments contribution. *Ocean Engineering.*

Zemic, 2023. *Type 1R1-K Load Cell,* Etten-Leur: Zemic.

Appendix A: Technical drawing of the floater

Below are the top, front and side view of the floater, black dots indicate the mooring line attachment points. Dimensions given in millimetres.

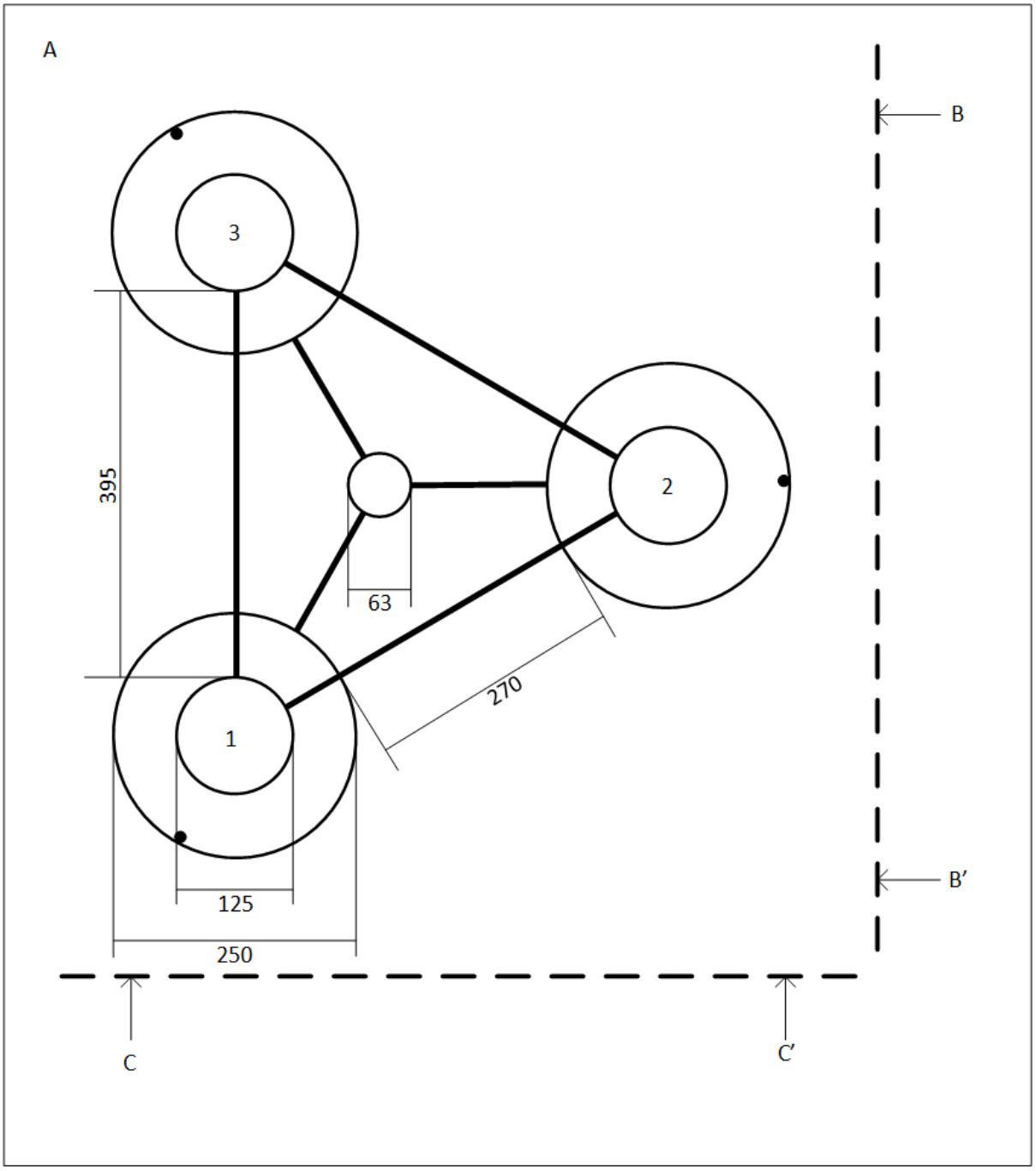

B-B’

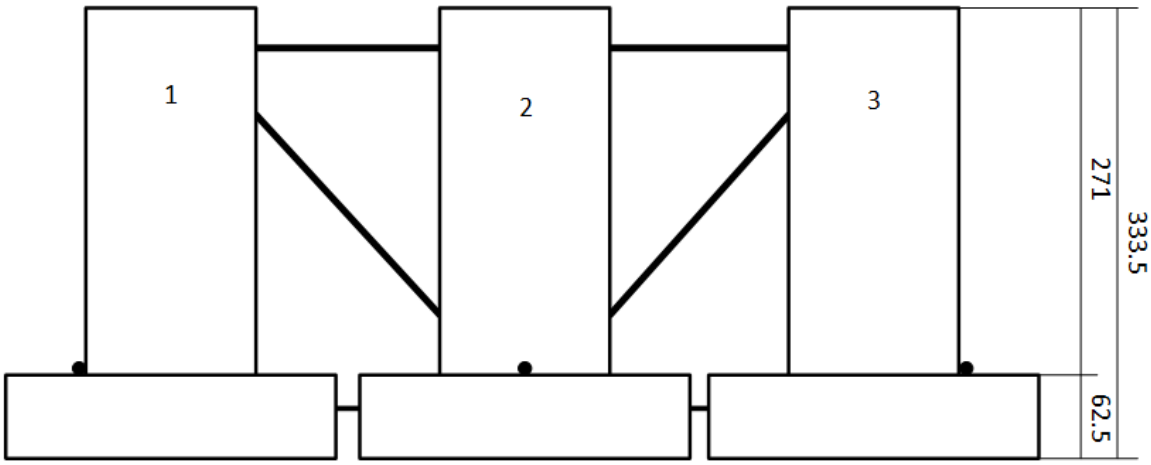

C-C’

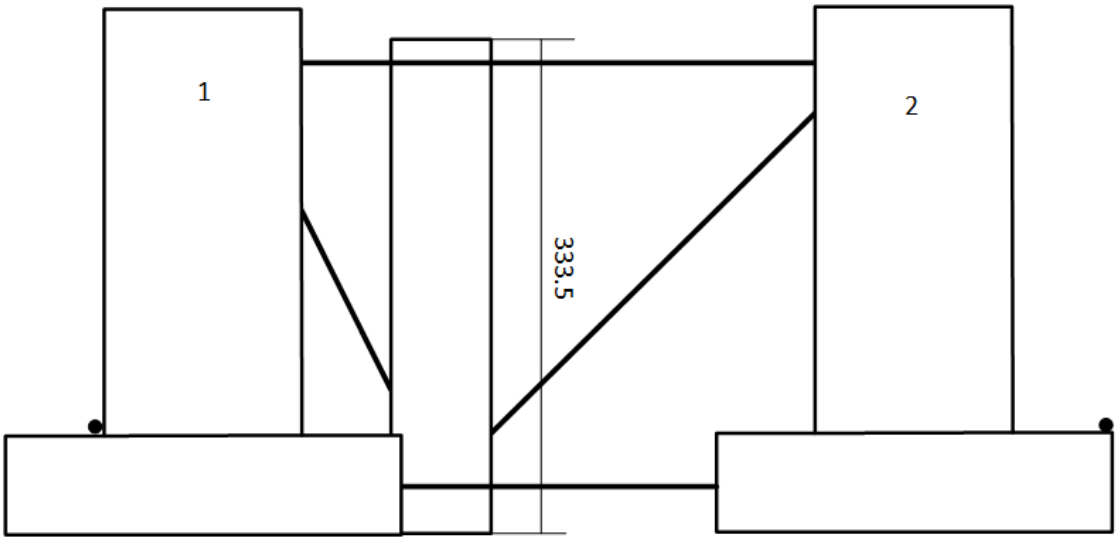

Appendix B: Data link and script

The raw data is provided via the repository of the TU Delft. The data is stored in comma separated values, so it should be easy to decode in most coding languages or even excel. The DOI to the data set is given below:

10.4121/a4ad6557-14a4-4c26-b699-a59314472f12

The script to that was used to generate the csv files is given below in Python code.

```
import numpy as np
import scipy.signal
import pandas as pd
import matplotlib.pyplot as plt
import scipy.io as spio
import scipy.optimize as so
import scipy.stats as sc
import nptdms as tdms
from nptdms import TdmsFile
from IPython.display import display
from openpyxl import Workbook
```

```
def datagen(experiment, freq = 10, posttrigger = 225, camera_index = 4,
threshold = 235):

    #file loading

    #experiment = 'b1' #b1wl_NM_2
    #camera_index = 4 #wissel tussen cameras bij fouten

    ########

    database =[['m1wav', 61],
               ['b1wav', 62],
               ['m2wav', 63],
               ['m3wav', 64],
               ['m4wav', 65],
               ['m5wav', 66],
               ['m6wav_nul', 67],
               ['m6wav', 68],
               ['m5wav_2_nul', 69],
               ['m5wav_2', 70],
               ['m6wav_2_nul', 71],
               ['m6wav_2', 72],
               ['b2wav_nul', 73],
               ['b2wav', 74],
               ['b3wav_nul', 75],
               ['b3wav', 76],
               ['b4wav_nul', 77],
               ['b4wav', 78],
               ['b5wav_nul', 79],
               ['b5wav', 80],
               ['m6wavs_nul', 81],
               ['m6wavs', 82],
               ['nulmeting', 83], #
               ['nulmeting', 84], #
```

```
                ['korte_golfburst', 85], #
                ['nulmeting', 86], #
                ['lange_golf', 87], #
                ['m1wav_2_nul', 88],
                ['m1wav_2', 89],
                ['b1wav_2_nul', 90],
                ['b1wav_2', 91],
                ['b3wav_2_nul', 92],
                ['b3wav_2', 93],
                ['m1t1_nul', 94],
                ['m1t1', 95],
                ['nulmeting', 96],
                ['m1t2_nul', 97],
                ['m1t2', 98],
                ['m1_nul', 99],
                ['m1', 100],
                ['m1wav_3_nul', 101],
                ['m1wav_3', 102],
                ['wind_nul', 103],
                ['wind', 104],
                ['m2_nul', 106],
                ['m2', 107],
                ['m3_nul', 108],
                ['m3', 109],
                ['m4_nul', 110],
                ['m4', 111],
                ['m5_nul', 112],
                ['m5', 113],
                ['m6_nul', 114],
                ['m6', 115],
                ['b1_nul', 116],
                ['b1', 117],
                ['b2_nul', 118],
                ['b2', 119],
                ['b4_nul', 120],
                ['b4', 121],
                ['b5_nul', 122],
                ['b5', 123],
                ['b3_nul', 124],
                ['b3', 125],
                ['nulmeting', 126],
                ['failed', 127],
                ['m1_2_nul', 128],
                ['m1_2', 129],
                ['m2_2_nul', 130],
                ['m2_2', 131],
                ['m3_2_nul', 132],
                ['m3_2', 133],
                ['m4_2_nul', 134],
                ['m4_2', 135],
                ['nulmeting', 136],
                ['verkeerde_wavefile', 137],
                ['m5_3_nul', 138],
                ['m5_3', 139],
                ['m6_2_nul', 140],
                ['m6_2', 141],
                ['b1_2_nul', 142],
                ['b1_2', 143],
```

```
                ['m6_3_nul', 144],
                ['foutemeting', 145],
                ['m6_3', 146],
                ['b2_2_nul', 147],
                ['b2_2', 148],
                ['b4_2_nul', 149],
                ['b4_2', 150],
                ['b5_2_nul', 151],
                ['b5_2', 152],
                ['wind_2_nul', 153],
                ['wind_2', 154],
                ['b3_2_nul', 153], #duplicate
                ['b3_2', 155],
                ['b1_3_nul', 156],
                ['b1_3', 157],
                ['b2_3_nul', 158],
                ['b2_3', 159],
                ['b4_3_nul', 160],
                ['b4_3', 161],
                ['b5_3_nul', 162],
                ['b5_3', 163],
                ['b3_3_nul', 164],
                ['b3_3', 165],
                ['b3XL_nul', 166],
                ['b3XL', 167],
                ['b3XL_2_nul', 168],
                ['b3XL_2', 169],
                ['b1wl_nul', 171],
                ['b1wl', 172],
                ['b2wl_nul', 173],
                ['b2wl', 174],
                ['b3wl_nul', 175],
                ['b3wl', 176],
                ['b4wl_nul', 177],
                ['b4wl', 178],
                ['b5wl_nul', 181],
                ['b5wl', 182],
                ['surgewl_nul', 183],
                ['surgewl', 185],
                ['heavewl_nul', 183],
                ['heavewl', 186],
                ['swaywl_nul', 183],
                ['swaywl', 187],
                ['swaywl_2_nul', 183],
                ['swaywl_2', 188],
                ['pitchwl_nul', 183],
                ['pitchwl', 189],
                ['rollwl_nul', 183],
                ['rollwl', 190],
                ['surge_nul', 183],
                ['surge', 191],
                ['surge_2_nul', 183],
                ['surge_2', 192],
                ['heave_nul', 183],
                ['heave', 193],
                ['sway_nul', 183],
                ['sway', 194],
                ['pitch_nul', 183],
```

```
                ['pitch', 195],
                ['roll_nul', 183],
                ['roll', 196],
                ['yaw_nul', 183],
                ['yaw', 198],
                ['yawwl_nul', 183],
                ['yawwl', 199],
                ['surgewl_2_nul', 183],
                ['surgewl_2', 200],
                ['b3wl_2_nul', 201],
                ['b3wl_2', 202],
                ['b2wl_2_nul', 203],
                ['b2wl_2', 204],
                ['b4wl_2_nul', 205],
                ['b4wl_2', 206],
                ['b1wl_2_nul', 207],
                ['b1wl_2', 208],
                ['b5wl_2_nul', 209],
                ['b5wl_2', 213],
                ['yaw_NM_nul', 219],
                ['yaw_NM', 220],
                ['yawwl_NM_nul', 219],
                ['yawwl_NM', 221],
                ['surgewl_NM_nul', 222],
                ['surgewl_NM', 223],
                ['heavewl_NM_nul', 222],
                ['heavewl_NM', 224],
                ['swaywl_NM_nul', 222],
                ['swaywl_NM', 225],
                ['pitchwl_NM_nul', 222],
                ['pitchwl_NM', 226],
                ['rollwl_NM_nul', 222],
                ['rollwl_NM', 227],
                ['surge_NM_nul', 222],
                ['surge_NM', 228],
                ['heave_NM_nul', 222],
                ['heave_NM', 229],
                ['sway_NM_nul', 222],
                ['sway_NM', 230],
                ['pitch_NM_nul', 222],
                ['pitch_NM', 231],
                ['roll_NM_nul', 222],
                ['roll_NM', 232],
                ['m1_NM_nul', 233],
                ['m1_NM', 234],
                ['m2_NM_nul', 235],
                ['m2_NM', 236],
                ['m4_NM_nul', 237],
                ['m4_NM', 238],
                ['m5_NM_nul', 239],
                ['m5_NM', 240],
                ['m6_NM_nul', 241],
                ['m6_NM', 242],
                ['wind_NM_nul', 243],
                ['wind_NM', 244],
                ['m2_NM_2_nul', 243], #duplicate
                ['m2_NM_2', 245],
                ['m4_NM_2_nul', 246],
```

```
                ['m4_NM_2', 247],
                ['m5_NM_2_nul', 248],
                ['m5_NM_2', 249],
                ['m6_NM_2_nul', 250],
                ['m6_NM_2', 251],
                ['b6_NM_nul', 252],
                ['b6_NM', 253],
                ['b5_NM_nul', 254],
                ['b5_NM', 255],
                ['b6_NM_2_nul', 256],
                ['b6_NM_2', 257],
                ['b5_NM_2_nul', 258],
                ['b5_NM_2', 259],
                ['wind_NM_2_nul', 260],
                ['wind_NM_2', 261],
                ['m1_NM_2_nul', 260],
                ['m1_NM_2', 262],
                ['b1_NM_nul', 263],
                ['b1_NM', 264],
                ['b1_NM_2_nul', 265],
                ['b1_NM_2', 266],
                ['b6wl_NM_nul', 267],
                ['b6wl_NM', 268],
                ['b5wl_NM_nul', 269],
                ['b5wl_NM', 270],
                ['b4_NM_nul', 271],
                ['b4_NM', 272],
                ['b4_NM_2_nul', 275],
                ['b4_NM_2', 276],
                ['b4wl_NM_nul', 277],
                ['b4wl_NM', 278],
                #['b4XL_NM_nul', 279],
                #['b4XL_NM', 280], #defunct
                ['b6wav_nul', 281],
                ['b6wav', 282],
                ['b6wav_2_nul', 283],
                ['b6wav_2', 284]]


    for i in range(len(database)):
        if database[i][0] == experiment:
            run = database[i][1]
        if database[i][0] == experiment+str('_nul'):
            runnul = database[i][1]

    ########

    tdms_file =
TdmsFile.read(f'E:\\thesis_data\\experiments\\{experiment}\\202220-
Run{run}.tdms')
    main = tdms_file.as_dataframe()

    tdms_file =
TdmsFile.read(f'E:\\thesis_data\\experiments\\{experiment}\\202220-
Run{runnul}.tdms')
    nul = tdms_file.as_dataframe()
```

```
    video =
cv.VideoCapture(f'E:\\thesis_data\\experiments\\{experiment}\\{experime
nt}_{camera_index}.avi')

    movmain =
pd.read_csv(f'E:\\thesis_data\\experiments\\{experiment}\\experiment_{e
xperiment}.csv', skiprows = 7)

    movnul =
pd.read_csv(f'E:\\thesis_data\\experiments\\{experiment}\\nulmeting_{ex
periment}.csv', skiprows = 7)

    ########

    #synchronisatie

    location_up_4_x = 562
    location_up_4_y = 1065

    location_up_6_x = 519
    location_up_6_y = 1056

    #threshold = 235

    if camera_index == 4:
        for i in range(400):
            frame = video.read()
            gray = cv.cvtColor(frame[1], cv.COLOR_BGR2GRAY)
            p1 = gray[int(location_up_4_x)][int(location_up_4_y)]
            p2 = gray[int(location_up_4_x-1)][int(location_up_4_y)]
            p3 = gray[int(location_up_4_x+1)][int(location_up_4_y)]
            p4 = gray[int(location_up_4_x-1)][int(location_up_4_y-1)]
            p5 = gray[int(location_up_4_x)][int(location_up_4_y-1)]
            p6 = gray[int(location_up_4_x)][int(location_up_4_y+1)]
            p7 = gray[int(location_up_4_x+1)][int(location_up_4_y+1)]
            p8 = gray[int(location_up_4_x+1)][int(location_up_4_y-1)]
            p9 = gray[int(location_up_4_x+1)][int(location_up_4_y-1)]
            bright = np.mean([p1, p2, p3, p4, p5, p6, p7, p8, p9])
            if bright > threshold:
                break

    if camera_index == 6:
        for i in range(400):
            frame = video.read()
            gray = cv.cvtColor(frame[1], cv.COLOR_BGR2GRAY)
            p1 = gray[int(location_up_6_x)][int(location_up_6_y)]
            p2 = gray[int(location_up_6_x-1)][int(location_up_6_y)]
            p3 = gray[int(location_up_6_x+1)][int(location_up_6_y)]
            p4 = gray[int(location_up_6_x-1)][int(location_up_6_y-1)]
            p5 = gray[int(location_up_6_x)][int(location_up_6_y-1)]
            p6 = gray[int(location_up_6_x)][int(location_up_6_y+1)]
            p7 = gray[int(location_up_6_x+1)][int(location_up_6_y+1)]
            p8 = gray[int(location_up_6_x+1)][int(location_up_6_y-1)]
            p9 = gray[int(location_up_6_x+1)][int(location_up_6_y-1)]
            bright = np.mean([p1, p2, p3, p4, p5, p6, p7, p8, p9])
            if bright > threshold:
                break
```

```
light = i

trigger = main.iloc[:, 14]
triggermoment = np.min(trigger[trigger>2.5].index)
triggermoment = np.nan_to_num(triggermoment)
triggermoment = int(triggermoment)


#array generator

ml1u = main.iloc[triggermoment:-1, 0]
ml2u = main.iloc[triggermoment:-1, 1]
ml3u = main.iloc[triggermoment:-1, 2]

wfu = main.iloc[triggermoment:-1, 3]
wtu = main.iloc[triggermoment:-1, 4]

wp1u = main.iloc[triggermoment:-1, 10]
wp2u = main.iloc[triggermoment:-1, 11]
wp3u = main.iloc[triggermoment:-1, 12]
wp4u = main.iloc[triggermoment:-1, 13]

timeu = movmain.iloc[light:-1,1]

rotXu = movmain.iloc[light:-1,2]
rotYu = movmain.iloc[light:-1,3]
rotZu = movmain.iloc[light:-1,4]

posXu = movmain.iloc[light:-1,5]
posYu = movmain.iloc[light:-1,6]
posZu = movmain.iloc[light:-1,7]

#freq downscaling

#freq = 10 #Hz

#posttrigger = 225 #sec

ml1 = []
ml2 = []
ml3 = []

wf = []
wt = []

wp1 = []
wp2 = []
wp3 = []
wp4 = []

time = []

rotX = []
rotY = []
rotZ = []

posX = []
```

```
posY = []
posZ = []

nt = int(1000/freq)
no = int(40/freq)

for i in range(freq*posttrigger):
    ml1 = np.append(ml1, np.mean(ml1u[nt*i:(nt-1)+nt*i]))
    ml2 = np.append(ml2, np.mean(ml2u[nt*i:(nt-1)+nt*i]))
    ml3 = np.append(ml3, np.mean(ml3u[nt*i:(nt-1)+nt*i]))

    wf = np.append(wf, np.mean(wfu[nt*i:(nt-1)+nt*i]))
    wt = np.append(wt, np.mean(wtu[nt*i:(nt-1)+nt*i]))

    wp1 = np.append(wp1, np.mean(wp1u[nt*i:(nt-1)+nt*i]))
    wp2 = np.append(wp2, np.mean(wp2u[nt*i:(nt-1)+nt*i]))
    wp3 = np.append(wp3, np.mean(wp3u[nt*i:(nt-1)+nt*i]))
    wp4 = np.append(wp4, np.mean(wp4u[nt*i:(nt-1)+nt*i]))

    time = np.append(time, np.mean(timeu[no*i:(no-1)+no*i]))

    rotX = np.append(rotX, np.mean(rotXu[no*i:(no-1)+no*i]))
    rotY = np.append(rotY, np.mean(rotYu[no*i:(no-1)+no*i]))
    rotZ = np.append(rotZ, np.mean(rotZu[no*i:(no-1)+no*i]))

    posX = np.append(posX, np.mean(posXu[no*i:(no-1)+no*i]))
    posY = np.append(posY, np.mean(posYu[no*i:(no-1)+no*i]))
    posZ = np.append(posZ, np.mean(posZu[no*i:(no-1)+no*i]))

#normaliseren naar nulmeting
ml1n = np.mean(nul.iloc[triggermoment:-1, 0])
ml2n = np.mean(nul.iloc[triggermoment:-1, 1])
ml3n = np.mean(nul.iloc[triggermoment:-1, 2])

wfn = np.mean(nul.iloc[triggermoment:-1, 3])
wtn = np.mean(nul.iloc[triggermoment:-1, 4])

wp1n = np.mean(nul.iloc[triggermoment:-1, 10])
wp2n = np.mean(nul.iloc[triggermoment:-1, 11])
wp3n = np.mean(nul.iloc[triggermoment:-1, 12])
wp4n = np.mean(nul.iloc[triggermoment:-1, 13])

rotXn = np.mean(movnul.iloc[light:-1,2])
rotYn = np.mean(movnul.iloc[light:-1,3])
rotZn = np.mean(movnul.iloc[light:-1,4])

posXn = np.mean(movnul.iloc[light:-1,5])
posYn = np.mean(movnul.iloc[light:-1,6])
posZn = np.mean(movnul.iloc[light:-1,7])

ml1 = ml1 - ml1n
ml2 = ml2 - ml2n
ml3 = ml3 - ml3n

wt = wt - wtn
wf = wf - wfn

time = time - time[0]
```

```
    wp1 = wp1 - wp1n
    wp2 = wp2 - wp2n
    wp3 = wp3 - wp3n
    wp4 = wp4 - wp4n

    rotX = rotX - rotXn
    rotY = rotY - rotYn
    rotZ = rotZ - rotZn

    posX = posX - posXn
    posY = posY - posYn
    posZ = posZ - posZn

    #omzetten naar panda
    data = pd.DataFrame()

    data['time'] = time

    data['mooring line 1'] = ml1
    data['mooring line 2'] = ml2
    data['mooring line 3'] = ml3

    data['wind force'] = wf
    data['wind torque'] = wt

    data['wave probe 1'] = wp1
    data['wave probe 2'] = wp2
    data['wave probe 3'] = wp3
    data['wave probe 4'] = wp4

    data['surge'] = posX
    data['sway'] = posZ
    data['heave'] = posY

    data['pitch'] = rotZ
    data['yaw'] = rotY
    data['roll'] = rotX
    return data
```

```
for i in range(len(database)):
    naam = database[i][0]
    lttr = list(naam)
    if lttr[-2] != 'u':
        print(naam)
        data = datagen(database[i][0], camera_index = database[i][2])
        data.to_csv(database[i][0]+'.csv')
```

Appendix C: Complete test matrix and codes

ms1 = mooring system 1, ms2 = mooring system 2

type	aspect	code
moored decay test	surge, without wind, ms1	surgewl
moored decay test	heave, without wind, ms1	heavewl
moored decay test	sway, without wind, ms1	swaywl
moored decay test	pitch, without wind, ms1	pitchwl
moored decay test	roll, without wind, ms1	rollwl
moored decay test	yaw, without wind, ms1	yawwl
moored decay test	surge, with wind, ms1	surge
moored decay test	surge, with wind, ms1	surgew_2
moored decay test	heave, with wind, ms1	heave
moored decay test	sway, with wind, ms1	sway
moored decay test	pitch, with wind, ms1	pitc
moored decay test	roll, with wind, ms1	roll
moored decay test	yaw, with wind, ms1	yaw

type	aspect	code
moored decay test	surge, without wind, ms2	surgewl_NM
moored decay test	heave, without wind, ms2	heavewl_NM
moored decay test	sway, without wind, ms2	swaywl_NM
moored decay test	pitch, without wind, ms2	pitchwl_NM
moored decay test	roll, without wind, ms2	rollwl_NM
moored decay test	yaw, without wind, ms2	yawl_NM
moored decay test	surge, with wind, ms2	surge_NM
moored decay test	heave, with wind, ms2	heave_NM
moored decay test	sway, with wind, ms2	sway_NM
moored decay test	pitch, with wind, ms2	pitch_NM
moored decay test	roll, with wind, ms2	roll_NM
moored decay test	yaw, with wind, ms2	yaw_NM

type	aspect	code
single wave no model	m1	m1wav
single wave no model	m2	m2wav
single wave no model	m3	m3wav
single wave no model	m4	m4wav
single wave no model	m5	m5wav
single wave no model	m6	m6wav
single wave no model	m5, repeat	m5wav_2
single wave no model	m6, repeat	m6wav_2

type	aspect	code
bichromatic wave no model	b1	b1wav
bichromatic wave no model	b2	b2wav
bichromatic wave no model	b3	b3wav
bichromatic wave no model	b4	b4wav
bichromatic wave no model	b5	b5wav
bichromatic wave no model	b6	b6wav
bichromatic wave no model	b1, repeat	b1wav_2
bichromatic wave no model	b3, repeat	b3wav_2
bichromatic wave no model	b6, repeat	b6wav_2

type	aspect	code
single wave model test	m1, ms1	m1
single wave model test	m2, ms1	m2
single wave model test	m3, ms1	m3
single wave model test	m4, ms1	m4
single wave model test	m5, ms1	m5
single wave model test	m6, ms1	m6
single wave model test	m1, ms1, repeat	m1_2
single wave model test	m2, ms1, repeat	m2_2
single wave model test	m3, ms1, repeat	m3_2
single wave model test	m4, ms1, repeat	m4_2
single wave model test	m5, ms1, repeat	m5_2
single wave model test	m6, ms1, repeat	m6_2

type	aspect	code
bichromatic wave model test	b1, ms1	b1
bichromatic wave model test	b2, ms1	b2
bichromatic wave model test	b3, ms1	b3
bichromatic wave model test	b4, ms1	b4
bichromatic wave model test	b5, ms1	b5
bichromatic wave model test	b1, ms1, repeat	b1_2
bichromatic wave model test	b2, ms1, repeat	b2_2
bichromatic wave model test	b3, ms1, repeat	b3_2
bichromatic wave model test	b4, ms1, repeat	b4_2
bichromatic wave model test	b5, ms1, repeat	b5_2
bichromatic wave model test	b1, ms1, repeat	b1_3
bichromatic wave model test	b2, ms1, repeat	b2_3
bichromatic wave model test	b2, ms1, repeat	b3_3
bichromatic wave model test	b2, ms1, repeat	b4_3
bichromatic wave model test	b2, ms1, repeat	b5_3
longer duration bichromatic wave model test	b3, ms1, extra-long	b3XL
longer duration bichromatic wave model test	b3, ms1, extra-long, repeat	b3XL_2

type	aspect	code
wind application test	wind, ms1	wind
wind application test	wind, ms1, repeat	wind_2
wind application test	wind, ms2	wind_NM
wind application test	wind, ms2, repeat	wind_NM_2

type	aspect	code
bichromatic wave model test, without wind	b1, no wind, ms1	b1wl
bichromatic wave model test, without wind	b2, no wind, ms1	b2wl
bichromatic wave model test, without wind	b3, no wind, ms1	b3wl
bichromatic wave model test, without wind	b4, no wind, ms1	b4wl
bichromatic wave model test, without wind	b5, no wind, ms1	b5wl
bichromatic wave model test, without wind	b1, no wind, ms1, repeat	b1wl_2
bichromatic wave model test, without wind	b2, no wind, ms1, repeat	b2wl_2
bichromatic wave model test, without wind	b3, no wind, ms1, repeat	b3wl_2
bichromatic wave model test, without wind	b4, no wind, ms1, repeat	b4wl_2
bichromatic wave model test, without wind	b5, no wind, ms1, repeat	b5wl_2

type	aspect	code
single wave model test	m1, ms2	m1_NM
single wave model test	m2, ms2	m2_NM
single wave model test	m4, ms2	m4_NM
single wave model test	m5, ms2	m5_NM
single wave model test	m6, ms2	m6_NM
single wave model test	m1, ms2, repeat	m1_NM _2
single wave model test	m2, ms2, repeat	m2_NM _2
single wave model test	m4, ms2, repeat	m4_NM _2
single wave model test	m5, ms2, repeat	m5_NM _2
single wave model test	m6, ms2, repeat	m6_NM _2

type	aspect	code
bichromatic wave model test	b1, ms2	b1_NM
bichromatic wave model test	b4, ms2	b4_NM
bichromatic wave model test	b5, ms2	b5_NM
bichromatic wave model test	b6, ms2	b6_NM
bichromatic wave model test	b4, ms2, repeat	b4_NM_2
bichromatic wave model test	b5, ms2, repeat	b5_NM_2
bichromatic wave model test	b6, ms2, repeat	b6_NM_2

type	aspect	code
bichromatic wave model test, without wind	b4, no wind, ms2	b4wl_NM
bichromatic wave model test, without wind	b5, no wind, ms2	b5wl_NM
bichromatic wave model test, without wind	b6, no wind, ms2	b6wl_NM

Appendix D: Calibration of measuring devices

run					Run	16							
					[kg]	[kg]	[V]	[V]	[N]	[V]	[V]	%	0,020%
date	7-Oct-22			step	mass step	massa	U	U correct	F	U calc	Residual	norm Res	
				1	0,00	0,05	0,16	0,10	0,49	0,10	-0,0003	-0,01%	1,43608E-08
chan	0			2	0,20	0,25	0,45	0,40	2,45	0,40	-0,0006	-0,03%	6,39053E-08
name	mooring line 1			3	0,40	0,45	0,75	0,69	4,41	0,69	-0,0001	-0,01%	2,6708E-09
				4	0,60	0,65	1,04	0,99	6,37	0,99	-0,0007	-0,03%	8,24422E-08
				5	0,80	0,85	1,33	1,28	8,33	1,28	-0,0006	-0,02%	5,96848E-08
sensor no	1			6	1,00	1,05	1,63	1,57	10,29	1,57	-0,0003	-0,01%	1,41505E-08
range	2	kg	positive	7	1,20	1,25	1,92	1,87	12,26	1,87	-0,0004	-0,02%	2,99622E-08
				8	1,60	1,65	2,51	2,46	16,18	2,46	0,0001	0,00%	2,01073E-09
amplifier	BMCM			9	1,20	1,25	1,92	1,87	12,26	1,87	0,0006	0,03%	6,72399E-08
range in	2	mV/V		10	1,00	1,05	1,63	1,57	10,29	1,57	0,0003	0,01%	1,74134E-08
range out	5	V		11	0,80	0,85	1,33	1,28	8,33	1,28	0,0000	0,00%	1,84401E-10
R neutral		uV/V		12	0,60	0,65	1,04	0,99	6,37	0,99	0,0004	0,02%	2,52041E-08
C neutral		uV/V		13	0,40	0,45	0,75	0,69	4,41	0,69	0,0005	0,02%	4,92887E-08
				14	0,20	0,25	0,45	0,40	2,45	0,40	0,0009	0,04%	1,50363E-07
calfact	6,6632	N/V		15	0,00	0,05	0,16	0,10	0,49	0,10	0,0001	0,01%	3,2185E-09
slope	0,1501	V/N		1		-0,05		0,00	-0,49	-0,04	0,0000	0,00%	
intercept	0,0297	V		2		-0,05		0,00	-0,49	-0,04	0,0000	0,00%	
sigma	0,000480108			3		-0,05		0,00	-0,49	-0,04	0,0000	0,00%	
95%	0,000960216			4		-0,05		0,00	-0,49	-0,04	0,0000	0,00%	
				5		-0,05		0,00	-0,49	-0,04	0,0000	0,00%	
Picas val (see orange box for ref.)				6		-0,05		0,00	-0,49	-0,04	0,0000	0,00%	
offset standing upright				7		-0,05		0,00	-0,49	-0,04	0,0000	0,00%	
0,011658	V			8		-0,05		0,00	-0,49	-0,04	0,0000	0,00%	
hanging positive bare				9		-0,05		0,00	-0,49	-0,04	0,0000	0,00%	
0,05416	V			10		-0,05		0,00	-0,49	-0,04	0,0000	0,00%	
hanging positive with hook plate				11		-0,05		0,00	-0,49	-0,04	0,0000	0,00%	
0,05416	V			12		-0,05		0,00	-0,49	-0,04	0,0000	0,00%	
hanging positive with plate and ha				13		-0,05		0,00	-0,49	-0,04	0,0000	0,00%	
0,157373	V			14		-0,05		0,00	-0,49	-0,04	0,0000	0,00%	
hanging negative with hook plate				15		-0,05		0,00	-0,49	-0,04	0,0000	0,00%	
	V												
hanging negative with plate and hanger				mass har	50								
	V			g				positive	negative				
hanging negative bare				mass pla	0		slope	0,15008	0,00000				
	V			g			intercept	0,0297	0,0000				
				attachments to sensor									
				0,05	kg								

ITTC-STANDARD			
g value ncg:	9,812	m/s^2	
calculation air den:	1,224	kg/m^3	
correction =	0,9999	[-]	
F = mg*correction			
	########	r'dam airport	
ambient pressure	1025	hPa	
R (gas-constant)	0,28669	kJ/(kg K)	
universal gas constant	8,314	kJ/(kmol K)	
molar mass	29	kg/kmol	
ambient temperature	19	deg C	
absolute temperature	292,15	K	
	1kg mean		
	0,999308	kg	

Fill in the orange fields, according to the values, that can be found on the knmi website: https://www.knmi.nl/nederland

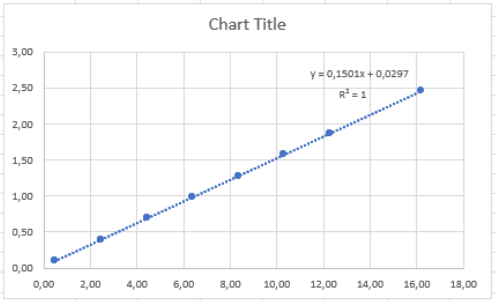

To get the correct values, we added the following steps:
- in the fields above this box, fill in the weather conditions (ittc standard), you can click the hyperlink

---

In the fields underneath '**Picas val**' fill in the following values

- a standing upright force transducer without any weight placed on it
- when the transducer is fixed to its hanging position, we take the next reading
- when we fix the hook-plate on it (the one holding the plate for the weights), we take another reading
- when we fix the plate for the weights we take a last reading

for the other direction we change the order, so first hanging with hook plate, hanging with plate and hanger and then after the calibration steps have been done we take off the hanger and hook-plate and take the reading for it just hanging.

Calibration page for mooring line 1

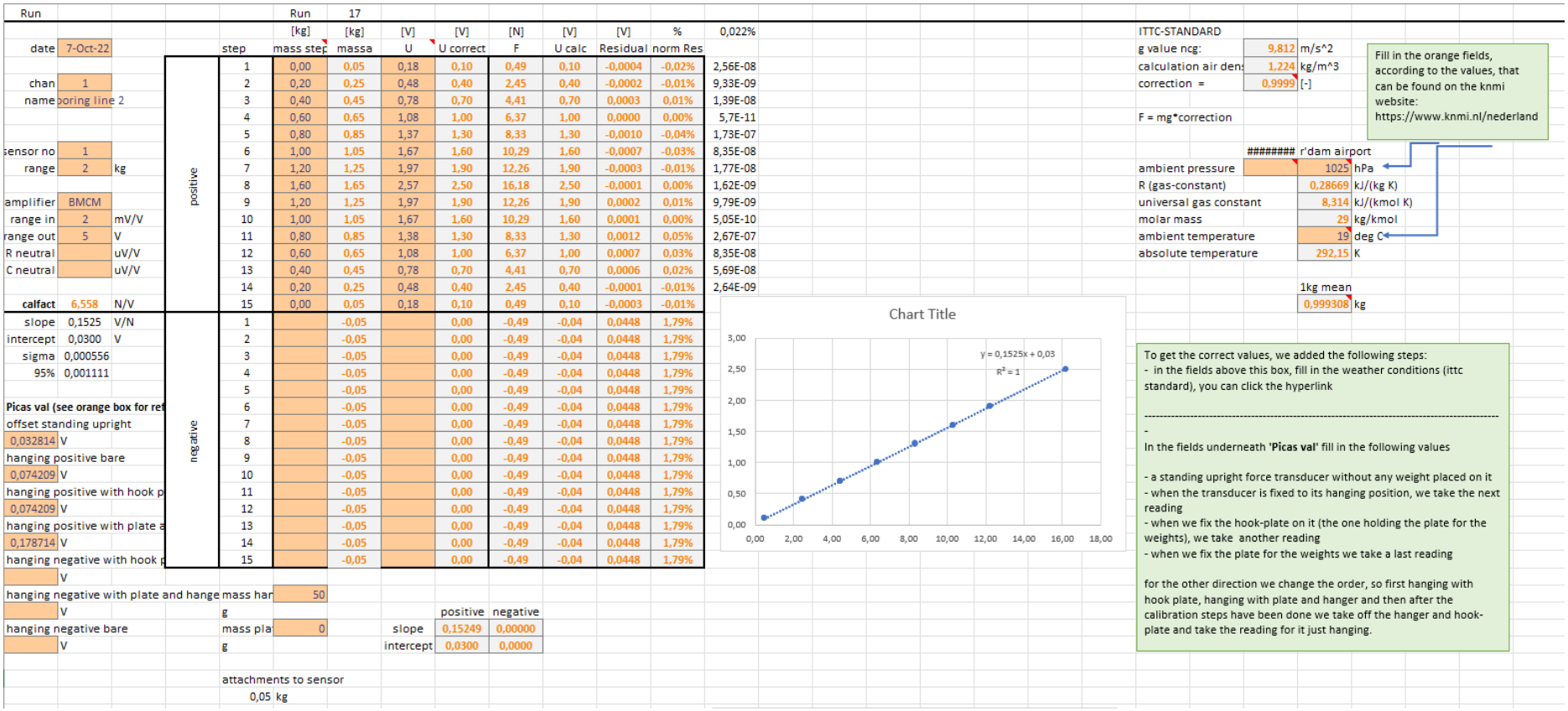

Run					Run	17							
					[kg]	[kg]	[V]	[V]	[N]	[V]	[V]	%	0,022%
date	7-Oct-22			step	mass step	massa	U	U correct	F	U calc	Residual	norm Res	
			positive	1	0,00	0,05	0,18	0,10	0,49	0,10	-0,0004	-0,02%	2,56E-08
chan	1			2	0,20	0,25	0,48	0,40	2,45	0,40	-0,0002	-0,01%	9,33E-09
name	boring line 2			3	0,40	0,45	0,78	0,70	4,41	0,70	0,0003	0,01%	1,39E-08
				4	0,60	0,65	1,08	1,00	6,37	1,00	0,0000	0,00%	5,7E-11
				5	0,80	0,85	1,37	1,30	8,33	1,30	-0,0010	-0,04%	1,73E-07
sensor no	1			6	1,00	1,05	1,67	1,60	10,29	1,60	-0,0007	-0,03%	8,35E-08
range	2	kg		7	1,20	1,25	1,97	1,90	12,26	1,90	-0,0003	-0,01%	1,77E-08
				8	1,60	1,65	2,57	2,50	16,18	2,50	-0,0001	0,00%	1,62E-09
amplifier	BMCM			9	1,20	1,25	1,97	1,90	12,26	1,90	0,0002	0,01%	9,79E-09
range in	2	mV/V		10	1,00	1,05	1,67	1,60	10,29	1,60	0,0001	0,00%	5,05E-10
range out	5	V		11	0,80	0,85	1,38	1,30	8,33	1,30	0,0012	0,05%	2,67E-07
R neutral		uV/V		12	0,60	0,65	1,08	1,00	6,37	1,00	0,0007	0,03%	8,35E-08
C neutral		uV/V		13	0,40	0,45	0,78	0,70	4,41	0,70	0,0006	0,02%	5,69E-08
				14	0,20	0,25	0,48	0,40	2,45	0,40	-0,0001	-0,01%	2,64E-09
calfact	6,558	N/V		15	0,00	0,05	0,18	0,10	0,49	0,10	-0,0003	-0,01%	
slope	0,1525	V/N	negative	1		-0,05		0,00	-0,49	-0,04	0,0448	1,79%	
intercept	0,0300	V		2		-0,05		0,00	-0,49	-0,04	0,0448	1,79%	
sigma	0,000556			3		-0,05		0,00	-0,49	-0,04	0,0448	1,79%	
95%	0,001111			4		-0,05		0,00	-0,49	-0,04	0,0448	1,79%	
				5		-0,05		0,00	-0,49	-0,04	0,0448	1,79%	
Picas val (see orange box for ref				6		-0,05		0,00	-0,49	-0,04	0,0448	1,79%	
offset standing upright				7		-0,05		0,00	-0,49	-0,04	0,0448	1,79%	
0,032814	V			8		-0,05		0,00	-0,49	-0,04	0,0448	1,79%	
hanging positive bare				9		-0,05		0,00	-0,49	-0,04	0,0448	1,79%	
0,074209	V			10		-0,05		0,00	-0,49	-0,04	0,0448	1,79%	
hanging positive with hook p				11		-0,05		0,00	-0,49	-0,04	0,0448	1,79%	
0,074209	V			12		-0,05		0,00	-0,49	-0,04	0,0448	1,79%	
hanging positive with plate a				13		-0,05		0,00	-0,49	-0,04	0,0448	1,79%	
0,178714	V			14		-0,05		0,00	-0,49	-0,04	0,0448	1,79%	
hanging negative with hook p				15		-0,05		0,00	-0,49	-0,04	0,0448	1,79%	
	V												
hanging negative with plate and hange				mass har	50								
	V			g				positive	negative				
hanging negative bare				mass pla	0		slope	0,15249	0,00000				
	V			g			intercept	0,0300	0,0000				
				attachments to sensor									
				0,05	kg								

ITTC-STANDARD			
g value ncg:	9,812	m/s^2	
calculation air dens	1,224	kg/m^3	
correction =	0,9999	[-]	
F = mg*correction			
	########	r'dam airport	
ambient pressure		1025	hPa
R (gas-constant)		0,28669	kJ/(kg K)
universal gas constant		8,314	kJ/(kmol K)
molar mass		29	kg/kmol
ambient temperature		19	deg C
absolute temperature		292,15	K
		1kg mean	
		0,999308	kg

Fill in the orange fields, according to the values, that can be found on the knmi website: https://www.knmi.nl/nederland

To get the correct values, we added the following steps:
- in the fields above this box, fill in the weather conditions (ittc standard), you can click the hyperlink

---

-
In the fields underneath '**Picas val**' fill in the following values

- a standing upright force transducer without any weight placed on it
- when the transducer is fixed to its hanging position, we take the next reading
- when we fix the hook-plate on it (the one holding the plate for the weights), we take another reading
- when we fix the plate for the weights we take a last reading

for the other direction we change the order, so first hanging with hook plate, hanging with plate and hanger and then after the calibration steps have been done we take off the hanger and hook-plate and take the reading for it just hanging.

Calibration page for mooring line 2

Run					Run	18								
					[kg]	[kg]	[V]	[V]	[N]	[V]	[V]	%	0,027%	
date	7-Oct-22			step	mass step	massa	U	U correct	F	U calc	Residual	norm Res		
			positive	1	0,00	0,05	-0,44	0,11	0,49	0,11	0,0008	0,03%	1,11E-07	
chan	2			2	0,20	0,25	-0,13	0,41	2,45	0,41	0,0002	0,01%	4,18E-09	
name	oring line 3			3	0,40	0,45	0,17	0,71	4,41	0,71	0,0005	0,02%	4,62E-08	
				4	0,60	0,65	0,47	1,02	6,37	1,02	0,0012	0,05%	2,44E-07	
				5	0,80	0,85	0,78	1,32	8,33	1,32	0,0004	0,02%	2,83E-08	
sensor no	3			6	1,00	1,05	1,08	1,62	10,29	1,62	0,0001	0,00%	1,23E-09	
range	2	kg		7	1,20	1,25	1,38	1,93	12,26	1,93	0,0004	0,02%	3,18E-08	
				8	1,60	1,65	1,99	2,53	16,18	2,53	0,0005	0,02%	3,46E-08	
amplifier	BMCM			9	1,20	1,25	1,38	1,93	12,26	1,93	-0,0001	0,00%	4,3E-10	
range in	2	mV/V		10	1,00	1,05	1,08	1,62	10,29	1,62	-0,0009	-0,04%	1,39E-07	
range out	5	V		11	0,80	0,85	0,78	1,32	8,33	1,32	-0,0010	-0,04%	1,78E-07	
R neutral		uV/V		12	0,60	0,65	0,47	1,02	6,37	1,02	-0,0007	-0,03%	7,29E-08	
C neutral		uV/V		13	0,40	0,45	0,17	0,71	4,41	0,71	-0,0008	-0,03%	1,08E-07	
				14	0,20	0,25	-0,14	0,41	2,45	0,41	-0,0006	-0,02%	5,52E-08	
calfact	6,457	N/V		15	0,00	0,05	-0,44	0,11	0,49	0,11	-0,0001	0,00%	5,83E-10	
slope	0,1549	V/N	negative	1		-0,05		0,00	-0,49	-0,05	0,0468	1,85%		
intercept	0,0291	V		2		-0,05		0,00	-0,49	-0,05	0,0468	1,85%		
sigma	0,000668			3		-0,05		0,00	-0,49	-0,05	0,0468	1,85%		
95%	0,001335			4		-0,05		0,00	-0,49	-0,05	0,0468	1,85%		
				5		-0,05		0,00	-0,49	-0,05	0,0468	1,85%		
Picas val (see orange box for ref				6		-0,05		0,00	-0,49	-0,05	0,0468	1,85%		
offset standing upright				7		-0,05		0,00	-0,49	-0,05	0,0468	1,85%		
-0,58733	V			8		-0,05		0,00	-0,49	-0,05	0,0468	1,85%		
hanging positive bare				9		-0,05		0,00	-0,49	-0,05	0,0468	1,85%		
-0,5437	V			10		-0,05		0,00	-0,49	-0,05	0,0468	1,85%		
hanging positive with hook p				11		-0,05		0,00	-0,49	-0,05	0,0468	1,85%		
-0,5437	V			12		-0,05		0,00	-0,49	-0,05	0,0468	1,85%		
hanging positive with plate a				13		-0,05		0,00	-0,49	-0,05	0,0468	1,85%		
-0,43875	V			14		-0,05		0,00	-0,49	-0,05	0,0468	1,85%		
hanging negative with hook p				15		-0,05		0,00	-0,49	-0,05	0,0468	1,85%		
	V													
hanging negative with plate and hange				mass har	50									
	V			g					positive	negative				
hanging negative bare				mass pla	0		slope		0,15487	0,00000				
	V			g			intercept		0,0291	0,0000				
				attachments to sensor										
				0,05	kg									

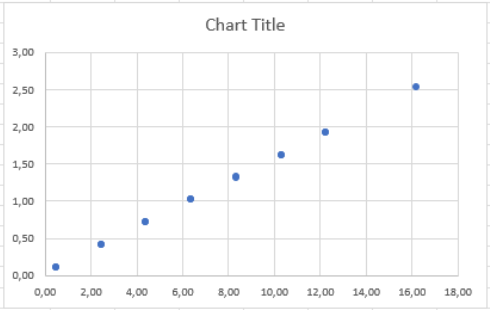

ITTC-STANDARD			
g value ncg:	9,812	m/s^2	
calculation air den:	1,224	kg/m^3	
correction =	0,9999	[-]	
F = mg*correction			
	########	r'dam airport	
ambient pressure		1025	hPa
R (gas-constant)		0,28669	kJ/(kg K)
universal gas constant		8,314	kJ/(kmol K)
molar mass		29	kg/kmol
ambient temperature		19	deg C
absolute temperature		292,15	K
		1kg mean	
		0,999308	kg

Fill in the orange fields, according to the values, that can be found on the knmi website: https://www.knmi.nl/nederland

To get the correct values, we added the following steps:
- in the fields above this box, fill in the weather conditions (ittc standard), you can click the hyperlink

---
-
In the fields underneath '**Picas val**' fill in the following values

- a standing upright force transducer without any weight placed on it
- when the transducer is fixed to its hanging position, we take the next reading
- when we fix the hook-plate on it (the one holding the plate for the weights), we take another reading
- when we fix the plate for the weights we take a last reading

for the other direction we change the order, so first hanging with hook plate, hanging with plate and hanger and then after the calibration steps have been done we take off the hanger and hook-plate and take the reading for it just hanging.

Calibration page for mooring line 3

Run					Run	23								
					[kg]	[kg]	[V]	[V]	[N]	[V]	[V]	%	0,458%	
date	10-Oct-22			step	mass step	massa	U	U correct	F	U calc	Residual	norm Res		
				1	0,00	0,04	-0,82	0,00	0,38	0,00	0,0003	0,41%	1,68E-05	
chan	3			2	0,05	0,09	-0,79	0,03	0,87	0,03	0,0002	0,23%	5,16E-06	
name	wind force			3	0,07	0,11	-0,78	0,04	1,07	0,04	-0,0006	-0,77%	5,97E-05	
				4	0,09	0,13	-0,77	0,05	1,26	0,05	-0,0004	-0,56%	3,19E-05	
				5	0,11	0,15	-0,75	0,06	1,46	0,06	-0,0001	-0,14%	1,98E-06	
sensor no	4			6	0,12	0,16	-0,75	0,07	1,56	0,07	-0,0001	-0,18%	3,27E-06	
range	2	kg		7	0,13	0,17	-0,74	0,08	1,66	0,08	-0,0003	-0,35%	1,21E-05	
			positive	8	0,14	0,17	-0,74	0,08	1,71	0,08	-0,0002	-0,20%	4,01E-06	
amplifier	BMCM			9	0,13	0,17	-0,74	0,08	1,66	0,08	0,0006	0,78%	6,05E-05	
range in		mV/V		10	0,12	0,16	-0,75	0,07	1,56	0,07	0,0000	0,00%	9,64E-12	
range out	5	V		11	0,11	0,15	-0,75	0,06	1,46	0,06	0,0000	0,02%	5,1E-08	
R neutral		uV/V		12	0,09	0,13	-0,77	0,05	1,26	0,05	0,0005	0,68%	4,58E-05	
C neutral		uV/V		13	0,07	0,11	-0,78	0,04	1,07	0,04	0,0006	0,73%	5,3E-05	
				14	0,05	0,09	-0,79	0,03	0,87	0,03	-0,0002	-0,25%	6,14E-06	
calfact	16,846	N/V		15	0,00	0,04	-0,82	0,00	0,38	0,00	-0,0003	-0,39%		
slope	0,0594	V/N		1		-0,04		0,00	-0,38	-0,05	0,0455	57,82%		
intercept	-0,0228	V		2		-0,04		0,00	-0,38	-0,05	0,0455	57,82%		
sigma	0,000374			3		-0,04		0,00	-0,38	-0,05	0,0455	57,82%		
95%	0,000747			4		-0,04		0,00	-0,38	-0,05	0,0455	57,82%		
				5		-0,04		0,00	-0,38	-0,05	0,0455	57,82%		
Picas val (see orange box for ref				6		-0,04		0,00	-0,38	-0,05	0,0455	57,82%		
offset standing upright				7		-0,04		0,00	-0,38	-0,05	0,0455	57,82%		
	V			8		-0,04		0,00	-0,38	-0,05	0,0455	57,82%		
hanging positive bare				9		-0,04		0,00	-0,38	-0,05	0,0455	57,82%		
-0,818	V			10		-0,04		0,00	-0,38	-0,05	0,0455	57,82%		
hanging positive with hook p				11		-0,04		0,00	-0,38	-0,05	0,0455	57,82%		
-0,818	V			12		-0,04		0,00	-0,38	-0,05	0,0455	57,82%		
hanging positive with plate a				13		-0,04		0,00	-0,38	-0,05	0,0455	57,82%		
	V			14		-0,04		0,00	-0,38	-0,05	0,0455	57,82%		
hanging negative with hook p				15		-0,04		0,00	-0,38	-0,05	0,0455	57,82%		
	V													
hanging negative with plate and hange				mass har	39									
	V			g				positive	negative					
hanging negative bare				mass pla	0		slope	0,05936	0,00000					
	V			g			intercept	-0,0228	0,0000					
				attachments to sensor										
				0,039	kg									

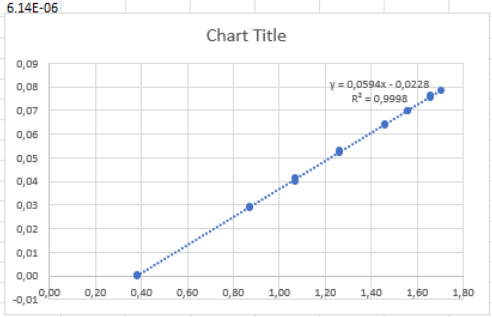

ITTC-STANDARD			
g value ncg:	9,812	m/s^2	
calculation air dens	1,224	kg/m^3	
correction =	0,9999	[-]	
F = mg*correction			
	########	r'dam airport	
ambient pressure		1025	hPa
R (gas-constant)		0,28669	kJ/(kg K)
universal gas constant		8,314	kJ/(kmol K)
molar mass		29	kg/kmol
ambient temperature		19	deg C
absolute temperature		292,15	K
		1kg mean	
		0,999308	kg

Fill in the orange fields, according to the values, that can be found on the knmi website: https://www.knmi.nl/nederland

To get the correct values, we added the following steps:
- in the fields above this box, fill in the weather conditions (ittc standard), you can click the hyperlink

---

In the fields underneath **'Picas val'** fill in the following values

- a standing upright force transducer without any weight placed on it
- when the transducer is fixed to its hanging position, we take the next reading
- when we fix the hook-plate on it (the one holding the plate for the weights), we take another reading
- when we fix the plate for the weights we take a last reading

for the other direction we change the order, so first hanging with hook plate, hanging with plate and hanger and then after the calibration steps have been done we take off the hanger and hook-plate and take the reading for it just hanging.

Calibration page for the wind force transducer

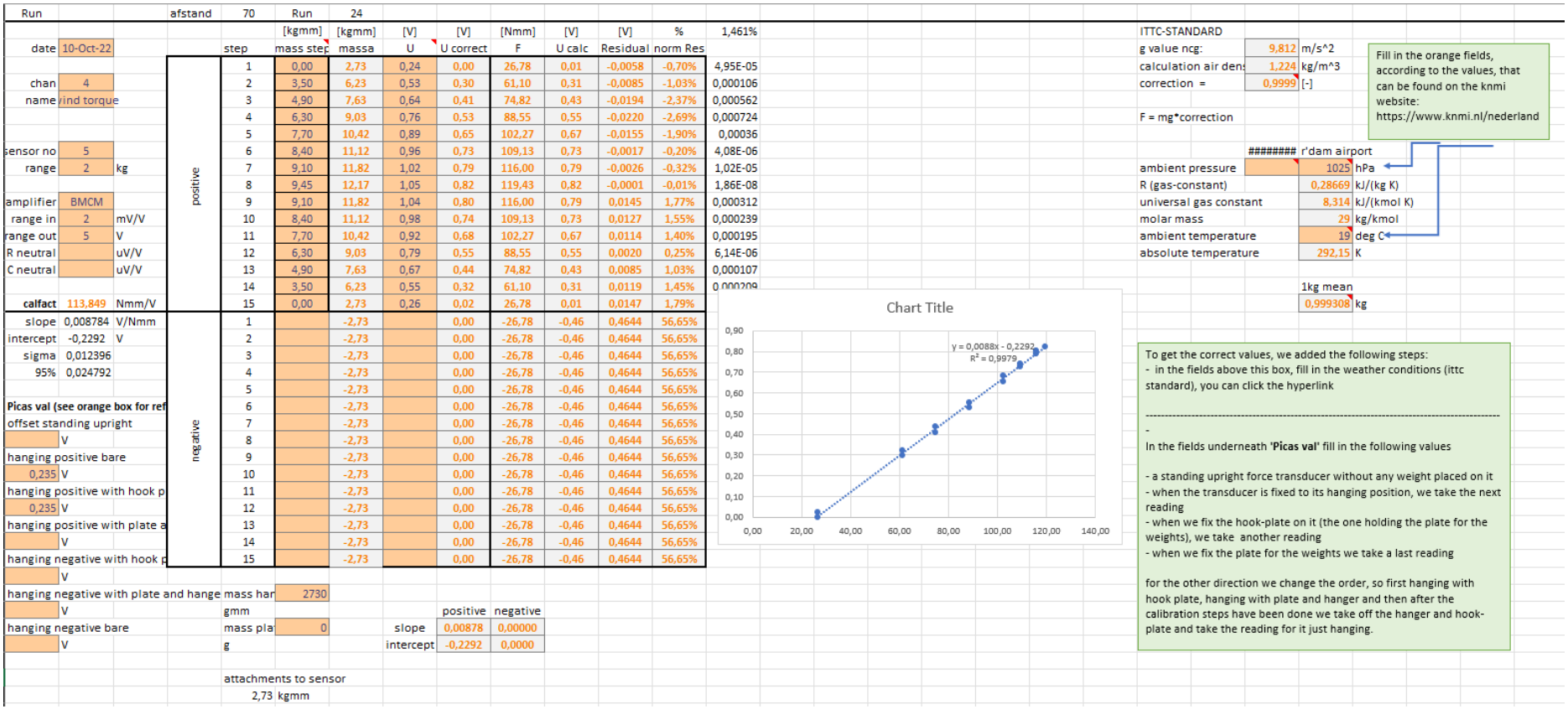

Run			afstand	70	Run	24							1,461%
					[kgmm]	[kgmm]	[V]	[V]	[Nmm]	[V]	[V]	%	
date	10-Oct-22			step	mass step	massa	U	U correct	F	U calc	Residual	norm Res	
			positive	1	0,00	2,73	0,24	0,00	26,78	0,01	-0,0058	-0,70%	4,95E-05
chan	4			2	3,50	6,23	0,53	0,30	61,10	0,31	-0,0085	-1,03%	0,000106
name	wind torque			3	4,90	7,63	0,64	0,41	74,82	0,43	-0,0194	-2,37%	0,000562
				4	6,30	9,03	0,76	0,53	88,55	0,55	-0,0220	-2,69%	0,000724
				5	7,70	10,42	0,89	0,65	102,27	0,67	-0,0155	-1,90%	0,00036
sensor no	5			6	8,40	11,12	0,96	0,73	109,13	0,73	-0,0017	-0,20%	4,08E-06
range	2	kg		7	9,10	11,82	1,02	0,79	116,00	0,79	-0,0026	-0,32%	1,02E-05
				8	9,45	12,17	1,05	0,82	119,43	0,82	-0,0001	-0,01%	1,86E-08
amplifier	BMCM			9	9,10	11,82	1,04	0,80	116,00	0,79	0,0145	1,77%	0,000312
range in	2	mV/V		10	8,40	11,12	0,98	0,74	109,13	0,73	0,0127	1,55%	0,000239
range out	5	V		11	7,70	10,42	0,92	0,68	102,27	0,67	0,0114	1,40%	0,000195
R neutral		uV/V		12	6,30	9,03	0,79	0,55	88,55	0,55	0,0020	0,25%	6,14E-06
C neutral		uV/V		13	4,90	7,63	0,67	0,44	74,82	0,43	0,0085	1,03%	0,000107
				14	3,50	6,23	0,55	0,32	61,10	0,31	0,0119	1,45%	0,000209
calfact	113,849	Nmm/V		15	0,00	2,73	0,26	0,02	26,78	0,01	0,0147	1,79%	
slope	0,008784	V/Nmm	negative	1		-2,73		0,00	-26,78	-0,46	0,4644	56,65%	
intercept	-0,2292	V		2		-2,73		0,00	-26,78	-0,46	0,4644	56,65%	
sigma	0,012396			3		-2,73		0,00	-26,78	-0,46	0,4644	56,65%	
95%	0,024792			4		-2,73		0,00	-26,78	-0,46	0,4644	56,65%	
				5		-2,73		0,00	-26,78	-0,46	0,4644	56,65%	
Picas val (see orange box for ref				6		-2,73		0,00	-26,78	-0,46	0,4644	56,65%	
offset standing upright				7		-2,73		0,00	-26,78	-0,46	0,4644	56,65%	
	V			8		-2,73		0,00	-26,78	-0,46	0,4644	56,65%	
hanging positive bare				9		-2,73		0,00	-26,78	-0,46	0,4644	56,65%	
0,235	V			10		-2,73		0,00	-26,78	-0,46	0,4644	56,65%	
hanging positive with hook p				11		-2,73		0,00	-26,78	-0,46	0,4644	56,65%	
0,235	V			12		-2,73		0,00	-26,78	-0,46	0,4644	56,65%	
hanging positive with plate a				13		-2,73		0,00	-26,78	-0,46	0,4644	56,65%	
	V			14		-2,73		0,00	-26,78	-0,46	0,4644	56,65%	
hanging negative with hook p				15		-2,73		0,00	-26,78	-0,46	0,4644	56,65%	
	V												
hanging negative with plate and hange				mass har	2730								
	V			gmm					positive	negative			
hanging negative bare				mass pla	0		slope		0,00878	0,00000			
	V			g			intercept		-0,2292	0,0000			
				attachments to sensor									
				2,73	kgmm								

ITTC-STANDARD			
g value ncg:	9,812	m/s^2	
calculation air dens	1,224	kg/m^3	
correction =	0,9999	[-]	
F = mg*correction			
	########	r'dam airport	
ambient pressure		1025	hPa
R (gas-constant)		0,28669	kJ/(kg K)
universal gas constant		8,314	kJ/(kmol K)
molar mass		29	kg/kmol
ambient temperature		19	deg C
absolute temperature		292,15	K
		1kg mean	
		0,999308	kg

Fill in the orange fields, according to the values, that can be found on the knmi website: https://www.knmi.nl/nederland

To get the correct values, we added the following steps:
- in the fields above this box, fill in the weather conditions (ittc standard), you can click the hyperlink

---

In the fields underneath '**Picas val**' fill in the following values

- a standing upright force transducer without any weight placed on it
- when the transducer is fixed to its hanging position, we take the next reading
- when we fix the hook-plate on it (the one holding the plate for the weights), we take another reading
- when we fix the plate for the weights we take a last reading

for the other direction we change the order, so first hanging with hook plate, hanging with plate and hanger and then after the calibration steps have been done we take off the hanger and hook-plate and take the reading for it just hanging.

Calibration page for the wind torque transducer

Appendix F: Division of time series data into sections

This appendix shows the division for all the bichromatic tests, concerning only the data for mooring line 2. The number next to the test indicates the amount of sections.

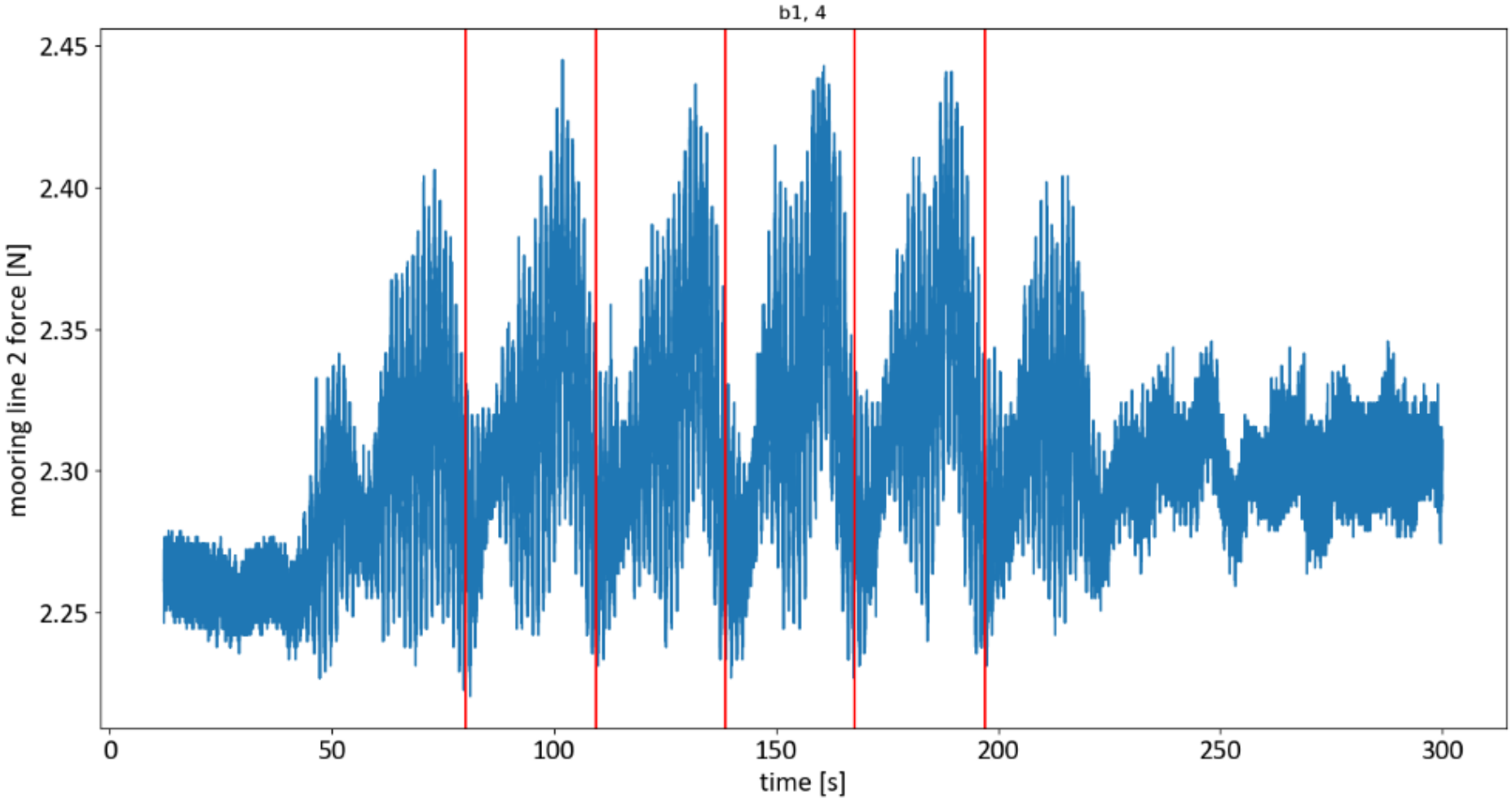

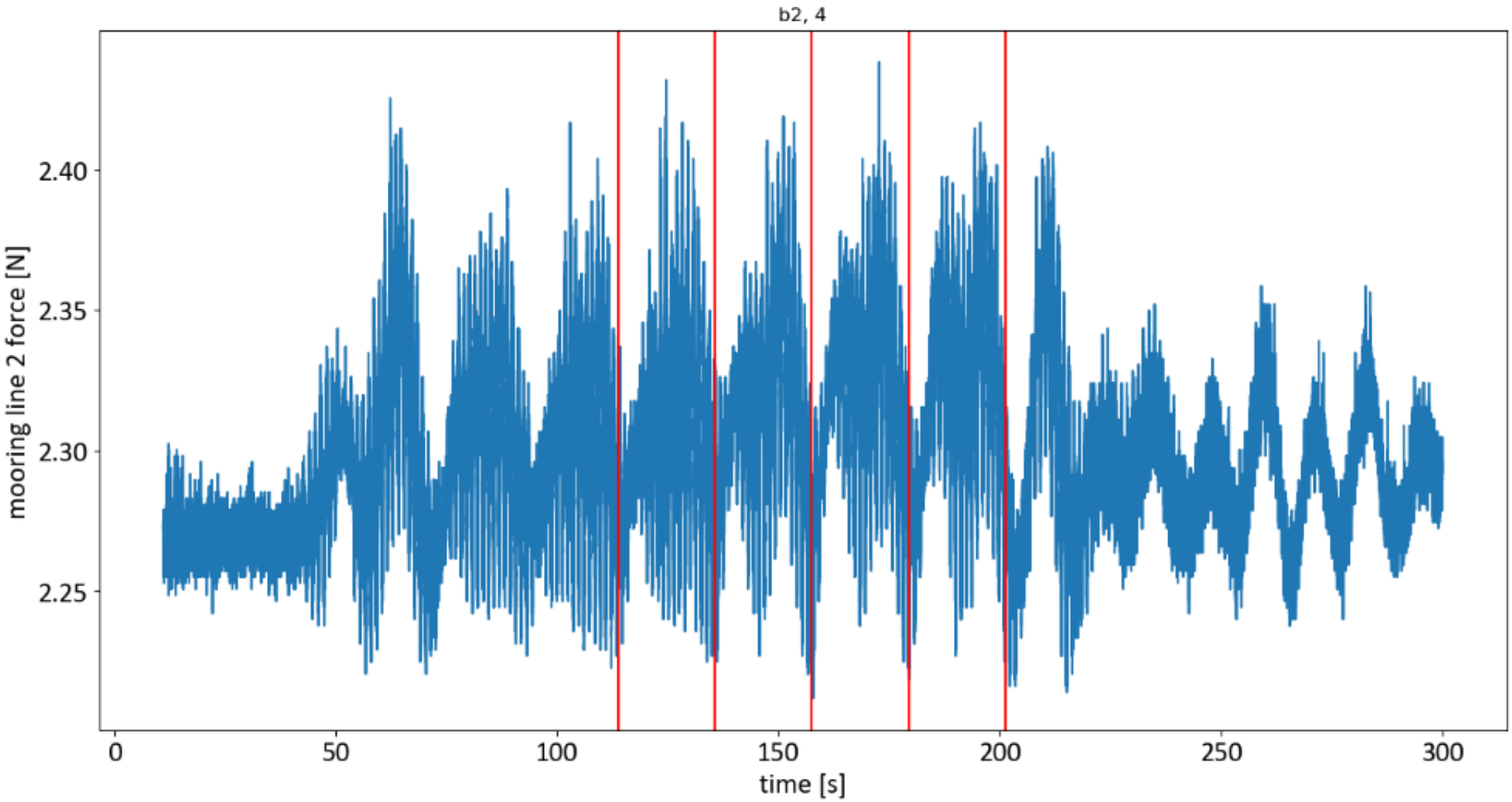
b2, 4
mooring line 2 force [N]
2.40
2.35
2.30
2.25
0
50
100
150
200
250
300
time [s]

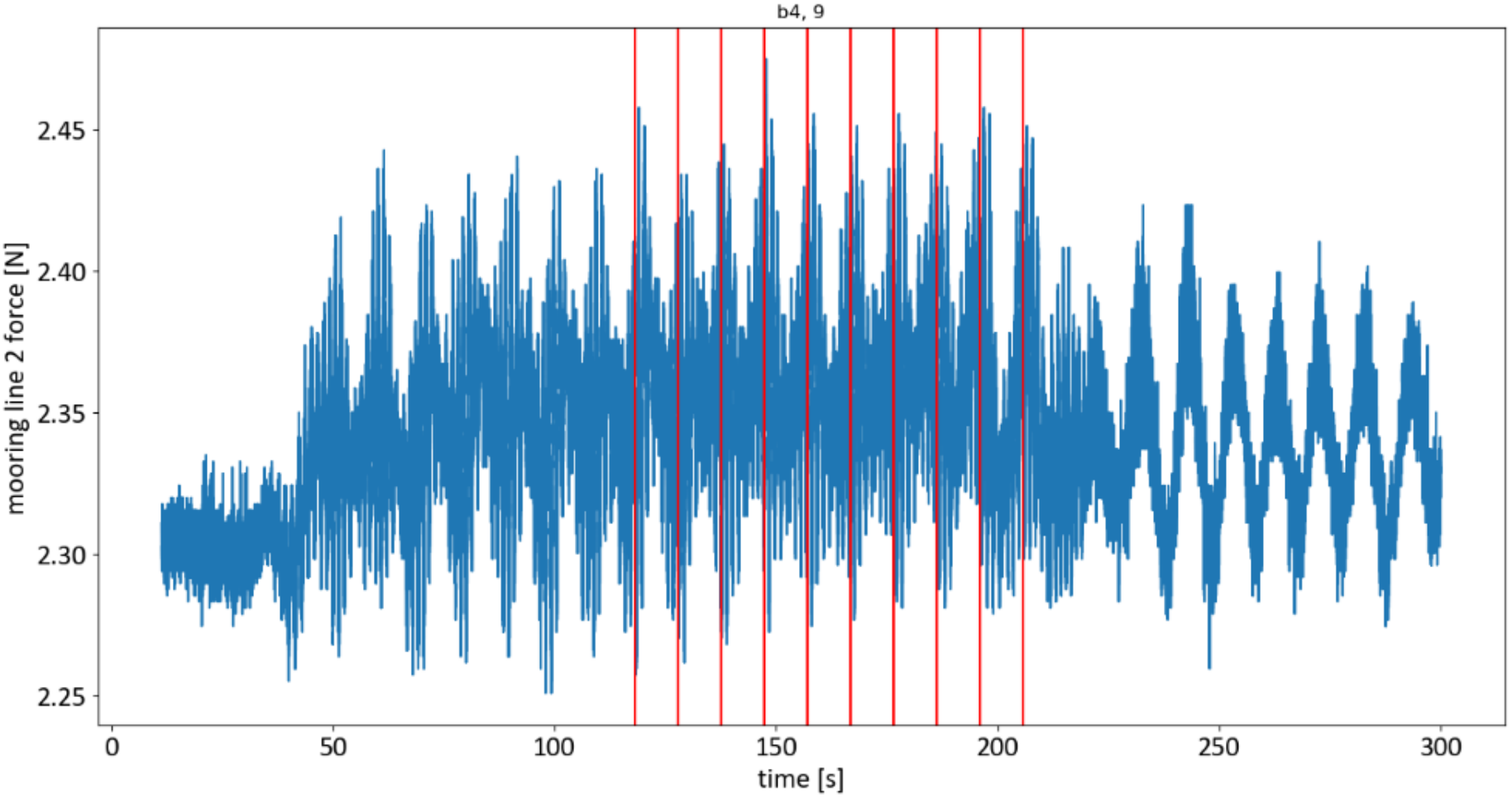
b4, 9
mooring line 2 force [N]
2.45
2.40
2.35
2.30
2.25
0
50
100
150
200
250
300
time [s]

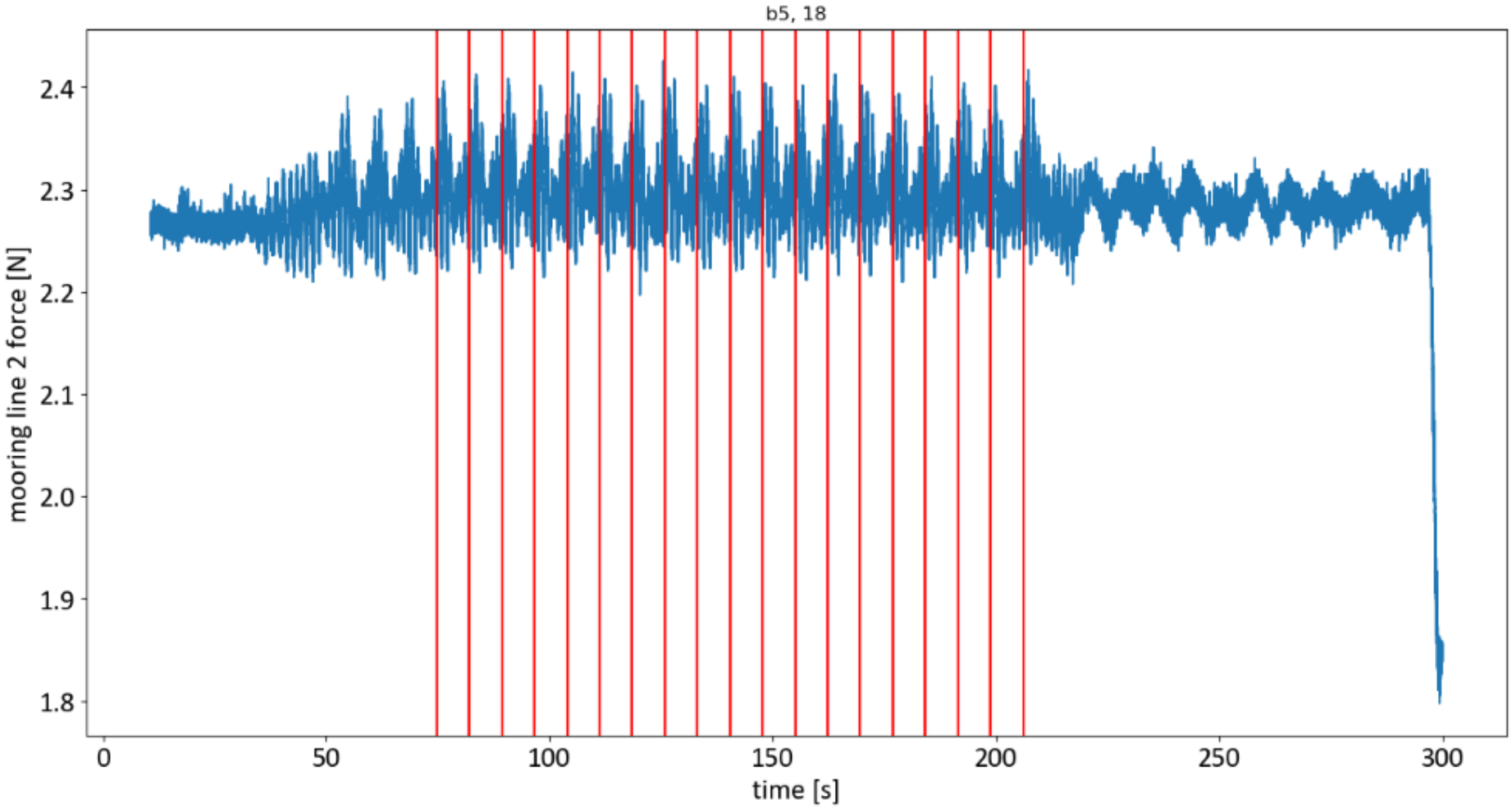
b5, 18
mooring line 2 force [N]
2.4
2.3
2.2
2.1
2.0
1.9
1.8
0
50
100
150
200
250
300
time [s]

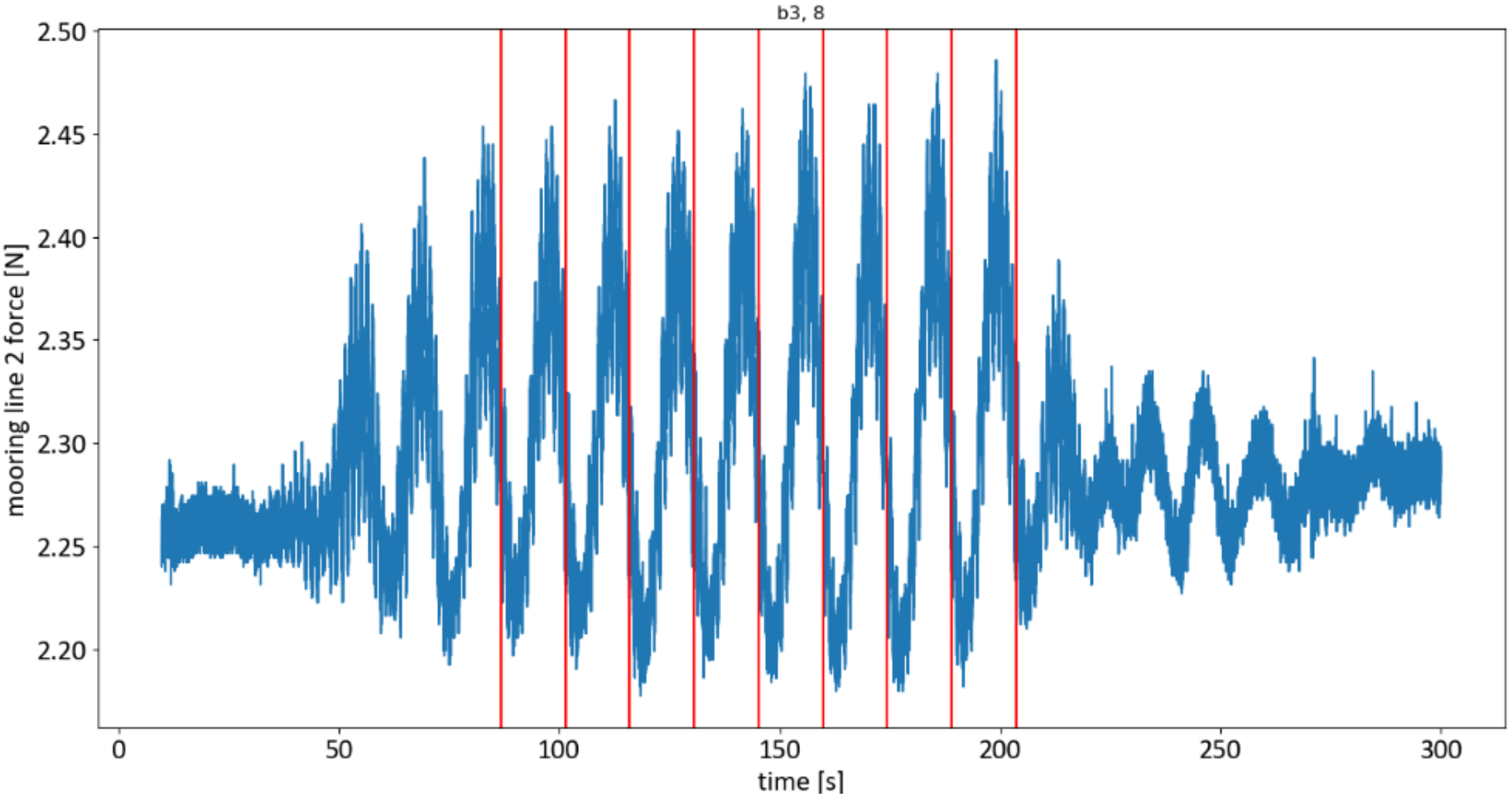
b3, 8
2.50
2.45
2.40
2.35
2.30
2.25
2.20
mooring line 2 force [N]
0
50
100
150
200
250
300
time [s]

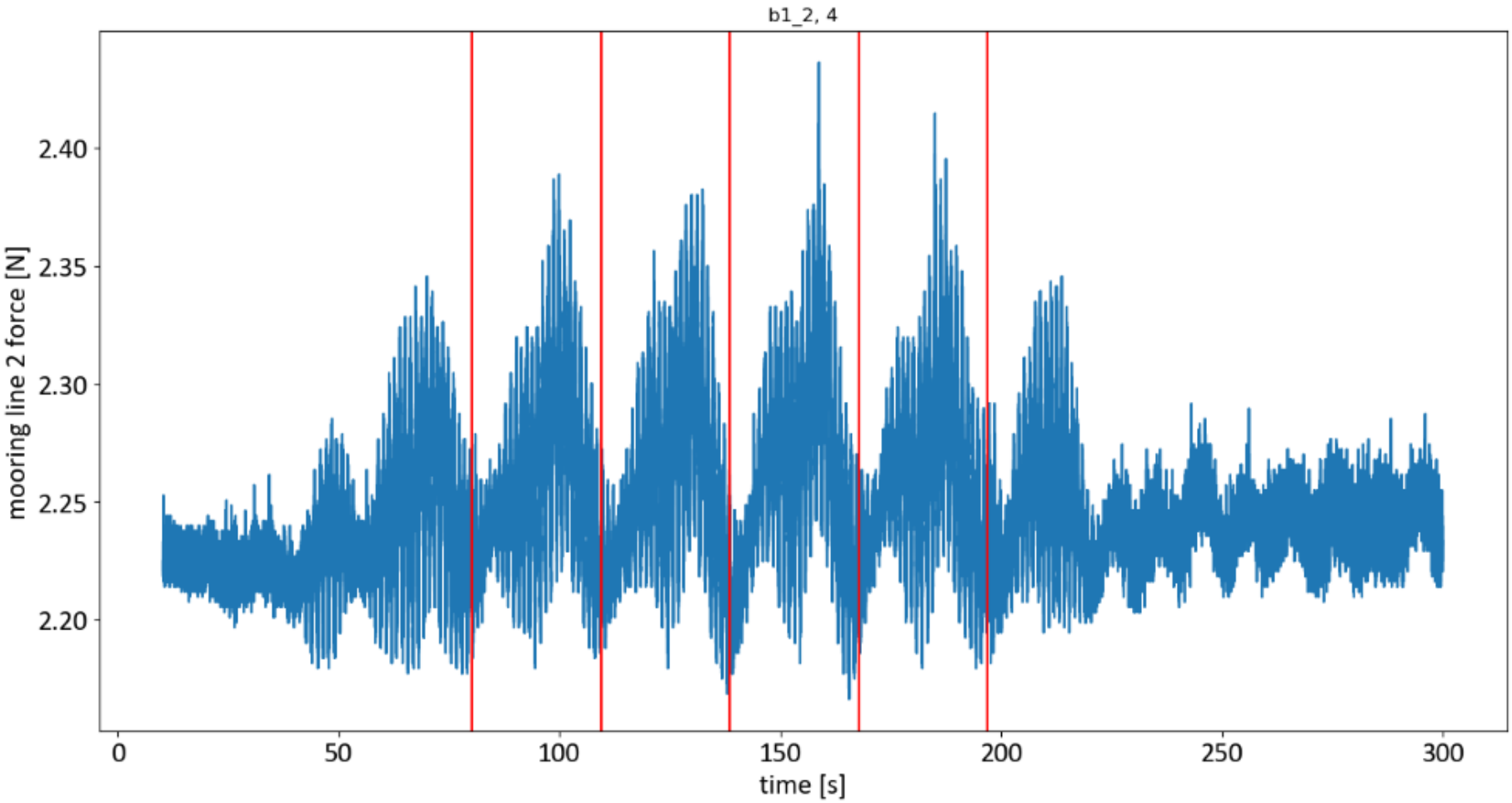
b1_2, 4
mooring line 2 force [N]
2.40
2.35
2.30
2.25
2.20
0
50
100
150
200
250
300
time [s]

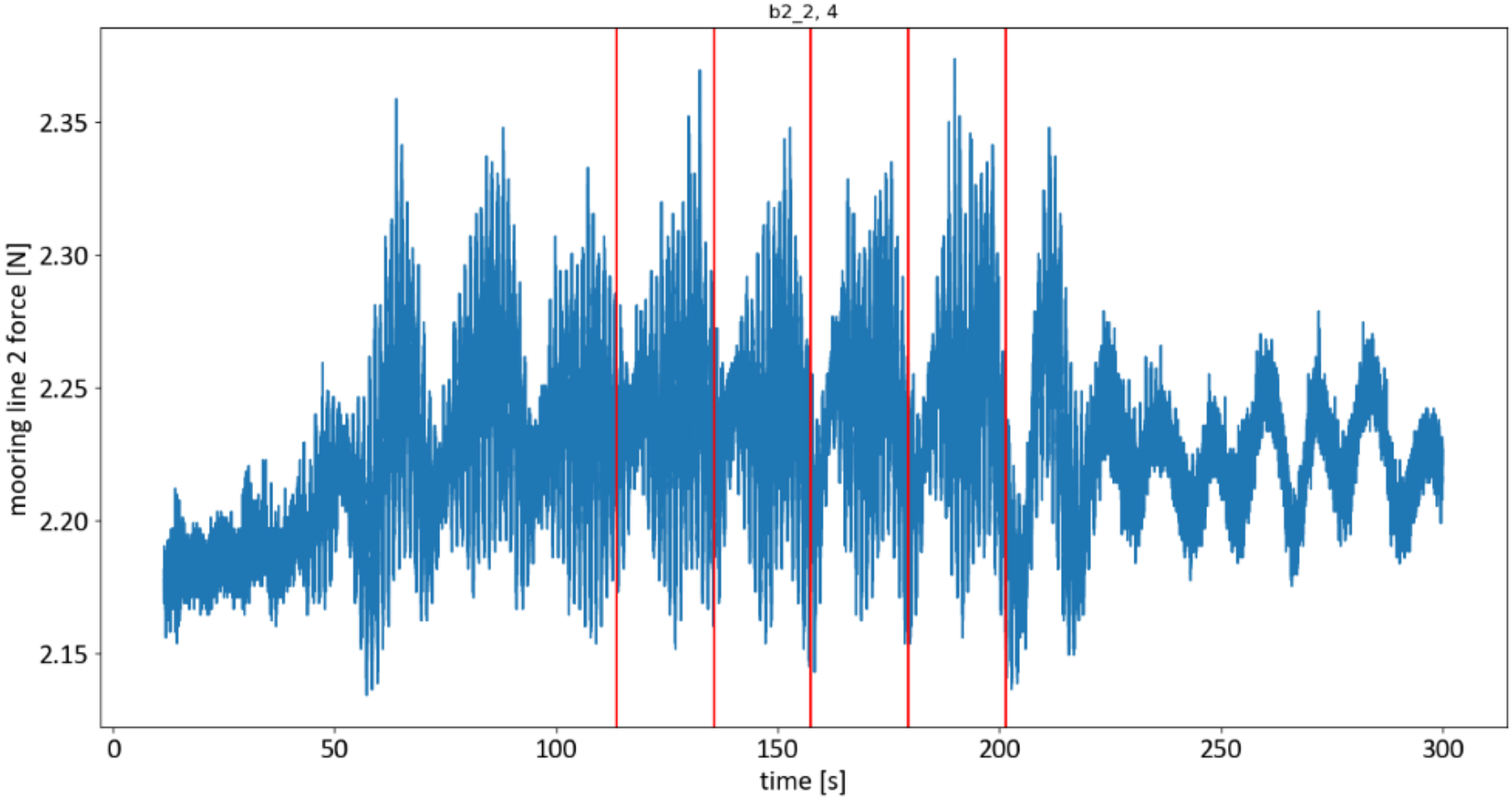
b2_2, 4
mooring line 2 force [N]
2.35
2.30
2.25
2.20
2.15
0
50
100
150
200
250
300
time [s]

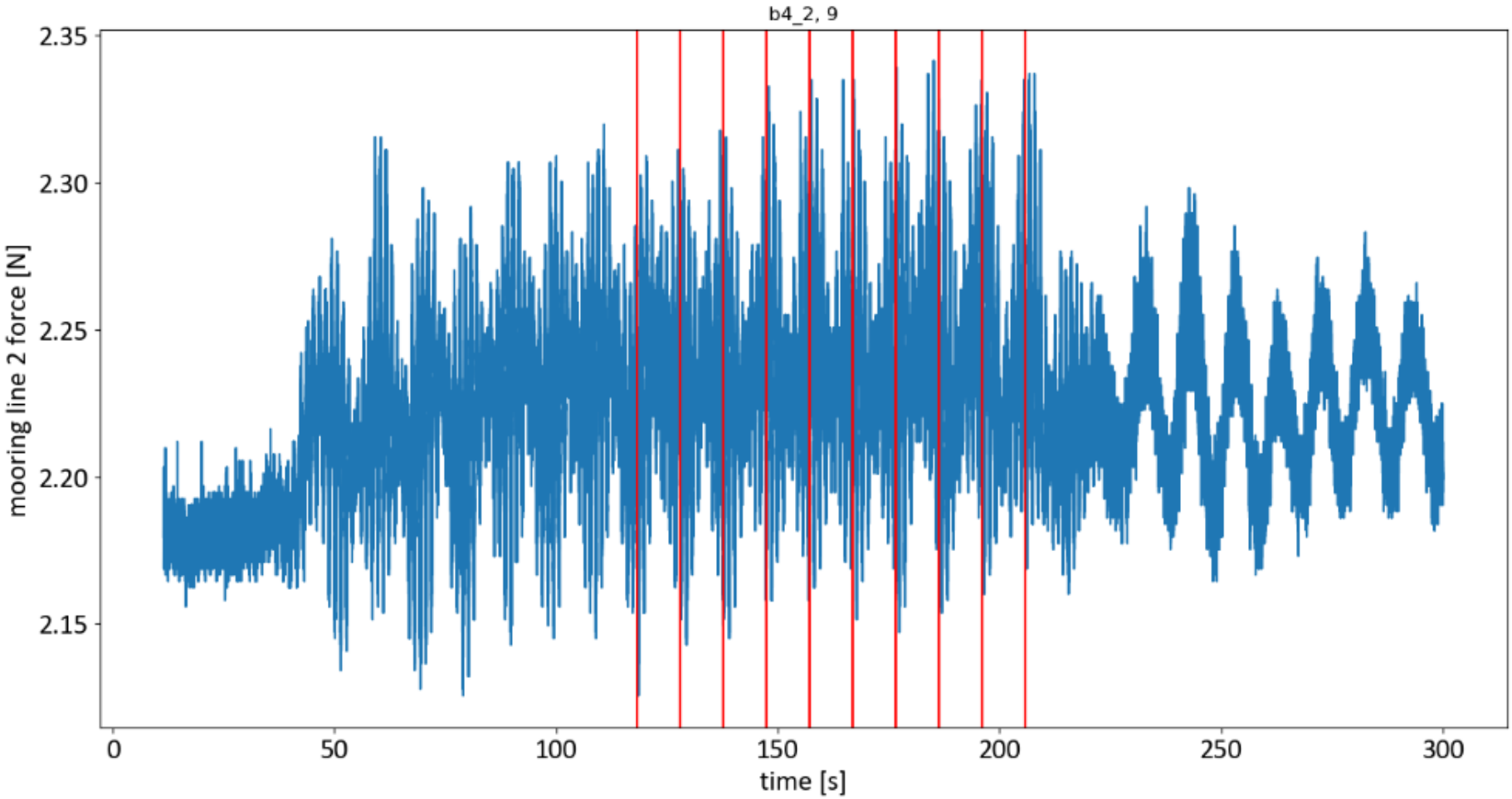
b4_2, 9
2.35
2.30
2.25
2.20
2.15
mooring line 2 force [N]
0
50
100
150
200
250
300
time [s]

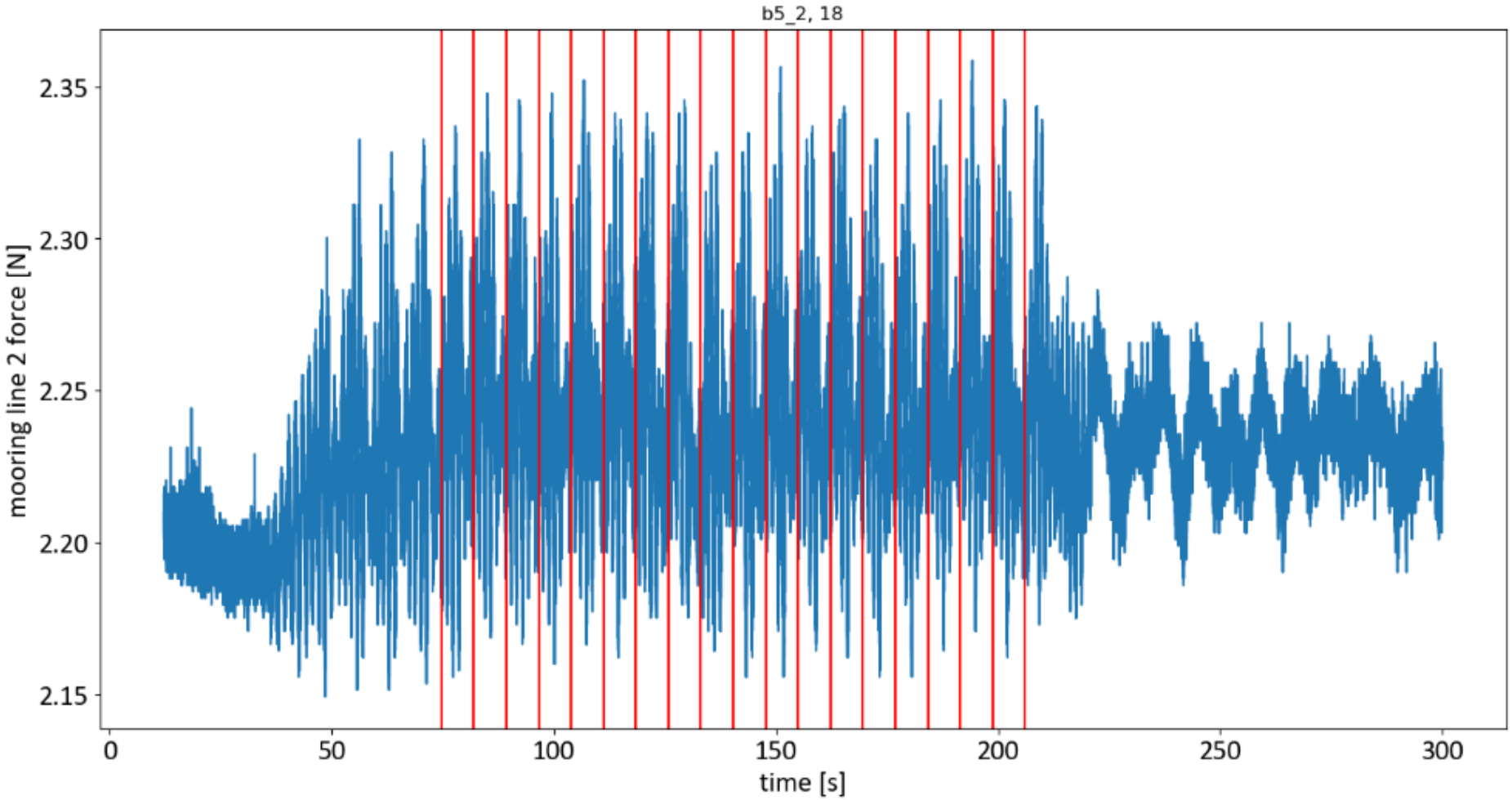
b5_2, 18
mooring line 2 force [N]
2.35
2.30
2.25
2.20
2.15
0
50
100
150
200
250
300
time [s]

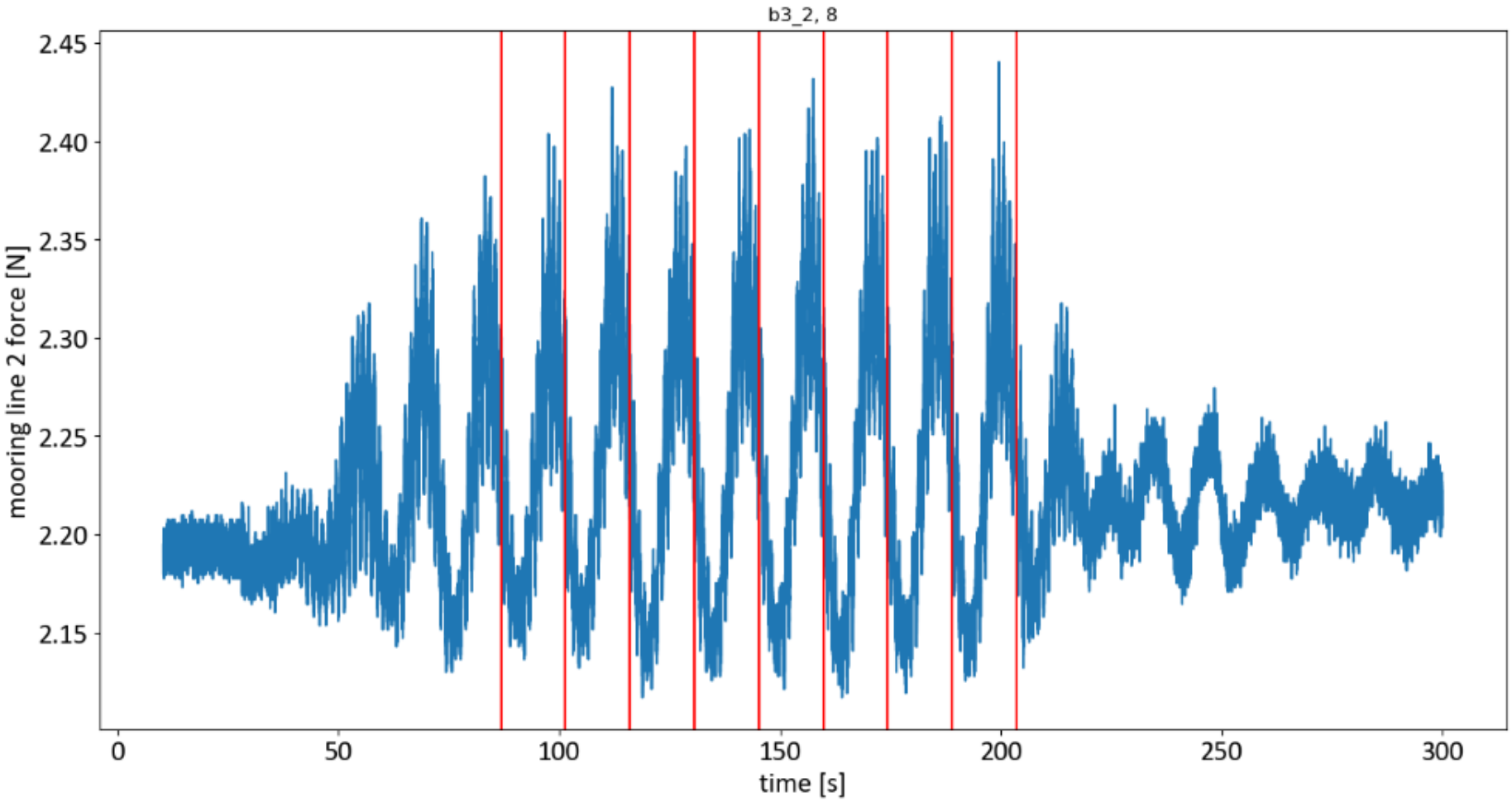
b3_2, 8
mooring line 2 force [N]
2.45
2.40
2.35
2.30
2.25
2.20
2.15
0
50
100
150
200
250
300
time [s]

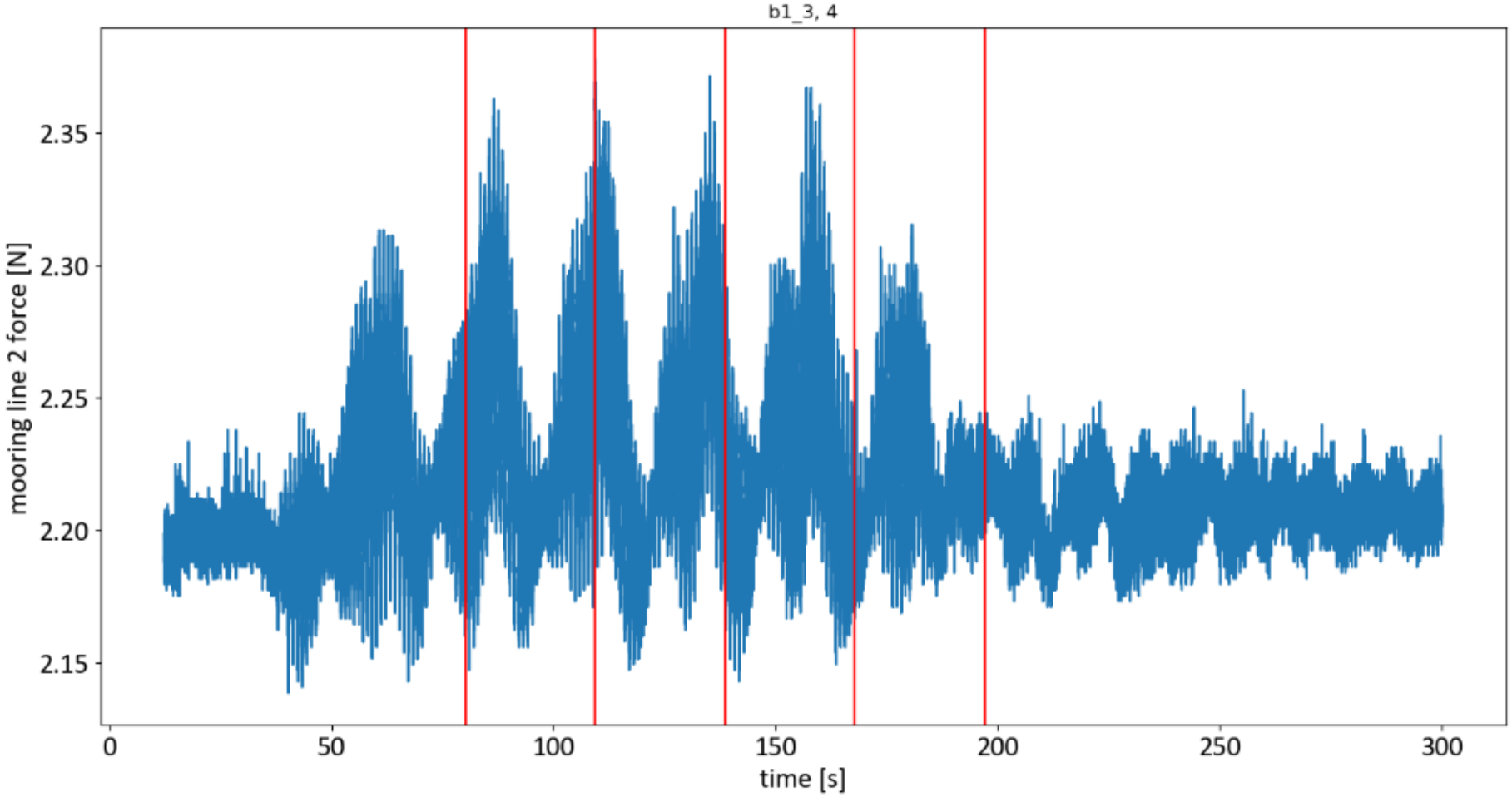
b1_3, 4
mooring line 2 force [N]
2.35
2.30
2.25
2.20
2.15
0
50
100
150
200
250
300
time [s]

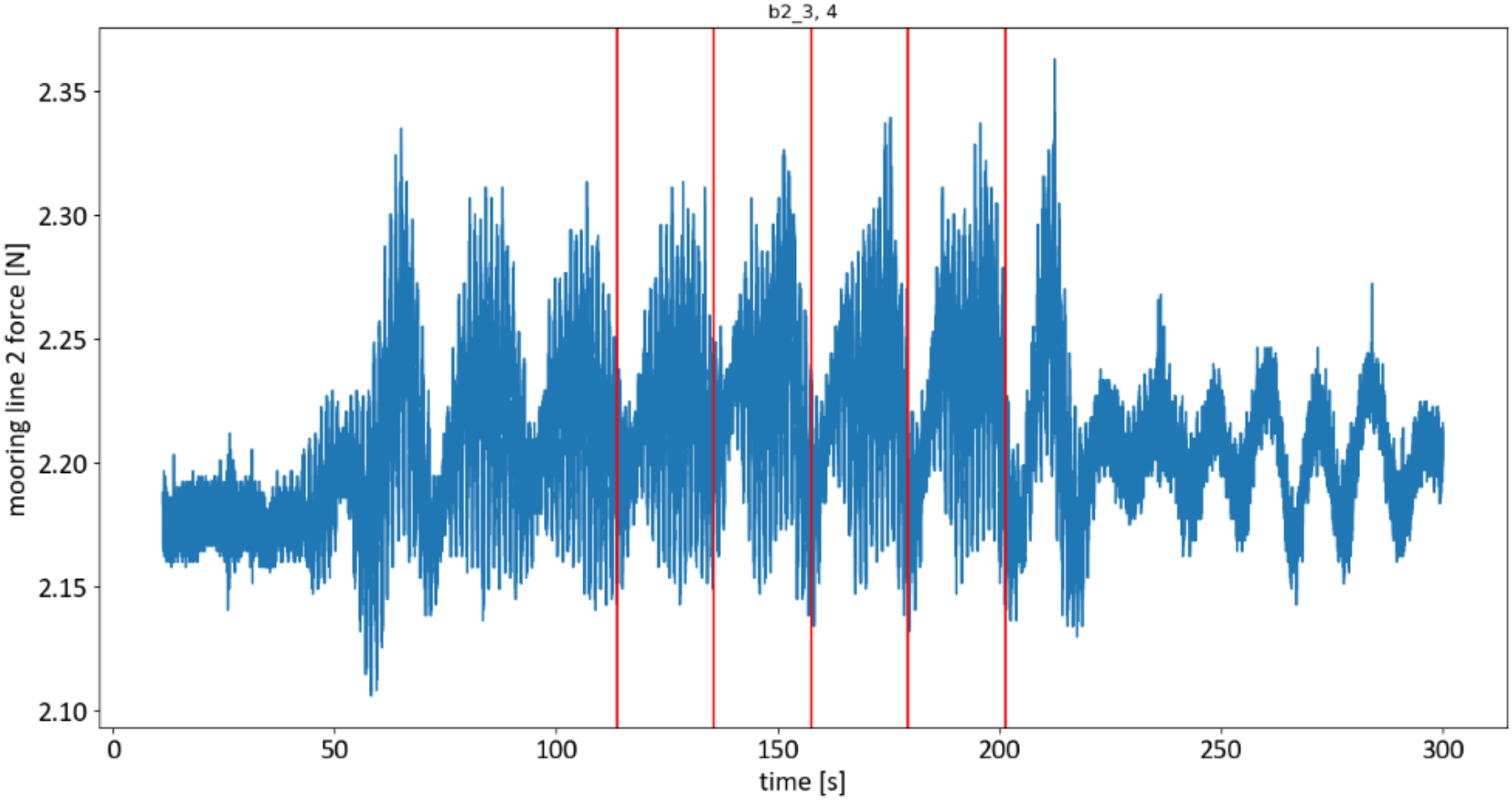
b2_3, 4
mooring line 2 force [N]
2.35
2.30
2.25
2.20
2.15
2.10
0
50
100
150
200
250
300
time [s]

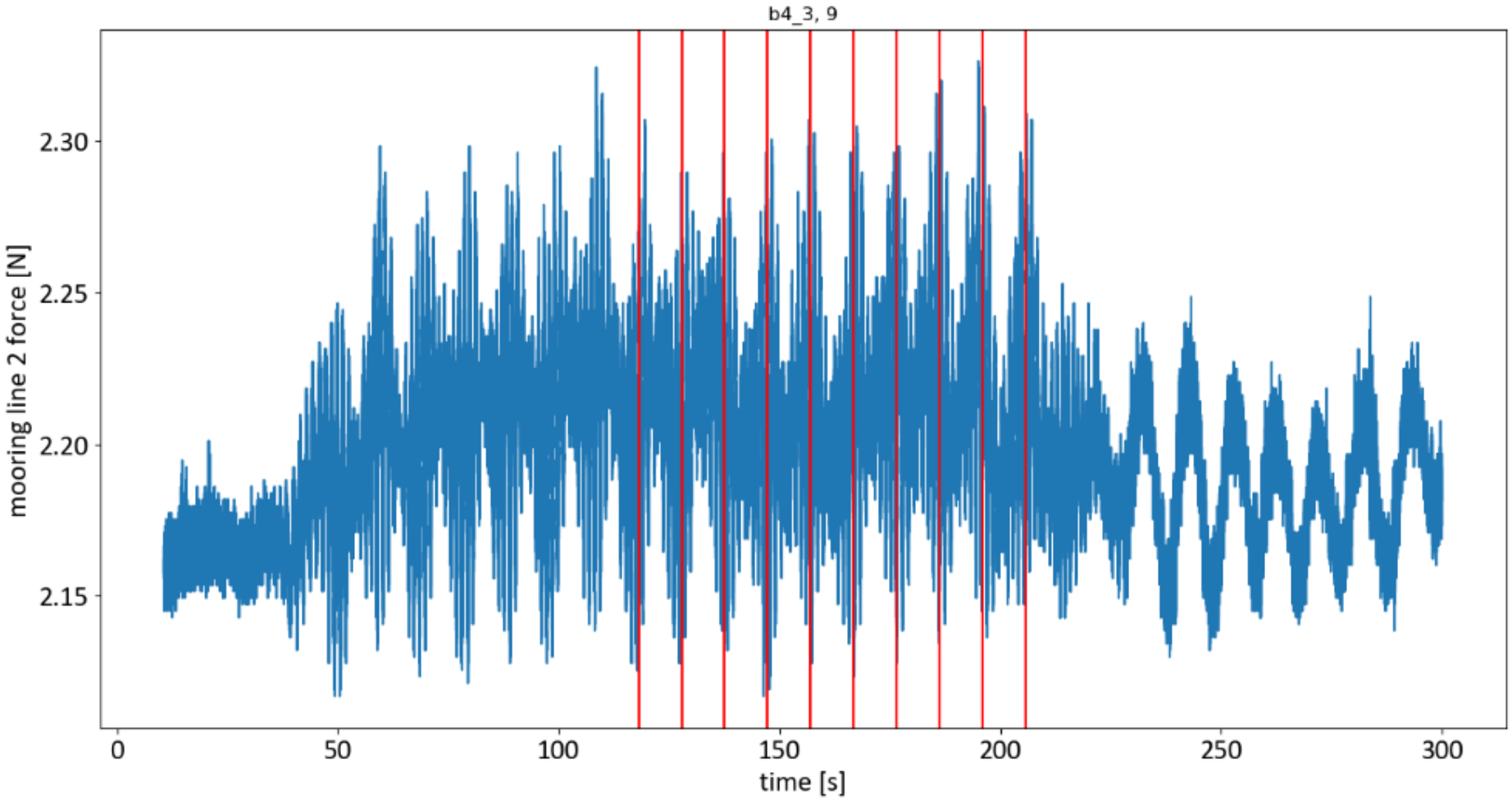
b4_3, 9
mooring line 2 force [N]
2.30
2.25
2.20
2.15
0
50
100
150
200
250
300
time [s]

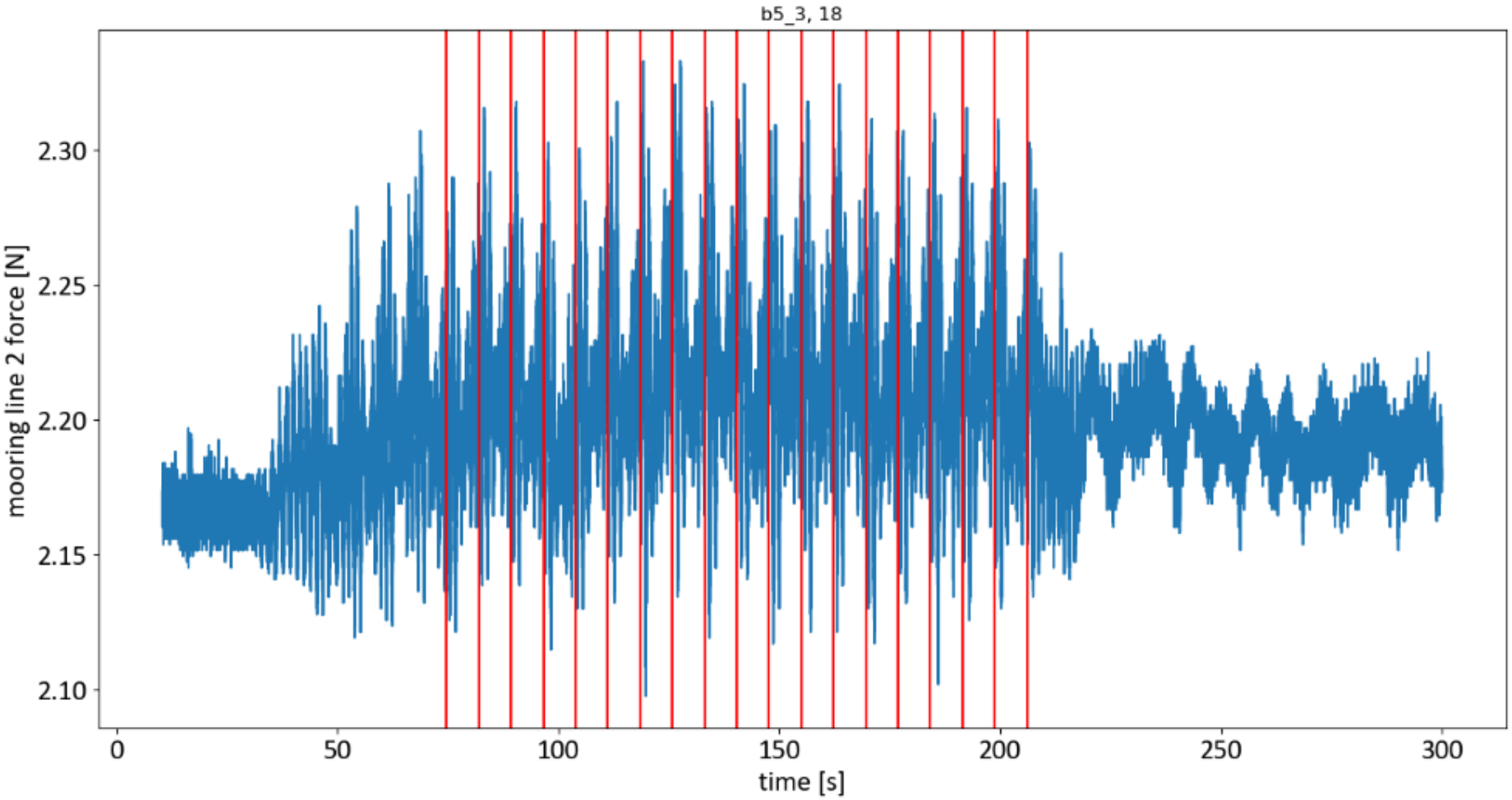
b5_3, 18
mooring line 2 force [N]
2.30
2.25
2.20
2.15
2.10
0
50
100
150
200
250
300
time [s]

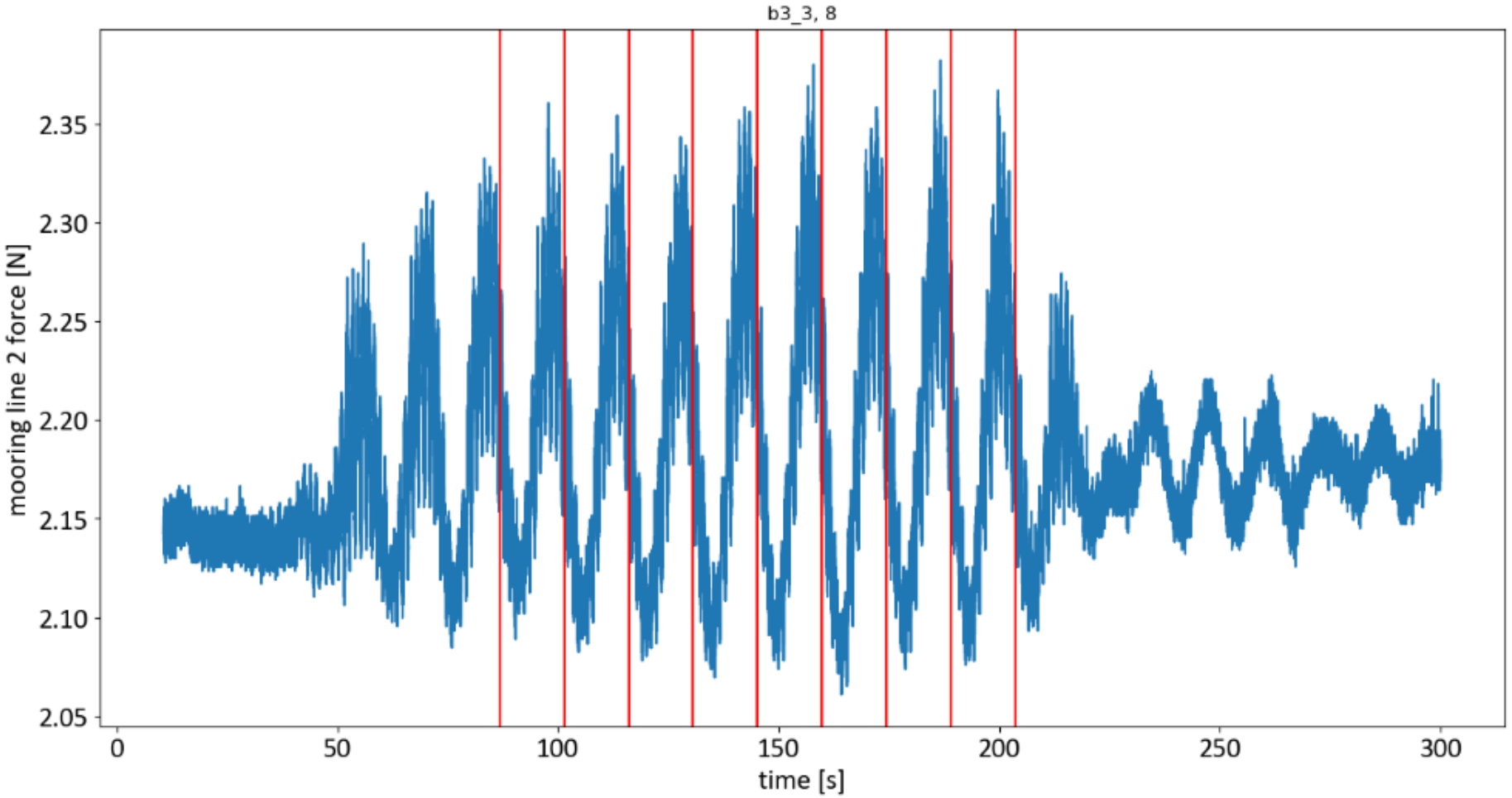
b3_3, 8
mooring line 2 force [N]
2.35
2.30
2.25
2.20
2.15
2.10
2.05
0
50
100
150
200
250
300
time [s]

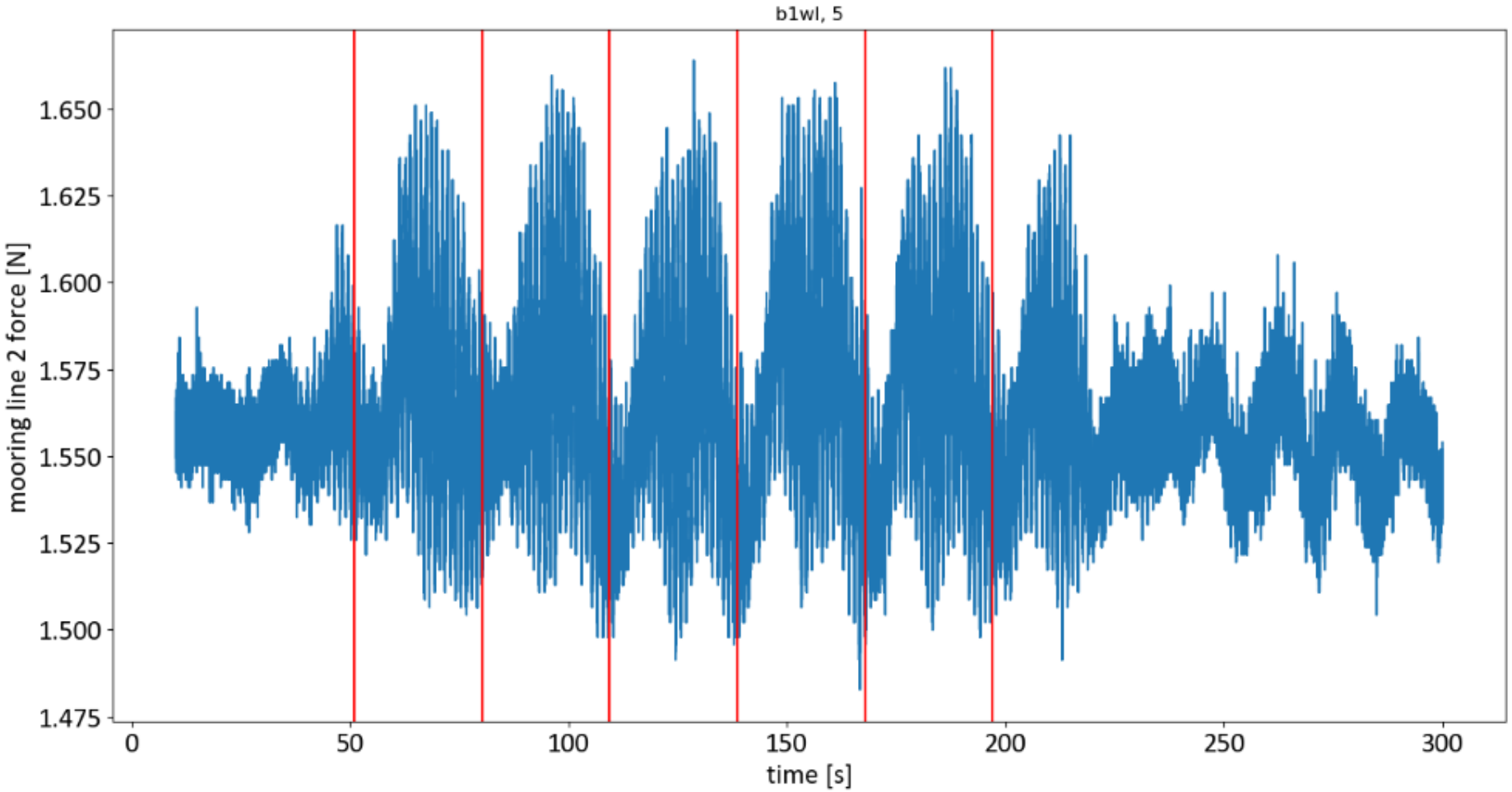
b1wl, 5
mooring line 2 force [N]
1.650
1.625
1.600
1.575
1.550
1.525
1.500
1.475
0
50
100
150
200
250
300
time [s]

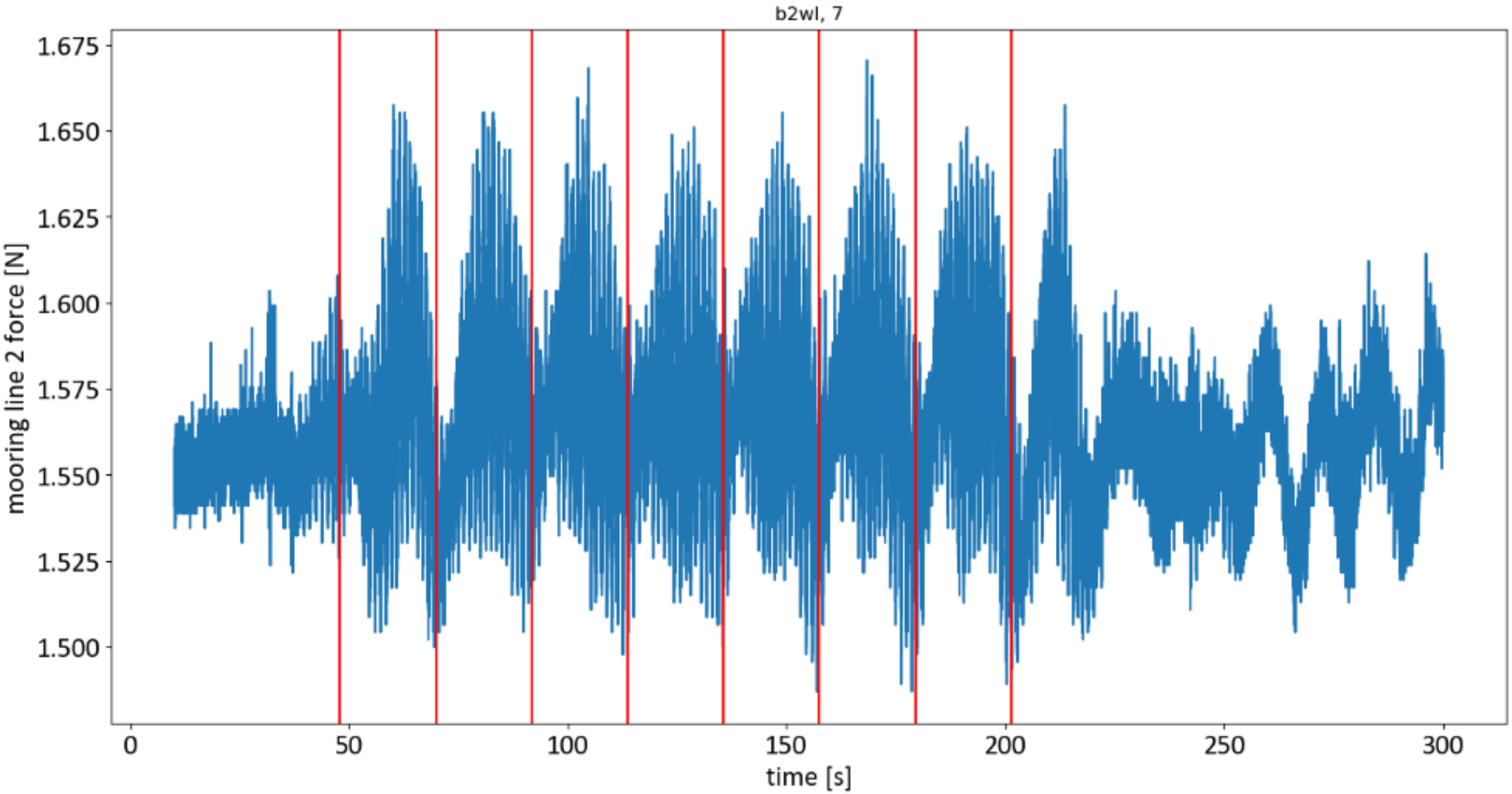
b2wl, 7
mooring line 2 force [N]
1.675
1.650
1.625
1.600
1.575
1.550
1.525
1.500
0
50
100
150
200
250
300
time [s]

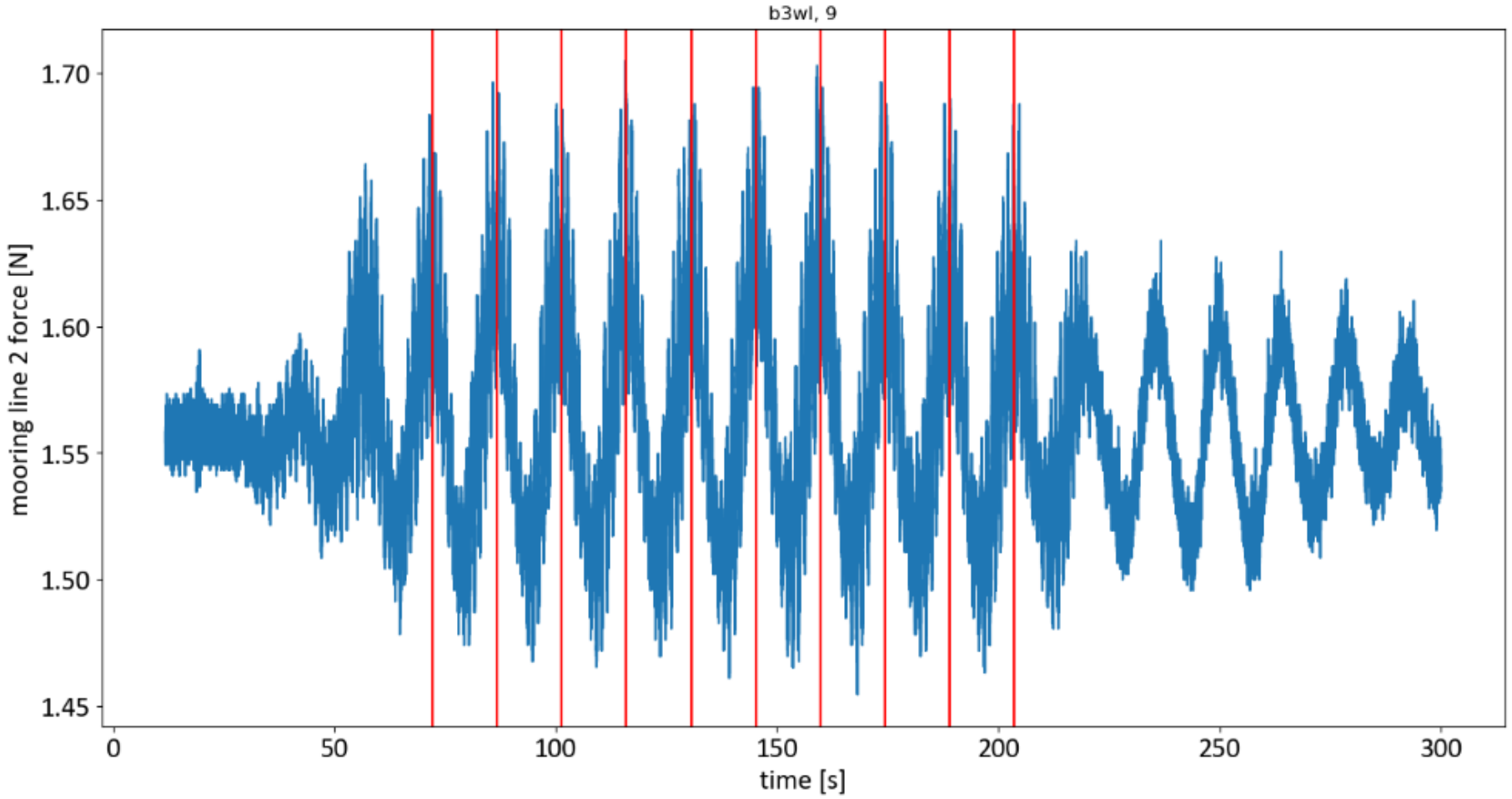
b3wl, 9
mooring line 2 force [N]
1.70
1.65
1.60
1.55
1.50
1.45
0
50
100
150
200
250
300
time [s]

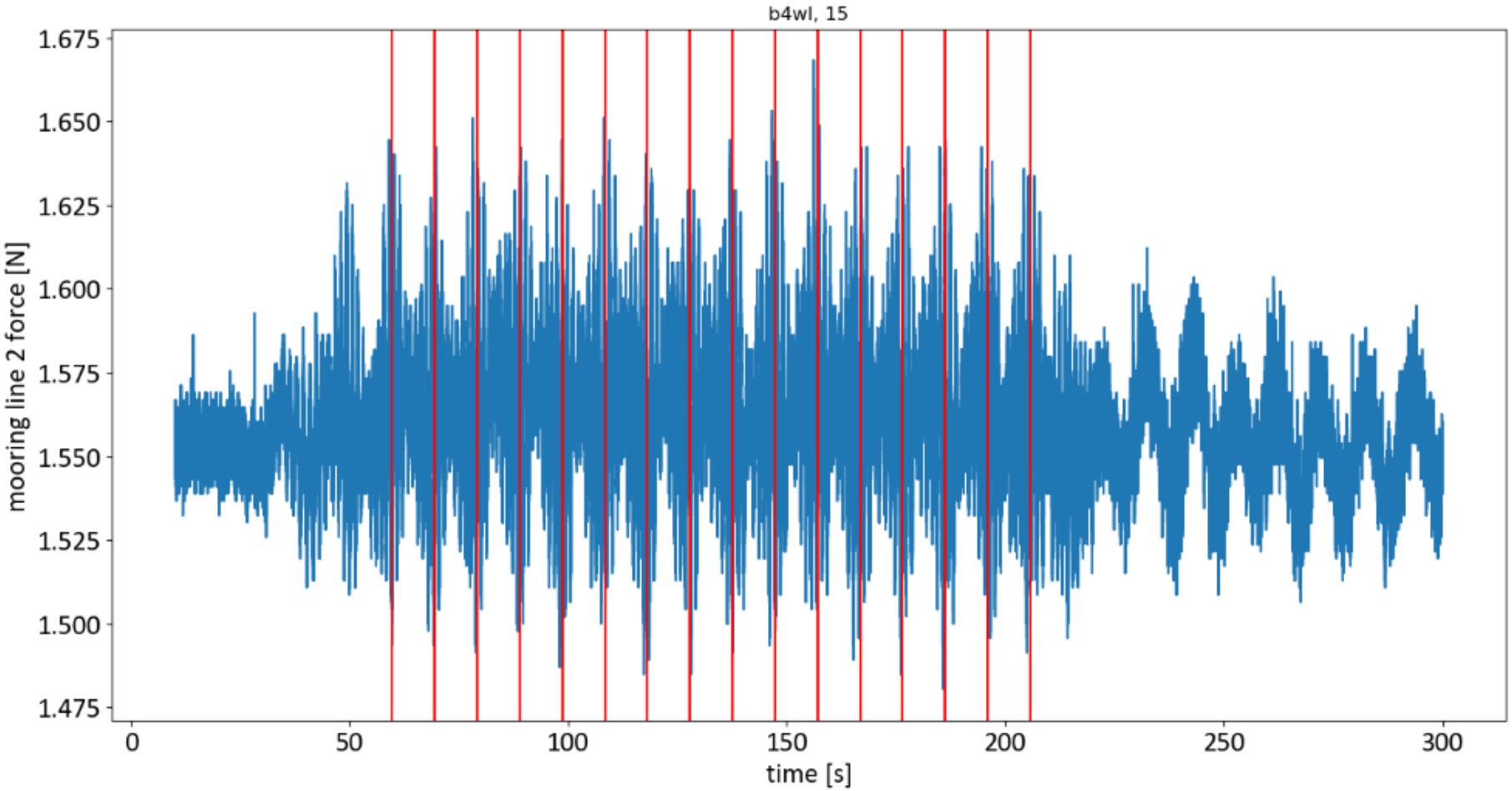
b4wl, 15
mooring line 2 force [N]
1.675
1.650
1.625
1.600
1.575
1.550
1.525
1.500
1.475
0
50
100
150
200
250
300
time [s]

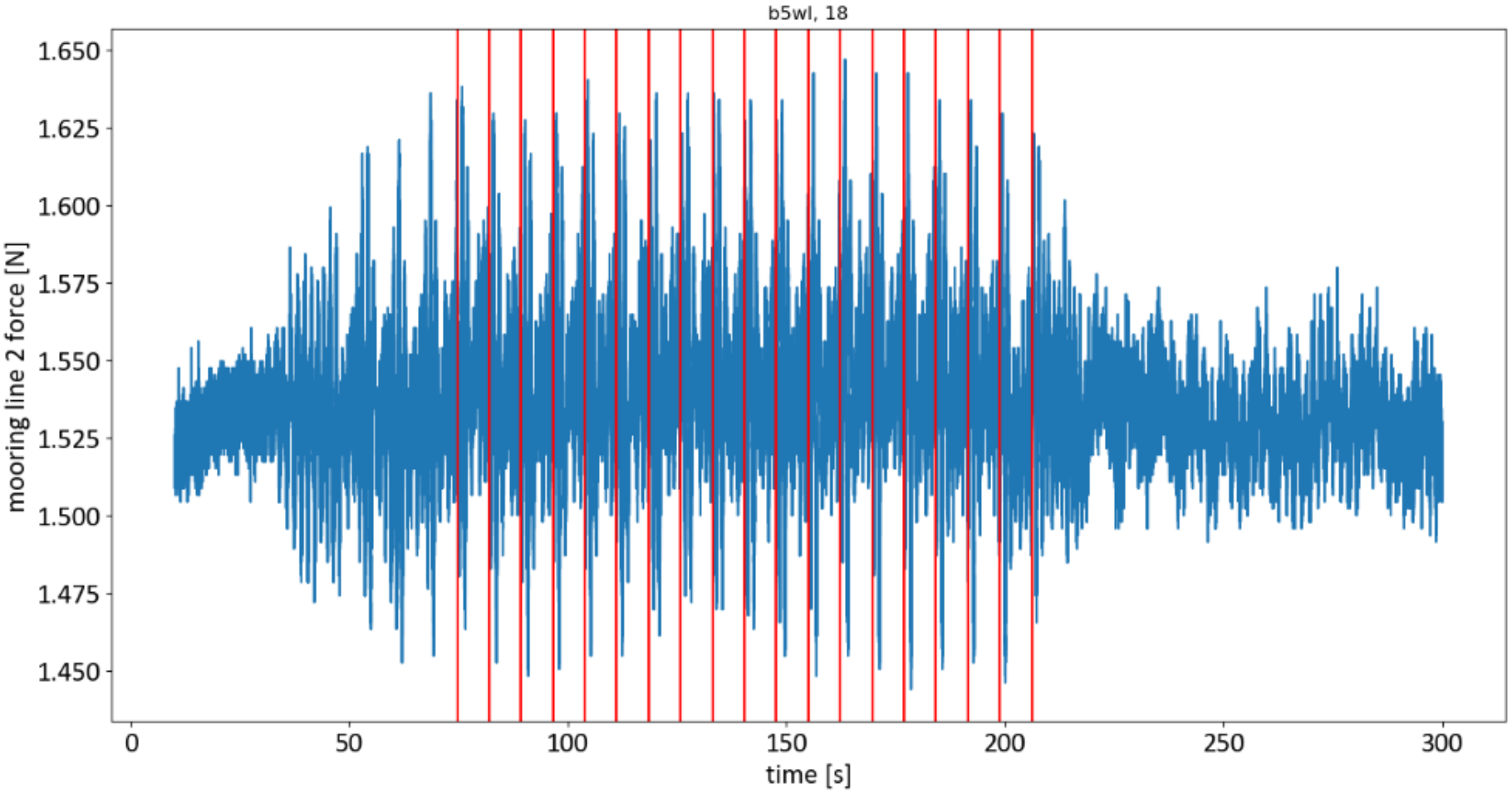
b5wl, 18
mooring line 2 force [N]
1.650
1.625
1.600
1.575
1.550
1.525
1.500
1.475
1.450
0
50
100
150
200
250
300
time [s]

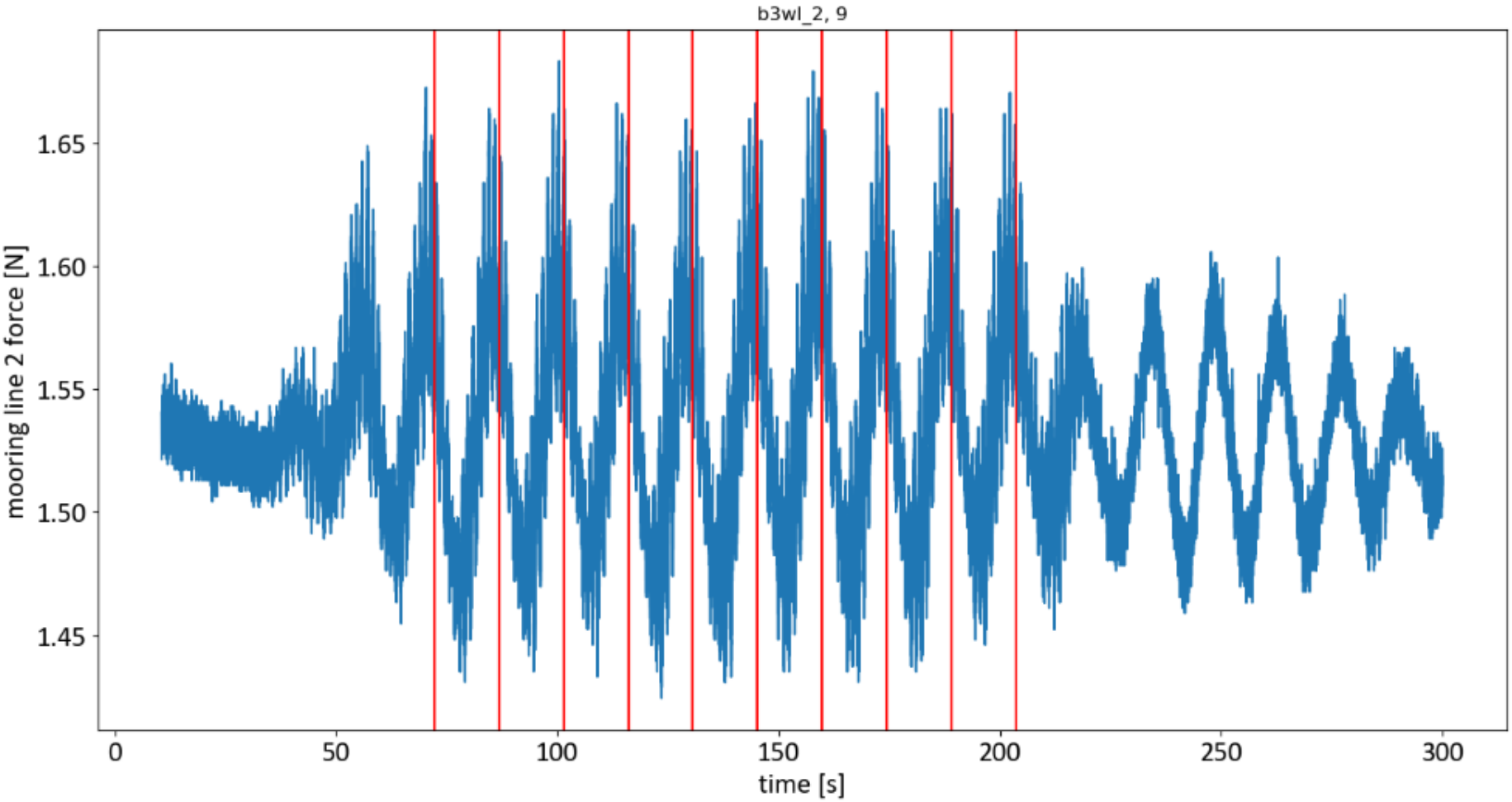
b3wl_2, 9
mooring line 2 force [N]
1.65
1.60
1.55
1.50
1.45
0
50
100
150
200
250
300
time [s]

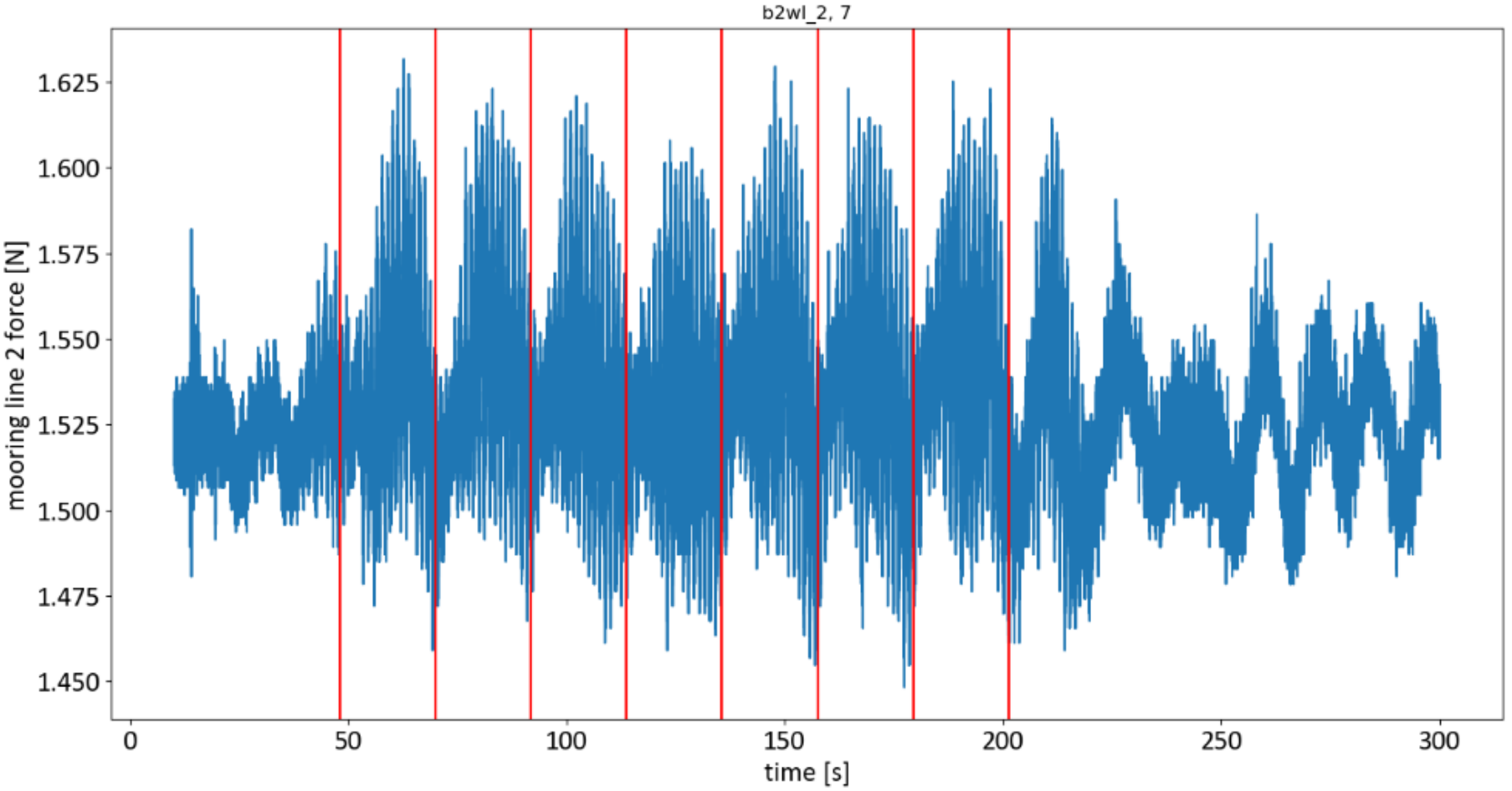
b2wl_2, 7
mooring line 2 force [N]
1.625
1.600
1.575
1.550
1.525
1.500
1.475
1.450
0
50
100
150
200
250
300
time [s]

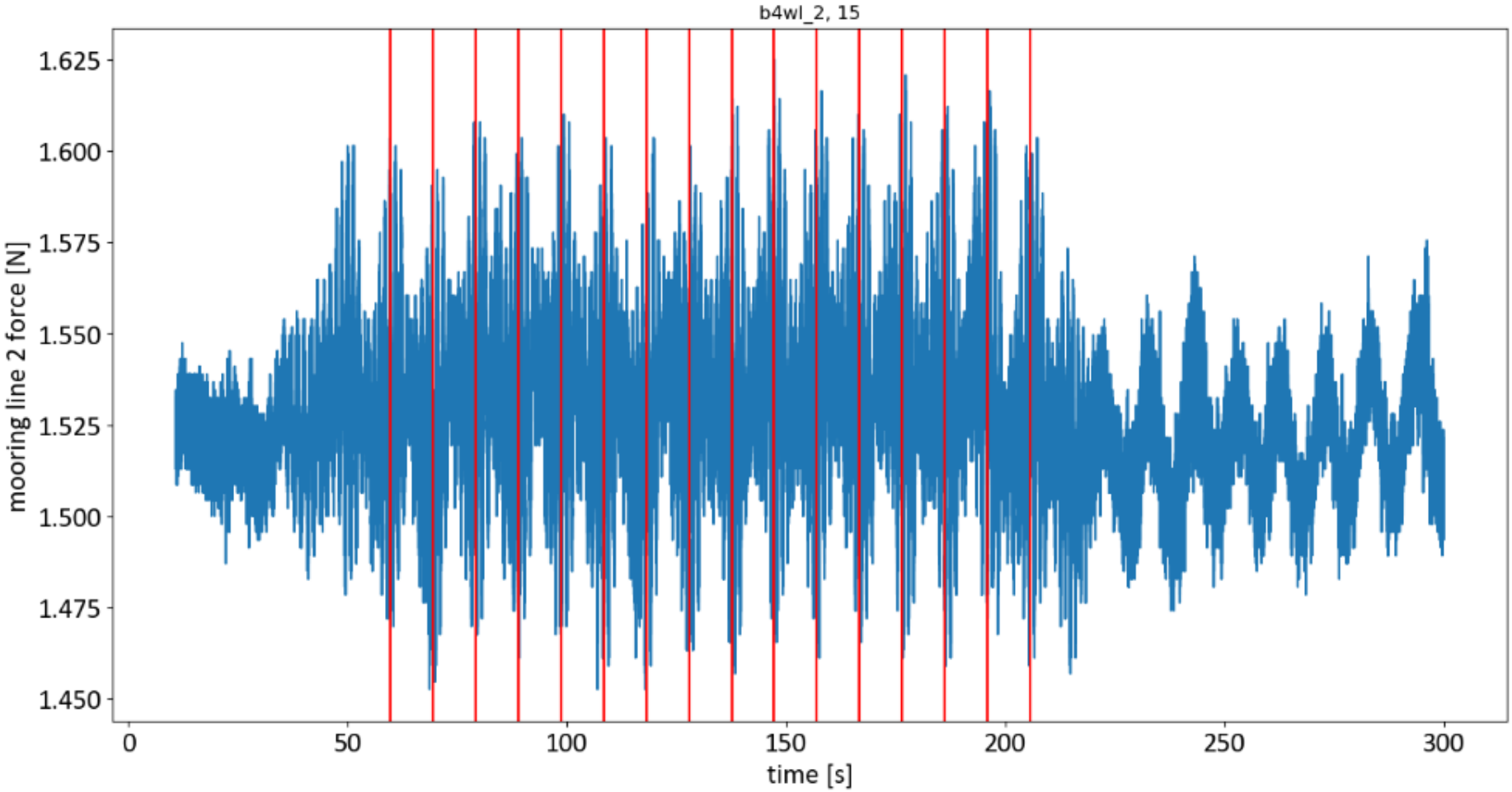
b4wl_2, 15
mooring line 2 force [N]
1.625
1.600
1.575
1.550
1.525
1.500
1.475
1.450
0
50
100
150
200
250
300
time [s]

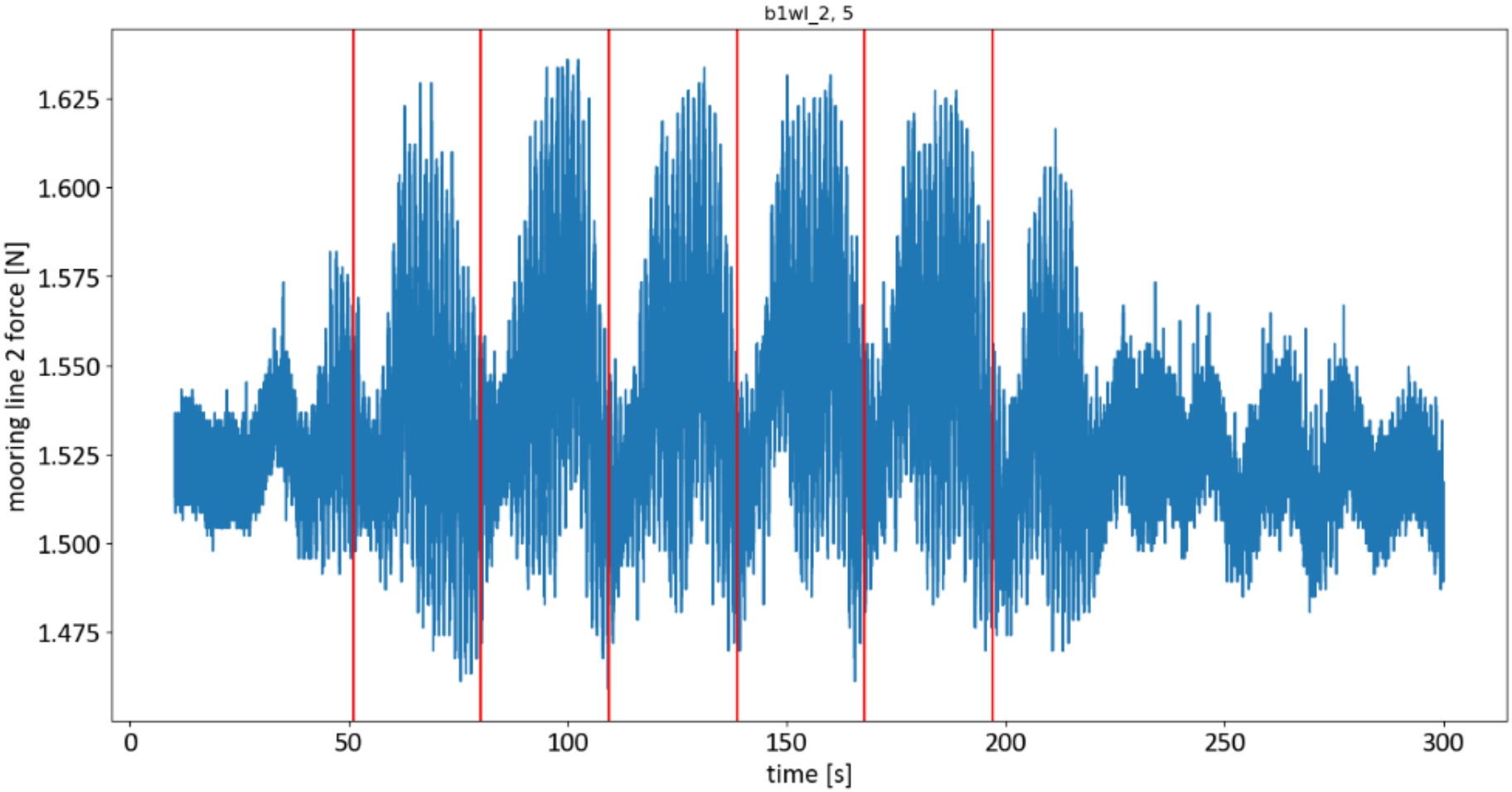
b1wl_2, 5
mooring line 2 force [N]
1.625
1.600
1.575
1.550
1.525
1.500
1.475
0
50
100
150
200
250
300
time [s]

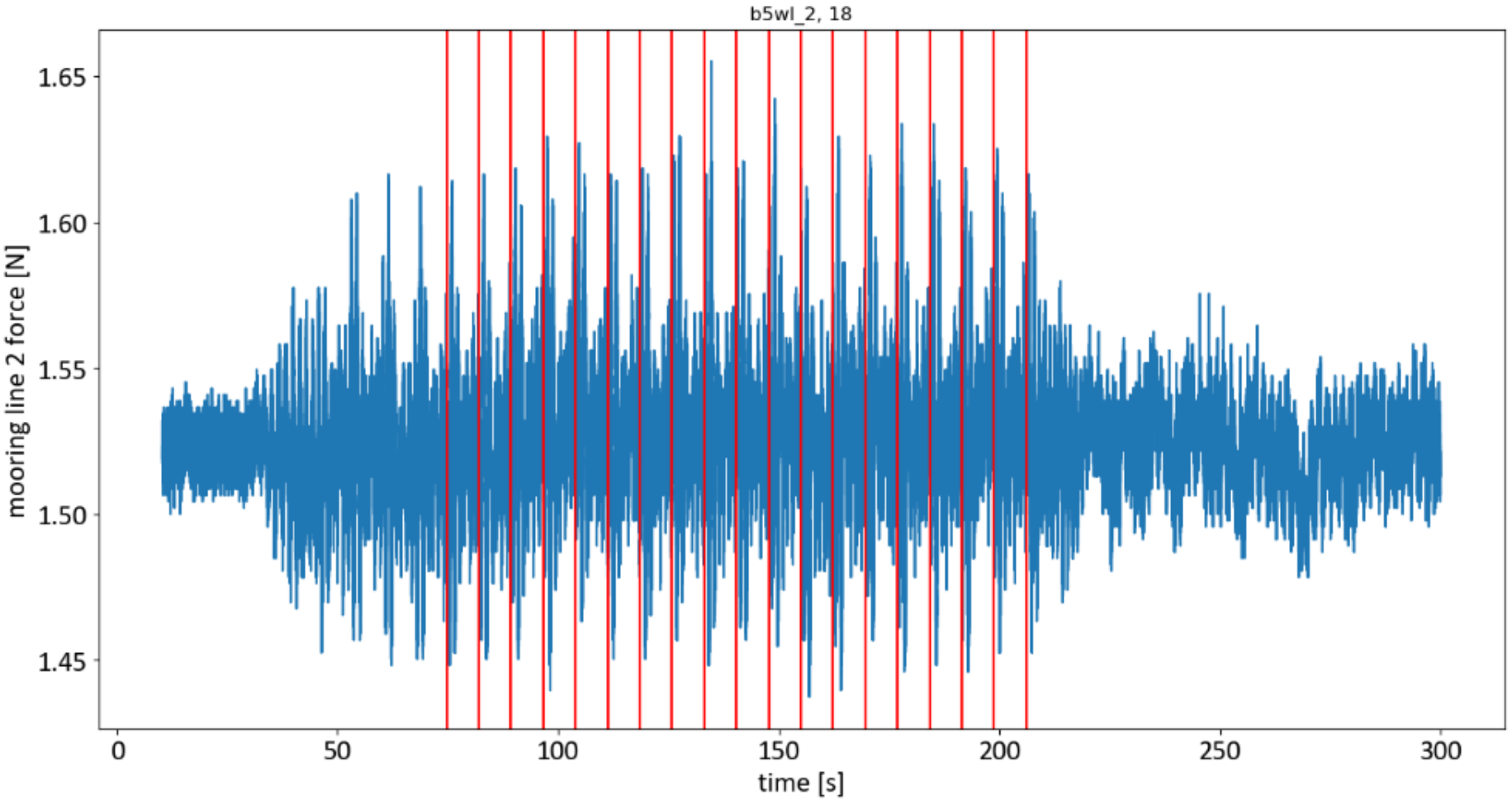
b5wl_2, 18
mooring line 2 force [N]
1.65
1.60
1.55
1.50
1.45
0
50
100
150
200
250
300
time [s]

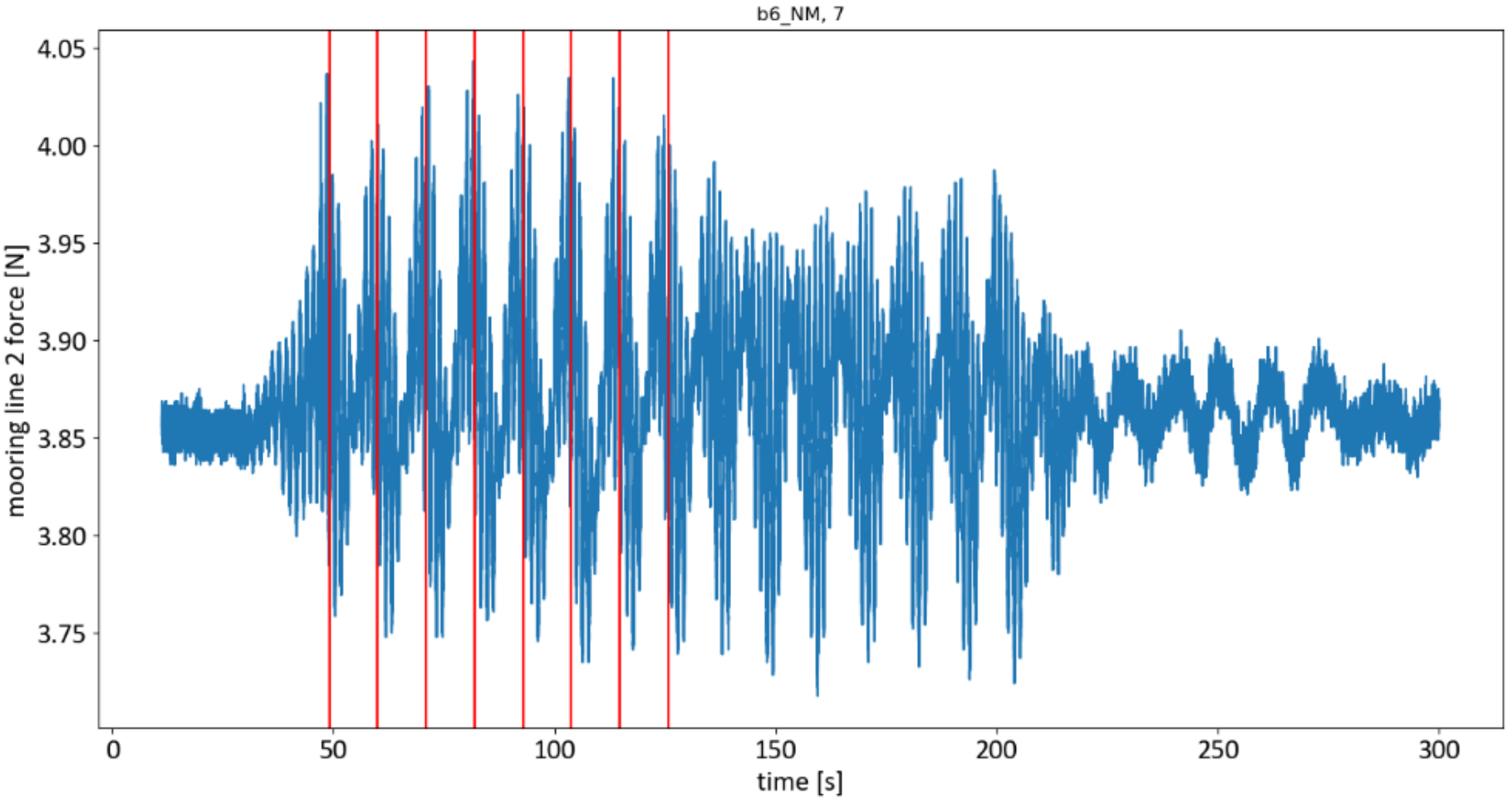
b6_NM, 7
mooring line 2 force [N]
4.05
4.00
3.95
3.90
3.85
3.80
3.75
0
50
100
150
200
250
300
time [s]

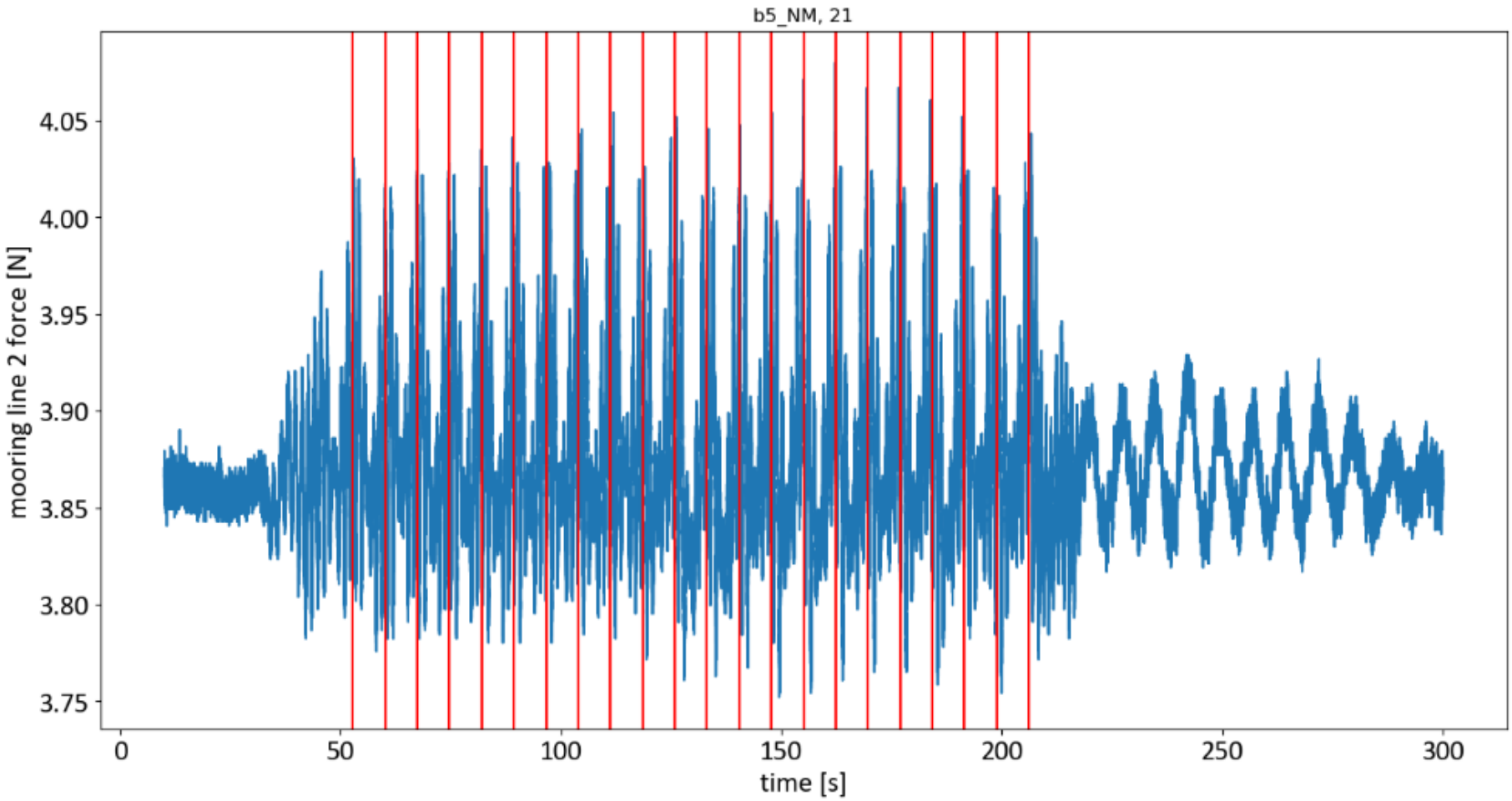
b5_NM, 21
mooring line 2 force [N]
4.05
4.00
3.95
3.90
3.85
3.80
3.75
0
50
100
150
200
250
300
time [s]

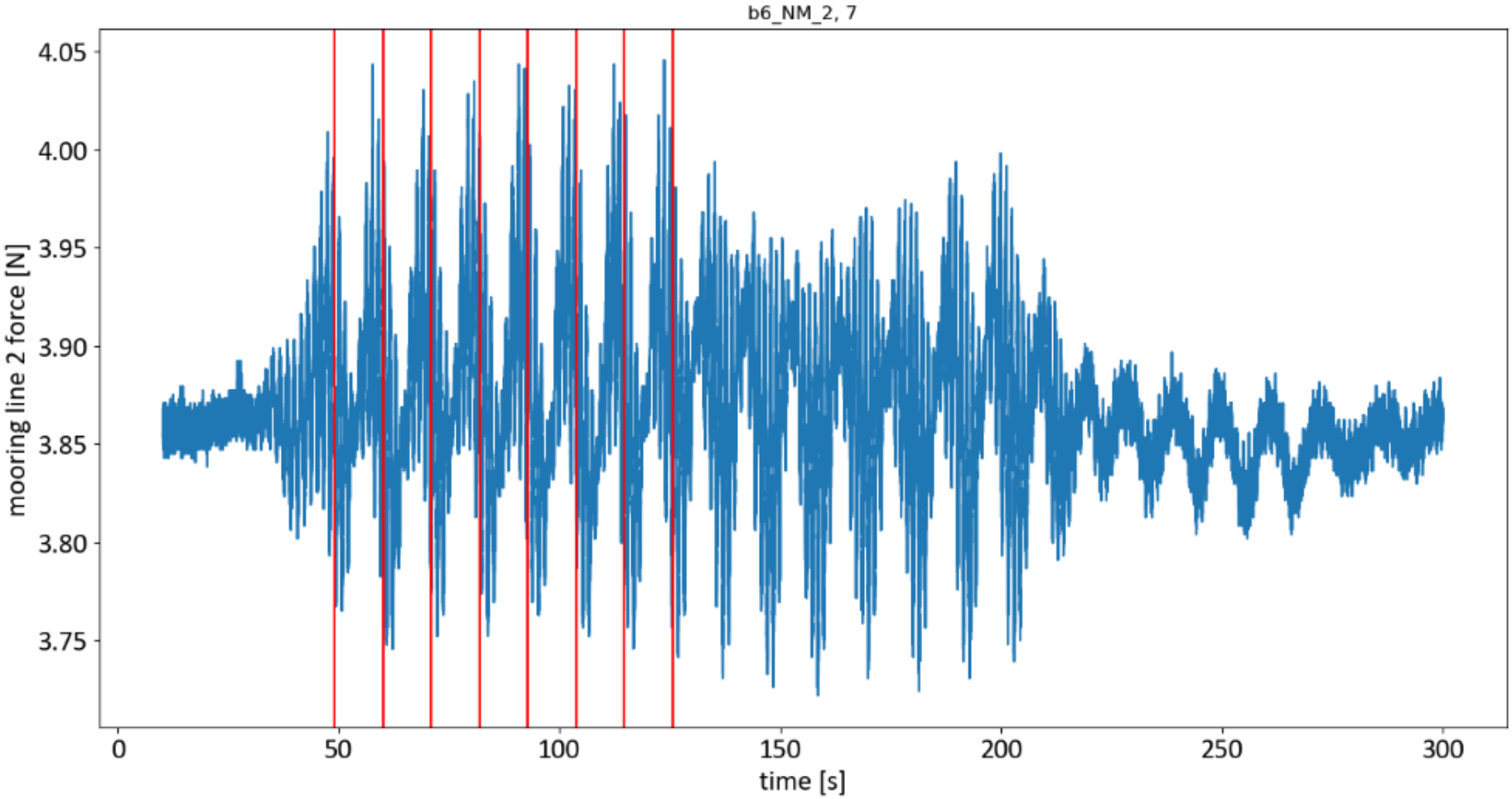
b6_NM_2, 7
mooring line 2 force [N]
4.05
4.00
3.95
3.90
3.85
3.80
3.75
0
50
100
150
200
250
300
time [s]

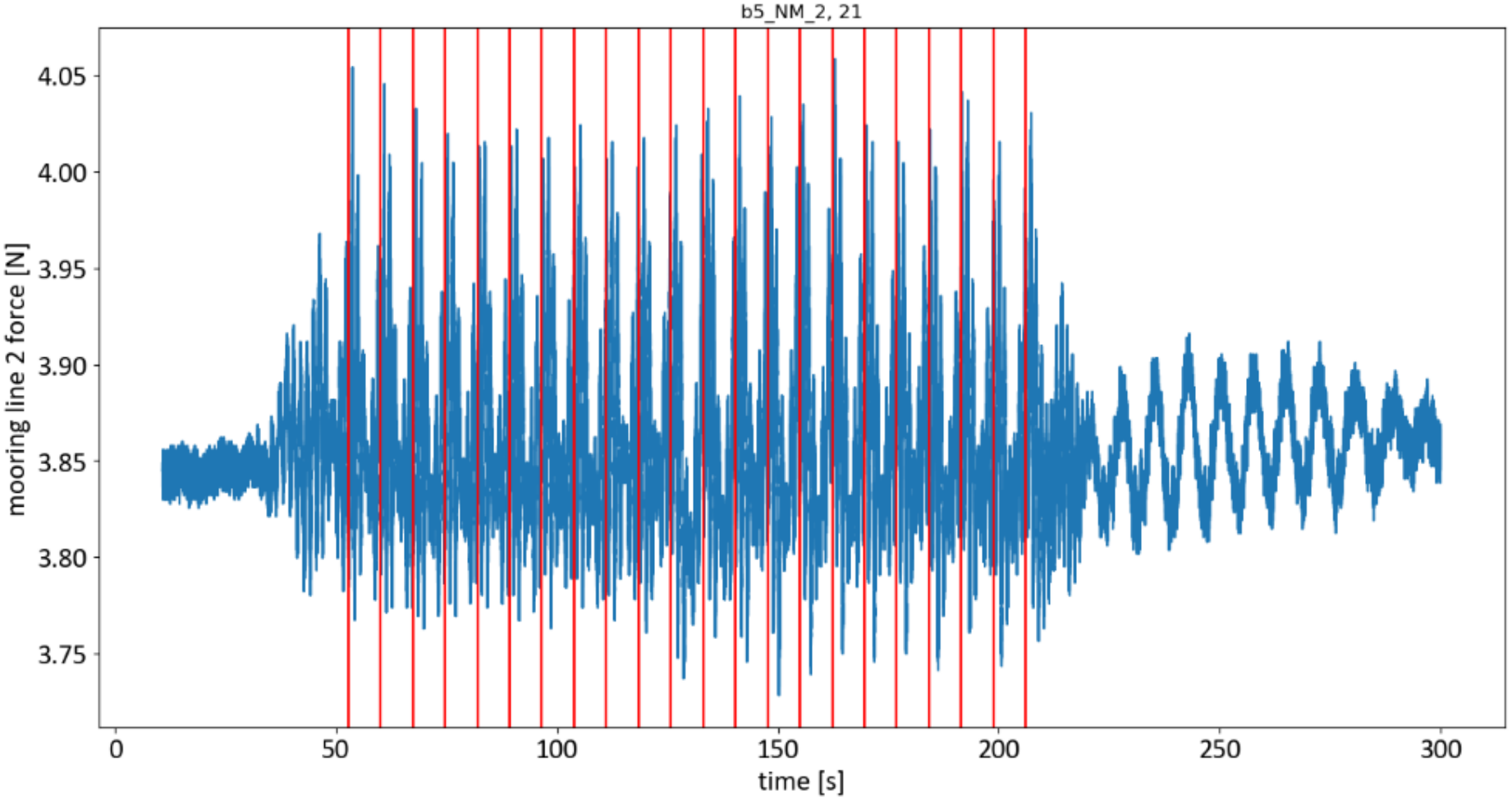
b5_NM_2, 21
mooring line 2 force [N]
4.05
4.00
3.95
3.90
3.85
3.80
3.75
0
50
100
150
200
250
300
time [s]

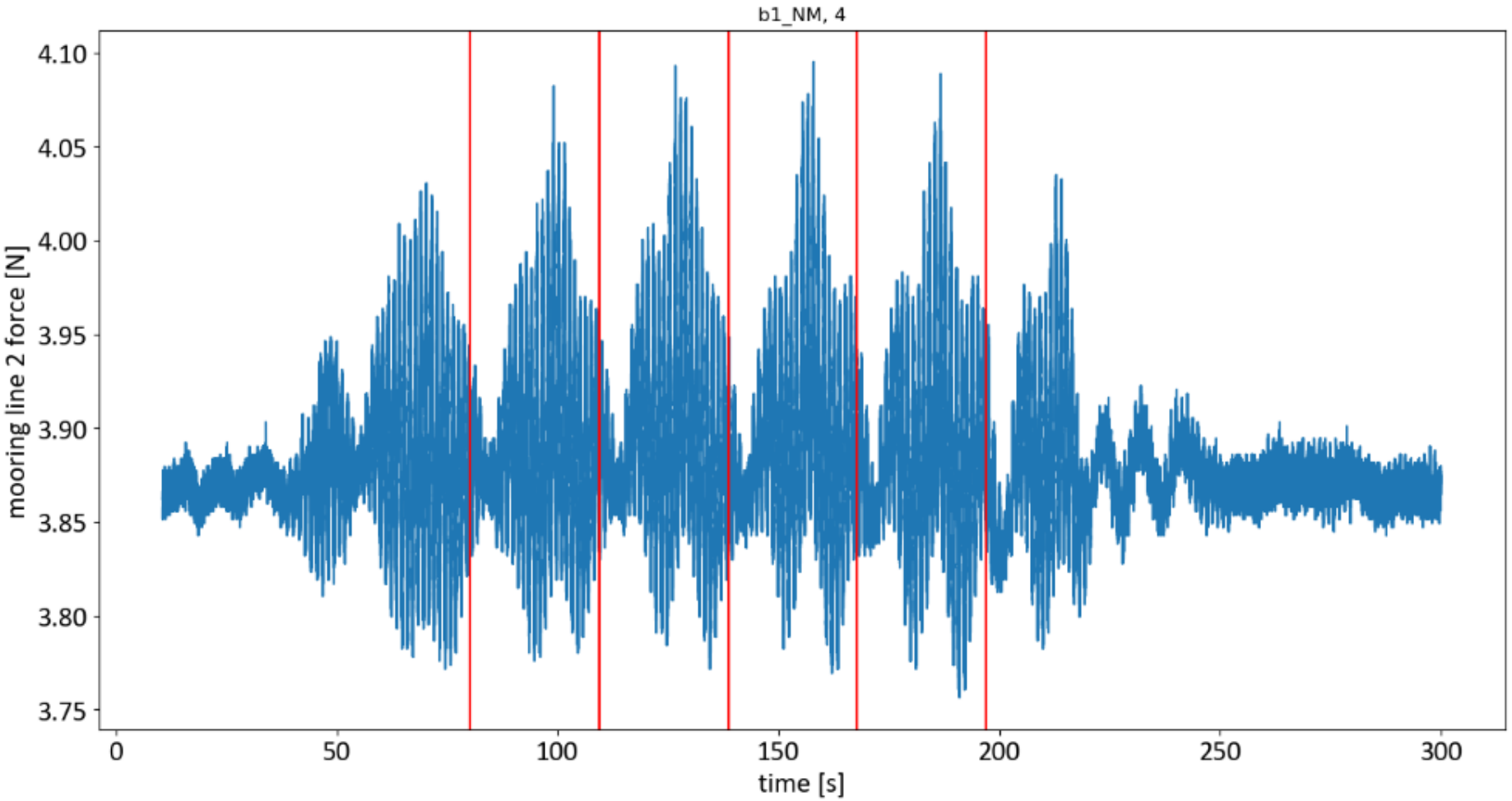
b1_NM, 4
mooring line 2 force [N]
4.10
4.05
4.00
3.95
3.90
3.85
3.80
3.75
0
50
100
150
200
250
300
time [s]

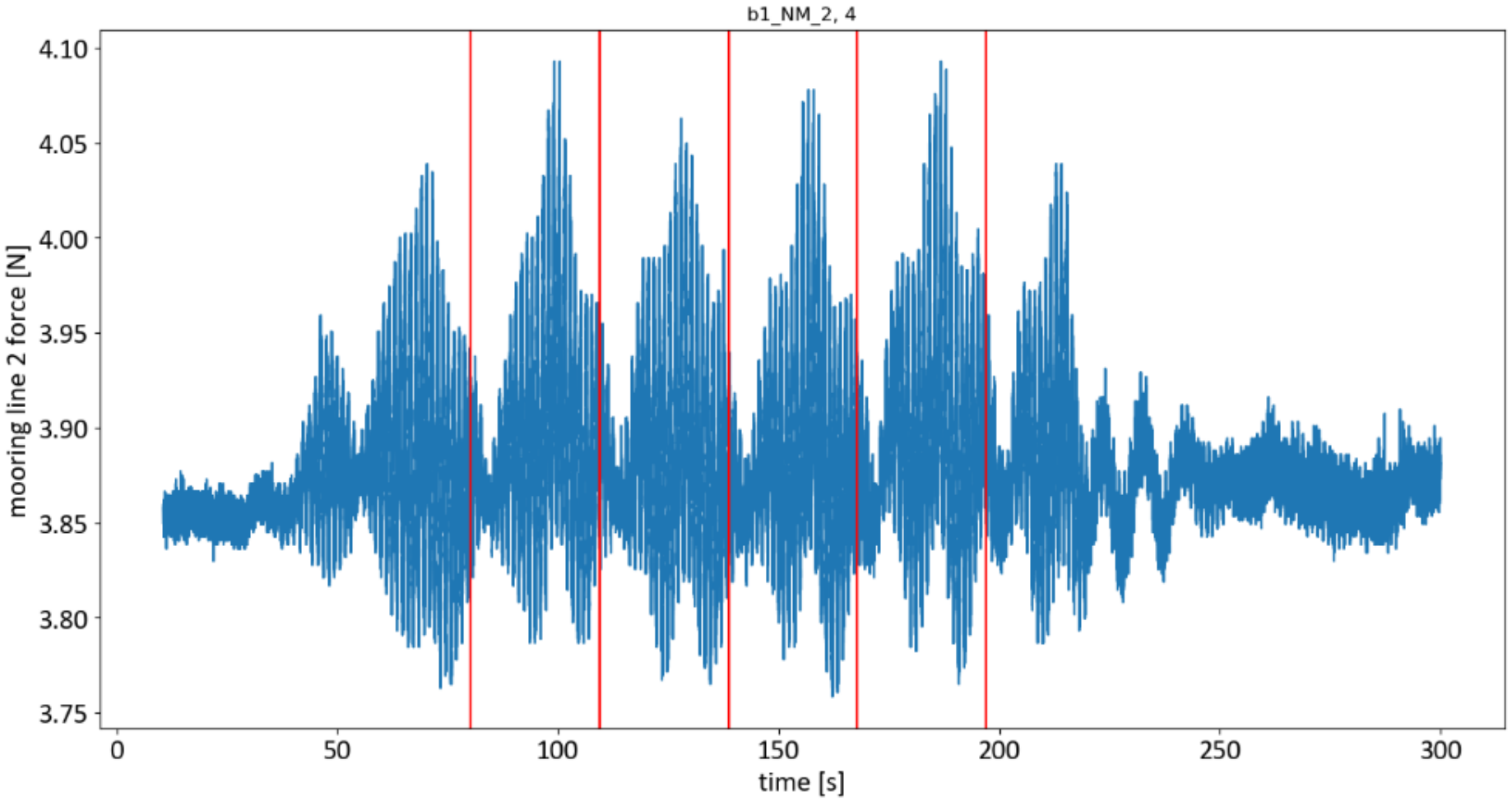
b1_NM_2, 4
mooring line 2 force [N]
4.10
4.05
4.00
3.95
3.90
3.85
3.80
3.75
0
50
100
150
200
250
300
time [s]

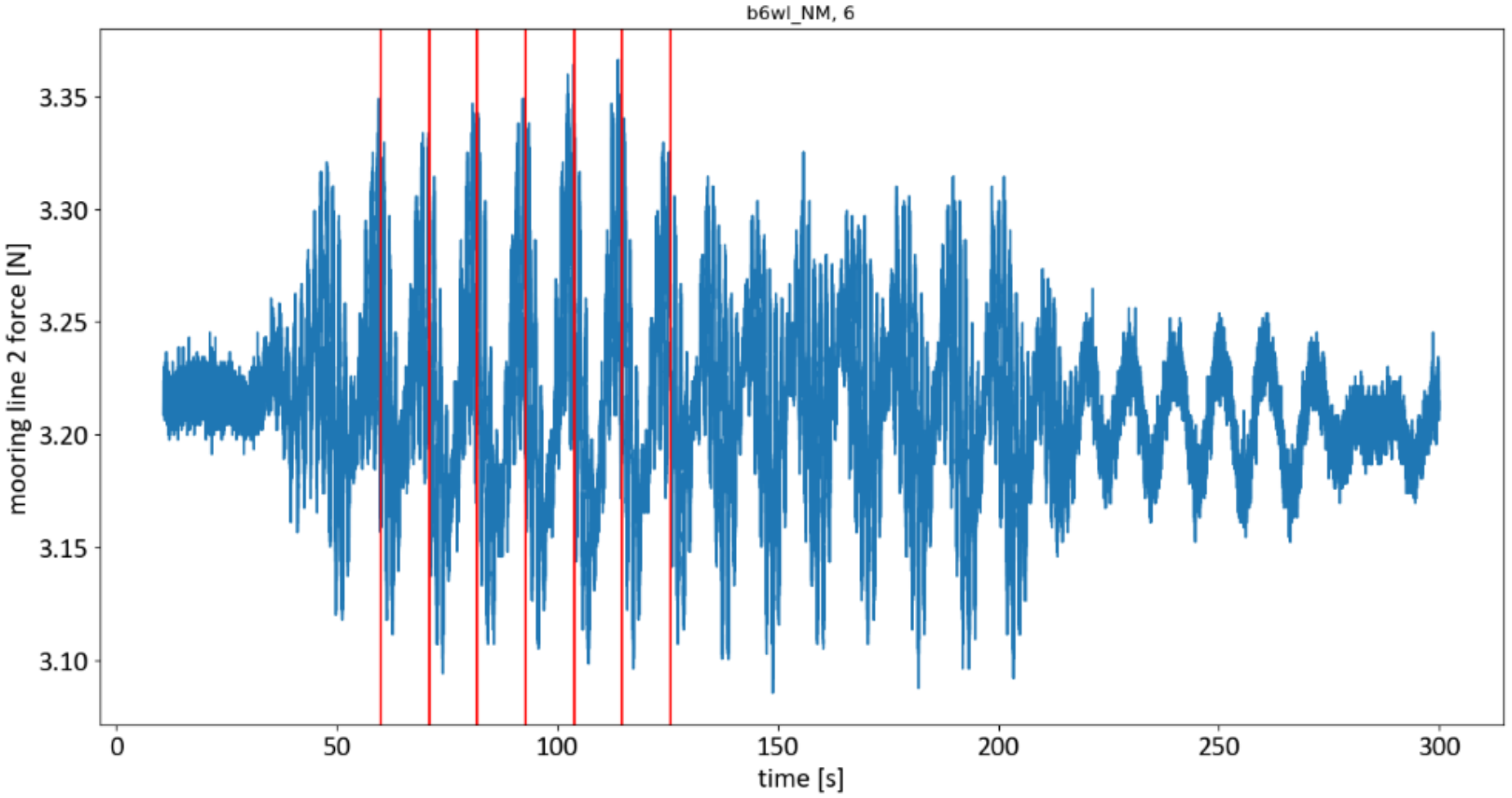
b6wl_NM, 6
mooring line 2 force [N]
3.35
3.30
3.25
3.20
3.15
3.10
0
50
100
150
200
250
300
time [s]

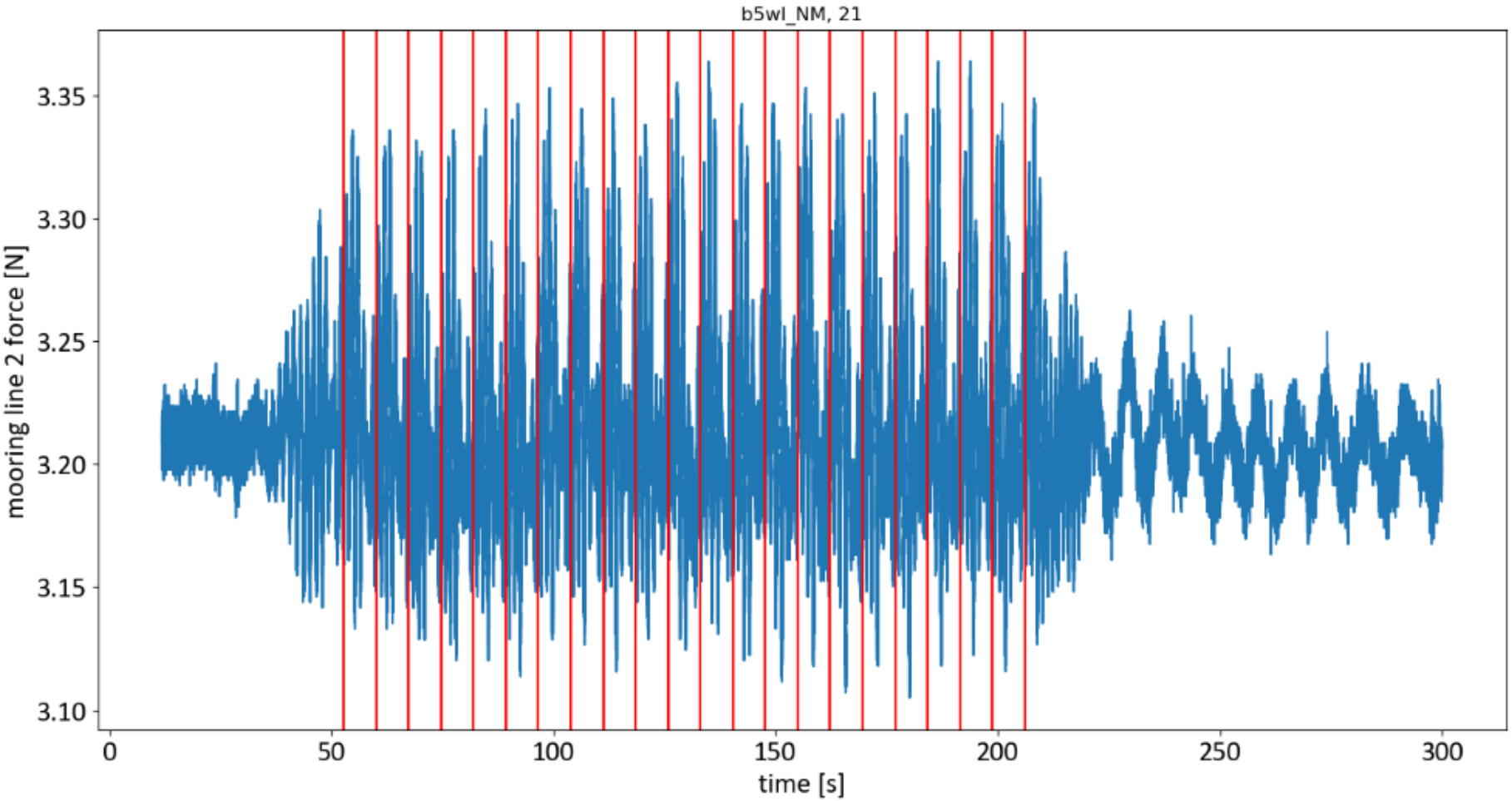
b5wl_NM, 21
mooring line 2 force [N]
3.35
3.30
3.25
3.20
3.15
3.10
0
50
100
150
200
250
300
time [s]

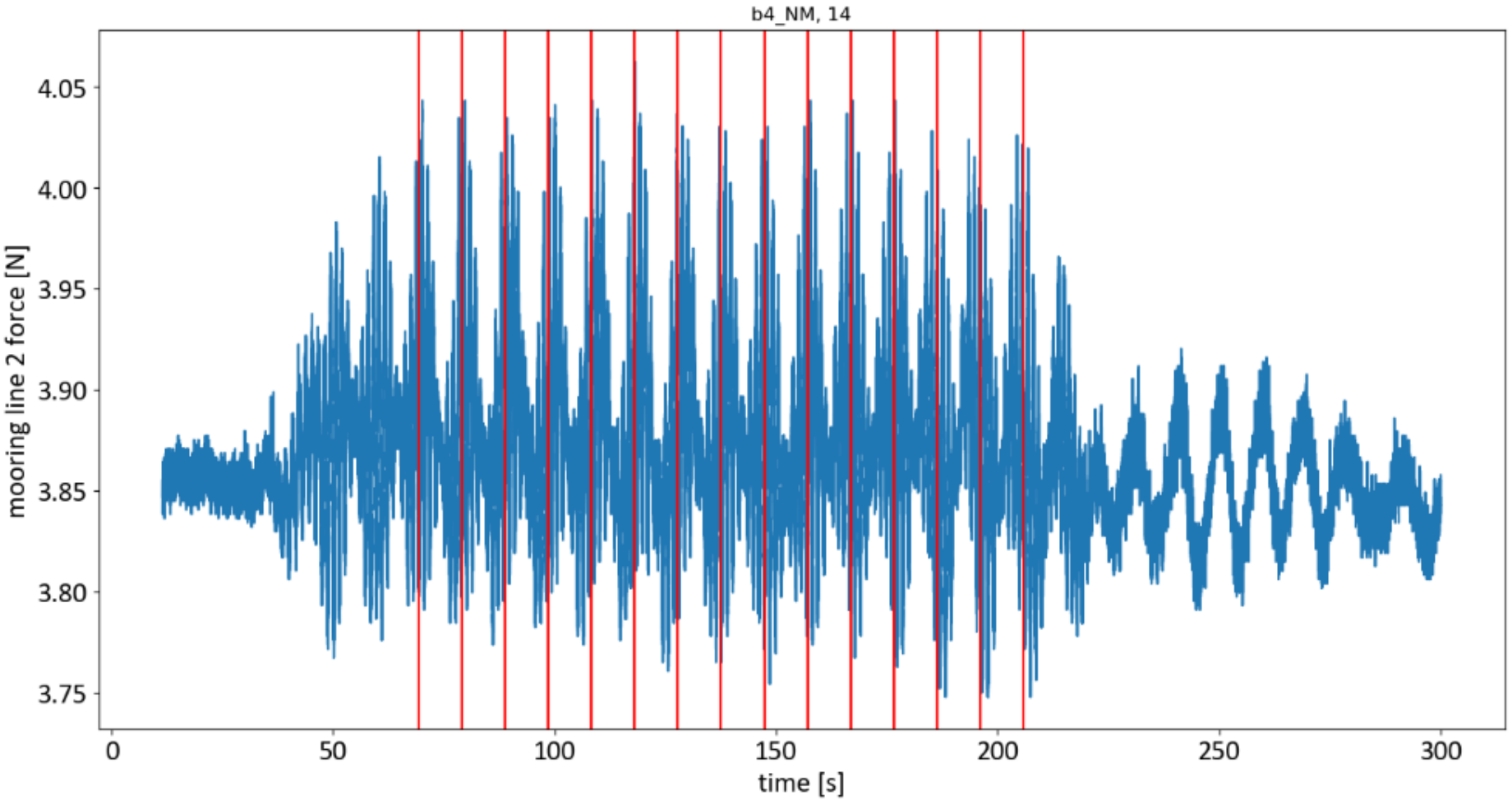
b4_NM, 14
mooring line 2 force [N]
4.05
4.00
3.95
3.90
3.85
3.80
3.75
0
50
100
150
200
250
300
time [s]

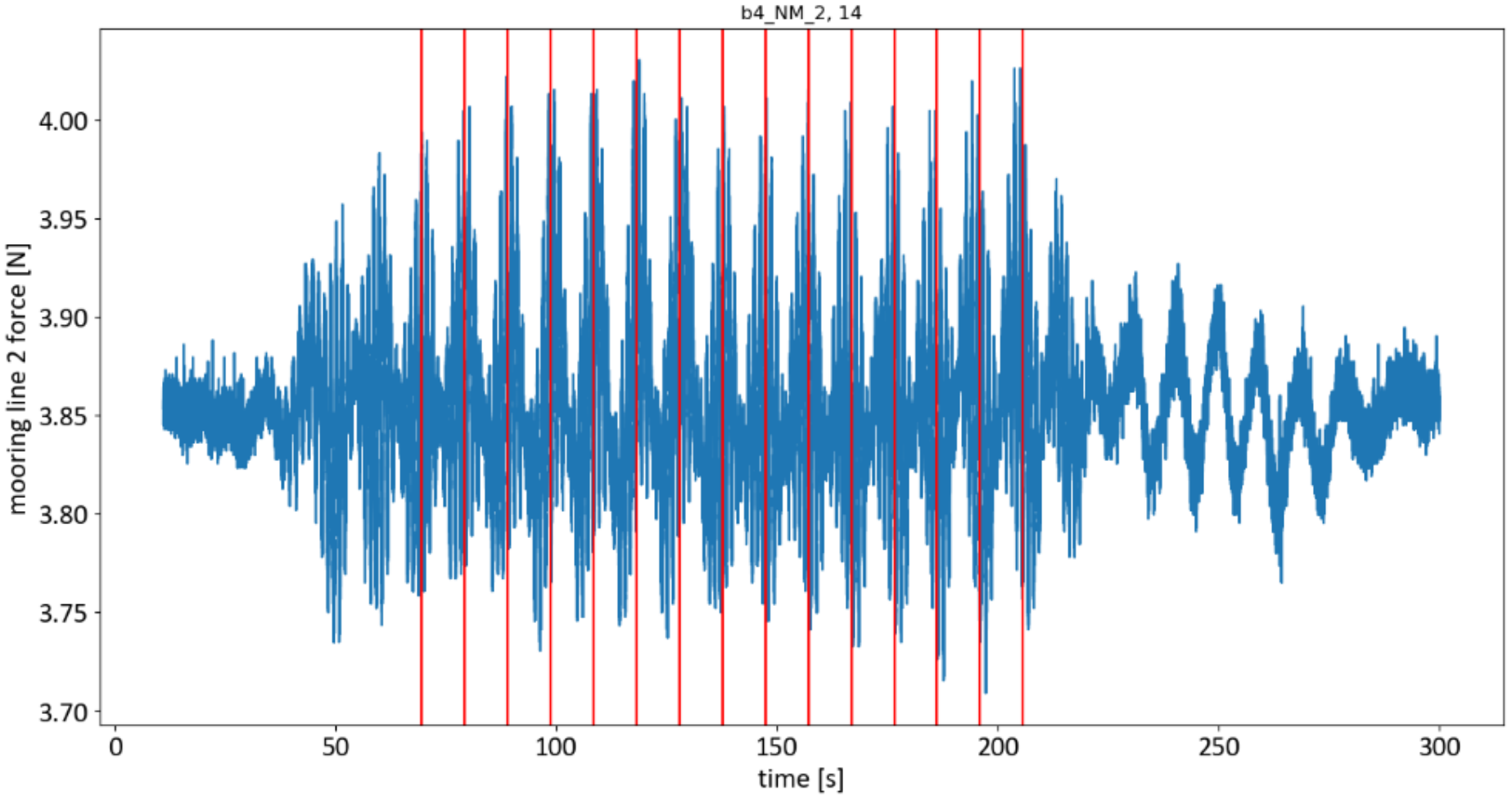
b4_NM_2, 14
mooring line 2 force [N]
4.00
3.95
3.90
3.85
3.80
3.75
3.70
0
50
100
150
200
250
300
time [s]

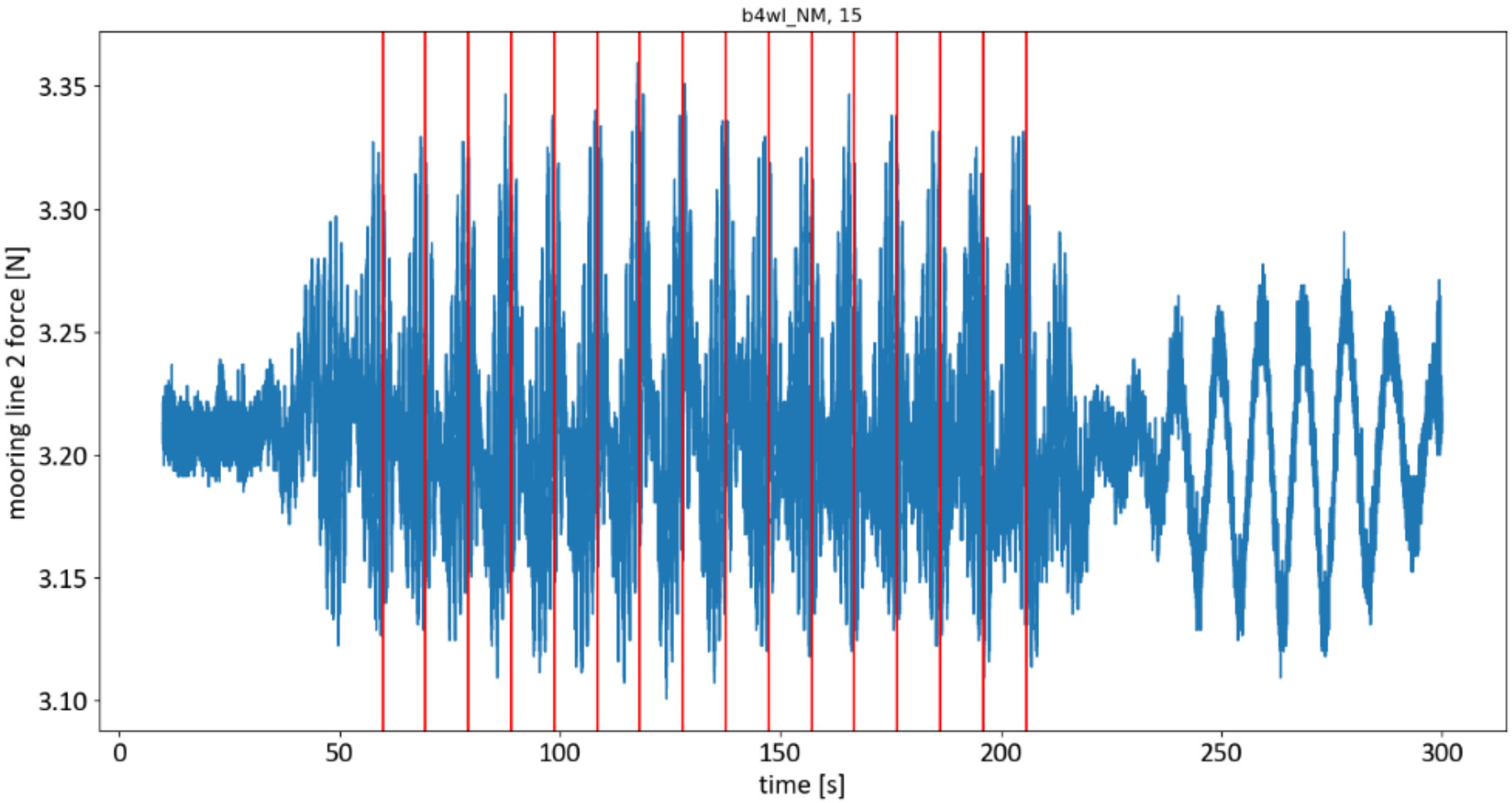
b4wl_NM, 15
mooring line 2 force [N]
3.35
3.30
3.25
3.20
3.15
3.10
0
50
100
150
200
250
300
time [s]

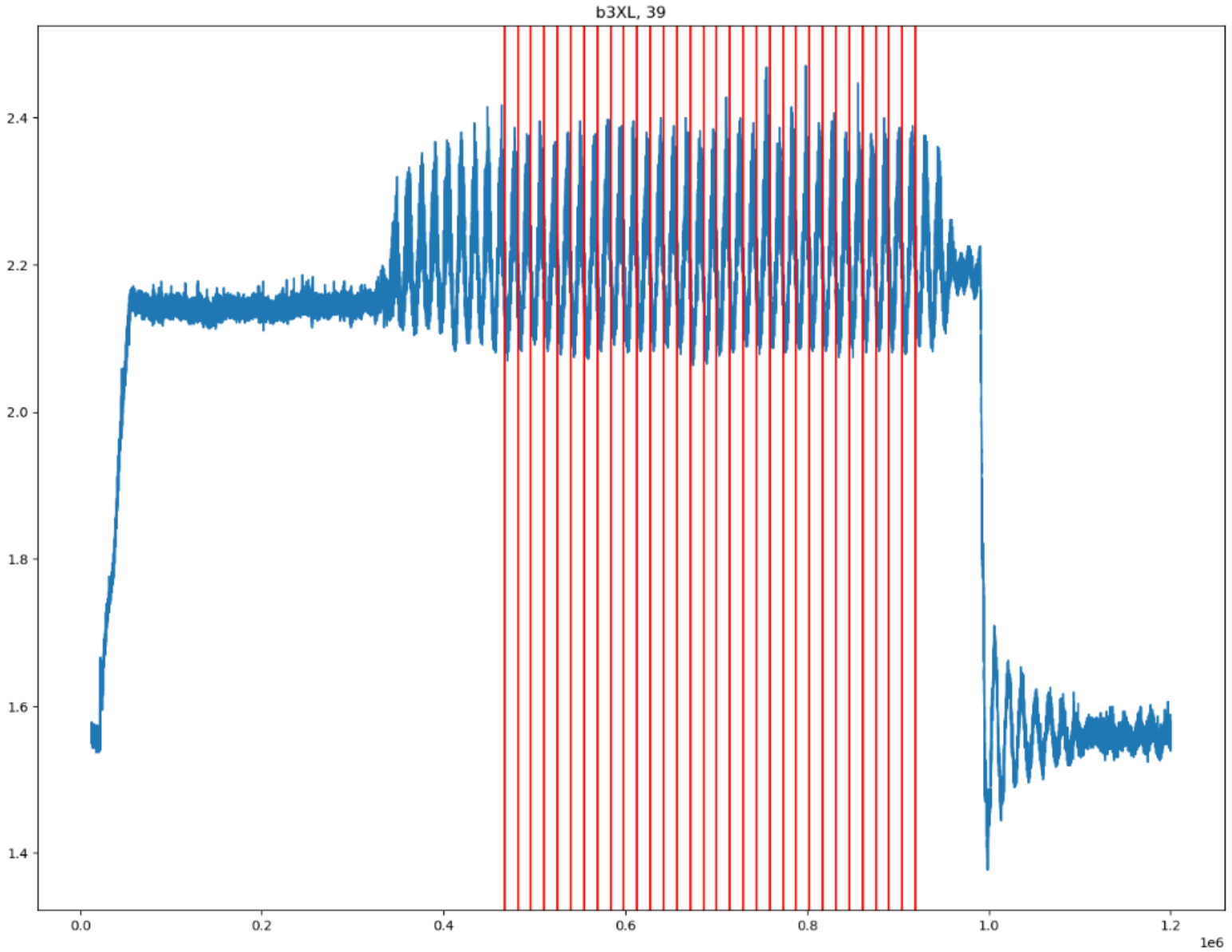
b3XL, 39
2.4
2.2
2.0
1.8
1.6
1.4
0.0
0.2
0.4
0.6
0.8
1.0
1.2
1e6

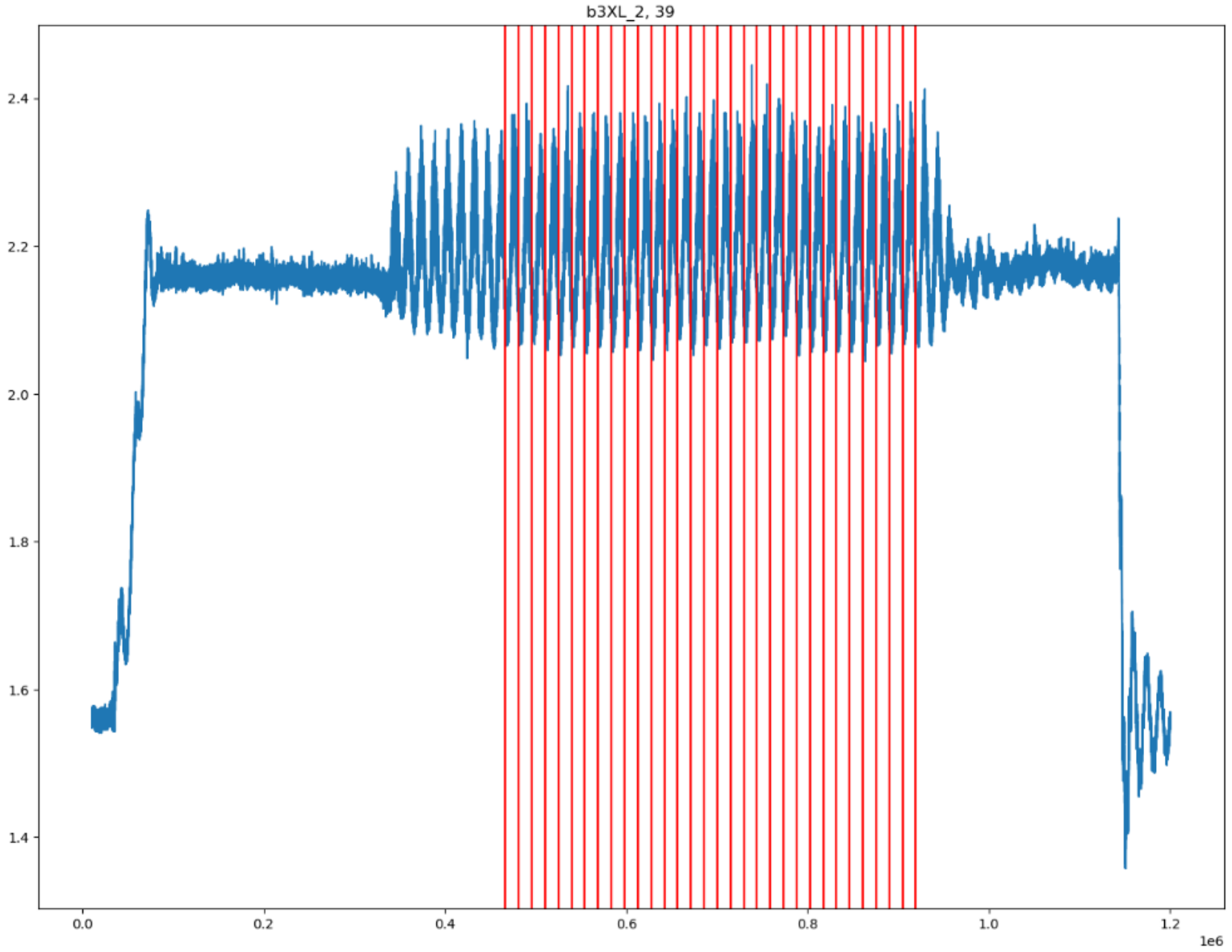
b3XL_2, 39
2.4
2.2
2.0
1.8
1.6
1.4
0.0
0.2
0.4
0.6
0.8
1.0
1.2
1e6

Appendix G: Calculations of the mooring line

To calculate the mooring line stiffness the known quantities are filled in. The reduction in effective depth caused by the rope of the chain part is estimated. Then the angle at the top of the chain is calculated using the known height, force and footprint. This angle is then used to get a better estimate of the reduction of effective depth. This is iterated a few times.

htank	1,25	m
xtot	0,92	m
rope length	0,65	m
rope hred est	0,625	m
h chain	0,425	m
Fx OC5	896900	N
Fx	1,013749	N
w, chosen chain	4,297525	N/m
xmax, est	0,398627	m
S0, chain on the bottom	0,521373	m
S, suspended ketting	0,617359	m
Stot	1,138732	m
chain perspective:		
Stot	1,138732	m
w	4,297525	N/m
h	0,425	m
Fx	1,013749	N
xtot	0,92	m
C, numerical	11,70079	N/m
C, analytical	13,72814	N/m
Fz	2,653117	N
alpha	1,205818	rad
hred, calc	0,607185	m
x, comp	0,232004	m

iteratie 1		
Stot	1,138732	m
w	4,297525	N/m
h	0,642815	m
Fx	1,013749	N
xtot	0,761635	m
C, numeriek	7,91955	N/m
C, analytisch	9,127054	N/m
Fz	3,637644	N
alpha	1,29901	rad
hred, berekend	0,62614	m
x, comp	0,174495	m

iteratie 2		
Stot	1,138732	m
w	4,297525	N/m
h	0,62386	m
Fx	1,013749	N
xtot	0,775984	m
C, numeriek	8,133545	N/m
C, analytisch	9,385883	N/m
Fz	3,553009	N
alpha	1,29286	rad
hred, berekend	0,625055	m
x, comp	0,178342	m

iteratie 3		
Stot	1,138732	m
w	4,297525	N/m
h	0,624945	m
Fx	1,013749	N
xtot	0,775165	m
C, numeriek	12,61037	N/m
C, analytisch	9,370596	N/m
Fz	3,557857	N
alpha	1,29322	rad
hred, berekend	0,62512	m
x, comp	0,178117	m
Ftot	3,699464	N
x, complete	0,953282	

Then x directed forces are applied and the excitation is recalculated for the line using more iterations. The stiffness is then numerically determined using the difference in force divided by the difference in excitation. This is then compared to the mooring line stiffness found in the documentation of the OC4 project (which uses the same lines as the OC5 project) . In blue is the stiffness found for the mooring line design, versus the desired stiffeness in the bottom right corner.

Stot	1,138732181	m
w	4,297525063	N/m
h	0,623062659	m
Fx	0,961748734	N
xtot, ketting	0,770914507	m
Fz	3,509999708	N
alpha	1,30335771	rad
hred, bereken	0,626893108	m
x, comp	0,171770286	m
x, complete	0,942684793	

Stot	1,138732	m
w	4,297525	N/m
h	0,626849	m
Fx	1,065749	N
xtot, ketti	0,779162	m
Fz	3,605433	N
alpha	1,283386	rad
hred, ber	0,623338	m
x, comp	0,184256	m
x, comple	0,963417	

delta x	-0,021				
delta Fx	-0,104				
C, comp	5,01627124	N/m			
				46,2	kN/m
				46200	N/m
				2nd power	96
kg				5,013020833	N/m

Appendix H: Set up of the recording device

As mentioned in the measuring devices section the wave gauges, mooring line force transducers, wind force and torque transducers and wave maker position measuring devices are all coupled to a central recording box and laptop. This happens trough an amplification and filtration device. The force transducers are located on one base and the other devices on a second base. A scheme showing the set-up is shown below. The devices used in the mooring lines and wind torque are a Zemic Type 1R1-K Load Cell (Zemic). For the wind force measurement an in-house shear force block was used. The wave gauges are General Acoustics USS 13-HF acoustic sensors (General Acoustics) fed to the amplifier via a Ultralab ULS advanced controller also from General Acoustics (General Acoustics). The acoustic sensors are calibrated via a fifth sensor measuring a constant known distance in the vicinity of the experimental set-up, thus taking account of environmental conditions, air humidity, for example. It should be noted that the wave gauge system has a delay consisting of 36 sampling periods plus 0.01 s, leading to a delay of 0.37 s at the 100 Hz used. Lastly the wavemaker positioning uses internal electronic components and an external potentiometer. A BMCM MA-UNI universal amplifier (BMCM), a BMCM AP8a backplane (BMCM) and a National Instruments USB 6211 I/O device (National Instruments) connect all systems to the laptop. All relevant device reports are provided via a zip-file along the dataset at <link naar repository>

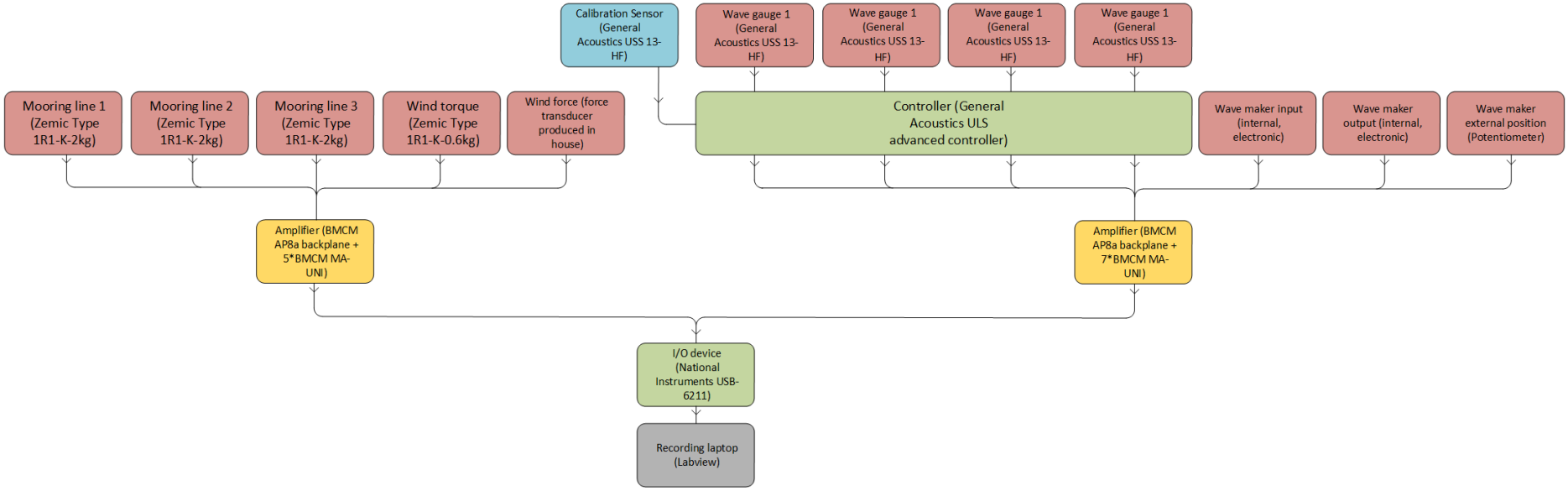

The force transducers use a strain gauge measurement system with an input of 2 mV/V for all systems. As can be seen in the photo below, this corresponds to a position 3 ON setting. The position 7 ON then corresponds to a cut off frequency of 100 Hz. The wiring can be seen going into the -EX, +EX, HI and LO locations, as is required with strain gauges.

The wave gauges and wave maker data inputs only have a position 7 ON setting, corresponding to the data cut off frequency of 100 Hz. The picture below shows the complete set-up (apart from the wave gauge controller) and although a bit hard to see the amplification blocks are set to a voltage measurement system with the wires in HI and LO. It also shows the input-output device in the blue metal box and the laptop connected via USB. As a little extra, the plastic tensioning coils used for the mooring system are also visible below the tape measure.